Atlantic Water in the Arctic Ocean - Mechanisms and Impacts

Morven Muilwijk

Thesis for the degree of Philosophiae Doctor (PhD)
University of Bergen, Norway
2021

UNIVERSITY OF BERGEN

Atlantic Water in the Arctic Ocean - Mechanisms and Impacts

Morven Muilwijk

Thesis for the degree of Philosophiae Doctor (PhD)
at the University of Bergen

Date of defense: 19.08.2021

Year: 2021

Title: Atlantic Water in the Arctic Ocean - Mechanisms and Impacts

Name: Morven Muilwijk

Print: Skipnes Kommunikasjon / University of Bergen

Scientific environment

This study was carried out at the Geophysical Institute at the University of Bergen, where I have been part of the Physical Oceanography group. Additionally, I have been affiliated with the Polar research group at the Bjerknes Center for Climate Research. A portion of the work presented in this thesis was conceptualized during the FAMOS (Forum for Arctic Modeling and Observational Synthesis) meetings, where I established fruitful collaborations. I have also been part of other useful scientific networks such as ASOF, and the N-ICE2015 consortium, from which I have gained a lot of knowledge and inspiration. A six-month-long research stay at Scripps Institution of Oceanography in San Diego was kindly hosted by Prof. Fiamma Straneo and incredibly valuable to the presented research. This would not have been possible without the support from the ACER and TRACEICE projects. I was honored to participate in the 2019 Emerging Leaders program during the Arctic Frontiers conference in Tromsø, and have also been enrolled in the Research School on Changing Climates in the Coupled Earth System (CHESS), which provided many relevant and interesting short courses and meetings that I participated in. Some exceptionally valuable experiences during my Ph.D. education are the Geophysical Fluid Dynamics (GFD) summer school on "ice-ocean interaction" in Woods Hole in 2017, the Arctic Field course in Qeqertarsuaq in 2017, the Advanced Climate Dynamics Course (ACDC) summer school on "the Anthropocene" in Yosemite in 2019, and the Trans-Arctic Change: Extending Interdisciplinary Collaborations on the Environment (TRACEICE) summer school in Fairbanks in 2018. Throughout my Ph.D. period, I have had a continuous strong collaboration with scientists at the Norwegian Polar Institute in Tromsø, through which I have participated in multiple research cruises in the Arctic region. This collaboration resulted in my largest fieldwork endeavor so far, as I participated as a member of Team Ocean during leg 4 of the MOSAiC (Multidisciplinary drifting Observatory for the Study of Arctic Climate) expedition from the beginning of May to the end of August 2020. Finally, it has been an honor to lead the Bergen Geophysical Society and serve as president for Geopsupen from 2017 to 2019.

CHESS
Research school on changing climates in the coupled earth system

UNIVERSITAS BERGENSIS

BJERKNES CENTRE
for Climate Research

"Today we are faced with a challenge that calls for a shift in our thinking, so that humanity stops threatening its life-support system. We are called to assist the Earth to heal her wounds and in the process heal our own - indeed to embrace the whole of creation in all its diversity, beauty and wonder. Recognizing that sustainable development, democracy and peace are indivisible is an idea whose time has come"

Wangari Maathai

Acknowledgements

Headwind, tailwind, smooth seas, and rough seas. Four years of exploring the wonders of the beautiful Arctic Ocean together with wonderful colleagues and friends. I want to acknowledge everyone who has supported me and made this journey possible. First and foremost, I want to thank my supervisor, Lars Henrik, for navigating me skillfully through this PhD with your unwavering support, motivation, and availability. Thank you for giving me free reins to explore my numerous side projects, engage in countless outreach activities, participate in cruises to the end of the world, and for setting boundaries when my scientific scope got too broad. I have had lots of fun on our shared adventures in San Diego, Fairbanks, Woods Hole, Svalbard, Tromsø, and the Bergen mountains. Thank you for all the scientific discussions, for providing me with exciting opportunities, and for always leaving me with good food for thought. We make a great team.

Helge, I am extremely grateful for having you as a co-supervisor. Thank you for your great scientific support and for sharing my passion for outreach and education. Your enthusiasm for dynamics is contagious, and you are the master of combining details with the big picture. You have taught me to focus on the "so what", and your capability of bridging the gap between science and society is incredibly inspiring to me. I have enjoyed working together to develop "Ekte data", row across Store Lungegårdsvann, and visit schools to teach about climate change. Thank you also to, Olaug, all the teachers, and the "Ekte data" team for all the joyful time spent providing scientific data and exercises to schools. Gabriel, thanks for being such a good buoy.

Mehmet, thank you so much for your very valuable support with the NorESM experiments in the early stages of my PhD and for introducing me to the marvelous world of numerical modeling. I would also like to extend my gratitude to Aleksi and Mats for always answering my (sometimes silly) questions and for all the technical and scientific support over the last few years. Mirjam; thank you for introducing me to the field of oceanography many years ago; your passion and excitement for the marvels of the ocean inspired me to become an oceanographer. Thanks also to Arild in Tromsø for fun collaborations and for inviting me to work on several exciting cruises in the Arctic.

Fiamma, thank you for kindly hosting and supervising me at Scripps for six months and for inspiring me to focus on the things that really matter and make a difference. I believe our scientific community will change over the years to come and hope that together we can bring science and communities closer together. Also, you're right - being a polar scientist in a tropical desert is not too bad.

This thesis has, of course, been a team effort, and I would therefore like to thank all my co-authors for their good contributions to my papers. Thank you to all the scientists and non-scientists at the Geophysical Institute and the Bjerknes Center; I have very

much enjoyed my nine years here. Special thanks to Gudrun for inviting me on board with fun outreach projects such as Klimavenn.

I am grateful to all people that have made my PhD time an extremely pleasant period, at and outside of work, in Bergen, San Diego, and remotely. Many thanks to the great PhD and postdoc community at GFI. In particular, thanks to all my GFI besties, in no particular order, Sonja, Elina, Anais, Eva, Xabier, Nadine, Marius, Laura, Ailin, Lander, Karita, Helene, Steffi, Meike, Maribel, AK, Jakob, Vår, and many more. Even though I keep drilling, there are not enough holes in the world that could contain all the laughter, happiness, and care you have given me. Algot, my partner for all the festive planning, I have very much enjoyed the beer brewing in the GFI basement and the numerous sheep heads devoured. Deserving special thanks are Margaret, Donald, and the lively Arenas gang in San Diego, all of whom are wonderful friends and whom I miss deeply. Sam, my friend, it has been really fun working and hanging out together. Having you all as friends has been essential to the success of my PhD and continues to be a privilege.

Also, special thanks to the amazing MOSAiC community; the long days out on the ice would not have been the same without you. Thanks also to the fantastic Adina team and all my friends and colleagues in Uganda, for allowing me to develop different skills and work with people in addition to numbers.

To my parents and extended family, thank you for always believing in me, supporting me, and for always showing interest in what I am doing. I know I am often busy and far away, but this makes it even better to come home to you. Finally, my girlfriend Zoe, you have been a constant source of encouragement, support, and joy. Thank you for all your help, patience and love. Also, thanks for agreeing with me that it should be pronounced narwhale instead of narwhal. I am deeply grateful for your partnership. You are my Arctic hero.

Morven Muilwijk
Bergen (southern boundary of the Arctic Ocean), May 2021

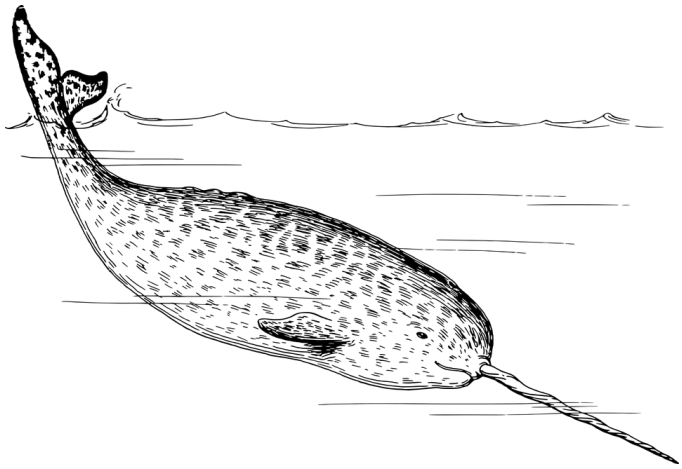

Abstract

The Arctic Ocean plays a fundamental role in regulating Earth's climate, and a changing Arctic will affect climate, weather, and life everywhere on the planet. Understanding the fundamental dynamics and mechanisms driving natural variability, and the effects of anthropogenic warming in the Arctic climate system is imperative to improve future climate predictions. Warm and saline Atlantic Water (AW) entering the region across the Greenland-Scotland Ridge is the primary heat source to the Arctic Ocean and plays an essential role in modulating the Arctic climate system. However, our knowledge is still insufficient to make skillful projections of future Arctic climate change with uncertainty levels similar to other regions. This thesis improves our understanding of the role of AW in the Arctic Ocean, focusing primarily on: its variations in the twentieth and twenty-first centuries; the underlying mechanisms governing this variability; and its proliferating regional impacts on sea ice, marine-terminating glaciers, and stratification.

First, we investigate the twentieth-century variability of AW heat transport through the gates of the Arctic Ocean. The analysis is based on a simulation from the global ocean-ice Norwegian Earth System Model (NorESM) supported by an extensive set of hydrographic observations dating back to 1900. We quantify prominent variability in both AW temperature and volume transport on near-decadal time scales, as well as significant positive trends in the most recent decades. Variations in volume transport were found to be linked to the wind forcing in the Nordic Seas and Subtropical North Atlantic, as manifested through the North Atlantic Oscillation, although the correlation is not constant over time and breaks down entirely in specific periods, such as the Early Twentieth Century Warming period. Variations in temperature are a combination of advected signals originating upstream and variations in atmospheric cooling over the Nordic Seas, which effectively dampen the AW heat anomalies along their path northward.

Secondly, we provide a further in-depth investigation of the relationship between the AW flow and wind forcing. Here, we analyze results from a coordinated wind perturbation experiment in a suite of nine different Arctic Ocean models, and calculate "Climate Response Functions" (CRFs) to isolate the effects of wind anomalies on AW circulation, sea ice, and hydrography. The CRFs show that anomalously strong/weak wind forcing over the Greenland Sea results in an intensification/weakening of the poleward AW flow and a reduction/increase in the Arctic sea ice cover. Despite biases in hydrography, all models respond in a similar manner to the anomalous winds and show a near-linear relationship between AW volume and heat transport, surface heat loss, and sea ice extent in the Barents Sea. Historical reconstructions show that the largescale wind forcing alone can explain 50% of the AW flow variance, indicating potential for

predictability.

Third, we focus on the export of meltwater from Upernavik Fjord in northwest Greenland as the combined result of melting caused by AW and the release of subglacial discharge at the fronts of marine-terminating glaciers. Using hydrographic observations collected between 2013 and 2019 we provide the first description of the hydrographic structure in Upernavik Fjord, explain the complex water mass transformation occurring in the fjord, and quantify the composition of the water mass exported from the fjord. We show that meltwater is heavily diluted and exported as "Glacially Modified Water" (GMW), which in summer is composed of 57.8 $\pm$8.1% AW, 41.0 $\pm$8.3% Polar Water, 1.0 $\pm$0.1% subglacial discharge, and 0.2 $\pm$0.2% submarine meltwater. Consistent with its composition, we show a close relationship between water mass properties on the continental shelf (AW and Polar Water) and the exported GMW properties, and estimate an exchange across the fjord mouth of 50 mSv. This study provides a first order parameterization for the exchange at the mouth of glacial fjords for large-scale ocean models.

Finally, we investigate changes in central Arctic Ocean stratification in the twentieth and twenty-first centuries. Observations show that from 1970 to 2017, the stratification in the Amerasian Basin has strengthened, whereas the stratification has weakened in parts of the Eurasian Basin. These contrasting results are due to competing effects of increasing AW influence ("Atlantification) and local freshening. Simulations from the Community Earth System Model Large Ensemble and a suite of nine CMIP6 models project that under a strong greenhouse-gas forcing scenario (RCP8.5/SSP585), the upper layers in the Amerasian Basin will become even more stratified in the future. In the Eurasian Basin, models show diverging results, with approximately half of the models projecting a strengthened stratification in the future and the other half projecting a weakened stratification. These differences are mainly a result of different balances between local processes and advected signals.

Combined, the four papers highlight the diverse yet significant role of AW in the Arctic environment and advance our knowledge of the broad-scale mechanisms governing AW variability and the impacts of AW on different components of the climate system. Our results provide a spatially and temporally inclusive progressed understanding of natural and anthropogenic climate change in the Arctic and ultimately contribute to improved projections of future Arctic climate change.

List of abbreviations

AB: Amerasian Basin

AMO: Atlantic Multidecadal Oscillation

AMOC: Atlantic Meridional Overturning Circulation

AW: Atlantic Water

BG: Beaufort Gyre

BSO: Barent Sea Opening

CMIP: Coupled Model Intercomparison Project

CRF: Climate Response Function

CTD: Conductivity Temperature Depth (instrument)

EB: Eurasian Basin

EEB: Eastern Eurasian Basin

ETCW: Early Twentieth-Century Warming

FS: Fram Strait

GSA: Great Salinity Anomaly

GMW: Glacially Modified Water

NAO: North Atlantic Oscillation

NorESM: Norwegian Earth System Model

OW: Overflow Water

PW: Polar Water (Pacific Water in Paper IV)

SML: Surface Mixed Layer

SST: Sea Surface Temperature

WEB: Western Eurasian Basin

The first temperature observations taken in the central Arctic Ocean during Fridtjof Nansen's Fram expedition 1893-1893. Foto: Norwegian National Library/Norwegian Polar Institute.

Outline

This thesis consists of an introductory part and four scientific papers. Chapter 1 consist of a short preamble and Chapter 2 gives an overview of the scientific background for the results presented. The objectives, data and methods are described in Chapter 3 and a brief summary of the papers is given in chapter 4. I share some future perspectives and concluding remarks in chapter 5. The scientific papers listed below are presented in Chapter 6.

List of papers

I. Muilwijk, M., Smedsrud, L. H., Ilicak, M., Drange, H. (2018). *Atlantic Water heat transport variability in the 20th century Arctic Ocean from a global ocean model and observations*. Journal of Geophysical Research: Oceans, 123(11), 8159-8179.

II. Muilwijk, M., Ilicak, M., Cornish, S.B., Danilov, S., Gelderloos, R., Gerdes, R., Haid, V., Haine, T.W., Johnson, H.L., Kostov, Y., Kovács, T., Lique, C., Marson, J.M., Myers, P.G., Scott, J., Smedsrud, L.H., Talandier, C., Wang, Q. (2019). *Arctic Ocean response to Greenland Sea wind anomalies in a suite of model simulations*. Journal of Geophysical Research: Oceans, 124(8), pp.6286-6322.

III. Muilwijk. M., Staneo, F., Slater, D., Smedsrud, L. H. , Wood, M., Holte, J., Andresen, C., Harden, B. (submitted to Journal of Physical Oceanography). *Export of ice sheet meltwater from Upernavik Fjord, West Greenland*.

IV. Muilwijk. M., Smedsrud, L. H. , Polyakov, I., Nummelin, A. (in prep) *Past, present, and future Arctic Ocean stratification from observations and CMIP6 simulations*.

Additional contributions

A Le Bras, I., Straneo, F., Muilwijk, M., Smedsrud, L. H., Li, F., Lozier, M. S., Holliday, N. P. (2021). *How much Arctic fresh water participates in the subpolar overturning circulation?*. Journal of Physical Oceanography.

B Svendsen, L., Keenlyside, N., Muilwijk, M., Bethke, I., Omrani, N. Gao, Y. (in review at Climate Dynamics) *Pacific contribution to decadal surface temperature trends in the Arctic during the twentieth century.*

C Smedsrud, L.H., Brakstad, A., Madonna, E., Muilwijk, M., Lauvset, S.K., Spensberger, C., Born, A., Eldevik, E., Drange, H., Jeansson, E., Li, C., Olsen, A., Skagseth, Ø., Slater, D.A., Straneo, F., Våge, K., Årthun, M. (submitted to Reviews

of Geophysics) *Nordic Seas Heat Loss, Atlantic Inflow, and Arctic Sea Ice cover over the last century* .

D Eldevik, T., Onarheim, I.H., Smedsrud, L.H., Steele, M., Dodd, P., Muilwijk, M., Årthun, M. (in prep) *How Atlantic heat makes Arctic sea ice retreat*

E Cornish, S.B., Muilwijk, M., Scott, J., Marson, J.M., Myers, P.G., Zhang, W., Wang, Q., Kostov, Y., Johnson, H.L. (in prep) *Ice trajectories under the Beaufort High can influence freshwater accumulation*

F Marshall, J. et al. (in prep) *Freshwater response of the Beaufort Gyre to a step change in the Beaufort High: model comparisons*

Contents

Chapter 1

Preamble: personal reflections

> "Scientists today are privileged to be able to indulge their passions for science and simultaneously to provide something useful to society. With these privileges comes serious responsibility."
>
> *Jane Lubchenko*

The output of a Doctorate in Philosophiae far exceeds a collection of scientific publications. Indeed this final submitted work is a compilation of the most significant scientific results I have worked on over the past four years set in a broader scientific context; however, the untyped, non-peer-reviewed, and personal work has been imperative. Over the course of my Ph.D. education I have been fixated on the "so what?" of academia, constantly cogitating on how this work contributes to society. As researchers, we are mainly evaluated on our scientific output, and there are unfortunately limited arenas to present outreach projects or other relevant research skills. There are also limited opportunities to properly present and discuss the shared challenges that arise at various stages of a scientific career. For example, some fundamental queries that have arisen during my Ph.D. education are: 1) How can we make our science more beneficial for the local communities?, 2) How can we ensure that the science we do is done most sustainably?, and 3) How can we address inequality in our scientific community? For me, these larger matters relevant to my Ph.D. education are equally important to the scientific outcomes. I have therefore chosen to dedicate a section of this thesis to pen some personal reflections on the often curtailed topics.

Although science for the sake of science is essential to make discoveries, a disconnect between natural sciences and society does a disservice to both. In 1998, environmental scientist Jane Lubchenko proposed a new social contract for natural scientists: "a commitment on the part of all scientists to devote their energies and talents to the most pressing problems of the day, in proportion to their importance, in exchange for public funding" (*Lubchenco*, 1998). Many natural scientists are turning their attention to problem-focused work for the benefit of society as is evident through the increase in trans-disciplinary science, for example. I believe that Lubchenco's ideas on science for society will continue to become more critical in the future as the cascading impacts of the Climate Crisis increasingly stress society. The primary output of my study of the Arctic climate system is enhanced understanding, hopefully contributing to improved climate projections. This is still mainly science for science sake, and I cannot

forget that the underlying problem of the ongoing change in the Arctic is already well established, and needs urgent political action rather than more research. I have therefore committed significant effort to connect this content beyond the peer-community. I will return to the motivation and objectives of my studies in Chapter 3. From my perspective, being a scientist is about producing high-quality scientific work as well as becoming an educator and a representative of the scientific community. I am notably interested in scientific outreach and strongly believe that it is one of my societal duties as a publicly funded scientists to communicate scientific content and enhance scientific literacy for a broader audience. One may argue that not all scientists have to do outreach, or that outreach should be left to communication professionals, but I challenge this dislocation of responsibility. It seems that science has entered a new era of public distrust in which the scientific process itself is open to public controversy, and provable facts are no longer considered objective, and as such I see outreach as paramount to a responsible research career. Especially in times of "fake news" and "alternative truth", the way science is presented and used further down the pipeline is of growing importance and scientists are best situated to moderate the dissemination and reverberation of their work. The increasing demand for good dissemination by funding agencies is further indicative of the importance of science communication.

1.1 SMART Outreach

> "People should treat the oceans like we do anything else that we care about it – with consideration – with care and affection. That's it. For that we must educate."
>
> *Walter Munk*

In lieu of university teaching, 25 % of my contract has been dedicated to an outreach project focused on high school students called "Ekte data (more information below). In addition to this primary project I have collaborated with many great colleagues on multiple exciting outreach projects focused on educating younger and older generations alike. Through these collaborations I have, for example, given talks at schools and public venues, made videos as part of the project "Værtinnen og Havmesteren", had my work featured in the US documentary series "True North" and a US planetarium documentary, and co-hosted a multiple-episode climate TV show for children, "Klimavenn". For many researchers, outreach is something that must be written into proposals or carried out to meet requirements, but training to develop communication skills in not often (if ever) paired with this requirement. As an example, Ph.D. candidates must preform a trial lecture on a given topic between submission and defense in which we are expected to be skilled scientific presenters but formal pedagogical training is not part of the Ph.D. curriculum.

Over the course of my outreach activities I have paid keen attention to what defines engaging, efficient, and impactful outreach in hopes of being able to use my experience and enthusiasm to assist other researchers with their public communication. I, therefore, propose a simple guideline to assist scientists when designing outreach projects; called SMART outreach.

- Strategic: think about how your outreach can have a large footprint or include as many people as possible from your target audience. Many "products" are limited on how many people they reach – can any of these obstacles be lowered?
- Meaningful: how can you relate your science to a specific target group? What values, experiences, comparisons, and approaches bring your content to the hearts of your audience?
- Accessible: easy to use. Create a product that is not too much dependent on your time.
- Reusable: outreach tools should be developed in such a way so that they can persist beyond your involvement, be used multiple times, are easily used by new users, and are integrated with exciting educational plans, curriculum, and courses. Not just a "one-time bridge" between scientists and the general public.
- Treat: Outreach should be fun, both for you and your target group!

High quality scientific outreach should achieve two main goals: (1) spread knowledge and understanding about the topic at hand, be it glaciers or bumblebees, and (2) develop or improve skills of scientific literacy, critical thought, and analytical understanding of real-world problems. By coupling these two goals when using the SMART outreach approach, the impact of the outreach is maximized. For though scientists tend to believe that knowledge transfer to the general public (or target audience) on their topic is the primary goal of outreach, I would argue that the skill transfer and improved scientific literacy is the outcome that has the more significant impact on society (or the target audience). These two goals have been foundational in the development of the "Ekte data" project, which I have been working on for the past four years. The project aims to (1) educate high school students about oceanography, meteorology, and climate observations, and (2) help them transfer their school-acquired skill sets to real-world problems such that they can interpret and understand uncertainty in "big data".

"Ekte data" — or "Real Data in English" — is a digital platform providing real-life scientific data for teaching mathematics and science at secondary high schools in Norway since 2015. In general, we see a gap between students' theoretical knowledge and applying their "mathematical toolbox" to real-world problems. This project aims to partly bridge the gap between theory and practical application while simultaneously giving students insight into the interpretation and uncertainty of "big data". The developed exercises use real-life oceanographic, meteorological, and climate observations to engage students by adapting learning outcomes integral to the curriculum (e.g., statistics, regression, modeling, thermodynamics) to relevant, real-world problems. We have built accessible exercises structurally and methodologically similar to those found in a textbook that allows students to engage with real-life data sets

rather than hypothetical problems or printed tables with static content. The web portal (https://ektedata.uib.no/) provides access to over 80 exercises on various topics, such as ocean circulation, acidification, arctic sea ice, wind energy, local weather, fish stocks, and climate change. The exercises are customized to the curriculum at different levels with data from both local and global observations. Integration of local data has been very successful and currently includes an extensive collection of weather stations placed on school rooftops and an advanced oceanographic buoy ("Gabriel") recording in a local fjord (https://ektedata.no/).

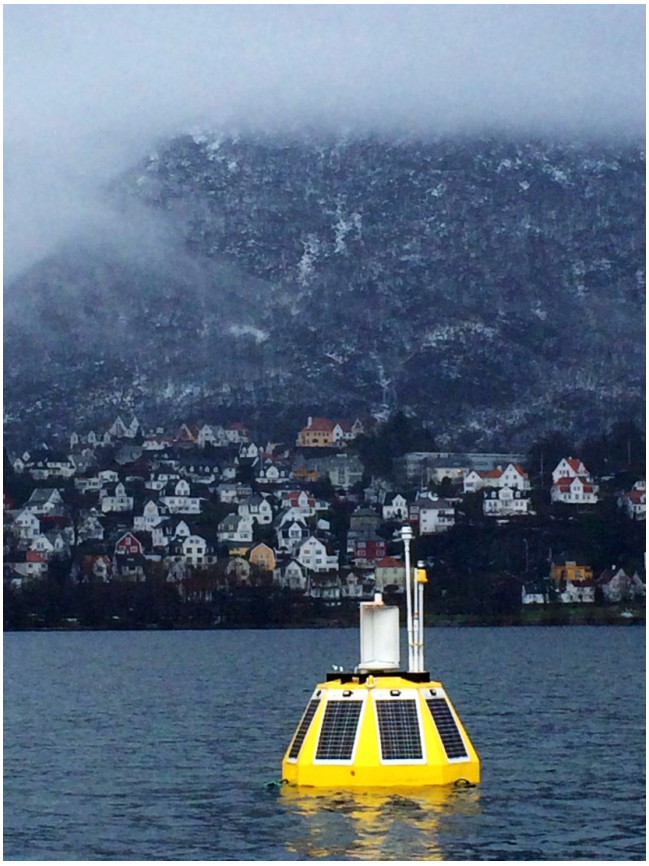

Figure 1.1: Data from the CTD-buoy "Gabriel" in a local fjord arm in the city of Bergen has provided data for high school mathematics and science exercises since 2015. As part of my Ph.D., I have been responsible for developing the "Ekte data" project, maintaining the buoy, and facilitating other scientific data for schools. Foto: Øyvind Paasche.

"Ekte data" and other SMART outreach projects have been a defining part of my Ph.D. candidacy; I am pleased to have the opportunity to share with you here. In the future I would like to further develop the SMART framework and reach out to scientists with the opportunity to grow and practice their science communication and pedagogical skills with hopes of improving the efficiency and enjoyability of their science outreach.

1.2 Sustainable science

> " We need to respect the oceans and take care of them as if our lives depended on it. Because they do."
>
> *Sylvia Earle*

The environmental footprint of our work, and particularly our traveling, is (rightly so) often a topic of debate. Most of the time, it is justified by the "for the greater good" argument or seen as necessary to produce good science. Physical meetings are crucial for good collaborations, although the global pandemic has shown that there are online alternatives for some types of meetings that have unique benefits, such as mitigating financial barriers to participation. This will likely be an ongoing dilemma for scientists in general, and arguably climate scientists in particular, for quite some time to come. A much less discussed aspect of our collective environmental footprint is that of our scientific practices in the field and lab. Due to the importance of this issue, I will take a moment to reflect. Oceanographic fieldwork is a prime example of research that needs to balance its environmental footprint with its return to science and society. Research vessels are essential for the understanding of the marine environment, but they are also polluters—- especially some of the ice breakers I have worked on. This is a dark side of science that is often not discussed due to the uncomfortable reality of the situation; we can do little more than maximize the efficient use of ship time.

Our instrumentation and methods, however, are something that we have significantly more control over. Some equipment is lost accidentally, but we also intentionally deploy not-insignificant amounts of equipment without the intention of recovery. Often the abandonment of equipment is justified because the footprint of recovery by ship exceeds that of the instrument itself, however there is no clear way to compare the impact of the plastics, chemicals, and heavy metals of the equipment to transportation emissions. The accumulation of litter and pollutants is a massive problem for the world's oceans and we as researchers ought to be on the forefront of innovative solutions, not consciously but quietly justifying the addition of our own waste. The primary barrier to addressing this issue is that there currently exists no environmentally friendly alternatives for most of these leave-behind instruments such as Meteorological radiosondes, XCTDs, and drifting buoys. The same lack of availability is also true of lab equipment such as gloves, bottles, pipettes, and other high-volume single-use products. As a community, we must acknowledge our contribution to the problem and demand better solutions from the manufacturers that provide our equipment.

It is not that the technology to make our equipment more environmentally friendly is lacking, but that demand is driven by a balance of price and quality as is amenable to scientific budgets. For this reason, I believe that efforts towards sustainable science − in a robust sense of the concept of sustainability − should be taken into account at the funding level. Currently, projects are evaluated on their scientific excellence, impact, and implementation, but there could also be room to consider environmental footprint. Where its not possible to eliminate negative impacts, transparent reporting on the consequences of our research should be common practice. Identification and quantification of the problem through mandatory reporting will also generate awareness and moti-

vate changes. This could potentially influence the community towards better practices and more open dialogue about the shared challenges we face. I have personally struggled with the deep-seeded realization that at the present moment my Ph.D. thesis has likely harmed the environment more than helped it. I hope, however, that its results improve our understanding and management of the vulnerable Arctic and that with time the net outcome of my work will be beneficial for the Ocean, her creatures, and society as a whole. I see a need for a shift in the paradigm of our scientific modes and methods such that the impacts of our work are minimized and thus lower the threshold we need to surpass to acutely substantiate the beneficial for the greater good argument. Over the course of my four month participation in the MOSAiC expedition the discussion of sustainable science was animated and ongoing – to me this indicates that the current and incoming generation of Early Career Researchers is ready for this change.

Figure 1.2: Research vessels are essential for the understanding of the marine environment, but there is room for improvement to make our scientific methods more sustainable. Here a picture from my recent fieldwork in the Arctic Ocean as part of the MOSAiC campaign.

1.3 Inclusive science

> "There is a playbook. It was written by men."
>
> *Sallie "Penny" Chisholm*

Though uncomfortable, the issue of bias and discrimination in science is one on which I am unwilling to remain silent. Great science results from great minds working together across disciplines and borders (both geographically and otherwise); that is to say, the quality of science is a product of the people who do it. Tragically, the research community is missing out on many great minds because of inherent issues of inequality in the academic system, both globally and in Norway. Women and minorities in oceanography and natural sciences are still navigating rough seas which means we are not harnessing humanity's full intellectual scope and capacity. This is intolerable because it is antithetical to the advancement of science for society, as is discussed in the previous section. The "#me-too" movement has led to more open discussion and increased accountability in some instances, but discrimination and an implicit gender bias still persist in our community. I have listened to many female and minority colleagues share their experiences of subtle discrimination, exclusion, and unwanted sexual attention, especially during fieldwork on ships, and this is not acceptable. The unequal treatment and discrimination in both large and microscopic ways cause many people to feel alienated in academia and ultimately pursue other careers. In contrast to the last two sections in this thesis preamble, I do not have, nor need, a proposed approach to this problem — the materials, organizations, initiatives, and policies are already in motion. What we need is commitment and accountability from our institutions, our colleagues, and ourselves to do the work. Over the years I have learned how important it is for, straight white males, like myself, to be supportive allies who: listen actively; support equality focused projects, policies, and programs; and speak up to create space for our colleagues when we notice things that are inappropriate.

The recent US-based documentary movie "Picture a Scientist" addresses gender and racial bias in science. This movie has helped spark discussions and keep the topic of equality on the agenda which I have seen to be beneficial for the UiB community. That being said, the data speaks for itself: of permanent staff at the faculty of natural sciences at UiB, only 15% of the professors are female. UiB is currently taking a leadership role with the United Nations Sustainable Development Goals, but if we want to be a true leadership institution, work must go beyond our hub target of Life Below Water (SDG 14) and focus on Gender Equality (SDG 5) as well.

Chapter 2

Scientific background

Compared to other regions of the world, the Arctic has been unexplored until fairly recently. Early cartographers in the period from the 1500s until the late 1800s were unsure whether to draw the region around the North Pole as land or water. Motivated by driftwood and artefacts along the coasts on Greenland originating from USS *Jeanette* that sunk on the opposite side of the Arctic in 1881, Fridtjof Nansen was the first to make a nautical crossing of the Arctic Ocean in 1893-96. The idea of the Arctic being an open ocean was finally dispelled. Even though he almost didn't carry enough rope and wire to measure the more than 4000 m deep Arctic basins during his expedition, Nansen observed and described the most important features of the ocean-ice system, laying the foundation for modern polar oceanography. Nansen found warm and saline water at depth, and while drifting with his ship the "Fram" across the Arctic Ocean for more then three years, he asked himself the most fundamental question in Arctic oceanography: Why does the heat present in the ocean below not melt the ice above? This question is the root to some of the science discussed in this thesis, and we can expand and rephrase it by asking: what are the mechanisms controlling the inflows of warm water masses to the Arctic Ocean and what are their impacts in the past, present and future? In this chapter we provide a brief summary of the state of the art scientific background for the results of this dissertation. We begin by a description of the Arctic Ocean, it's role in the global climate system and the oceanographic setting (Chapter 2.1). We then present the current understanding of how and why the northward flow of warm water masses has changed in the past (Chapter 2.2), before we describe the impacts of these waters (Chapter 2.3).

2.1 Study area and oceanographic setting

2.1.1 Regional description

The Arctic Ocean is Earth's northernmost body of water, and it is also the smallest of the world's five major oceans. In this thesis we study the wider definition of the Arctic Ocean (*Aagaard et al.*, 1985), consistent with the official Arctic Ocean definition of the International Hydrographic Office (*IHO*, 1953; *Jakobsson and Macnab*, 2006), which includes both the Central Arctic Ocean, the Barents Sea and the Nordic Seas, a region often termed the Arctic Mediterranean following *Sverdrup et al.* (1942). The Central

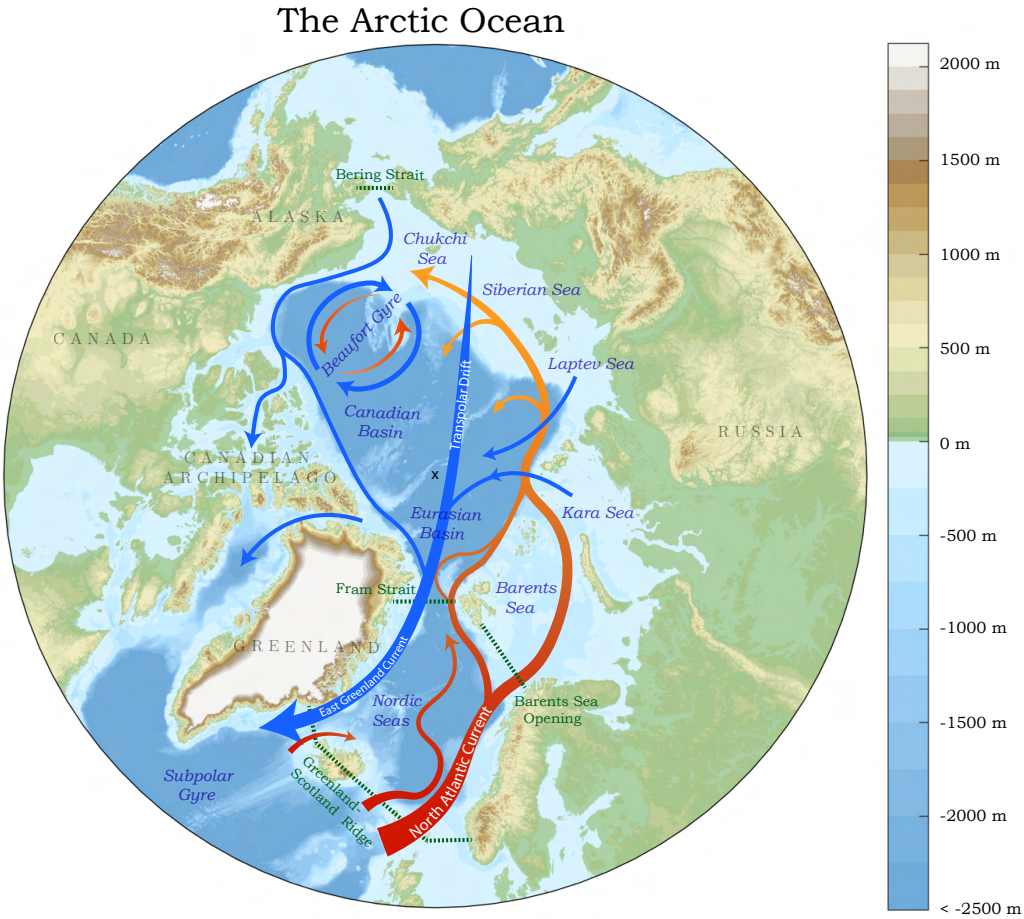

Figure 2.1: Schematic circulation of the Arctic Ocean. The pathways of warm Atlantic inflow and cold Polar Water outflow are shown by red and blue arrows, respectively. Red arrows represent circulation at intermediate depths, whereas blue arrows represent a near surface circulation. Color shading represent the bathymetry and land topography from ETOPO2, and relevant topographic features, basins, seas and gateways are named.

Arctic Ocean consists of five shallow (<500 m) shelf seas (the Beaufort, Chukchi, East Siberian, Laptev and Kara Seas) and two main deep (>2500 m) basins (the Eurasian Basin and Canadian/Amerasian Basin) separated by the subsurface Lomonosov Ridge (Figure 2.1, *Rudels* (2015)). The two deep basins are each subdivided by less prominent ridges; the Nansen-Gakkel Ridge, which separates the Eurasian Basin into the Amundsen and Nansen basins, and the Alpha-Mendeleyev Ridge, separating the Canadian/Amerasian Basin into the Canada and Makarov basins. The Nordic Seas comprise the deep (>3500 m) Norwegian, Greenland, and Iceland Seas, and serve as the main gateway connecting the subpolar North Atlantic in the south to the Central Arctic Ocean and Barents Sea in the north. They connect to the Eurasian Basin via the deep (∼2500 m) Fram Strait (*Klenke and Schenke*, 2002) and to the Barents Sea through the shallow (∼300 m) Barents Sea Opening (*Aagaard et al.*, 1985). The southern boundary is the Greenland-Scotland Ridge (GSR), a submarine ridge extending from Greenland via Iceland and the Faroe Islands to Scotland. This ridge acts as a solid barrier below 850 m, which is the sill depth of the Faroe Bank Channel (*Hansen and Østerhus*, 2007). The Arctic Ocean is further connected to the Pacific Ocean through Bering Strait (<90 m) between Alaska and Russia and to Baffin Bay through the various channels of the Canadian Arctic Archipelago. In this study we briefly also touch upon the oceanography of Baffin Bay west of Greenland, but note that from an oceanographic perspective this is not well connected with the other Arctic basins and seas (*Hopkins*, 1991).

The Arctic Ocean and Earth's climate

"What happens in the Arctic, doesn't stay in the Arctic."

Acting as the Northern Hemisphere's refrigerator, the Arctic region contributes actively to regulating Earth's climate (*IPCC et al.*, 2019). In terms of Earth's energy balance the Arctic is a region of net outgoing radiation at the top of the atmosphere which balances the net radiation surplus near the equator. The inequality in the amount of solar radiation received near the poles compared to the tropics gives rise to a gradient in atmospheric temperatures which drives a poleward circulation of heat and air, and hence regulates temperatures further south (*Marshall and Plumb*, 2008). Also the oceans carry a vast amount of heat poleward, and the general cooling of the ocean in the Arctic plays a vital role for the global ocean circulation. Furthermore, the Arctic climate system has a number of feedback mechanisms which affect the global climate. For example, a seasonal sea ice cover modifies the poleward temperature gradients trough its high albedo (*Pistone et al.*, 2019), which results in solar radiation being reflected back to space. The sea ice also plays a role as an insulating layer atop the Arctic Ocean, capping oceanic heat, and preventing it from warming the lower atmosphere (*Thomas and Diekmann*, 2003). These are just some of the properties which help cool the Arctic and the planet. A loss of sea ice will therefore result in a feedback loop which will result in increased warming (*Pistone et al.*, 2019). Among its other important functions, the Arctic Ocean also acts as a sink for carbon dioxide, although it's role in the global carbon cycle is still poorly understood. The Arctic is also home to a large ice sheet and multiple glaciers, storing a large portion of Earth's freshwater, which in turn determines global sea level and has the potential to affect ocean circulation (*IPCC et al.*, 2019). Furthermore, the vast area of permafrost, storing large amounts of methane (*Schuur et al.*, 2015), as well as subsea permafrost carbon stocks (*Sayedi et al.*, 2020),

is also tightly coupled to the climate state of the Arctic Ocean. This is a very simplified summary of the complex role of the Arctic Ocean in the global climate system, but it is needless to say that changes in the Arctic will affect climate, weather and life not only locally, but elsewhere on the planet as well.

The Arctic Ocean in a warming climate

The Arctic region is changing in response to global warming more dramatically than anywhere else on the planet as observed by surface air temperature. The ongoing increase of greenhouse gas concentrations due to anthropogenic emissions leads to enhanced absorption of outgoing longwave radiation and hence increased surface air temperatures. In the Arctic region these surface air temperatures have warmed at more than twice the global rate, a feature often termed "Arctic Amplification" (*Cohen et al.*, 2014, 2020; *Landrum and Holland*, 2020; *Serreze et al.*, 2007). An intensive loss of Arctic sea ice (Figure 2.2, Chapter 2.3.1) and glacial ice (Chapter 2.3.2) is one of the results of this warming, which in turn sustains fundamental global and local climate feedbacks (*IPCC et al.*, 2019). For example, on a global scale the loss of sea ice impacts Earth's planetary albedo (*Pistone et al.*, 2019), large-scale atmospheric circulation (e.g. *Deser et al.* (2015); *Screen* (2017)), weather at lower latitudes (e.g., *Francis and Vavrus* (2012); *Liptak and Strong* (2014); *Overland and Wang* (2010); *Sorokina et al.* (2016); *Yang and Christensen* (2012)), and ocean circulation (*Sévellec et al.*, 2017).

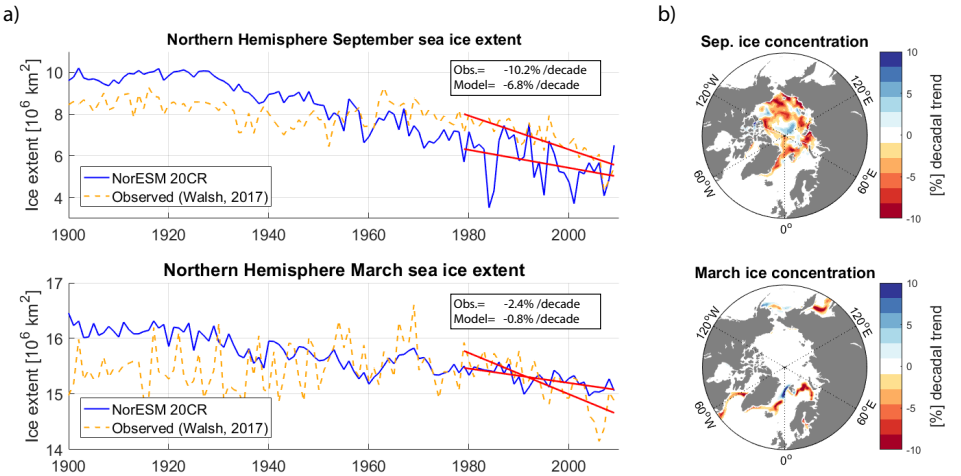

Figure 2.2: a) Time series of observed sea ice extent from Walsh et al. (2017) and simulated by NorESM (Paper I in this thesis) for September (upper panels) and March (lower panels). Linear trends from 1980 to 2009 are indicated in red for both the model and observations. Time series are cut in 2009 due to the length of the twentieth century NorESM simulation. b) Maps showing the spatial decadal september (upper panel) and march (lower panel) trend in sea ice concentration from 1900 to 2009 from the NorESM model.

Locally, the diminishing sea ice cover impacts marine ecosystems (e.g. *Lannuzel et al.* (2020); *Meier et al.* (2014); *Wassmann et al.* (2011)), ocean stratification (*Polyakov et al.*, 2020), ocean accidification (*Terhaar et al.*, 2020), and human activity

(*Meier et al.*, 2014; *Stocker et al.*, 2020; *Wei et al.*, 2020). The ongoing Arctic Ocean warming (*Polyakov et al.*, 2010; *Timmermans et al.*, 2018; *Woodgate*, 2018), freshening (*Haine*, 2020; *Solomon et al.*, 2020), and changing stratification (Paper IV) also link back again to the sea ice trough various feedback loops.

The observed changes in the Arctic Ocean are unprecedented in more than 1000 years (*Kinnard et al.*, 2011; *Polyak et al.*, 2010) and closely linked human activity (*Fyfe et al.*, 2013; *Najafi et al.*, 2015). Most recent climate projections show a continued Arctic warming (*Davy and Outten*, 2020) and loss of sea ice (*Årthun et al.*, 2021; *Keen et al.*, 2021; *Notz and Community*, 2020), but there is high uncertainty in the projected trends because of spread amongst the models resulting from different model resolutions, parameterizations, physics and biases (e.g. *Danabasoglu et al.* (2016); *Heuzé and Årthun* (2019); *Ilicak et al.* (2016); *Massonnet et al.* (2012); *Shu et al.* (2019, 2020); *Wang et al.* (2016a)), and internal climate variations (*Årthun et al.*, 2021; *Desmarais and Tremblay*, 2021; *Swart et al.*, 2015). We will discuss model uncertainties and differences further on in this thesis.

2.1.2 Circulation in the Arctic-Atlantic region

The general Arctic Ocean circulation is associated with a large northward heat transport and is mainly constrained by geological boundary conditions such as the large shelf seas, deep ridges and narrow gateways connecting the deep basins to the Pacific and North Atlantic Oceans (*Aagaard and Carmack*, 1989). The dominating features include a large scale intermediate cyclonic flow of Atlantic Water (AW), an anticyclonic surface circulation in the Beaufort Gyre, and a transpolar drift of sea ice and surface waters across the Central Arctic Ocean from the Siberian region towards Greenland and the Fram Strait (Figure 2.1, *Rudels* (2015)). Relatively warm and saline AW enters the Arctic Ocean across the eastern parts of the GSR as several branches stemming from the North Atlantic Current extension of the Gulf Stream (Figure 2.3, *Hansen et al.* (2008); *Rudels* (2015); *Timmermans and Marshall* (2020)). The AW propagates further north through the Norwegian Sea as it is topographically steered into a western and eastern branch of the Norwegian Atlantic Current (*Orvik and Niiler*, 2002). North of the Lofoten area, the Norwegian Atlantic Current splits again, and the AW finally enters the Central Arctic Ocean through two distinct gateways: one branch enters through the eastern part of the deep ($\sim$ 2500 m) Fram Strait as the West Spitsbergen Current (*Fahrbach et al.*, 2001; *Schauer*, 2004), while the other branch flows into the Barents Sea and enters through the 600 m deep St. Anna Trough in the northern Kara Sea (*Ingvaldsen et al.*, 2002; *Schauer et al.*, 2002). The division of these two branches is further investigated in Paper I in this thesis, but earlier studies indicate that although they contribute with roughly equal amounts of AW volume, the northward heat transport is higher through the Barents Sea ($\sim$ 70 TW, *Smedsrud et al.* (2013)) than through the Fram Strait ($\sim$ 40 TW, *Schauer and Beszczynska-Möller* (2009)) relative to a zero degree reference temperature. Some of the AW recirculates in the Fram Strait or further upstream in the Norwegian Sea and never makes it to the Central Arctic Ocean (*Beszczynska-Möller et al.*, 2012; *Hattermann et al.*, 2016; *Orvik and Niiler*, 2002; *Schauer*, 2004). North of the Kara Sea the AW branches converge again (*Schauer et al.*, 2002) and form a geostrophic and topographically trapped boundary current named the

Arctic Circumpolar Boundary Current which flows around the Eurasian and Canadian Basins along the continental shelf break at intermediate (200–500 m) depth (*Aagaard and Carmack*, 1989). A portion of the AW diverges from the boundary current into the deep Central Arctic Ocean basins, and its various pathways have mainly been inferred from the spatial distribution of maximum AW temperature (*Timmermans and Marshall*, 2020) and satellite altimetry-derived dynamic ocean topography (*Morison et al.*, 2021). These methods suggest multiple cyclonic recirculation branches within the deep Eurasian and Makarov Basins (*Karcher*, 2003; *Polyakov*, 2005; *Woodgate*, 2013; *Woodgate et al.*, 2001) as originally schematized by *Rudels et al.* (1994). Although not of specific interest in this thesis, we note that mesoscale eddies play a very important role for redistributing AW mass and heat in the Arctic Ocean interior (*Hunkins*, 1974; *Meneghello et al.*, 2021; *Timmermans and Marshall*, 2020; *Zhao and Timmermans*, 2015).

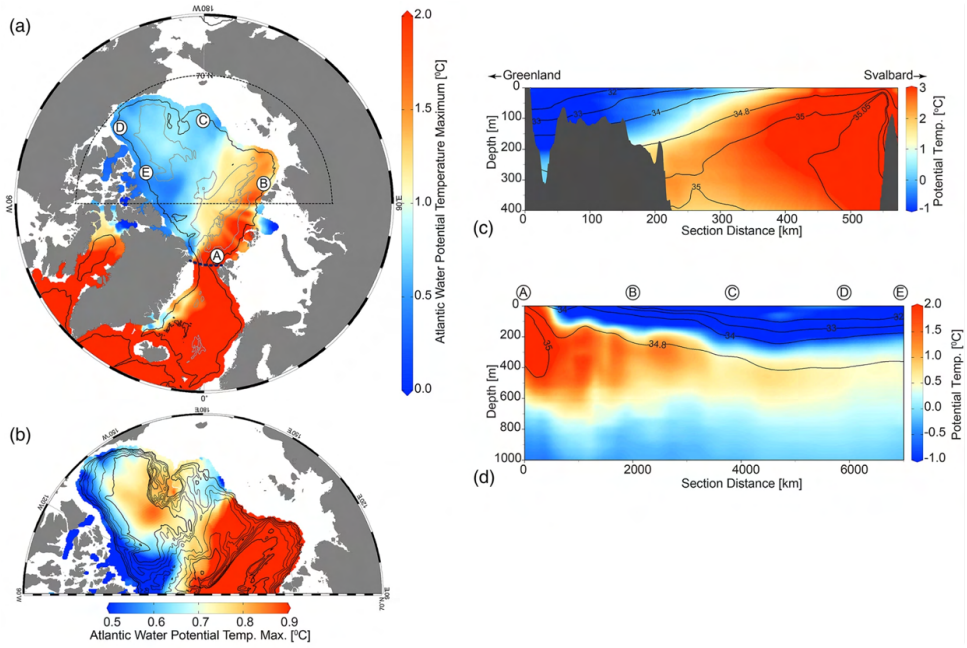

Figure 2.3: Atlantic Water potential temperature maximum for the a) Arctic Ocean and b) the sector bounded by the thin dotted black lines in a). In c), a section of potential temperature (color shading) and salinity (contours) across Fram Strait is shown; cooler, fresher water in the west flows south, while the warmer, saltier water to the east flows north. d) shows a section along the 1000 m isobath moving cyclonically around the Central Arctic Ocean with letters A–E corresponding to their locations marked in panel a). Figure and caption from Timmermans and Marshall (2020).

Below the AW layer, the deep Arctic Ocean circulation is, like the intermediate circulation, nearly barotropic and presumed to also follow cyclonic pathways in the Eurasian and Canadian Basins (*Jones*, 2001; *Rudels*, 2015). However, observations of the deep Arctic Ocean are incredibly sparse and there is high uncertainty related to the flow and properties of these deep water masses (*Morison et al.* (2021) and Section 2.1.3).

We will describe the forcing mechanisms driving the main Arctic circulation in further detail in Section 2.2.2, but note that typical ocean dynamics, such as Sverdrup balance, are not applicable in the Arctic Ocean (*Nøst and Isachsen*, 2003) since the north south gradient of the Coriolis parameter is very small, and there exists no meridional boundary along which a boundary current can form. The circulation is instead driven by a combination of buoyancy forcing related to a general freshwater input (*Lambert et al.*, 2016), heat loss to the atmosphere (*Smedsrud et al.*, 2021), and the larger scale wind patterns related to the dominating atmospheric circulation centers: the Icelandic Low and Beaufort High, introducing cyclonic and anticyclonic vorticity tendencies, respectively.

Observations of the AW inflow to the Arctic Ocean estimate a northward transport of 8.0 $\pm$ 0.7 Sv across the GSR (*Østerhus et al.*, 2019; *Tsubouchi et al.*, 2021). Two secondary inflows are relatively minor in terms of volume, but important in terms of Arctic Ocean hydrography (*Haine et al.*, 2015; *Woodgate et al.*, 2010). Approximately 0.8 Sv of Pacific Water enters the Arctic Ocean through the Bering Strait (*Woodgate et al.*, 2006) and approximately 0.1 Sv of freshwater enters as river runoff (*Carmack et al.*, 2016). The Pacific Water is mainly confined to circulate on the Canadian side of the Lomonosov Ridge below the Surface Mixed Layer (SML)(*MacKinnon et al.*, 2021; *Mclaughlin et al.*, 1996), whereas the river runoff remains near the surface before it finally is exported from the region mixed with other fresher upper Arctic Ocean waters (*Haine et al.*, 2015). The major outflows of the Central Arctic Ocean basins occur through the numerous straits in the Canadian Arctic Archipelago (*LeBlond*, 1980; *Münchow et al.*, 2006) and in the East Greenland current that flows south on the western side of the Fram Strait (e.g. *Aagaard and Coachman* (1968); *de Steur et al.* (2009); *Rudels* (1987)). Additionally, a large volume of freshwater is exported trough the Fram Strait in the form of sea ice (*Smedsrud et al.*, 2017). Eventually all these outflows enter the North Atlantic through the Davis Strait and Denmark Strait. Here, we generally divide the outflows into a shallow component consisting of cold and relatively fresh Polar Waters (PW), and dense Overflow Waters (OW) at depth (*Le Bras et al.* (2021), Figure 2.13). In summary, the Arctic Ocean is an active region for water mass transformation processes, including deep water formation, contributing to the global overturning circulation, and it acts like a double estuary, with AW as the main inflow and two outflows: cold and fresh PW at the surface and dense OW in the abyss (*Eldevik and Nilsen*, 2013; *Lambert et al.*, 2016).

2.1.3 Hydrography of the Arctic Ocean

The hydrography of the Arctic Ocean is characterized by a strong density stratification. Given the low temperatures, salinity dominates density, and much of the Arctic Ocean is therefore a so-called beta ocean (where beta refers to the saline contraction coefficient) - as opposed to alpha oceans in the subtropics where the upper layers are permanently stratified by temperature (*Carmack*, 2007; *Nansen*, 1902). In the Arctic Ocean the water column generally consists of three distinct layers: a relatively fresh and cold surface mixed layer on top, an intermediate layer between 200 m and 800 m of warmer and more saline Atlantic and Pacific waters, and a deep layer including various bottom waters below 800 m (Figure 2.4, *Rudels* (2015)). AW was already by *Nansen* (1902)

and *Helland-Hansen and Nansen* (1909) identified as the main heat source to the Arctic Ocean, and it is the warmest and most saline water mass found in the Arctic Ocean. In the Nordic Seas the AW is found near the surface, but after it reaches the sea ice and fresh surface layers in the Central Arctic Ocean the layer is only found at intermediate depths with a core of maximum temperatures at approximately 30–400 m (*Timmermans and Marshall*, 2020).

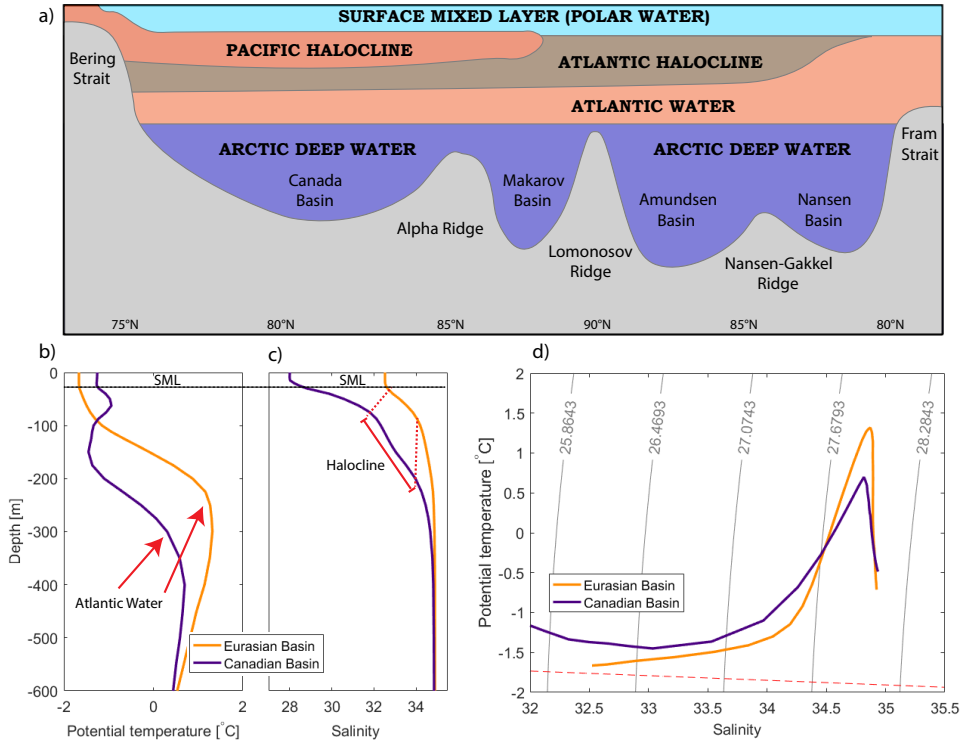

Figure 2.4: Simplified schematic illustration of the most important water masses and their vertical distribution along a section crossing the Central Arctic Ocean from Bering Strait to Fram Strait (a). For a more detailed division of water masses see Rudels (2015). Figure adapted from Goncalves-Araujo (2016) and Aagaard and Carmack (1989). Typical profiles of temperature (b) and salinity (c), and a temperature-salinity diagram (d) for the Eurasian and Canadian Basin from the MIMOC climatology (Schmidtko et al., 2013).

Specific to the the Central Arctic Ocean is a fourth layer in between the surface and intermediate layers, called the cold halocline (Figure 2.4). Here salinity increases rapidly with depth, whereas the low surface temperatures extend to the lower part of the halocline. The resulting salinity stratification is very strong and effectively decouples the surface layer from the warm intermediate layers below as mixing trough this barrier is difficult. The halocline is formed by the advection of cold shelf waters and local convection which are both a result from sea ice formation and brine rejection during winter (*Steele and Boyd*, 1998). In the Canadian Basin it is also influenced by the Bering Strait inflows of cold Pacific Water during winter and warm Pacific Water during summer (*MacKinnon et al.*, 2021; *Rudels*, 2015; *Steele*, 2004; *Woodgate et al.*, 2010).

Overall, the halocline plays an essential role in the Arctic climate system, as it caps the AW and limits its heat fluxes to reach the sea ice cover (*Aagaard et al.*, 1981). How the Arctic Ocean stratification and halocline properties will change in a warming climate is still an open question, which we address in Paper IV of this thesis.

Relevant to the question of stratification and halocline properties is the flux of freshwater into the cold surface mixed layer. The Central Arctic Ocean is an important storage and source of freshwater to the North Atlantic (*Haine et al.*, 2015; *Solomon et al.*, 2020). It receives its freshwater (0.3 Sv in total) from river runoff (0.13 Sv), net precipitation (0.07 Sv), meltwater from Greenland (0.01 Sv) and inflow of relatively fresh Pacific Water (0.08 Sv, *Haine et al.* (2015)). The river runoff constitutes 10% of the global river runoff, while the Arctic Ocean only constitutes 1% of the global ocean volume (*Aagaard and Carmack*, 1989), and this comes predominately from the 6 largest Arctic rivers (Ob, Yenisey, Lena, Kolyma, Yukon, and Mackenzie; *Holmes et al.* (2012)). As described in Chapter 2.1.1 the freshwater leaves the Central Arctic Ocean mainly as liquid freshwater (75%) through the East Greenland Current and the Canadian Arctic Archipelago. Also the Nordic Seas receive a large amount of freshwater in the form of precipitation (0.012 Sv), runoff from Greenland (0.005 Sv), runoff from Scandinavia (0.012 Sv) and sea ice melt (0.071 Sv; *Le Bras et al.* (2021)). Sea ice acts as sink of freshwater from the Central Arctic Ocean, since 25% is exported as sea ice through the Fram Strait, but acts as a source of freshwater to the Nordic Seas as it melts here. In *Le Bras et al.* (2021) we show that approximately half of the Arctic freshwater volume is exported out of the region at the surface (the estuarine part), and that the other half participates in the overturning limb of the circulation creating overflow water. As the freshwater contributes to the strong density stratification in the surface it is of high interest how the freshwater fluxes might change in the future. For example, projections of a warming global climate suggest a spin up of the hydrological cycle (*Held and Soden*, 2006) and hence increased runoff (*Lehner et al.*, 2012; *Nummelin et al.*, 2015; *Wang et al.*, 2021). Several studies have observed an increase in Arctic freshwater content (e.g. *Haine* (2020); *Proshutinsky et al.* (2019); *Rabe et al.* (2014)), but in the 2010s the trend has somewhat stabilized relative to the 2000s (*Solomon et al.*, 2020). Model studies performed by *Nummelin et al.* (2015) indicate that increased runoff will result in a strengthened Arctic Ocean stratification, but it is yet unclear how these mechanisms are effected by for example increased AW heat transport and ongoing "Atlantification" processes (Section 2.2.1). The future changes in freshwater pathways will also be investigated in Paper IV of this thesis.

The depth to which the SML extends, before it transitions into a halocline, is also an important characteristic of the Arctic Ocean. Again, this varies a lot between the Nordic Seas where deep convection occurs and in the Central Arctic Ocean where deep convection is is unlikely to happen. However, in both regions it varies a lot seasonally, and the mixed layer acts as a medium for seasonal storage of heat and receives most of the momentum from the atmopshere above (*Rudels*, 2015). Whereas there is a general upwelling over the Nordic Seas, the Central Arctic Ocean generally experiences an Ekman downwelling due to the anticyclonic winds here. This downwelling helps deepen the surface mixed layer and hence also the halocline, especially in the Beaufort Gyre (*Timmermans and Marshall*, 2020). As a result the halocline resides at approximately 250 m in the Canadian Basin and at 80 m in the Eurasian Basin (*Polyakov et al.*, 2020). Besides the wind forcing, the SML depth is also determined by the growth and melt of

sea ice (*Lemke and Manley*, 1984; *Steele et al.*, 1989) and affected by tides (*Fer et al.*, 2015, 2020).

Although not particularly investigated in this thesis we acknowledge the existence and importance of Pacific Water and Deep Water in the Arctic Ocean. In the Canadian Basin the Pacific Water resides at intermediate depth in-between the AW and the halocline, hereby strengthening the stratification even further (*MacKinnon et al.*, 2021; *McLaughlin et al.*, 2004). It experiences large seasonal variations (*Woodgate et al.*, 2005), and has a large local impact on the sea ice cover in the Canadian Basin (*MacKinnon et al.*, 2021; *Woodgate et al.*, 2012). The deep waters residing in the Central Arctic Ocean are relatively uniform in temperature and salinity, with some differences between the Euarasian and Canadian Basins (*Aagaard et al.*, 1981, 1985; *Schauer et al.*, 2002). Most of these deep water masses are assumed to be of Atlantic origin (*Anderson et al.*, 1994), but some of the densest water masses likely originate from shelf slope plumes, which develop through cooling and rejection of salt during sea-ice growth (*Arthun et al.*, 2011; *Meincke et al.*, 1997). Due to the geographic constraints much of the deep water in the Canadian and Eurasian Basins is confined there. Some of the dense and deep waters produced in the Nordic Seas, however, overflow the western sills of the GSR and contribute to the the important overturning circulation (*Brakstad et al.*, 2019; *Håvik et al.*, 2019; *Le Bras et al.*, 2021; *Semper et al.*, 2020; *Swift and Aagaard*, 1981). We investigate the overflow waters and water mass transformation processes in detail in *Le Bras et al.* (2021) and *Smedsrud et al.* (2021), but this is not included in this thesis.

While the importance of AW to the Arctic climate system has been known for more than 120 years (*Helland-Hansen and Nansen*, 1909; *Nansen*, 1902), much of the variability and the mechanisms governing this variability are still unclear. In the following chapter we summarize some recent science regarding AW variability and trends.

2.2 Atlantic Water inflows to the Arctic Ocean

2.2.1 Observed long-term variability and trends

On various timescales, the AW flow has been subject to variations in volume transport, temperature and salinity – all major drivers of high latitude climate variability. Given its important role in the Arctic climate system, there are numerous studies investigating the AW inflow and its properties over time, unfortunately too many to all mention here. One of the longest continuous temperature records in our domain is the Kola section in the Barents Sea. Here AW temperature has been measured in the upper 200 m since 1850. These records show large interannual variations (Figure 2.5), a strong warming trend in recent decades, an early warm period in the 1940s, and two cooler periods in the early 1900s and in the 1960s-70s. Snapshots of similar variability have been observed both upstream and downstream of the Kola Section (see summary by *Yashayaev and Seidov* (2015)), and show existence of multidecadal variations. For example, an early warm period was also documented in the AW layer in the Central Arctic Ocean by *Polyakov* (2005); *Polyakov et al.* (2004, 2009), who also suggested it might be part of a long term multidecadal oscillation. These low frequency variations in AW temperature agree well with the Atlantic Multidecadal Oscillation (AMO) in-

dex of *Sutton and Hodson* (2005), representing the large-scale sea surface temperature variation throughout the North Atlantic Ocean.

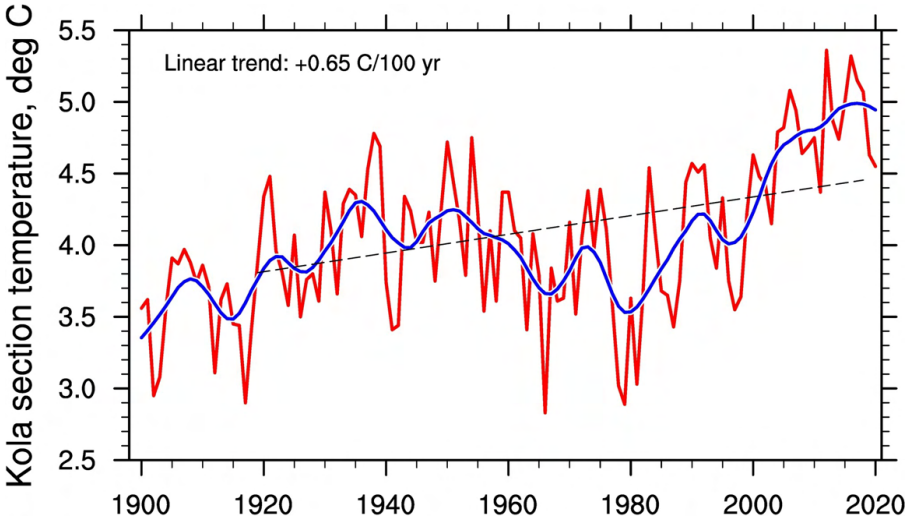

Figure 2.5: Observed Atlantic Water temperature over the upper 200 m of the water column along the Kola section in the Barents Sea. Temperature data from The Nikolai M. Knipovich Polar Research Institute of Marine Fisheries and Oceanography (PINRO) and ICES (https://ocean.ices.dk/core/iroc. Figure courtesy: Helge Drange (https://folk.uib.no/ngfhd/Climate/climate.html).)

The mechanisms behind the early twentieth century warming in the Arctic have been discussed in many papers (see review by *Yamanouchi* (2011)), as has the origin of the AMO (e.g. *Chylek et al.* (2009, 2010); *Drinkwater et al.* (2014); *Otterå et al.* (2010)). Overall, the Arctic temperature variability (in both ocean and atmosphere) has been attibuted to a combination of external forcing and internannual variability (*Day et al.*, 2012; *Delworth and Dixon*, 2000; *Kay et al.*, 2011; *Zhang*, 2015) but their relative importance remains unclear. For example, in *Svendsen et al.* (2021) we show that there are important contributions from the Pacific Ocean to the decadal surface temperature trends and the early twentieth century warming in the Arctic (see also *Svendsen et al.* (2018)). Other recent studies, on the other hand, argue that there is no evidence for an internally generated multidecadal AMO, and that it is all an artifact of pulses of volcanic activity during the preindustrial era (*Mann et al.*, 2021). Whether the early twentieth century warming is part of a large scale climate oscillation or not remains unclear. However, we do know that temperature variations in the AW are a result of atmospheric forcing locally in the Nordic Seas (*Asbjørnsen et al.*, 2019; *Carton et al.*, 2011; *Mork et al.*, 2014), and atmospheric forcing remotely, resulting in advected temperature anomalies into the region (*Asbjørnsen et al.*, 2019; *Ingvaldsen et al.*, 2002). These advected anomalies are clearly shown in both observations (*Chepurin and Carton*, 2012; *Furevik*, 2000; *Helland-Hansen and Nansen*, 1909; *Holliday et al.*, 2008; *Sutton and Allen*, 1997) and models (*Årthun and Eldevik*, 2016; *Asbjørnsen et al.*, 2019; *Krahmann et al.*, 2001; *Langehaug et al.*, 2019). The contributions of local and remote atmospheric forcing may be difficult to separate, but we dive deeper into some of the

mechanisms related to the early AW warming and temperature variability in Paper I in this thesis.

Just like temperature, there have been observed large interannual variations in AW salinity (*Yashayaev and Seidov*, 2015). Salinity largely increases and decreases in parallel with temperature (*Carton et al.*, 2011), but some large salinity anomalies appear to be disconnected from the temperature changes. The largest observed salinity anomaly was a freshening episode from 1975 to 1982 (*Dickson et al.*, 1988), which has been traced throughout the whole North Atlantic and Arctic Ocean, and subsequently named the "Great Salinity Anomaly" (GSA). Three post-GSA low-salinity events, two of which were particularly strong, occurred between 1985 and 2005 (*Carton et al.*, 2011; *Yashayaev and Seidov*, 2015). We will not discuss the origin of AW salinity anomalies further here as the main focus of this thesis is related to AW heat. However, we note that there is limited local influence on AW salinity (as opposed to SML salinity) and that most salinity anomalies appear to be advected in from the North Atlantic (*Carton et al.*, 2011; *Glessmer et al.*, 2014; *Yashayaev and Seidov*, 2015).

The AW volume transport across the GSR also varies (Paper I in this thesis and *Smedsrud et al.* (2021)), but unfortunately observations of current velocities are more sparse than temperature and salinity observations. At the Svinøy section, near the AW inflow to the Nordic Seas, the instrumental record of ocean currents dates back to 1995 (*Orvik et al.*, 2001), whereas the Barents Sea Opening and the Fram Strait were monitored continuously since 1997 (*Beszczynska-Möller et al.*, 2012; *Fahrbach et al.*, 2001; *Ingvaldsen*, 2004). These records show variations on the order of 1–2 Sv from year to year, but they are too short to reveal possible decadal changes. Variations in AW volume are dominant over temperature in terms of regulating the northward heat transport (Paper I in this thesis and *Asbjørnsen et al.* (2019)), but determining the dominant mechanisms on regulating the volume transport remains an ongoing discussion. We give an overview over these various mechanisms in Section 2.2.2.

Recent trends

Over the past decades, the AW layer in the Nordic Seas and Central Arctic Ocean has warmed dramatically (Paper I in this thesis, *Asbjørnsen et al.* (2020); *Lind et al.* (2018); *Skagseth et al.* (2020); *Tsubouchi et al.* (2021)). Early signs of this warming in the central Arctic Ocean were documented by *Schauer* (1997), *Schauer et al.* (2002), and *Rudels et al.* (2000). In 2012, however, *Polyakov et al.* (2012) showed, using unique historical data (Chapter 3.2.3), that the warming of the AW layer had already begun in the 1970s. This Central Arctic Ocean Warming is in agreement with measurements taken annually further upstream in the West Spitsbergen Current that show an overall warming in the AW core of 1.1 $^{\circ}C$ since 1979 (*Eldevik et al.*, 2021; *Muilwijk*, 2016). Since interannual variabilty is pronounced, the general warming trend is observed as warm "pulses", with cold years in between (*Dmitrenko et al.*, 2008; *Polyakov et al.*, 2010). In more recent years the AW temperature and volume transport have continued to increase (*Lind et al.*, 2018; *Polyakov et al.*, 2017; *Smedsrud et al.*, 2021), resulting in a systematic change often dubbed the "Atlantification" of the Northern Barents Sea and Eurasian Basin (*Årthun et al.*, 2012; *Reigstad et al.*, 2002; *Wassmann et al.*, 2004). The concept of Atlantification is generally understood as an Arctic-ward expansion of the "Atlantic domain" - a regional transition from typical Central Arctic like condi-

tions (with Central Arctic Ocean ecosystems and a thick seasonal ice cover) towards more Nordic Seas like conditions (with typical North Atlantic ecosystems, warmer AW closer to the surface and open water conditions throughout the year, Figure 2.6). From a hydrographic perspective, Atlantification has been characterised by warm AW extending further poleward and/or occupying a larger part of the water column (Figure 2.6 and 2.10). Both these processes result in a warming and salinification of the upper ocean, and hence a weaker stratification and enhanced AW heat fluxes further northeast along the AW pathways. Recently it has been inferred that the Atlantification has reached as far into the Central Arctic Ocean as the Laptev Sea region (*Polyakov et al.*, 2017, 2020). Despite a general salinification of the Eurasian Basin, the AW inflow does not have a very clear trend in salinity in the Fram Strait (*MOSJ*, 2021), nor at the GSR (*González-Pola et al.*, 2018).

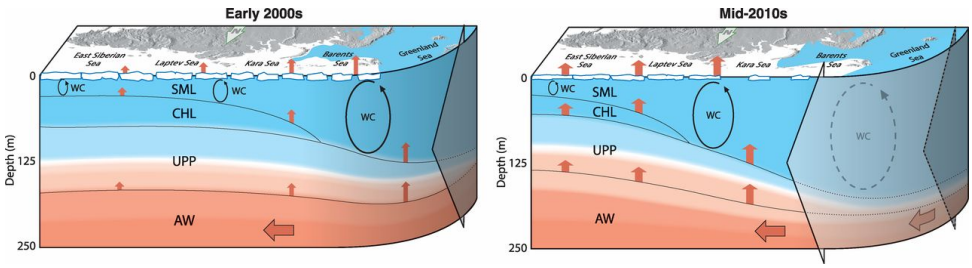

Figure 2.6: Schematic illustration of the ongoing "Atlantification" of the Eastern European Basin. Processes associated with Atlantification are marked: increased flow of Atlantic Water (AW) or increased heat content, reduction of sea ice cover, increased surface heat fluxes (red arrows) and increased depth of winter convection (WC). CHL indicates the cold halocline layer, SML indicates the surface mixed layer and UPP indicates the upper permanent pycnocline. Figure and figure caption from Polyakov et al. (2017).

Parallel to the ongoing Atlantification, there has been observed an anomalous strong advection of warm and fresh Pacific Water through the Bering Strait, resulting in a recent change in the Canadian Basin we refer to as "Pacification" (*Polyakov et al.*, 2020). These joint effects of Atlantification and Pacification are referred to as a "Borelazation" (a shift in the northward range and associated ecosystem change) of the Arctic Ocean, which includes changes in both the physical, geochemical, and biological environments. The recent changes in the Arctic- Atlantic region are likely linked to anthropogenic induced global warming, but to the extent multidecadal variations are present, then it is also possible that the recent warming trend is a combination of both global warming and internal variability. A scientific demanding and societal important question is therefore what will happen in the next fifty years: will global warming completely dominate the trends or is there internal multidecdal variability (e.g. *Mann et al.* (2021); *Otterå et al.* (2010); *Svendsen et al.* (2018)) which will temporarily dampen – or amplify – the warming signal? The results from Paper I in this thesis are relevant for this discussion, as we study the effect of multidecadal variations in our region. Nonetheless, since current climate model simulations project the AW heat transport to continue to increase with future global warming (*Årthun et al.*, 2019; *Auclair and Tremblay*, 2018; *van der Linden et al.*, 2019), we may expect a continued Borelazation of the Arctic Ocean, with possible severe impacts on future Arctic Ocean ecosystems,

sea ice (Chapter 2.3.1), marine terminating glaciers (Chapter 2.3.2) and water mass transformation (Chapter 2.3.3).

2.2.2 Mechanisms

From the previous sections it is documented that the AW inflow is of great relevance to the Arctic climate and that it is subject to both natural variations and anthropogenically induced trends. But what drives the AW flow and what impacts the volume transport variations? The atmosphere is instrumental in driving the circulation, but its impact can been divided into two distinctly different types of forcing; a wind and a buoyancy driven forcing (*Smedsrud et al.*, 2021). It may be viewed as a tug of wars between a "push" and a "pull" mechanism. Both are important, but their relatively importance is still not well understood (*Timmermans and Marshall*, 2020), and likely varies depending on the timescale of interest. A further complication is that the two forcing mechanisms are coupled through e.g. cold-air advection. Here we briefly describe the major mechanisms driving the AW flow (see also review by *Timmermans and Marshall* (2020)).

Pull: an estuary perspective

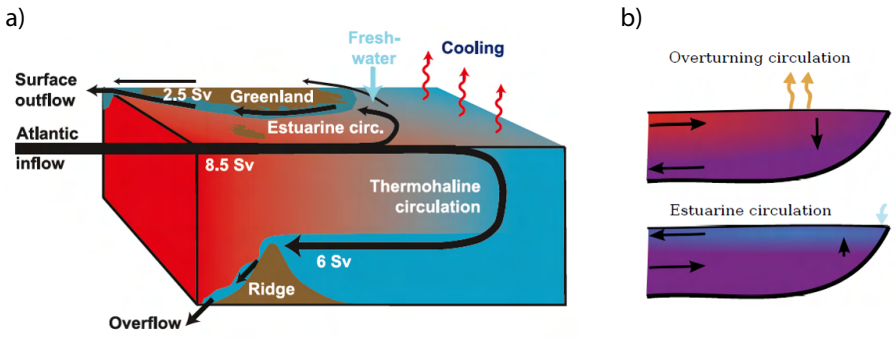

Figure 2.7: The "pull" mechanism - a double estuary perspective. a) Schematic illustration of two circulation systems which are proposed to drive the northward (and southward) flow of Atlantic Water. A freshwater driven estuary circulation and a buoyancy (cooling) driven thermohaline circulation. Figure from (Hansen et al., 2008). b) Same as a) but divided in two separate parts. Figure courtesy: Erwin Lambert.

Aagaard et al. (1985) was the first to describe the Arctic Ocean circulation based on a freshwater/buoyancy driven, estuary like circulation. This framework is built on the idea that warm inflow into the Nordic Seas is simply balanced by an outflow of (relatively) fresh PW, and that upper ocean mixing in the Central Arctic Ocean is what sets the exchange fluxes. Later on this framework was extended by considering the circulation as a so-called double estuary (Figure 2.7, *Eldevik and Nilsen* (2013); *Lambert et al.* (2016)). The freshwater input in the Central Arctic Ocean is one part of the double estuary, which results in a positive buoyancy forcing (the positive estuary). The other part is a negative buoyancy forcing in the Nordic Seas as the atmosphere cools and densifies the AW as it progresses northward on the eastern side of the boundary current system

(*Eldevik et al.*, 2009; *Mauritzen*, 1996). The heat loss in the Nordic Seas drives an overturning circulation, whereas the freshwater input drives and estuarine circulation. Both of these mechanisms, however, act as a "pull" mechanism on the AW flow across the GSR. *Lambert et al.* (2016) even found that the AW inflow can persist even in the absence of deep convection and overturning in the Nordic Seas. This is important because the link between the northward flow of AW and the Atlantic Meridional Overturning Circulation (AMOC) is a hot topic. A similar combination of these buoyancy driven mechanisms were presented by (*Spall*, 2013), who made a simple conceptual model of the Arctic Ocean circulation. He noted that horizontal eddy fluxes and vertical mixing in the Central Arctic Ocean have an important effect on the AW inflow as well. Based on these frameworks, variations in freshwater input, atmospheric cooling and mixing in the Arctic might affect AW inflow variation. Recent studies indicate that these processes are perhaps equally important as the wind driven circulation described below (*Smedsrud et al.*, 2021; *Timmermans and Marshall*, 2020). Also, this is inherently a "chicken or egg" discussion, as most of the processes described above are dependent on wind forcing.

Push: a wind driven flow

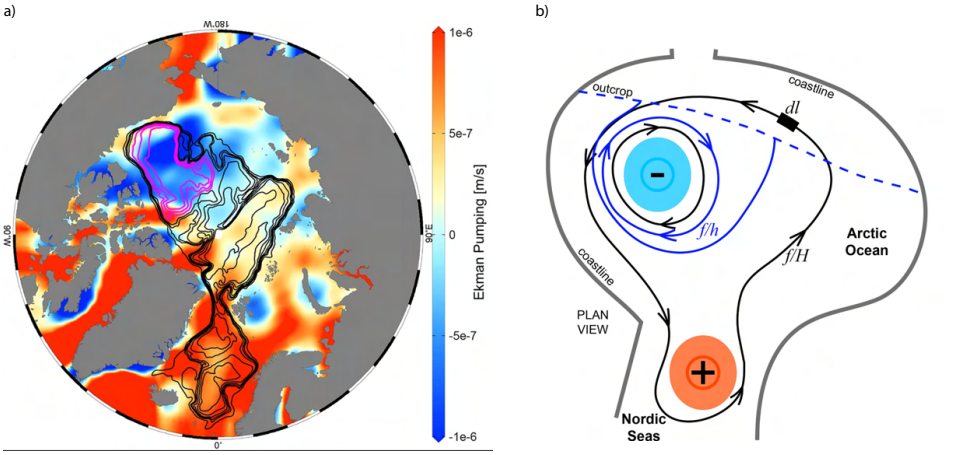

Figure 2.8: The "push" mechanism - a wind driven flow. a) Annual average Ekman pumping (color shading, 2005-2017) and a selection of closed f/H contours which the barotropic flow follows (Nøst and Isachsen, 2003). Black contours enclose an area for which the area integral of windstress curl is positive and magenta where the integral is negative. Figure from Timmermans and Marshall (2020). b) Schematic showing the winddriven circulation. f/H contours are shown in black with the direction of circulation along the contour governed by the sign of the windstress curl. Figure and figure caption adapted from Timmermans and Marshall (2020).

The "push" mechanism describes the mean cyclonic flow, as well as the variability, in the Arctic Ocean to be mainly driven by wind stress (*Morison et al.*, 2021; *Nøst and Isachsen*, 2003; *Timmermans and Marshall*, 2020). Since the Coriolis parameter is so small, Sverdrup Balance effect has limited effect, and *Nøst and Isachsen* (2003) hence showed that the barotropic flow in the Arctic Ocean is mainly controlled by bathymetry. They describe that in the Arctic Ocean potential vorticty contours (f/H) coincide with

the isobaths, and therefore the vorticity-conserving barotropic flow (following f/H contours) is directed to follow the bathymetric contours (Figure 2.8). The forcing is set by the wind stress curl integrated over the area within the f/H contours in question. In the Arctic Ocean this curl consists of a strong cyclonic forcing in the Nordic Seas related to the northern mode of the North Atlantic Oscillation (the Icelandic Low) and a somewhat weaker anticyclonic forcing in the Canadian Basin related to the Beaufort High. Since the cyclonic wind stress dominates, the circulation is cyclonic throughout the whole Arctic Ocean, and technically the cyclonic flow around the Eurasian and Canadian basins is driven by the wind forcing further south in the Nordic Seas.

The effect of the wind stress curl in the Nordic Seas and the Icelandic low on northward AW heat transport has been further investigated in Paper I and Paper II in this thesis. However, it has already been suggested by *Nilsen et al.* (2003) and by *Bringedal et al.* (2018) that the wind forcing influences the short term variability across the GSR, and *Dickson et al.* (2000) related the strength of the AW flow on longer time scales to an increasingly positive phase of the NAO (stronger Icelandic Low). Also simulations of future climate by *Årthun et al.* (2019) indicate that a possible increased northward flow of AW would be connected to a deepening of the Icelandic Low. However, the connectivity of the various processes and the mechanisms of future Arctic ocean circulation are not yet fully understood (*Timmermans and Marshall*, 2020). We show in *Smedsrud et al.* (2021) that heat loss and wind forcing combined drive the variability of the flow, but again the two mechanisms might be interconnected on the different timescales. Some studies suggest that the AMOC influences Arctic surface temperatures and sea ice on decadal timescales, because a stronger AMOC is associated with a strong AW flow (*Delworth and Zeng*, 2016; *Yeager et al.*, 2015; *Zhang*, 2015). However, the AMOC is projected to weaken and the AW inflow is projected to increase (*Årthun et al.*, 2019; *Nummelin et al.*, 2017). This is just an example that the relationships between various mechanisms are complex and not completely clear. It is likely that both internal and external variations are important (*Årthun et al.*, 2019; *Oldenburg et al.*, 2018) and the dynamics of the flow could therefor change with a changing climate (*Smedsrud et al.*, 2021).

2.3 Impacts and relevance of Atlantic Water in the Arctic Ocean

2.3.1 Impacts on sea ice

Throughout winter most of the Central Arctic Ocean is covered by sea ice characterized by an average thickness of around 2 m (*Kwok*, 2018). The sea ice cover has a large seasonal cycle, with summer extent in recent years generally around one third of the winter extent, and also experiences large inter-annual variations(*Notz*, 2017). Since satellite observations began in 1979, we have observed a decline in the total area covered by sea ice in each month of the year (*Comiso et al.*, 2017; *Stroeve and Notz*, 2018). Changes in sea ice extent are generally larger in summer (-12.8 % per decade ± 2.3 % relative to 1981–2010 mean) than in winter (-2.7% per decade ± 0.5% relative to 1981–2010 mean, *Onarheim et al.* (2018)), and accompanied by a general thinning as well (*Chevallier et al.*, 2017; *Kwok*, 2018; *Laxon et al.*, 2013; *Renner et al.*, 2014).

Both the variations and trends in Arctic sea ice extent and thickness are mainly linked to direct atmospheric forcing (e.g. *Olonscheck et al.* (2019); *Stroeve and Notz* (2018)). For example, approximately 50% of the observed Arctic summer sea ice loss is driven by higher Arctic surface temperatures due to increasing atmospheric greenhouse gas concentrations (e.g. *IPCC et al.* (2019); *Notz and Marotzke* (2012); *Notz and Stroeve* (2016)), which is amplified by processes such as the sea ice albedo feedback (*Pistone et al.*, 2019), radiative feedbacks related to clouds (*Morrison et al.*, 2018), and moist air intrusions (*Woods and Caballero*, 2016), just to mention a few.

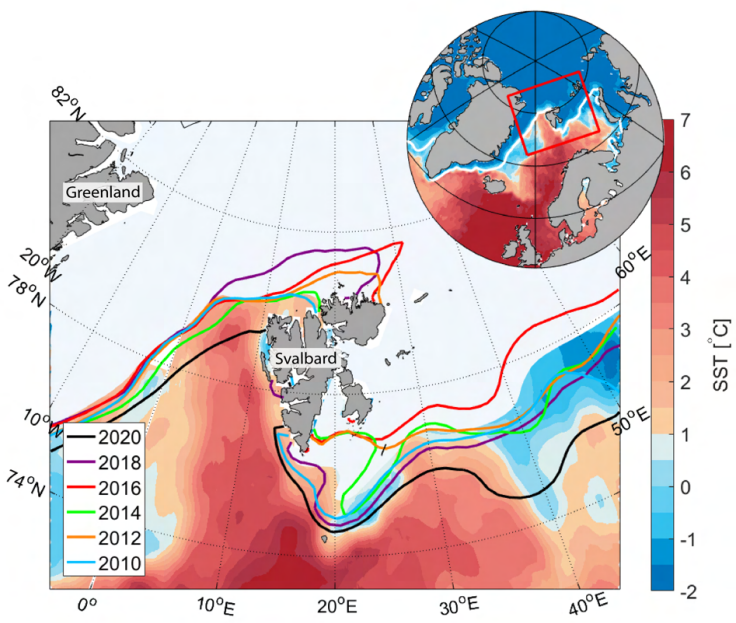

Figure 2.9: Atlantic Water heat influences the sea ice edge location north of Svalbard. Mean winter sea ice extent for 5 years between 2010 and 2020 are shown as contours. The temperature distribution is illustrated by satellite sea surface temperature (SST; colour shading) and the ice extent (white; the limit of 15% ice concentration) for April 2015.

In some regions, however, the ocean plays an important (and even dominant) role in regulating the sea ice extent, and this influence is likely to increase (*Carmack et al.*, 2015). In their early work, *Helland-Hansen and Nansen* (1909) noted that varying inflow of AW influences the seasonal sea ice cover by determining the amount of winter freezing near the AW inflow region. Indeed, the Barents Sea and Svalbard region is the hotspot of winter sea ice variability and retreat (*Onarheim et al.*, 2018), with prominent changes along the AW inflow path and into the Nansen Basin (*Duarte et al.*, 2020; *Onarheim and Årthun*, 2017; *Onarheim et al.*, 2014; *Rudels*, 2016). Here, multiple studies have shown that the position of the sea ice edge (Figure 2.9) can be directly linked to variations in the inflow of AW (*Årthun et al.*, 2012, 2017; *Duarte et al.*, 2020; *Ivanov et al.*, 2016, 2012; *Koenigk and Brodeau*, 2017; *Lien et al.*, 2017; *Onarheim and Årthun*, 2017; *Onarheim et al.*, 2015; *Sandø et al.*, 2014), something we also show and

investigate in paper II in this thesis. Furthermore, in *Eldevik et al.* (2021) we present a simple analytical model which describes how winter sea ice extent variability and trend north of Svalbard are explained by a tug-of-war between wind driven drift pushing sea ice southward and the AW pushing ice-free conditions northward. This is consistent with other recent studies that show that the sea ice in this region is mainly controlled by a combination of AW heat variations and large scale ice-drift (*Lundesgaard et al.*, 2021).

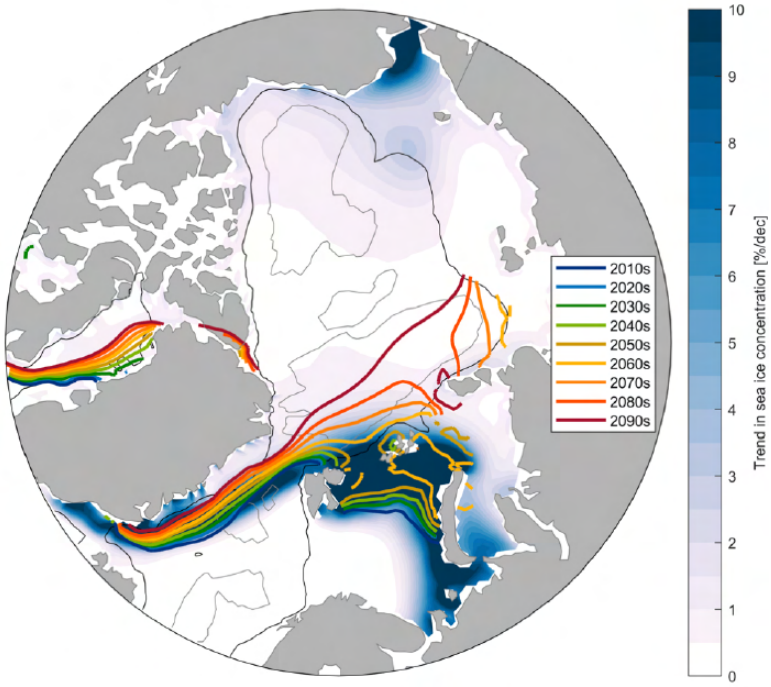

Figure 2.10: The ongoing and projected future expansion of the Atlantic domain "Atlantification" into the Arctic represented by the 0 °C isotherm at 100 m depth as projected by the CESM large ensemble simulation (RCP8.5 scenario). Color shading shows the decadal trends in sea ice concentration, illustrating the likely growing impact of Atlantic Water on sea ice in the inflow regions. Figure courtesy: Marius Årthun.

Further north into the Central Arctic the exchange of heat from AW to the sea ice above is generally suppressed because of the strong stratification (*Carmack et al.*, 2015; *Lind et al.*, 2016; *Padman and Dillon*, 1987), but polynyas occasionally mirror the AW pathways (*Ivanov et al.*, 2016), and increased upward mixing of heat as a result from wind forcing may result in direct bottom melting of sea ice as observed during the N-ICE2015 campaign by (*Koenig et al.*, 2016; *Muilwijk*, 2016; *Peterson et al.*, 2017; *Provost et al.*, 2017), and simulated by (*Sandø et al.*, 2014). In addition, as the sea ice becomes thinner and more mobile, it facilitates the creation of more open-water areas and leads. This may lead to another positive feedback, since more open water may result in the increased input of momentum from wind, which results in

more turbulent mixing, which again could assist in bringing more AW heat upward (*Peterson et al.*, 2017). With continuously increasing AW heat transport and projected future continuation of the ongoing Atlantification processes (*Årthun et al.*, 2019), the processes described above might become even more dominant (Figure 2.10), and we might be transitioning towards a new Arctic climate state, with a substantially greater role for Atlantic inflow (*Polyakov et al.*, 2017). A key question is what will happen in the future when the Fram Strait and Barents Sea AW branches eventually meet in winter open water area north of Franz Josef Land. Will the domain of where the AW inflow regulates the sea ice edge location simply increase in size?

2.3.2 Impact on marine terminating glaciers

Similarly to the Arctic sea ice cover, the Greenland ice sheet is loosing mass in response to global warming (*IPCC et al.*, 2019; *Mouginot et al.*, 2019; *Shepherd et al.*, 2020). The loss of ice mass is generally due to two processes: 1) anomalous surface melting in congruent with increased air temperatures, and 2) increased ice discharge resulted from the speed up, thinning and retreat of multiple marine-terminating glaciers (*Mouginot et al.*, 2019). The mechanisms and forcings behind the increased ice discharge are complex (*Straneo et al.*, 2013), but multiple studies have recently attributed the retreat and acceleration of these glaciers to increased oceanic forcing (*Holland et al.*, 2008; *Rignot et al.*, 2012; *Seale et al.*, 2011; *Straneo et al.*, 2013; *Wood et al.*, 2018, 2021). Numerous marine-terminating glaciers are in contact with the ocean in narrow fjords that connect to the continental shelf (*Straneo et al.*, 2012). In two comprehensive reviews, *Straneo et al.* (2013) and *Straneo and Cenedese* (2015) explain how the variability and trends in subsurface AW drive this retreat through submarine melting of the ice fronts and icebergs (Figure 2.11a). For example, in northeast Greenland, AW variability is understood to control the melting of Greenlands largest remaining ice shelf at 79 °N (*Lindeman et al.*, 2020; *Schaffer et al.*, 2020; *Wilson and Straneo*, 2015). Also along the western coast of Greenland, *Holland et al.* (2008) and *Wood et al.* (2018) show that anomalous ocean temperatures trigger glacier retreat. Recent results from the NASA project Oceans Melting Greenland (OMG) compare the degree of oceanic influence for glaciers all across the coast of Greenland (*Wood et al.*, 2021).

Slater et al. (2019) developed a parameterization relating the glacier terminus position to the ocean temperature on the continental shelf, the subglacial discharge and surface melt. In *Smedsrud et al.* (2021) we used this parameterization to quantify the impact of AW variability on the glaciers of northeast Greenland throughout the twentieth and the beginning of the twenty-first century (Figure 2.11b). These results show that over the past 120 years, the AW variability alone explains a significant proportion of the advance and retreat of marine terminating glaciers. As AW has an important role for forcing the glaciers, it also triggers an important feedback mechanism where the glaciers force the ocean. Enhanced subglacial melting results in an increased flux of freshwater into the ocean, which in turn contributes to global sea-level rise, and has the potential to affect the regional and large-scale ocean circulation, including the AMOC (*Bamber et al.*, 2012, 2018; *Böning et al.*, 2016; *Caesar et al.*, 2021; *Frajka-Williams et al.*, 2016; *Gillard et al.*, 2016; *Le Bras et al.*, 2021; *Shepherd et al.*, 2020). In paper III in this thesis we investigate this freshwater flux, and the indirect effect of AW

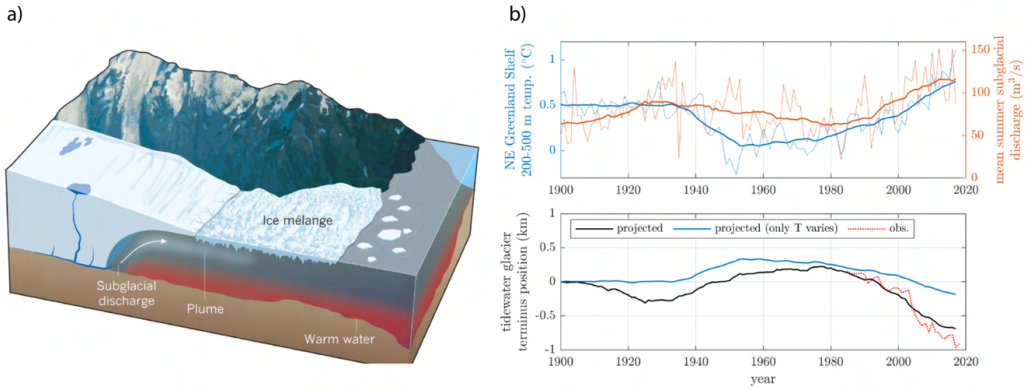

Figure 2.11: a) Illustration of warm subsurface Atlantic Water entering glacial fjords and reaching the front of marine terminating glaciers where it induces submarine melt. Figure from Straneo et al. (2013). b) Top panel: Simulated AW temperature averaged over the NE Greenland continental shelf (left axis) and simulated summer subglacial discharge from NE Greenland's marine-terminating glaciers (right axis). Lower panel: Simulated advance and retreat of NE Greenland's marine-terminating glaciers. The projected terminus position (black) is based on the parameterization described by Slater et al. (2019) using the ocean temperature and subglacial discharge shown in the top panel. The blue line shows the projected terminus position when subglacial discharge is held constant, and thus isolates the impact of the ocean on the glaciers. The red dashed line shows the observed terminus positions (Slater et al., 2019). Figure from Smedsrud et al. (2021).

induced glacial melting, for a large fjord system in northwest Greenland.

2.3.3 Relevance for water mass transformation and global ocean circulation

The AW inflow to the Arctic Ocean does not only affect climate locally. Its variability and interaction with the atmosphere influences the various water mass transformation processes that occur here, which in turn influence the ocean circulation in the North Atlantic further south (*Chafik and Rossby*, 2019; *Heuzé*, 2017; *Lozier et al.*, 2019). The AW undergoes a variety of transformations before a large part eventually flows south again across the western parts of the GSR as dense OW (Section 2.1.3). The most important transformation is that the AW looses most of its heat to the cold atmosphere, particularly in the Nordic Seas (Figure 2.12, *Smedsrud et al.* (2021)). As a consequence, the AW becomes denser, and the heat loss is thus the primary driver for forming dense water masses which fill the deep North Atlantic (*Chafik and Rossby* (2019); *Gebbie and Huybers* (2011); *Smedsrud et al.* (2021), Figure 2.13). Most of this dense water formation occurs in the Nordic Seas, with recent studies naming the Greenland Sea as an important region *Huang et al.* (2020); *Våge et al.* (2015). Previously this dense water formation occurred mainly trough the process of deep convection (*Helland-Hansen and Nansen*, 1909), but in recent decades only convection to intermediate depths has been observed (*Brakstad et al.*, 2019; *Karstensen et al.*, 2005; *Latarius and Quadfasel*, 2016; *Lauvset et al.*, 2018). Recent changes in dense water formation have been attributed to: 1) changes in sea ice cover in the Greenland Sea (*Visbeck et al.*,

1995), which can be partly linked to AW heat (*Chatterjee et al.*, 2021), 2) anomalous wind forcing (*Meincke et al.*, 1992), and 3) salinity anomalies advected northward with the AW (*Brakstad et al.*, 2019; *Glessmer et al.*, 2014; *Lauvset et al.*, 2018). An increase in AW salinity increases the upper ocean density and hence lowers the water column stability, favoring convection. In an opposite manner, increased freshwater transport from the Central Arctic Ocean or from Greenland runoff limits convection (*Brakstad et al.*, 2019).

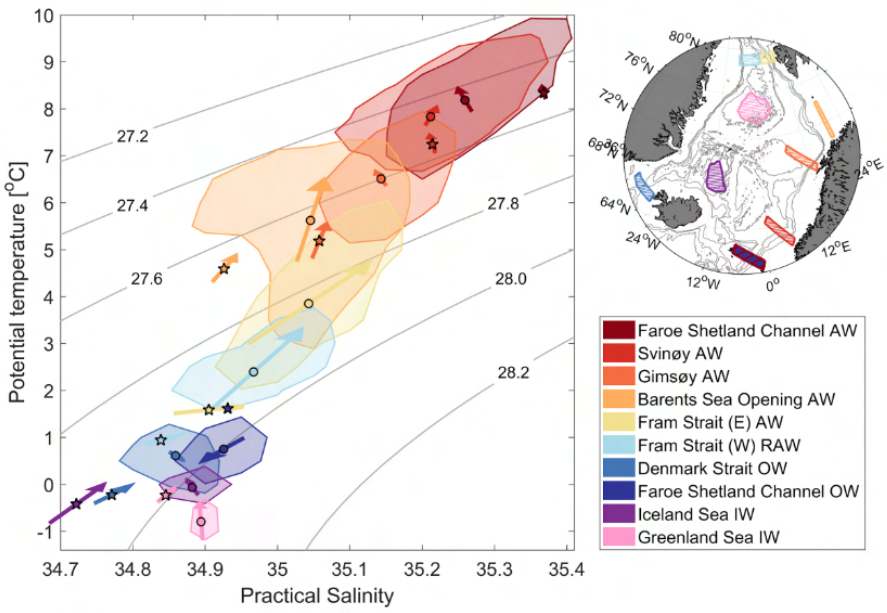

Figure 2.12: a) Temperature-Salinity diagram of selected water masses observed in the Nordic Seas (1950–2019), illustrating the water mass transformation occurring in the region: Warm and saline AW gradually cools and freshens along its pathway northward, and is further transformed in the Central Arctic Ocean and Nordic Seas into denser Overflow Waters (OW) and Intermediate Waters (IW) which are eventually exported from the region in the West. Fresh and light Polar Water masses are not included here, but these are investigated in Le Bras et al. (2021). The range of each water mass is based on the frequency of occurrence and illustrated by patches outlining 60 % of the observations. Circles show the observed median values, and arrows show the linear trends from 1950 to 2019. Stars show the simulated NorESM (Paper I in this thesis) median values and the related arrows the NorESM trends from 1950 to 2009. Figure courtesy: Ailin Brakstad (from Smedsrud et al. (2021)).

The importance to dense water formation is one reason why we investigated the Nordic Seas heat loss more closely in Paper I in this thesis and in *Smedsrud et al.* (2021). Here we find that the amount of cooling is closely linked to the AW heat transport across the GSR, but also that local atmospheric variability plays an important role. Also *Asbjørnsen et al.* (2019), *Mork et al.* (2014), and (*Mork et al.*, 2019) documented that approximately half of the interannual variabilty in ocean heat content in the Nordic Seas is explained by local air-sea fluxes. Nonetheless, AW variability has both direct and indirect implications for the water mass transformation in the Nordic Seas. Recent work by *Lozier et al.* (2019) further discusses what was implied by *Eldevik et al.*

(2009); namely that the transformation of warm and saline AW to cold and fresh OW in the Nordic Seas is largely responsible for the overturning and its variability in the North Atlantic. The AW inflow properties and subsequent transformation in the Nordic Seas may thus have far reaching impacts.

Another important water mass transformation process affected by the AW inflow is the dense water formation in the Arctic shelf seas (*Rudels*, 2015; *Schauer*, 1997). If the water column here is stratified and sufficiently cooled, sea ice is formed, resulting in brine release and cold and dense water cascades from the continental shelf (*Arthun et al.*, 2011). Especially in the Barents and Kara Seas, this sea ice production is directly linked to the AW inflow (Section 2.3.1). Furthermore, as the Arctic sea ice cover is projected to continue to shrink in the future (*Årthun et al.*, 2021; *Notz and Community*, 2020), the areas for possible dense water formation can be expected to shift northward. For example, *Lique and Thomas* (2018) illustrate, based on results from a future climate model simulation, that future dense water formation and deep convection can occur as far north as the Eurasian Basin. Already, observations show an indication of this being plausible, with dense waters being formed on the previously sea-ice-covered East Greenland shelf (*Våge et al.*, 2018) and along the AW boundary current north of Svalbard (*PérezHernández et al.*, 2019). We will discuss the potential of deep water formation in the Central Arctic Ocean more in Paper IV in this thesis.

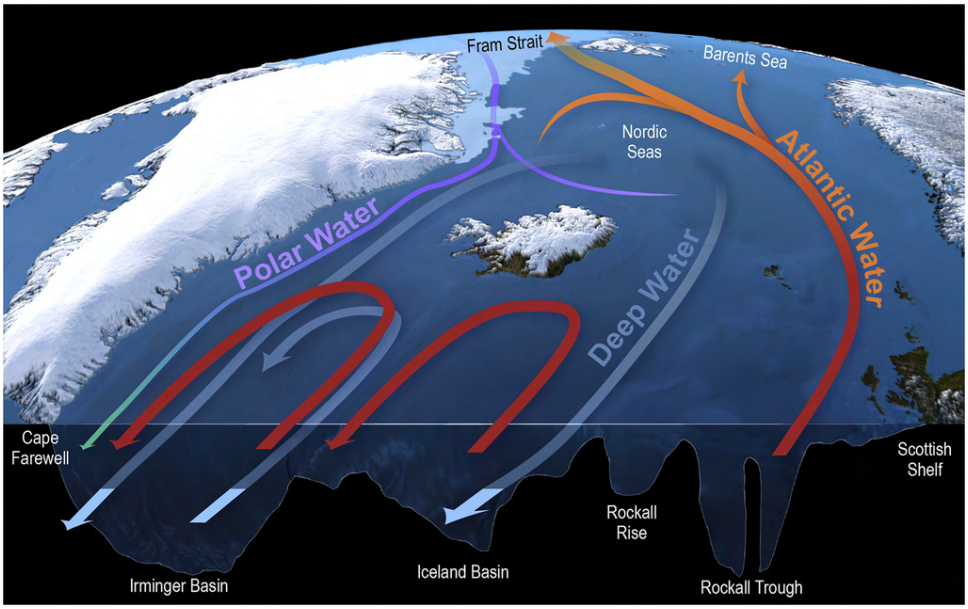

Figure 2.13: Schematic illustration of the circulation and AMOC in the subpolar North Atlantic. Red arrows depict warm and saline Atlantic Water; the light blue arrows depict cold, less salty, dense Deep Waters; and the purple/green arrows depict cold, fresh, light Polar Waters. Figure from Le Bras et al. (2021).

Chapter 3

This study

This thesis aims to obtain a better understanding of the role of AW in the Arctic Ocean, focusing primarily on: its variability in the twentieth and twenty-first centuries; the underlying mechanisms governing this variability; and its regional impacts on sea ice, marine-terminating glaciers, and the subsequent ocean circulation and water mass transformation. This chapter outlines the primary motivation and objectives for the presented work (Section 3.1) and describes the methods used to achieve these objectives (Section 3.2).

3.1 Motivation and Objectives

Global climate change is most pronounced in the Arctic region, with the unprecedented loss of sea ice and an overall warming at more than twice the global rate (Figure 3.1a, *Landrum and Holland* (2020); *Serreze et al.* (2007)). The Arctic Ocean may become ice-free during the 21st century (*Notz and Community*, 2020), and such dramatic changes are likely to echo through the climate system. Further to local changes, effects may extend beyond the Arctic itself, potentially impacting northern hemisphere atmospheric circulation, global teleconnections, and lower latitude weather (e.g., *Francis and Vavrus* (2012); *IPCC et al.* (2019); *Liptak and Strong* (2014); *Overland and Wang* (2010); *Sorokina et al.* (2016); *Yang and Christensen* (2012)). The observed and projected changes include, but are not limited to, changes in ocean circulation (*Sévellec et al.*, 2017), atmospheric circulation (*Screen*, 2017), the cycling of carbon (*Hinzman et al.*, 2013), and marine ecosystems (*Wassmann et al.*, 2011).

Assessing the impacts of global climate change in the Arctic is further complicated by the large amount of uncertainty inherent to the underobserved region. As an example, the uncertainty of projected warming in the Arctic is more than double anywhere else on the planet (Figure 3.1b). The spatially and temporally scarce observational record also contributes to our lack of understanding of critical key processes. To improve future climate predictions, a better understanding of mechanisms driving Arctic climate variability and trends on different time scales is essential. *Nansen* (1902) identified AW as the primary heat source to the Arctic Ocean already in the early 1900s and thus it is known that AW has a critical role in modulating the Arctic climate system. However, despite this long accepted coupling our knowledge is still insufficient to create climate predictions with uncertainty levels similar to other regions. To ad-

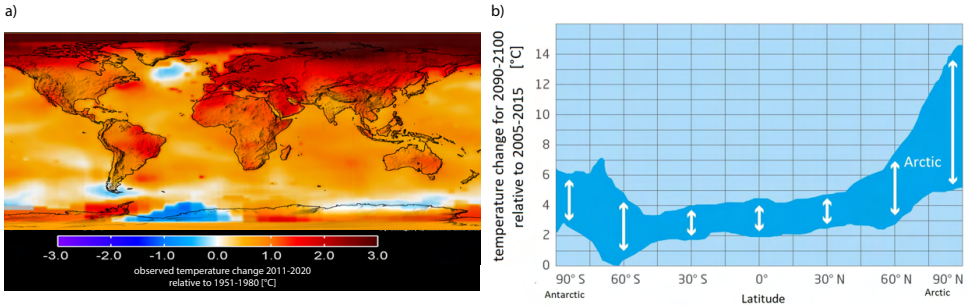

Figure 3.1: a) Global near surface temperature change (nine year average 2011-2020 relative to 1951-1980). Data:NASA/GISS. Figure courtesy: Helge Drange. b) Uncertainty in projected temperature change per latitude by the end of the twenty-first century for CMIP5 models under a strong climate gas forcing scenario (RCP8.5). The envelope represent the minimum and maximum temperate range for the suite of models. Figure courtesy: Alfred-Wegener-Institut / Yves Nowak.

dress this we must further our understanding of the mechanisms driving AW variability and the subsequent proliferating impacts throughout the marine and climate system. In summary, the main research questions of this thesis are:

1. What are the interannual to decadal-scale variations in poleward ocean heat transport in the twentieth century, and what are the underlying mechanisms responsible for these variations? (Paper I)

2. How does poleward ocean heat transport respond to anomalous wind forcing over the Greenland Sea, and what are the downstream effects of these wind anomalies on Arctic sea ice? (Paper II)

3. What is the effect of AW variability on Greenland's marine-terminating glaciers and the subsequent export of glacially modified waters from Greenland's fjords? (Paper III)

4. How will future AW inflows affect Central Arctic Ocean stratification and halocline properties? (Paper IV)

3.2 Data and methods

In this thesis, the topic of AW in the Arctic Ocean is addressed through a relatively broad range of methods and approaches. The papers span multiple spatial and temporal scales as well as geographical regions (Figure 3.2), each providing unique insight into the mechanisms and impacts of AW in the Arctic Ocean. In the process of addressing the above listed research questions, I have used a broad range of methodologies and data products such as in-situ observations, reanalysis data, and regional and global climate models. Physical oceanographers often group themselves into modelers and observationalists, with the mindset that one can never be good at both, though I disagree with this ideology. I argue that continually combining observations and numerical models is the only way to make scientific progress. Throughout my Ph.D. candidacy, I have developed a considerable collection of useful modeling skills such as

running experiments using the NorESM model, adapting model code, analyzing model output (from a range of different models types), and using more simple idealized models such a 1-D convection model and a buoyant plume model for subglacial discharge. In addition to my modeling work, I have contributed to multiple research cruises and have advanced my skills in observational data processing and oceanographic instrumentation such as CTDs, ADCPs, Microstructure profilers, autonomous gliders, and mooring deployment and recovery. The opportunity to develop as both a modeling and observational oceanographer has been foundational to my academic practice, and I am deeply grateful to my supervisors and collaborators who have supported my advancement in both worlds.

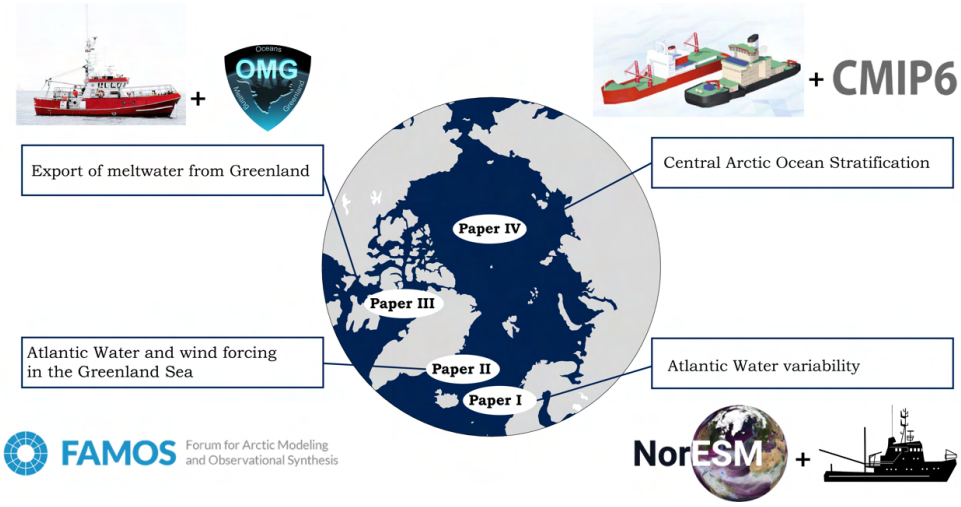

Figure 3.2: Overview over the four main topics, their geographic anchoring, and the associated projects/data sources for each paper of this thesis.

Accurate high-resolution data are needed to understand and predict variability of any climate system. This data is collected from both observations and models – each with their respective strengths and weaknesses. By combining both types of data we develop a more robust understanding of the system, harnessing the strengths of one method to enhance the other . The primary limiting factor for the utility of ocean observing systems is that they are expensive and logistically challenging (*Weller et al.*, 2019). This is especially true in the Arctic Ocean, where harsh weather conditions and sea ice cover limit accessibility resulting in sparse observational data. The observations that are available provide a necessary direct description of reality, but especially in the inaccessible Arctic Ocean, numerical models are needed to supplement temporal and spatial gaps in observational data. In contrast to observational data, numerical models provide spatially and temporally complete data but are limited by spatial resolution and their capability to accurately simulate the real world (*McWilliams*, 1996). The primitive equations ultimately calculating the time-evolving, three-dimensional ocean circulation in the models are discretized according to the model's time step and spatial grid. By definition, many essential processes such as turbulent mixing, diffusion, and eddies are excluded and therefore need to be parameterized, which results in high uncertainty

(*Fox-Kemper et al.*, 2019; *Wunsch and Ferrari*, 2018). Pairing observational data with a model can help to constrain these parameterizations. The combination of observations and models enhances researchers ability to understand and describe the system as a whole and discern its role in the global climate system. In the Arctic Ocean, however, this approach is hindered by limited observations, especially in winter, and rapid environmental change in response to Global Climate change which results in this region having the most imperfect simulations on the planet. Therefore, it is crucial to improve the models and collect more observational data while continuously discussing the weaknesses and suitability of each for the research questions at hand.

There is a vast ocean of literature on model intercomparisons (e.g. CMIP3, CMIP5 and CMIP6 papers), many of which conclude a wide spread in the models' capability to simulate specific processes, or that the models have significant biases compared to observations (Figure 3.3 and e.g. *Danabasoglu et al.* (2016); *Ilicak et al.* (2016); *Tsujino et al.* (2020); *Wang et al.* (2016b)). This topic is addressed in paper II and IV, where we compare many different models; however, we note that simply describing model differences and biases is not helpful beyond individual model development. The strength in model intercomparison projects lies in using the similarities and differences to gain a better mechanistic understanding of the systems at hand. The primary data products and tools used are described briefly in the following sections.

3.2.1 NorESM, FAMOS and CMIP6 climate models

This dissertation's backbone is the "in-house" Norwegian Earth System Model, NorESM (previously called the Bergen Climate Model). A general description of the model's first version (NorESM1) used in Paper I and II are given by *Bentsen et al.* (2013), whereas a description of the updated version (NorESM2) used in Paper IV and *Le Bras et al.* (2021) is given by *Seland et al.* (2020). The ocean model, Bergen Layered Ocean Model (BLOM), is an updated version of the Miami Isopycnic Coordinate Ocean Model (MICOM) used in NorESM1. BLOM consists of 51 near-isopycnic interior layers and two variable density layers in the SML. The isopycnal layering is an essential difference in comparison to other global circulation models, which generally use set depth coordinates. NorESM uses a tripolar grid with two poles over Greenland and Siberia, which allows for higher spatial resolution in the high latitudes. At the equator, the grid resolution is 1° zonally and 1/4° meridionally. The grid gradually becomes more isotropic as latitude increases, and the typical horizontal resolution in the Arctic Ocean is 40 km. The sea ice model is based on the Los Alamos Sea Ice Model (CICE, *Hunke et al.* (2015)) configured with eight layers of ice and three of snow, using the same horizontal grid as the ocean model. A NorESM2-specific change to CICE includes the effect of wind drift of snow into the ocean following (*Lecomte et al.*, 2013). For our results, it is essential to note that NorESM does not resolve mesoscale eddies and relies on eddy parameterizations such as *Gent and Mcwilliams* (1990) to represent cross-shelf transport due to mesoscale eddies. For studying AW in the Arctic Ocean, the parameterization of shear-induced mixing is also imperative. In NorESM1, this was parameterized using the local gradient Richardson number according to *Large et al.* (1994). In NorESM2, this has been replaced by a one-equation second-order turbulence closure model (*Ilcak et al.*, 2008; *Umlauf and Burchard*, 2005). We have not

investigated the detailed effects of these changes.

In Paper I of this thesis, we have first performed a historical simulation using the ocean and sea-ice components of the model's first version (NorESM1) forced by a twentieth-century atmospheric reanalysis forcing ($20CR_{adj}$), which is a blended dataset derived from the ensemble mean version of the 20th Century Reanalysis (20CRv2; *Compo et al.* (2011)), satellite observations, and the corrected Coordinated Ocean-ice Reference Experiments phase-II (CORE-II) forcing for the period 1871 to 2009 (*Griffies et al.*, 2012). This is the same model setup used by *He et al.* (2016), who analyzed the forcing dataset in detail and found that the original 20CRv2 resulted in large SST and SSS biases. The same model setup was used again in Paper II, where we performed a set of coordinated CRF experiments in which we perturbed the atmospheric forcing (Section 3.2.2). Furthermore, we use the output from the updated model (NorESM2) both in the fully coupled configuration (Paper IV) and the stand-alone ocean-sea ice configuration (used in *Le Bras et al.* (2021)) forced by the Japanese 55-year Reanalysis (*Tsujino et al.*, 2018). The NorESM2 data are provided as part of the CMIP6 contributions to the *Histocial* and future *ScenarioMIP* decks (*Eyring et al.*, 2016; *Gidden et al.*, 2019) and OMIP2 (Ocean Model Intercomparison Project Phase II, *Griffies et al.* (2016)) experiments.

In addition to NorESM, we analyzed output from a range of other models provided by other modeling groups. In paper II, we analyze output from eight other ocean-sea ice models, both regional and global, provided through the Forum for Arctic Ocean Modeling and Observational Synthesis (FAMOS, *Proshutinsky et al.* (2016)) network, the successor of the Arctic Ocean Model Intercomparison Project (AOMIP, *Proshutinsky et al.* (2011). In paper IV, we additionally analyze the output of nine other global CMIP6 models that contributed to the *Histocial*, and future *ScenarioMIP* experiments (*Eyring et al.*, 2016; *Gidden et al.*, 2019).

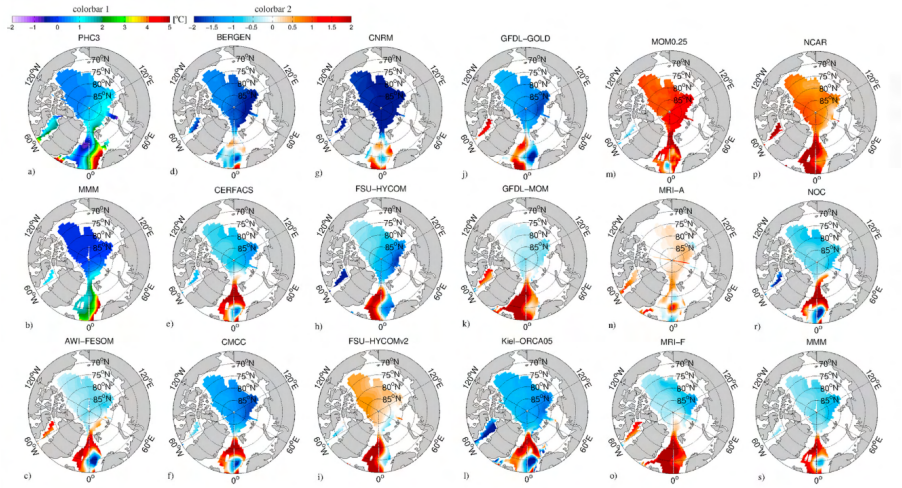

Figure 3.3: As of today global climate models still have large biases when it comes to simulating Arctic Ocean hydrography and circulation. Here we show temperature bias at 400 m depth relative to the PHC3.0 climatology for a suite of global ocean-ice models as part of the CORE-II model intercomparison project. MMM is the multimodel mean. Figure from Ilicak et al. (2016).

3.2.2 The Climate Response Function Experiments

Coordinated Climate Response Function (CRF) experiments involving the participation of several international modeling groups' are imparative to this dissertation. The experiments were originally proposed by *Marshall et al.* (2017), in collaboration with modeling groups under the auspices of FAMOS, to investigate the behavior of so-called "key switches" in the Arctic Climate System. A CRF experiment entails observing how a numerical model responds to an abrupt and sustained change in some aspect of the model forcing. These experiments have shown to be very useful to outline "linear" relationships in the climate system, such as the response to changes in greenhouse gases (*Good et al.*, 2011, 2013), ozone (*Marshall et al.*, 2014) or freshwater input (*Lambert et al.*, 2019). A CRF (also called step response function) is the time integral of the characteristic impulse function (*Marshall et al.*, 2017), it can provide simple climate prediction measures. For example, if we calculate the CRF of sea ice extent to a step-change in surface temperature, we may then construct the linear response of sea ice extent to any record (past or future) of sea surface temperature forcing. In other words, as per linear response theory (e.g., *Hasselmann* (1993)), a convolution of the CRF and a time history of the forcing yields a time history of the response:

$$R(t) = \int_0^t CRF(t-t')\frac{\partial F}{\partial t}(t')dt', \tag{3.1}$$

where F is the anomalous forcing and $CRF(t)$ is the time-dependent response to a unit step change in forcing. Of course, the system is likely not linear (especially in the example of sea ice, which we know includes many feedback mechanisms), and thus the predictive skill is limited. That being said, a strength of the CRF is that one may check the predictive skill a-posteriori by comparing the convolution of a historical forcing time series and the CRF with the actual observed diagnostic parameter.

The FAMOS collaboration resulted in two major international studies: one experiment designed to investigate a variety of responses to changes in the strength of the Greenland Sea (GS) Low, an effort led by M. Muilwijk (Paper II in this thesis); and another experiment designed to understand the response of the Beaufort Gyre (BG) to abrupt wind-driven changes in the strength of the Beaufort High, an effort led by authors J. Marshall, G. Meneghello, and J. Scott (manuscript in preparation). Early results from the Beaufort Gyre experiment prompted an additional follow-up study led by S. Cornish and M. Muilwijk (manuscript in preparation, not included in this thesis) on the effect of sea ice divergence and ice-ocean turning angles on wind-driven freshwater adjustment of the Beaufort Gyre.

The BG and GS experiments' procedure involved perturbing a wide range of ice-ocean models (many with different resolution, domains, and atmospheric forcing) with an identical 10 m wind anomaly by adding this perturbation pattern to the original forcing. The anomaly patterns correspond to an anonymously strong or weak Beaufort High (BG+ and BM-) and an anonymously strong or weak Icelandic Low (GS+ and GS-), representing the dominant atmospheric sea level pressure patterns in the Arctic Ocean. The perturbations' peak magnitude is 4 hPa, this was chosen to be representative of multi-year to decadal trends (*Marshall et al.*, 2017). The 10 m winds are then computed using the relationship to the geostrophic wind as described by *Proshutinsky*

and Johnson (1997):

$$W_s = 0.7 \times \begin{bmatrix} \cos 30 & -\sin 30 \\ \sin 30 & \cos 30 \end{bmatrix} \times W_g \tag{3.2}$$

The perturbations are applied abruptly to a control simulation and sustained for a minimum of 25 years. The CRFs were then derived by subtracting the non-perturbed control simulation from the perturbed simulation. We note that CRFs may also be derived directly from long control runs of fully coupled models using a statistical approach (e.g., *Cornish et al.* (2020); *Johnson et al.* (2018); *Kostov et al.* (2017)).

Although not included in this thesis, the BG experiment results are essential for this thesis's paper IV results. As shown by *Cornish et al.* (2020), the BG experiments indidcate an increase/decrease in Arctic freshwater content in response to weaker or stronger anticyclonic winds driving convergent Ekman flow on the surface of the Beaufort Gyre. Interestingly, after a decade of anomalous forcing, the magnitude in response across models differs by a factor of five despite the forcing being the same. These differences can be explained by differences in sea ice distribution, which mediate the transfer of stress through a process known as the ice-ocean governor (*Meneghello et al.*, 2018). Additionally, Cornish and Muilwijk (manuscript in prep) have found that how the angle between wind and ice motion is simulated can influence the accumulation of freshwater beneath the Beaufort High; the divergence of ice is sensitive to the angle at which ice moves in response to rotational winds. Due to the stabilizing feedback of ice thickness on the growth rate, ice export from the gyre is partially compensated by enhanced ice growth within the gyre, resulting in a sink of freshwater.

3.2.3 Hydrographic observations of the Nordic Seas and Central Arctic Ocean

The observational data used in this thesis is comprised of many different datasets. For quality control and model evaluation, we have used climatological datasets such as the World Ocean Atlas (WOA13) global climatology (*Boyer et al.*, 2013), the World Ocean Atlas (WOA18) global climatology (*Locarnini et al.*, 2018), the Polar Science Center Hydrographic Climatology (PHC3) (*Steele et al.*, 2001), and a global monthly isopycnal upper-ocean climatology (MIMOC, *Schmidtko et al.* (2013)). In paper III, we performed an extensive analysis of the regional AW variability (in Baffin Bay), using the EN4 dataset (*Good et al.*, 2013) and ECCOv4 ocean state estimate (*Forget et al.*, 2015). However, much of this work was not included in the final paper due to space limitations. One conclusion was that EN4 did not contain enough data to provide trustworthy information on Baffin Bay variability, whereas ECCOv4 captured variability well compared to mooring data from the Davis Strait.

The primary observational data set for the Nordic Seas used in Paper I is the NOAA Climatological Atlas of the Nordic Seas and Northern North Atlantic (*Korablev et al.*, 2014) which was initially developed at the Arctic and Antarctic Research Institute (AARI) in the late 1980s. This dataset builds on an enhanced collection of in situ observations from the beginning of the twentieth century until 2012 and contains vast amounts of Russian observations. These observations were then updated to include new international data, and subsequently converted to a new database format using modern

software for quality control. The temporal distributions of the station numbers and seasonal bias in the duplicate controlled database is illustrated in Figure 3.4. Spatial and temporal data coverage and seasonal biases are significant concerns – however, the uncertainty resulting from this and other errors are discussed in detail by (*Korablev et al.*, 2014). In Paper I, we argue that data quality is good enough to estimate large-scale AW variability in the Nordic Seas from 1920 and onward, with gaps during WW2. We have performed manual quality control of all the profiles used in this study. We note, however, that now a newly updated dataset of Nordic Seas hydrography exists, which was used in *Smedsrud et al.* (2021). This dataset is a combination of the dataset used in *Huang et al.* (2020) which covers the period 1980-2019 and is a collection from various archives, including the Unified Database for the Arctic and Subarctic Hydrography (UDASH, *Behrendt et al.* (2018)) and the NISE dataset (Norwegian Iceland Seas Experiment, *Nilsen et al.* (2008)) which also covers multiple archives over the period 1900-2006.

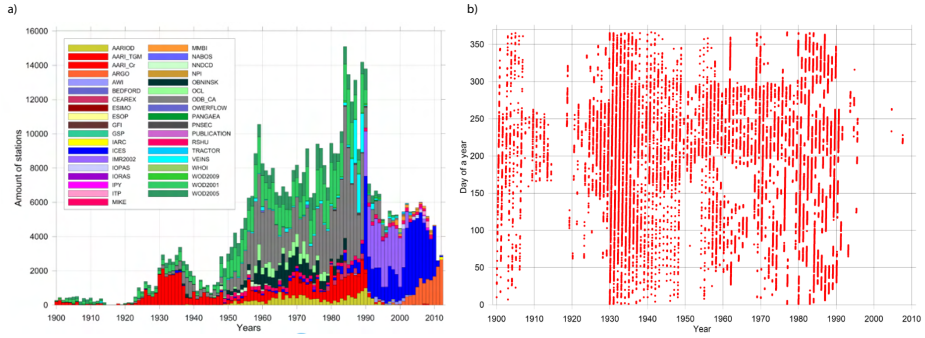

Figure 3.4: a) Number of oceanographic stations in the he NOAA Climatological Atlas of the Nordic Seas and Northern North Atlantic used in paper I in this thesis. Colors indicate the various data sources used to create the atlas. b) Same as a) but here red dots show the data distribution by day and by years. Figures from Korablev et al. (2014).

Historical data is relatively sparse in the Nordic Seas, though it is much more sparse in the Central Arctic Ocean. *Nansen* (1902) provided the first oceanographic measurements of the Central Arctic Ocean from his famous drift on board the Fram, which drifted across the Arctic Ocean following the transpolar drift from 1893 to 1896. However, systematic oceanographic observations only began in the 1930s and 40s, when Russians started a program consisting of crewed ice–drift stations and winter aircraft surveys (*Polyakov et al.*, 2004). The first basin-wide surveys were conducted by Russian aircraft in 1955. During the 1960s and 1970s, the Russians increased their aircraft surveys, resulting in occasional hydrographic observations using Nansen bottles. During the 1980s and 1990s, the increased use of icebreakers and submarines resulted in a significant increase in hydrographic profiles. The bulk of historical data before 2000 was finally gathered to construct the climatological atlases of the Arctic Ocean by *Gorshkov* (1980), *Treshnikov* (1985), and the *Environmental Working Group* (1997). Much of the (Russian and American) historical raw data is still classified and only publicly available as part of these climatological atlases.

In paper IV, we use a unique 47-year long archive of the Central Arctic Ocean

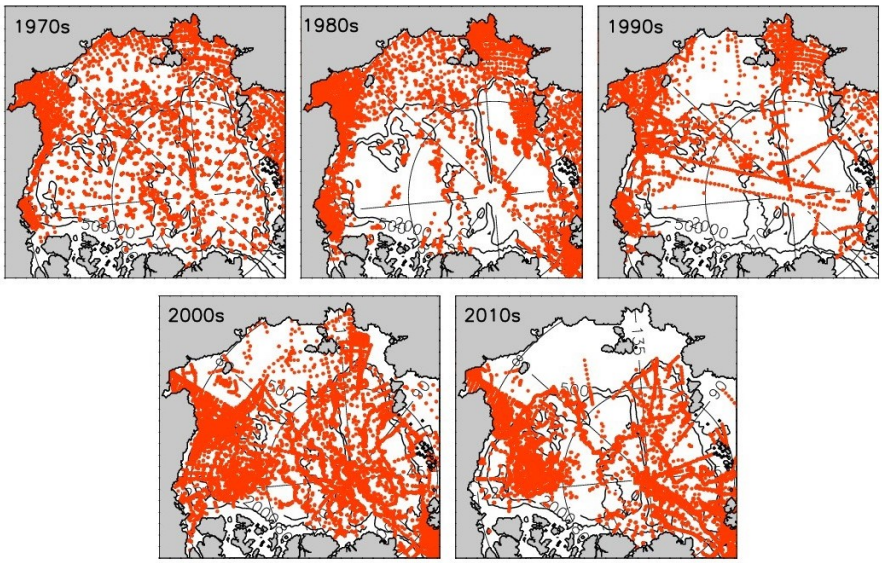

Figure 3.5: Maps showing Central Arctic Ocean data coverage of oceanographic profiles (red dots) from the data set used in Paper IV. Depth is shown by 500- and 2000-m contours. Figure courtesy: Igor Polyakov.

hydrography covering the period 1970 to 2017 which was provided by Igor Polyakov at the University of Fairbanks, Alaska; including most of the historical data and its complete temporal information which is unavailable in the public atlases. The dataset includes Russian, American, Canadian, European ship and aircraft expeditions, year-round crewed drift-stations, autonomous drifters, and Russian and American submarine data. This is an updated version of the archive previously used by *Polyakov et al.* (2004, 2008, 2013, 2018, 2020). Since the 2000s, a significant part of the data stems from ship-based measurements complemented by drifting ITPs, conducting CTD profiles down to 800 m. Figure 3.5 shows the temporal and spatial data availability of this unique dataset. As many historical observations used Nansen bottles to take water samples and measure temperatures and salinity at standard levels, the accuracy of these data and the vertical resolution is relatively low. As such, especially the depth information of the old measurements must be considered to be highly uncertain (Paper IV). Nonetheless, *Polyakov et al.* (2003) and (*Polyakov et al.*, 2004) show that these old records still allow the AW core temperature and salinity to be calculated quite accurately. In recent years, the accuracy from CTDs has increased to more than an order of magnitude greater than the bottle measurements.

3.2.4 Greenland fjord data

In paper III, we use a set of hydrographic observations collected in and around Upernavik Fjord in northwest Greenland between 2013 and 2019. Using these data, we are the first to describe the hydrographic conditions of Upernavik Fjord and evaluate the close relationship between fjord and shelf properties. In 2013, temperature, con-

ductivity, and pressure data from Upernavik were collected from the research vessel R/V Porsild during a field campaign to collect sediment cores and bathymetric measurements (*Andresen et al.*, 2014). Data for the remaining years was provided by the NASA campaign Oceans Melting Greenland (*OMG Mission*, 2020). During 2015 and 2016, stations were occupied by M/V Cape Race, a commercial tourist vessel, and the S/Y Ivilia, a sailing vessel, which were both equipped with a CTD. For the years 2016-2019, we used hydrographic profiles collected from Airborne eXpendable Conductivity, Temperature and Depth (AXCTD) probes (*Fenty et al.*, 2016). Every summer, since 2015, OMG deploys about 250 probes from an aircraft to measure the temperature and salinity of the fjords and shelf around Greenland (see a schematic of the deployment Figure 3.6). The AXCTDs send their temperature and salinity data back to the aircraft from a temporary surface buoy and calculate the depth based on a constant fall-rate. Although somewhat less accurate than ship-based CTD measurements (accuracy discussed in (*Childers and Brozena*, 2005)), this methodology has resulted in an incredibly valuable dataset of Greenland's fjords due to its high spatial resolution.

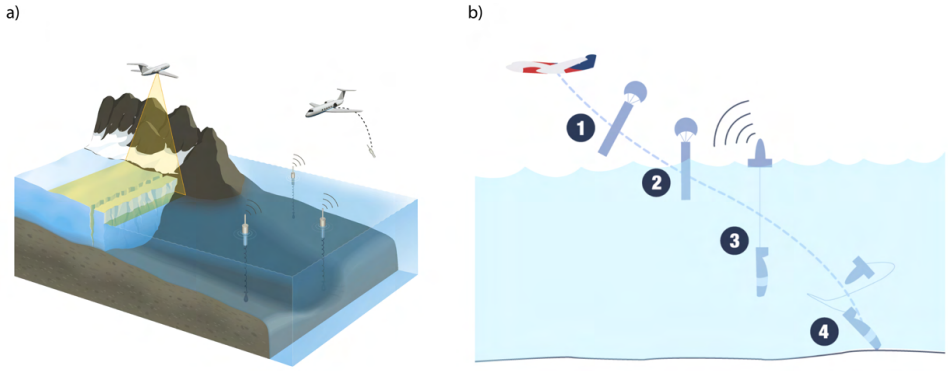

Figure 3.6: a) Illustration showing deployment of AXCTD probes in glacial fjords and on Greenland's continental shelf as part of the OMG project. b) Illustration showing the AXCTD deplomentprocedure: 1) Probe is dropped from the plane, parachute opens, 2) Probe lands in the water, 3) Buoy floats to the surface and transmits data back to the plane, while probe sinks 4) After 15 minutes, both buoy and probe sink to the ocean floor and eventually decompose. Figures and caption from the OMG project website (`https://omg.jpl.nasa.gov/portal/`).

Chapter 4

Summary of papers

Paper I: **Atlantic Water heat transport variability in the 20th century Arctic Ocean from a global ocean model and observations**

Muilwijk, M., Smedsrud, L. H., Ilicak, M., Drange, H. (2018), Journal of Geophysical Research: Oceans, 123(11), 8159-8179.

Paper I investigates the twentieth-century variability of ocean heat transport (temperature and volume) through the gates of the Arctic Ocean. We focus on the variability of AW heat, which dominates the Arctic Ocean heat transport and link the variability to upstream conditions in the Nordic Seas. The analysis is built on a simulation with the global ocean-ice Norwegian Earth System Model (NorESM) forced by a reanalysis atmospheric forcing and supported by an extensive set of hydrographic observations dating back to 1900. We reveal prominent variability in both AW temperature and volume transport on $5-6$ and on $8-9$ year time scales, as well as strong positive trends in the most recent decades. Temperature variability is mainly an advective signal originating further upstream, whereas variations in volume transport appear to be strongly linked to the wind forcing in the Nordic Seas and Subtropical North Atlantic, often manifested through the North Atlantic Oscillation (NAO). However, an important finding is that the correlation between the large scale wind forcing, NAO, and AW volume transport is not constant over time and breaks down entirely in specific periods. The Early Twentieth-Century Warming (ETCW) during the 1930s and 1940s is clearly manifested in our results, and this is an example of a period where the volume transport across the Greenland Scotlan Ridge (GSR) is not correlated with the NAO-like wind forcing. We also show that the oceanic ETCW is mainly a temperature anomaly, which was strong in the North because it was subject to an anomalously low atmospheric dampening in the Nordic Seas. In general, we show that the atmospheric forcing in the Nordic Seas contributes to approximately half of the ocean heat variability, consistent with *Mork et al.* (2014) and *Asbjørnsen et al.* (2019), and that it effectively dampens the oceanic anomalies along their pathway northward. Interestingly, our results also show that temperature trends increase northward, although this was not studied in detail . Furthermore, we document the division of the AW branch north of the Lofoten region and investigate how the variability is split between the Fram Strait (FS) and the Barents Sea Opening (BSO). We find that volume transport variability dominates the variability in heat transport through the BSO, but temperature plays a larger role in the

FS. Local winds in the FS and BSO regions are essential in determining the division between the two branches and the large re-circulation occurring in FS. On a centennial timescale, the AW dominated both the mean and variability in ocean heat transport into the Central Arctic Ocean.

Paper II: Arctic Ocean response to Greenland Sea wind anomalies in a suite of model simulations

Muilwijk, M., Ilicak, M., Cornish, S.B., Danilov, S., Gelderloos, R., Gerdes, R., Haid, V., Haine, T.W., Johnson, H.L., Kostov, Y., Kovács, T., Lique, C., Marson, J.M., Myers, P.G., Scott, J., Smedsrud, L.H., Talandier, C., Wang, Q. (2019), Journal of Geophysical Research: Oceans, 124(8), pp.6286-6322.

Paper II investigates the effects of anomalous wind forcing over the Greenland Sea (GS) on the northward AW flow, Arctic sea ice, and Nordic Seas hydrography. This work results from a larger international intermodel comparison experiment, initiated as part of the FAMOS (Forum for Arctic Modeling and Observational Synthesis) network, focused on analyzing the key "switches" of the Arctic climate system. We calculate Climate Response Functions (CRFs, Chapter 3.2.2) and analyze results from a suite of nine different Arctic Ocean model simulations. The CRF's show that anomalously strong/weak GS wind forcing results in an intensification/weakening of the poleward AW flow and a reduction/increase in the Arctic sea ice cover. These anomalous wind patterns are comparable in strength to winds resulting from a strong positive/negative North Atlantic Oscillation index. The wind forcing in the Nordic Seas affects the AW circulation and hydrography throughout all Arctic Ocean basins, but the release of passive tracers also reveals significant intermodel differences and weaknesses in terms of Central Arctic Ocean circulation. Despite biases in hydrography, all models agree on the general response to the anomalous winds and show a linear relationship between AW volume and heat transport, surface heat loss, and sea ice extent in the Barents Sea. Most of the anomalous AW heat transport resulting from a strong wind forcing is lost to the atmosphere, aided by loss of sea ice in the Barents Sea , and thus effective ocean cooling. Although slightly non-intuitive, we thus show that through surface heat loss and Ekman pumping, the depth-integrated heat content in the Arctic Ocean generally decreases due to intensified AW flow and vice versa for a weakened flow. Linear convolutions of the CRFs and historical time series of SLP produce reconstructions showing that the GS wind forcing can explain 50% of the historical AW flow variance. This gives rise to a potential for predictability of the Arctic-Atlantic circulation based on wind forcing anomalies and CRFs. The response and potential for predictability on Arctic sea ice is limited for forced ocean-ice models due to the lack of ocean-atmosphere feedbacks, but should be better captured in fully coupled model simulations. Although not included in this manuscript, the GS wind anomalies also have a large effect on the outflows of the Central Arctic Ocean, mainly export of sea ice, and thus also play an essential role in the total Arctic freshwater budget. In general, the CRF approach has proven to be a valuable tool for isolating key drivers of climate variability and their downstream effects, in addition to evaluating differences in climate model dynamics.

Paper III: **Export of ice sheet meltwater from Upernavik Fjord, West Greenland**

Muilwijk, M., Staneo, F., Slater, D., Smedsrud, L. H., Wood, M., Holte, J., Andresen, C., Harden, B., submitted to Journal of Physical Oceanography.

Paper III investigates the subsequent effects resulting from AW interaction with marine-terminating glaciers in northwest Greenland. Ice loss from Greenland translates into a large freshwater flux into the North Atlantic. This freshwater generally enters the ocean at the head of Greenland's glacial fjords through seasonal runoff, melting of icebergs, and submarine melting of marine-terminating glaciers. Most of the runoff is released as so-called subglacial discharge at depth, near the glacier's grounding line, resulting in the rise of turbulent buoyant plumes at the glacier fronts. The plumes entrain warm AW, which has entered the deep fjord from the shelf, and melts the glacier at depth. After the plume reaches neutral buoyancy, it further mixes with other intermediate fjord water masses and iceberg meltwater, resulting in complex water mass transformation. Finally, the diluted freshwater is exported from the fjord at intermediate depths as a newly formed water mass; "Glacially Modified Water" (GMW). In this paper, we present the first description of the hydrographic structure in Upernavik, a major glacial fjord in northwest Greenland, and focus on the export properties of GMW from this fjord. We suggest a technique to identify GMW based on comparison of hydrographic measurements collected on the continental shelf and inside the fjord, and then use observations from six years to identify variations in the water masses that flow into and out of the fjord. Furthermore, we propose a new method based on an Optimum Multi-Parameter technique across multiple years, and show that GMW in summer is composed of 57.8 $\pm$8.1% AW, 41.0 $\pm$8.3% Polar Water, 1.0 $\pm$0.1% subglacial discharge and 0.2 $\pm$0.2% submarine meltwater. Consistent with its composition, we show a close relationship between water mass properties on the continental shelf (AW and Polar Water) and the exported GMW properties. Our results are supported by a buoyant plume model, but we also show that such a buoyant plume model alone cannot accurately reproduce GMW properties. This is because the plume model does not account for further mixing that occurs after the plume has reached neutral buoyancy. The obtained mixing ratios enable us to derive a rough estimate of the exchange across the fjord mouth during summer on the order of 50 mSv, without having any current measurements. This study provides a first-order parameterization of fjord-shelf exchange for large-scale ocean models.

Paper IV: **Past, present, and future Arctic Ocean stratification from observations and CMIP6 simulations**

Muilwijk, M., Smedsrud, L.H., Polyakov, I., Nummelin, A.

Paper IV investigates changes in Central Arctic Ocean stratification in the twentieth and twenty-first centuries. Because of large amounts of river runoff, ice melt, net precipitation, and a relatively fresh Pacific inflow, the Central Arctic Ocean is one of the most stratified oceans on Earth (*Li et al.*, 2020). This strong stratification is critical to the system's physical, biological and biogeochemical components, as it effectively shields

the sea ice cover from oceanic heat found at depth, limits primary production due to reduced nutrient fluxes, and reduces the ocean's capability to take up atmospheric CO2. In a future warming climate, the freshwater flux into the Central Arctic Ocean is expected to increase, likely strengthening the stratification. Simultaneously, however, the AW and Pacific Water inflows are expected to warm and shoal, and possibly increase, and the sea ice cover is expected to shrink with a warming atmosphere −− changes which could potentially result in a weakened stratification. This can be seen as a "tug of war" between the ongoing "Atlantification" and local freshening, and as of today, there is no scientific consensus on which process will dominate under future global warming. We present the first in-depth investigation of Arctic Ocean stratification in different regions from future simulations aided by a unique archive of historical observations. Using this 47-year long observational record, we synthesize the observed changes before we compare these with simulations from the Community Earth System Model large ensemble simulation (CESM-LE) and an ensemble of 9 climate models from the Coupled Model Inter-comparison Project Phase 6 (CMIP6). We present a new indicator of stratification and show that from 1970 to 2017, the stratification of the upper Central Arctic Ocean has generally increased. On average, over the observational period, the halocline layers have warmed Arctic-wide, and this is projected to continue throughout the twenty-first century. In the Amerasian Basin, the halocline has freshened, whereas, in the Eurasian Basin, a moderate increase in salinity has been observed. Within the Amerasian Basin, there is agreement between models that the upper layers will become fresher and more stratified in the future. On the other hand, there is a divergence between the models regarding future stratification within the Eurasian Basin. Approximately half of the suite of models project a strengthened future stratification in the Eurasian Basin, and the other half project a weakened future stratification. All models show an overall freshening in the upper layers of the Eurasian Basin, but some models show a substantial freshening in the AW layer as well. The different vertical distributions of the freshening results in different effects on the stratification. Models which only simulate a freshening near the surface show increased stratification. In contrast do models that simulate equally strong freshening in the AW layer show a weakened stratification. The AW freshening appears to be an advective signal. Models thus differ in large-scale circulation and in the propagation of salinity anomalies, ultimately affecting the stratification in the Eurasian Basin. Although Atlantification continues well into the future, it is apparent that local freshening is a dominant process regarding future stratification changes. Whether the Eurasian Basin becomes more or less stratified in the future may depend on to which degree salinity anomalies from the Arctic outflows ultimately return with the AW inflow.

Chapter 5

Perspectives and outlook

The Arctic Ocean is literally a hotspot of the ongoing global warming. It is thoroughly established that the coupled ocean-sea ice system is an active and amplifying component of the global climate system, but many of the mechanisms governing Arctic Ocean climate trends and variations, and their linkage to lower latitudes, are not yet fully understood. Also, how the Arctic Ocean dynamics might change as the region continues to warm and the sea ice cover continues to decline remain uncertain. The poleward oceanic heat transport and its naturally varying fluctuations are central and essential pieces of this puzzle, as it governs the climate in the Atlantic sector of the Arctic.

This thesis addresses some central aspects of AW variability, the underlying forcing mechanisms, and subsequent impacts on sea ice and marine-terminating glaciers. The analysis presented in the papers shows the essential role of wind forcing on the AW inflow while also eluding to the role of atmospheric cooling and buoyancy forcing. The findings indicate a complex balance between local (freshening) processes and advective (Atlantification) processes in the Eurasian sector of the Central Arctic Ocean, which becomes more and more essential — and at the same time more uncertain — in the future (Paper IV).

The work furthermore demonstrates both strengths and weaknesses of Arctic Ocean model simulations. As an example, it is shown in Paper I that the variations in the simulations agree well with available observations. In Paper II we show that forced model experiments yield valuable information on how the system responds to external forcing despite significant model differences and biases. This conclusion is based on the fact that very different model systems respond similarly to the same external forcing. Nonetheless, our results show that state-of-the-art Arctic Ocean simulations still have a large spread in hydrography and circulation patterns, and therefore have high uncertainty for hindcasts and future projections.

The model divergence is generally larger in the Arctic than elsewhere on the planet, much because of the complex — and non-linear — coupling between atmosphere, sea ice and ocean (*Winton*, 2008). Therefore, we make the point that for studies of the Arctic Ocean, relying on the output from a single model system is insufficient — a multi-model approach is necessary to increase the confidence in the results. Also, many ensembles from a single model system may skew the results towards specific model biases or physical/thermodynamical deficiencies. Due to the inherent uncertainty of the models, studies of the Arctic Ocean must be grounded in and validated by observations. Direct observations of the ocean, sea ice and atmosphere, and particularly long

time series remain essential to identify and understand leading mechanisms acting on different time scales and possibly changing as a result of changes in the background climate, and subsequently implications of Arctic variations and potential predictability. The work presented in this thesis naturally points towards several open questions, some of which will be discussed here.

5.1 AW temperature variability

In Paper I we discuss the interannual to near decadal variability of AW in the Nordic Seas and the Arctic gateways. Observational records and simulations also show evidence of multidecadal variability in AW temperature from 1900 to today, with an Early Twentieth-Century Warming (ETCW) followed by a colder period and another warming from approximately the 1980s. This was not a major focus in our paper, but we contributed to the topic by concluding that the ETCW is mainly a result of a temperature anomaly and not a volume transport anomaly, and that the ETCW period was subject to weak atmospheric damping. We also concluded that during the ETCW, there was nearly no correlation between the AW flow in the Nordic Seas and the NAO and the wind stress curl. The ETCW is undoubtedly a real warming signal, but whether this was just a singular warm period (*Mann et al.*, 2021) or part of a repeated pattern (AMO, *Otterå et al.* (2010)) remains debated. Our simulation was not long enough nor had enough model members to statistically assess this question, and there is still uncertainty regarding the forcing mechanisms governing a potential AMO. This is an important question because we do not know whether the current warm period (1980→ today) is a pure global warming signal or a combination of global warming and multidecadal variations. This raises the follow-up question whether the future will be entirely dominated by a steadily increasing global warming signal or if the trends will be somewhat dampened and amplified by multidecadal variations. Future work is required on disentangling the possible co-existence of multidecadal variations and a global warming signal, especially if we are to improve our predictable skills.

In paper I and *Smedsrud et al.* (2021), we found that AW temperature trends and anomalies increase poleward in the Nordic Seas. This was evident from observations and the NorESM simulations, but the mechanisms were not investigated in detail. In some follow up analysis we found no apparent south-to-north increase in trends, but that it is more spatially varying. In other words, there are some "hotspots" where the AW, but also SST, trends are stronger than in other places. This is especially the case around Svalbard and in the Barents Sea. Surface fluxes are a likely cause (*Skagseth et al.*, 2020), and in *Smedsrud et al.* (2021) we discussed that the increase in poleward directed anomalies was mainly due to a large trend in AW temperature advection, and a fairly constant heat losses in the Nordic Seas, resulting in larger anomalies further north. Further elaboration on this topic could be an interesting contribution to the general understanding of Arctic-Atlantic variability.

In general, the role of surface fluxes and sea ice on AW heat variability is not discussed in great detail in Paper I. The overall heat loss in the Arctic Ocean contributes to significant variations in AW heat transport over time. This has been subject to fur-

ther investigations in *Smedsrud et al.* (2021). In paper I and in *Asbjørnsen et al.* (2019), it has been shown that the local atmospheric forcing contributes to approximately half of the variation in AW heat transport, confirming earlier results of *Mork et al.* (2014). In *Smedsrud et al.* (2021) we found that much of the variability in the surface heat fluxes are linked to the frequency of cold air outbreaks and cyclones. The trends are relatively small, which is interesting since increasing SST implies stronger cooling. However, the atmosphere also warms and the stability of the marine boundary layer and advection may change, likely leading to small changes to the local the heat budget. In the twentieth century, the trends in heat loss are largest in the Barents Sea and Central Arctic Ocean, primarily due to loss of sea ice. The sea ice efficiently insulates the ocean. Furthermore, during sea ice is formation, latent heat is released to the atmosphere, implying that the ocean only cools once and where the sea ice melts (*Smedsrud et al.*, 2021). As the open water area continues to increase into the future, potential heat loss increases. This might again change the balance between the importance of local cooling versus advected anomalies on the AW heat variability. In the Nordic Seas in the twentieth century, there has been a sea ice loss, but only a small (and not significant) trend in heat loss. In *Smedsrud et al.* (2021) we argue that this is because the ice loss occurred over a region with cold surface water. Nonetheless, future studies should continue to investigate the various mechanisms of Arctic-Atlantic heat anomalies (*Asbjørnsen et al.*, 2019) in a warming and more ice-free Arctic, as the current relationships will likely prevail in the future. Potential changes in the large-scale atmospheric circulation must also be considered. In Paper I, we show that there is a good correlation between the large-scale atmospheric circulation and the AW inflow strength, but that this relationship is temporarily varying. The major governing circulation patterns discussed in Paper I and II might therefore undergo changes in the future.

Despite having a cold bias in the Nordic Seas and Central Arctic Ocean, the NorESM model used in Paper I, II, *Smedsrud et al.* (2021) and *Le Bras et al.* (2021) captures most of the observed variability well but loses its oceanic heat too quickly on the way northward. This is a common feature for many global models (*Ilicak et al.*, 2016), but the reasons are not yet fully understood. The coarse spatial resolution and the fact that models generally are too diffusive in the horizontal plane might be a possible explanation (*Docquier et al.*, 2020). Highly uncertain vertical mixing parameterizations in the Arctic — often tuned to represent the global ocean — is another possible explanation. Furthermore, and related to the spatial resolution factor, NorESM does not resolve eddies. A large part of the AW is recirculated before it reaches the FS and BSO, and what sets how much is being recirculated is still not completely clear to us. Furthermore, the results presented in Paper II showed that the models have very different AW circulation in the Central Arctic Ocean. The Lomonosov Ridge creates a potential vorticity barrier, so differences among the momentum advection schemes and momentum closure schemes might lead to differences among the models. These are all important problems, and in order to achieve more accurate projections, these should be topics for in-depth analyses and model developments. It is also important to note that the above problems are likely not automatically solved with increased spatial resolution. Significant improvement in mixing paramterizations are needed, and twin-type of experiments with different resolutions and different model systems are required to better understand the effect of resolution changes (*Docquier et al.*, 2020).

Ocean heat transport is calculated and discussed in papers I, II, and *Smedsrud et al.* (2021). We acknowledge that technically heat transport is only correctly calculated as a heat-transport convergence in a closed budget, which we do partly in Paper I and in *Smedsrud et al.* (2021). Heat transports through single straits cannot be independent of the reference temperature, and technically these are so-called "temperature-transports (*Schauer and Beszczynska-Möller*, 2009). In paper I, we still compare straits and sections to each other but argue that this is possible since we use the same reference temperature for all. In Paper II, the assumption of 0°C as a reference temperature in the BSO is equivalent to the assumption that all outflowing water masses (on the northern end of the Barents Sea) has this temperature. Time series of the heat transport through the northern gates of the Barents Sea was not available for all models in that study, but we know from earlier work (e.g., *Årthun et al.* (2012)) that the 0°C reference is an acceptable and working value for the Barents Sea. The Davis Strait outflow has a positive heat contribution (Paper I) because the outflow is colder than the reference temperature of °C. We do not believe that this is pertinent for our study but we have not investigated this further. The cold outflow could affect variability in the Labrador Sea, hence being important for the hydrographic conditions and sea ice here and in the Baffin Bay. What controls the cold outflow variability is not investigated in this paper either, but we assume that Arctic sea ice and conditions in the BG are important here.

5.2 AW forcing mechanisms

As discussed in Chapter 2.2.2, there are two perspectives on what drives the poleward AW flow: a "push" and a "pull" mechanism. However, which is the most important driver, and what governs temporal variations? Both the double-estuary (pull) perspective and the f/H following wind-driven (push) perspective provide good explanations, and these processes work together to facilitate AW inflow and circulation around the Arctic Ocean (*Timmermans and Marshall*, 2020). On their own, neither of these perspectives can provide a complete picture: in the double-estuary explanation, there is no role for topography or wind, and in the f/H frame work, the flow is barotropic, whereas strong stratification exists along the AW pathway (*Timmermans and Marshall*, 2020). The governing factor for the variability is likely a question of timescales; different processes might be more important at different timescales. This was further investigated in (*Smedsrud et al.*, 2021), where we particularly focused on the relationship between the volume transport and cooling in the Nordic Seas. Here were found that over long (+5 year) timescales, the overall relationship between the heat loss and inflow volume is clear, as was also suggested by *Eldevik and Nilsen* (2013). However, on a year-to-year basis, the wind variability appears to dominate (*Smedsrud et al.*, 2021). There is an especially high correlation between the simulated inflow across the GSR and the along-coast wind strength since the along-coast winds drive Ekman transport towards the coast, which drives a barotropic inflow. This strengthens our findings in papers I and II, where we show a clear relationship between NAO-type wind forcing in the Greenland Sea and the poleward AW volume transport. It also strengthens results from *Bringedal et al.* (2018), who studied the AW inflow across the GSR over the observed

period (1996–2016) and concluded that wind forcing drives much of the seasonal and interannual variability. Nonetheless, as discussed above, the importance of wind versus buoyancy forcing might change in the future as the Arctic continues to warm, the sea ice cover reduces, and the freshwater-driven estuarine forcing increases. The topic therefore warrant continued studies, and long-term observations across the AW inflow, such as the straits along the GSR and along the OSNAP array further south, are critical. Furthermore, long-term variations and trends in the wind field will likely affect the AW inflow in the future. Several studies have documented an increase in wind speed in some regions of the world ocean, which also needs to be continuously studied.

A general weakness of the experimental setup in Paper II was the permanent location of the wind stress anomaly, which was decided prior to our analysis. A lateral shift is explained briefly in Paper II, and the position and extension of the wind anomalies were chosen to match observed variability by *Marshall et al.* (2017), but we did not have the chance to investigated spatial changes fully because it would involve running nine different models with new forcing. The relative intensity of AW recirculation and FS/BSO inflows are likely impacted by the exact location of the northern edge of the wind stress anomaly. As a result, the importance of the lateral shift of the NAO-like SLP pattern remains unknown. It would be very interesting to see studies that investigate how the exact location of wind anomalies and the direction of different wind patterns affect the AW flow. Nevertheless, we expect the conclusions drawn in paper II to be robust and only mildly sensitive to lateral shifts of the wind anomalies. Another interesting impact of the GS wind forcing is the effect on the Arctic outflows. Our Paper II only focused on the impact of the northward flow, but results also indicated clear impacts on the outflow of PW and sea ice through the western parts of the FS, which was not subject to further analysis due to time limitations. Future work could expand the CRF approach on Arctic freshwater exports, building on the work by *Smedsrud et al.* (2017), who found clear relationships between sea ice export and local wind in the FS.

An ultimate motivation for understanding the mechanisms driving Arctic climate variability on different timescales is to improve projections of future changes, both on shorter interannual timescales and longer climate timescales. Such projections are useful not only for climate science but also for security and the management of fisheries, shipping, tourism, and other industries. For example, the relationship between ocean heat transport and sea ice anomalies has allowed for skillful predictions of the winter sea ice cover on interannual to decadal time scales (*Årthun et al.*, 2017; *Onarheim et al.*, 2015; *Yeager et al.*, 2015). The CRF method applied in Paper II allows for skillful prediction of the AW flow in the Nordic Seas and the Barents Sea based on wind anomalies. This methodology could be further advanced by looking at CRFs on different timescales, for example, seasonal timescales (*Lambert et al.*, 2019). Different predictors could also be tested. The methodology only works if there are not too many (interacting) feedback mechanisms but appears very valuable for systems where the response has a certain delay. We suggest that the CRF methodology could be used on other systems where there is a societal need for predictability and a know memory or delay in the system. The effect of runoff from Greenland is one example where CRFs could be useful. Using a step-change function on a proper fjord-ocean parameteriza-

tion (Section 5.4) could be an improvement of traditional "hosing experiments" (e.g. *Fichefet et al.* (2003); *Swingedouw et al.* (2013); *Yu et al.* (2016)).

Although not directly investigated in this thesis, our work connects to studies focusing on the larger scale ocean variability and the AMOC. We will not go into detail, but the AMOC has for obvious reasons been subject to numerous studies over the last decades and was truly popularized as it featured in the movie "Day after tomorrow" in 2004. Several studies associate a strengthened AMOC with increased poleward ocean heat transport, which leads to the AMOC influencing Arctic sea ice and Arctic temperatures indirectly (*Yeager et al.*, 2015; *Zhang*, 2015). Furthermore, the AMOC is likely influenced by the flux of Arctic freshwater originating from high northern latitudes (*Lozier*, 2012; *Lozier et al.*, 2019). On the other hand, the inflow of AW to the Nordic Seas is projected to increase, whereas the AMOC is projected to weaken (*Årthun et al.*, 2019; *Nummelin et al.*, 2017). It thus appears that we do not yet have a complete mechanistic understanding of how the northward flow of AW and the AMOC is connected. Another possibility is that their connection changes completely in the future. Nonetheless, Arctic variability, how it connects to variability further south, and all the feedback loops involved remain an important topic of research.

5.3 Arctic Ocean stratification

Paper IV investigates the past, present, and future changes of Arctic Ocean stratification. This is still a manuscript in progress but already inspires some elaborations. A major finding from this work is that in the future, some CMIP6 models simulate an EB freshening both at the surface and in the AW layer, whereas some models simulate an EB freshening in the surface layer only. The mechanisms behind these different freshening regimes and the debate of local freshwater forcing versus remote (AW/Pacific Water) forcing are not yet completely certain. Based on analysis of spatial salinity trends in NorESM and CESM-LE (Paper IV), we speculate that the AW freshening in the NorESM is a signal that originates in the Arctic and propagates to the North Atlantic Subpolar Gyre before it returns to the AW inflow. In CESM-LE, the Arctic freshening leaves the Arctic and does not return, perhaps due to differences in the large-scale circulation and different balances between the horizontal and overturning parts of the circulation. However, this cannot be confirmed without investigating long-term freshwater transports through the Arctic gates as recently done by *Zanowski et al.* (2021). Future analysis potentially included in this manuscript is a complete freshwater budget of the Central Arctic Ocean. Comparing the various contributions of freshwater to the Arctic Ocean in the future and temporal variations and changes for an ensemble of different model systems might shed light on the mechanisms at play. Factors that could be included are river runoff, contributions from sea ice melt/freeze, precipitation minus evaporation, and AW and Pacific Water contributions. Paper IV furthermore confirms the statement in the introduction to this chapter; that a multi-model approach is necessary when investigating Arctic Ocean dynamics. We show that although there is an agreement in the BG, the models have some fundamental differences, leading to opposite projections of future stratification in the EB region. This might have consequences for the local sea ice cover and the potential for dense water formation at new loca-

tions (*Lique and Thomas*, 2018), as observed in the Barents Sea (*Skagseth et al.*, 2020) and north of Svalbard (*Athanase et al.*, 2020; *PérezHernández et al.*, 2019). There is no way to tell which projection is more realistic, but this "negative result" is still very important.

5.4 Fjord exchange parameterizations

In Paper III, we lay the foundation for what could become a parameterization of fjord-ocean exchange in Greenland. Coupling the Greenland ice sheet and active ice sheet models to the ocean and ocean models is an ongoing and important research topic. The impact of Greenland's meltwater on ocean circulation is still poorly known but could potentially be serious. Most ocean models do not include the water mass transformation which occurs in the fjord as a process. The models either dump the freshwater input (e.g., *Bamber et al.* (2018)) as a virtual salinity flux at the surface or the freshwater is evenly distributed in the uppermost layers. The upwelling and mixing with AW within the fjord are usually not included. Therefore, the relationships we have found between shelf and GMW properties and the dilution coefficients provide a solid prospect for a parameterization of GMW export. However, we only investigated a single glacier-fjord system in northwest Greenland. The GMW properties need to be investigated in multiple fjord systems along the Greenland coast. It is possible that similar results can be obtained from other fjords that share characteristics with Upernavik, such as a deep sill and limited spatial variability within the fjord (*Straneo et al.*, 2012). On the other hand, there are also many fjord systems in Greenland with completely different circulation regimes such that our methods might not work. We did not discuss the details of circulation in Upernavik in Paper III, as we did not have access to current observations. Previous studies investigating Greenland fjord circulation found that the circulation is complicated and forced by multiple external factors *Straneo et al.* (2011); *Sutherland et al.* (2014). For example, *Sutherland et al.* (2014) found evidence in Kangerdlusauq and Sirmilik fjords in southeast Greenland of a seasonally varying intermediary circulation, superimposed on the weaker estuarine circulation. They also showed that the estuarine circulation part is complicated because it consists of multiple outflows (at the surface and intermediate-depth as GMW). The intermediary circulation could be forced by density variations near the fjord mouth, driven by local winds, or tides (*Sutherland et al.*, 2014). This circulation depends on the detailed fjord bathymetry and geography and is likely to vary greatly from fjord to fjord. Another example of a completely different fjord system where our methods are not likely to work is the Sherard Osborn fjord in northern Greenland, where a shallow sill limits the inflow of warm AW, effectively shielding the Ryder glacier from the warm subsurface waters (*Jakobsson et al.*, 2020). Observations of many different fjord systems are required to produce a more accurate parameterization that could work for different fjord systems or perhaps a certain region. There is also a need for longer-term observations, including current measurements, to properly resolve the seasonal variability. Furthermore, observations need to be obtained both inside the fjords and on the continental shelf outside the fjord's mouth. Future work should also include a method to include the surface layer in the GMW export. We know that the surface layer includes a significant portion of the runoff and meltwater, but it is not easy to separate the different freshwater sources without noble

gases. The surface layer is also highly variable over short time periods and can be difficult to observe due to icebergs and ice melange.

5.5 Concluding remarks

In order to better understand the variability and impacts of the northward AW flow in the Arctic Ocean and skillfully predict future climate, continuous monitoring of the gateways is of paramount importance. Long observational time series of the Central Arctic Ocean basins also remain critical to further improve our understanding of the complex Arctic Ocean climate system. Furthermore, continued focus on improving parameterizations of key ocean processes such as water mass transformation, mixing, and brine release in large-scale ocean circulation models is needed. The effect and importance of model resolution also warrant further investigations. Improved understanding of these factors — and of the Arctic Ocean as a part of the global ocean and climate system — can only be reached through continuously combining modeling efforts with observations. By assessing the AW variability, its forcing mechanisms, and the impacts of this variability, the four papers that constitute this thesis emphasize the importance of warm and saline AW in the Arctic climate system. In summary, the main conclusions are:

- AW heat transport variability dominates the oceanic heat transport variability in the Northern Hemisphere (Paper I)
- AW volume transport changes mainly due to wind stress curl, and AW temperature mainly due to advection and local atmospheric forcing (Paper I)
- Stronger/weaker winds over the Greenland Sea results in stronger/weaker flow of Atlantic Water in the Nordic Seas and into the Arctic Ocean (Paper II)
- In the Barents Sea, there is a linear relationship between Atlantic Water volume and heat transport, surface heat loss, and sea ice extent (Paper II)
- Freshwater from Upernavik fjord in northwest Greenland is exported as a diluted water mass at depth named “Glacially Modified Water (GMW), which consists of major parts AW and PW and only minor parts subglacial discharge and meltwater (Paper III)
- Variations in GMW properties reflect variations in the AW and PW source waters, emphasizing a close relationship between the shelf properties and export from Upernavik fjord (Paper III)
- CMIP6 simulations project that under a strong global warming scenario (SSP585), the AW will continue to warm throughout the twenty-first century, and the entire Arctic Ocean will undergo a strong freshening (Paper IV)
- CMIP6 models consistently project a strengthened stratification in the Amerasian Basin in the future, whereas in the Eurasian Basin, half of the models investigated show a weakened stratification in the future and half of the models show a strengthened stratification (Paper IV)

Chapter 6

Scientific results

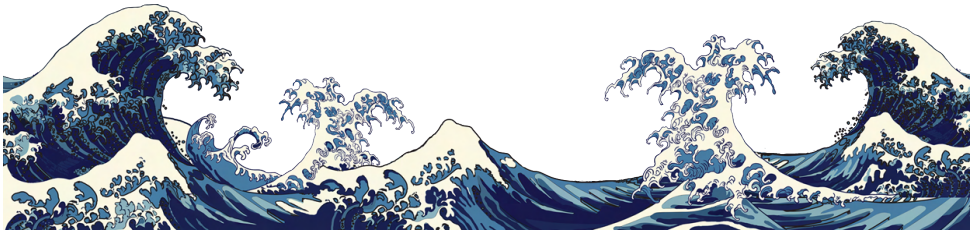

Paper I

Atlantic Water heat transport variability in the 20th century Arctic Ocean from a global ocean model and observations

Muilwijk, M., Smedsrud, L.H., Ilicak, M., Drange, H.
Journal of Geophysical Research: Oceans, **123(11)** (2018)

Journal of Geophysical Research: Oceans

RESEARCH ARTICLE
10.1029/2018JC014327

Special Section:
Forum for Arctic Modeling and Observational Synthesis (FAMOS) 2: Beaufort Gyre phenomenon

Atlantic Water Heat Transport Variability in the 20th Century Arctic Ocean From a Global Ocean Model and Observations

Morven Muilwijk[1,2], **Lars H. Smedsrud**[1,2,3], **Mehmet Ilicak**[4], **and Helge Drange**[1,2]

[1]Geophysical Institute, University of Bergen, Bergen, Norway, [2]Bjerknes Centre for Climate Research, Bergen, Norway, [3]University Centre in Svalbard, Longyearbyen, Svalbard, [4]Eurasia Institute of Earth Sciences, Istanbul Technical University, Istanbul, Turkey

Key Points:
- Atlantic Ocean heat transport variability dominates in the Northern Hemisphere and on centennial scale
- Volume transport changes due to wind stress curl and temperature due to advection and local forcing
- Ocean heat transport in the Fram Strait is dominated by temperature variability but in the Barents Sea Opening by volume variability

Supporting Information:
- Supporting Information S1

Correspondence to:
M. Muilwijk,
morven@uib.no

Citation:
Muilwijk, M., Smedsrud, L. H., Ilicak, M., & Drange, H. (2018). Atlantic Water heat transport variability in the 20th century Arctic Ocean from a global ocean model and observations. *Journal of Geophysical Research: Oceans*, *123*. https://doi.org/10.1029/2018JC014327

Received 3 JUL 2018
Accepted 12 OCT 2018
Accepted article online 18 OCT 2018

Abstract Northward ocean heat transport and its variability influence the Arctic sea ice cover, contribute to surface warming or cooling, or simply warm or cool the Arctic Ocean interior. A simulation with the forced global ocean model NorESM20CR, aided by hydrographic observations since 1900, show large decadal fluctuations in the ocean heat transport, with the largest variations in the Atlantic sector. The simulated net poleward ocean heat transport over the last century is about 68 TW, and 88% of this occurs in the Barents Sea Opening (45 TW) and the Fram Strait (15 TW). Typical variations are 40 TW over time scales between 5 and 10 years, related to thermohaline and wind stress forcings. The mean heat transport in the Davis Strait is about 10 TW, and less than 5 TW flows north in the Bering Strait. The core temperature of the Atlantic Water (AW) entering the Arctic Ocean has increased in recent decades, consistent with an ongoing expansion of the Atlantic domain (Atlantification), but earlier warm events are also documented. The temperature of the northward-flowing AW thus plays a vital role, with decadal variations of around 0.5 °C. The Nordic Seas atmosphere contributes with thermodynamic forcing, dampening the advected heat anomalies. In the Barents Sea, variations in the inflow volume flux dominate, while variations in temperature dominate the heat transport in the Fram Strait. There are significant trends over recent decades, also dominated by the Barents Sea that presently has 1 Sv higher volume transport and +1.0 °C warmer AW than the long-term mean.

Plain Language Summary Ocean currents bring heat northward into the Arctic Ocean. This ocean heat influences the sea ice cover regionally and warms the Arctic Ocean surface and interior. Warm and salty Atlantic Water that enters the Arctic Ocean through the Fram Strait and the Barents Sea dominates the oceanic heat contribution to the Arctic Ocean in the 20th century. In this study, we have investigated how this ocean heat transport has varied over time and which physical mechanisms that influence these variations. Understanding these natural variations is important for explaining ongoing Arctic change today. Our main tool for investigation is a global ocean model driven by observed atmospheric variations, and we compare this model with observations of temperature and salinity in the Nordic Seas. We find that the ocean heat transport has varied on different time scales and that these variations are linked to changes in the wind systems in the Nordic Seas, atmosphere-ocean heat exchanges, and, to some extent, local winds in the straits. Overall, the ocean heat transports and Atlantic Water temperatures have increased during recent decades. These changes are especially large at the Barents Sea entrance where the water has warmed about 1 °C.

1. Introduction

A shrinking cryosphere, including accelerated loss of Arctic sea ice, is one of many indicators of global-scale warming. The Arctic, as an example, has lost more than half of its sea ice volume over the last 40 years (Carmack et al., 2015; Comiso, 2012). The rise of surface air temperature has also been anomalously large at high northern latitudes, a feature often termed *Arctic Amplification* (Chylek et al., 2009; Serreze et al., 2006; Serreze & Barry, 2011). In recent years the surface warming has been the largest in the Barents Sea, where the position of the sea ice edge has been linked to variations in the inflow of Atlantic Water (AW; Årthun et al., 2012; Koenigk & Brodeau, 2017; Onarheim & Årthun, 2017; Onarheim et al., 2015, 2018; Sandø et al., 2014). For the future decades and century, it is still an open research question to which extent the Arctic Ocean will be dominated by enhanced warming through the surface or by an increased poleward ocean heat transport (Burgard

& Notz, 2017). Here we investigate how ocean heat transport toward the Arctic Ocean has varied in the 20th century and what the controlling mechanisms are. We present a century-long model simulation, supported by long-term observations, exploring variations in heat transport to the Arctic Ocean since the end of the 19th century. The model used is the ocean and sea ice component of the Norwegian Earth System Model (NorESM-O), forced by a reanalysis data set for the period 1871–2009 (He et al., 2016). The following topics are addressed: (i) identification of the interannual- to decadal-scale variations in the poleward heat transport, (ii) the underlying mechanisms responsible for these variations, and (iii) explanation of how the variations are distributed across the main straits connecting the Arctic to the global ocean.

Oceanic heat enters the Arctic Ocean as AW through Fram Strait (FS) and the Barents Sea and as Pacific Water (PW) through the Bering Strait (Carmack et al., 2015). Based on early observations, Aagaard (1989) suggested that AW should be the most important oceanic heat supply to the Arctic Ocean. Historical observations show a warming trend in core temperature of AW entering the Arctic Ocean over the last few decades (1977–2015; Alexeev et al., 2013; Polyakov et al., 2012, 2017; Quadfasel et al., 1991). The interaction between AW, PW, and Arctic sea ice has in previous studies been discussed due to the strongly stratified cold halocline layer, with temporal and spatial variations (Ivanov et al., 2016; Woodgate et al., 2006; R. Zhang, 2015). The sea ice near the inflow regions may respond passively to variations in AW and PW heat transports, and recent studies now suggest a direct effect on sea ice loss both in the Eurasian and Canada Basins (Polyakov et al., 2017; Woodgate et al., 2010).

The recent change in the Eurasian Basin has by Polyakov et al. (2017) been discussed as part of an *Atlantification* of the Arctic Ocean, that is, an expansion of the Atlantic domain. Nansen (1902) already identified AW as the key heat source for the Arctic Ocean. Roles of the different AW branches in transporting heat variability are still not clear, especially on decadal and multidecadal time scales. A portion of the suggested Atlantification and recent warming has been attributed to the current, human-induced global warming. However, past periods of warm AW, like the *Early Twentieth Century Warming* (ETCW) during the 1930s and 1940s have been thoroughly documented (Bengtsson et al., 2004; Yamanouchi, 2011). Thus, it is reasonable to assume that the AW warming trend in the Arctic Ocean should be a manifestation of both anthropogenic forcing and multidecadal variations.

The paper is organized as follows: A summary of the ocean heat transport toward the Arctic Ocean and its variability is given in section 2. In section 3, the model, available observations, and methods are outlined. The simulated volume and heat transports through Arctic Ocean straits, the observed AW variability, and the model's ability to simulate the observed variability are presented in section 4. We then discuss the drivers of heat and volume transport variations and the covariability between the main gateways in section 5. Finally, we summarize our conclusions in section 6.

2. Background

2.1. AW and PW in the Arctic Ocean

The warm and salty AW enters the Nordic Seas (consisting of the Greenland, Iceland, and Norwegian Seas) close to the eastern coast of Iceland and through the Faroe- Shetland Channel close to Shetland (Orvik & Niiler, 2002; Figure 1). After it has entered the Nordic Seas, the AW continues northward toward the Arctic Ocean in two different branches, a western branch that feeds the interior of the Norwegian Sea and an eastern branch, more commonly known as the Norwegian Atlantic Slope Current, flowing northward as a near barotropic shelf-edge current (Orvik et al., 2001).

Off the northern coast of Norway, the Norwegian Atlantic Slope Current divides in two branches, one entering the Barents Sea between the Bear Island and Norway, hereafter called the Barents Sea Opening (BSO), and one, the West Spitsbergen Current, flowing northward past Svalbard and into the FS (Aagaard & Carmack, 1989). A large part of the latter current recirculates westward in the FS (Hattermann et al., 2016) and joins the southward flowing East Greenland Current toward the Denmark Strait, forming a cyclonic loop in the Nordic Seas. The Barents Sea is one of the shallow (approximately 200 m deep) shelf seas that is part of the Arctic continental shelf. The AW that enters here is cooled before it enters the deep Arctic Ocean through the St. Anna Trough (Smedsrud et al., 2013; Figure 1).

Relatively warm and saline PW enters the Arctic Ocean through the shallow (50 m) and narrow (85 km) Bering Strait (Rudels, 2015). This PW then flows through the Chukchi Sea, where it is modified by heat exchange, runoff, ice formation, and ice melt, before it finally enters the deep Canadian Basin at the shelf break (McLaughlin et al., 2004). The PW is less saline and colder than the AW and is mainly confined to the Canadian

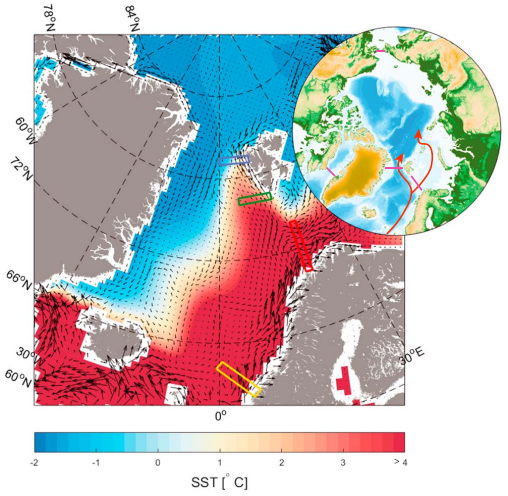

Figure 1. Overview map of the Atlantic Water inflow (red arrows) in the Nordic Seas and Arctic Ocean (circular) with simulated Sea Surface Temperature (SST) from the NorESM20CR simulation. Black arrows show the long-term annual mean barotropic current from the model (vertical and temporal mean). Four regions along the Atlantic Water flow path are outlined with colored lines: Svinøy (gold), the Barents Sea Opening (red), Sørkapp (green), and the Fram Strait (blue). The Arctic Ocean straits are shown in magenta in the overview map.

Basin (Rudels, 2015). Although the mean PW temperature is quite low, the summer PW is relatively warm and plays an important role for the hydrographic conditions and sea ice in the region (Woodgate et al., 2010).

Several mooring arrays have been deployed for more than 20 years in the different gateways with the aim of closing the Arctic Ocean heat, volume, and salt budgets. These recordings show a strongly seasonally varying AW flow in the FS, with volume transports in winter twice as large as in summer (4 and 2 Sv, where 1Sv = 10^6 m^3/s; Beszczynska-Möller et al., 2012). The corresponding heat transport varies from around 28 TW in summer to 46 TW in winter (relative to a reference temperature of 0 °C; Beszczynska-Möller et al., 2012; Schauer, 2004). A portion of this heat recirculates in the FS without entering the Arctic Ocean, with an annual net inflow into the Arctic Ocean through the FS of about 40 TW (Schauer & Beszczynska-Möller, 2009). In the BSO, the seasonal difference is smaller, with a winter mean volume transport of 1.7 Sv and a summer mean of 1.3 Sv (Ingvaldsen et al., 2004a). The observed heat transport through the BSO is about 70 TW (Skagseth et al., 2011).

Woodgate et al., (2006, 2010) gave an estimate of the mean volume transport of PW through the Bering Strait at around 1 Sv, with a corresponding mean heat transport of approximately 12 TW. Volume transports vary from 0.4 Sv in winter to 1.3 Sv in summer, and temperatures vary from freezing temperature in winter to 4 °C in summer (Woodgate, 2005). Variability in volume is explained by a combination of local winds and variation of the large scale pressure difference between the Pacific and the Arctic (Woodgate et al., 2010). Despite its comparatively small volume and heat contribution, the inflow of PW through the Bering Strait, and especially the timing of heat input, has a large impact on the sea ice cover in the western Arctic Ocean (Woodgate et al., 2010).

A final connection between the Arctic Ocean and the Atlantic Ocean is through the Canadian Arctic Archipelago via the Davis Strait (Figure 1; Beszczynska-Möller et al., 2011; Rudels, 2015). The net outflow through Davis Strait is estimated between 2.3 and 2.6 Sv (Beszczynska-Möller et al., 2011; Curry et al., 2011). Due to the low temperatures (negative) of the outflow, the heat transport through Davis Strait has a maximum positive value of 18–20 TW (Cuny et al., 2005; Curry et al., 2011).

Here we mainly focus on the interannual- to decadal-scale variations and therefore mainly consider annual mean transports. For temperature and salinity evaluation, a cross section across the FS is defined at 79° N (blue box in Figure 1) and one further south at Sørkapp (76° N), the latter aligned with a repeat hydrological section operated by the *Norwegian Institute of Marine Research* (Lind & Ingvaldsen, 2012; green box in Figure 1). The BSO section is defined between the islands *Fugløya* and *Bear Island*, where we also have a long record of observations (red box in Figure 1). AW properties have also been investigated in a section at 64° N, commonly known as the *Svinøy section* (yellow box in Figure 1).

2.2. AW Long-Term Variability

Based on available observations, the inflow of AW into the Arctic Ocean has varied both in temperature, volume, and salinity. For example, over the last few decades, the AW layer in the Arctic Ocean has been subject to warming and shoaling. Early evidence of this warming was found in the Nansen Basin in 1990 (Quadfasel et al., 1991). In the years to follow, several studies have confirmed the warming trend of AW at different locations in the Arctic Ocean (Carmack et al., 1995; Grotefendt et al., 1998; Morison et al., 1998, 2000; Rudels et al., 2000; Schauer et al., 1997, 2002; Steele & Boyd, 1998; Swift et al., 1997). Although the absolute warming has been spatially variable, the maximum core temperature of the AW has increased with 1–2 standard deviations from the 1970s to the early 2000s (Polyakov et al., 2012). This change has, at least partially, been attributed to global warming (Banks et al., 2000; Barnett et al., 2001, 2005; Kay et al., 2011; Levitus et al., 2000; Polyakov et al., 2010).

The AW warming has not been constant in time. A local maximum was observed in the mid-1990s (Polyakov et al., 2010), followed by a minimum where the warming slowed and a slight cooling in the late 1990s (Boyd & Steele, 2002). Remnants of this signal arrived in the Canadian Basin in the early 2000s (Shimada, 2004). It appears that the warming of AW occurs as pulses. For example, the AW temperatures in the FS were lower in 1997 than in the mid-1980s (Rudels et al., 2000) but increased again after 1998, indicating a new warm pulse (Dmitrenko et al., 2006, 2008; Polyakov, 2005).

Although the recent anomalies in the AW inflow are warmer than previously observed, it has been suggested that some of the changes described above can in part be attributed to multidecadal fluctuations with a time scale of 50–80 years (Polyakov, 2005; Polyakov et al., 2004, 2009; Smedsrud et al., 2013). The AW temperature records in the Arctic Ocean show two warmer periods, one in the 1930s to 1940s (ETCW) and one in the 1990s to 2000s, and two colder periods, one early in the 1900s and the second one in the 1960s to 1970s (Polyakov, 2005; Polyakov et al., 2004). Also in the Barents Sea, the AW temperature shows substantial variations on decadal time scales. Observations from the Kola section since 1900 (Tereshchenko, 1996) show a cold period in the early 20th century, a warm period between 1930 and 1950, followed by a cold period until the 1970s, and finally the ongoing warming. These low frequency variations in AW temperature agree well with the Atlantic Multidecadal Oscillation index of Sutton and Hodson (2005), representing the large-scale sea surface temperature variation throughout the North Atlantic Ocean.

The AW inflow volume transport to the Arctic Ocean also varies, but unfortunately, the current observations are more sparse than hydrographic observations. In BSO and FS, currents have been observed continuously by moorings since 1997 (Beszczynska-Möller et al., 2012; Fahrbach et al., 2001; Ingvaldsen et al., 2004a). At the Svinøy section, near the AW inflow to the Nordic Seas, the instrumental record of ocean currents dates back to 1995 (Orvik et al., 2001). All these time series show a relatively large (1–2 Sv) year-to-year variability, with an exception of the Svinøy section volume transport that increased with more than 3 Sv in 1997. However, the time series are too short to reveal any decadal or multidecadal variations.

Helland-Hansen and Nansen (1909) were the first to give a comprehensive description of the hydrographic conditions in the Norwegian and the Barents Seas and the relationship between the two. They indicated, for example, a 2-year delay in the temperature signal from Sognesjøen (61° N) to the Russian Kola section downstream in the Barents Sea. We now know from several other studies that temperature anomalies propagate northward from the North Atlantic along the path of the Norwegian Atlantic Slope Current (Furevik, 2000; Holliday et al., 2008; Yashayaev & Seidov, 2015). This poleward propagation is not only the case for temperature anomalies but also for salinity. For example, Årthun and Eldevik (2016) and Holliday et al. (2008) showed that interannual to decadal ocean heat anomalies propagate persistently toward the Arctic, and Glessmer et al. (2014) showed the same for salinity anomalies.

2.3. Forcing Mechanisms Controlling AW Variability

Both thermodynamic atmospheric forcing and changes in ocean volume transport have been suggested to explain the above-mentioned temperature and heat anomalies in the Nordic Seas (Årthun & Eldevik, 2016; Carton et al., 2011; Furevik, 2001; Mork et al., 2014; Skagseth et al., 2008). Mork et al. (2014) found that heat fluxes are responsible for about half of the observed interannual heat content variability but that the fraction is nonstationary in time. Variations in AW volume are clearly important, but explaining the forcing mechanisms for this flow is an ongoing research question (Skagseth et al., 2008). The flow is likely to be both thermohaline and wind driven, with the relative role of the forcing components varying on different time scales (Skagseth et al., 2008).

A major part of the thermohaline forcing is the cooling of AW as it moves northward. This generates an outflow of denser waters from the Nordic Seas. This outflow lowers the sea surface height in the Nordic Seas and acts as a "pull" mechanism on the AW. Hansen et al. (2010) showed that this is the case for the AW inflow through the Iceland-Faroe branch, and Richter et al. (2012) showed that 22% (Iceland-Faroe branch) and 38% (Faroe-Scotland branch) of the variations in the volume transport can be explained using direct observations of sea surface height.

A number of previous studies have investigated the wind-driven forcing (Herbaut et al., 2017; Orvik & Skagseth, 2003; Richter et al., 2009; Sandø et al., 2012; Skagseth, 2004; Skagseth & Orvik, 2002). Alongshore winds at the Norwegian coast, for example, induce Ekman transport toward the coast which is balanced by an along-slope current. This mechanism is one of the key drivers of variations in the AW inflow and can be linked

to atmospheric lows with a typical trajectory toward northeast (Skagseth, 2004; Skagseth & Orvik, 2002). Orvik and Skagseth (2003) also found correlation between the Svinøy section volume transport and the wind stress curl at 55° N. However, Sandø and Furevik (2008) showed that the latter relationship breaks down after 2004 and suggested that the correlation is only high when the winter mixed layer is shallower than the sill depth across the Greenland-Scotland Ridge, which happens in years when the atmospheric forcing is relatively weak. Furthermore, Sandø et al. (2012) showed that the variability of AW inflow is anticorrelated with the dense overflow in the Denmark Strait and Faroe-Shetland Channel and that this also covaries with an atmospheric pattern resembling the North Atlantic Oscillation (NAO) (Hurrell, 1995). The NAO is the dominant mode of variability in the North Atlantic region (Hurrell, 1995) and has been associated with interannual and decadal variations in the AW inflow by a number of studies (Blindheim et al., 2000; Dickson et al., 1988a; Hurrell & Deser, 2009; Krahmann et al., 2001).

It has also been suggested that the NAO affects the volume of AW entering the Barents Sea and hence the fraction of water that recirculates or reaches the FS. Furevik (1998), Lien et al. (2017), and J. Zhang et al. (1998) showed that during periods with strong NAO, the AW inflow was stronger and had an anomalous eastward extension, resulting in less water being recirculated in the Nordic Seas and more entering the Barents Sea. However, Ingvaldsen et al. (2004b) and Lien et al. (2017) found that the flow through the BSO is also highly dependent on the local wind pattern and positive wind stress curl in the Barents Sea which in turn sets up Ekman transport toward the coast. Finally, Smedsrud et al. (2013) found that the NAO correlation broke down after 2000, and Lien et al. (2013) showed that the flow into the BSO was strongly affected by northern Barents Sea winds.

3. Data and Methods

3.1. Model Description

The global ocean-ice components of the Norwegian Earth System Model (NorESM) are used in this study. A general description of the model is given by Bentsen et al. (2012), while the setup of our simulation is similar to that described in He et al. (2016). The model originates from the Miami Isopycnic Coordinate Model but is extensively updated, and the sea ice component is the Los Alamos Sea Ice Model version 4 (Hunke et al., 2008). The sea ice and ocean components are configured on the same grid and fully coupled within the Community Earth System Model version 1 framework (Hurrell et al., 2013). For the experiments presented here, a tripolar grid is used with approximately 1° zonal resolution along the equator. The Northern Hemisphere grid singularities are located in Canada and Siberia. This gives a typical resolution in the Nordic Seas-Arctic Ocean of approximately 40 km. In the vertical, the ocean model has 51 isopycnals referenced to 2,000 dbar, and a surface mixed layer divided into two nonisopycnic layers. The ocean-ice model is forced by a 20th century atmospheric reanalysis forcing ($20CR_{adj}$) which is a blended data set derived from the ensemble mean version of the 20th Century Reanalysis (20CRv2; Compo et al., 2011), satellite observations, and the corrected Coordinated Ocean-ice Reference Experiments phase-II (CORE-II) forcing for the period 1871 to 2009 (He et al., 2016). The original 20CRv2 resulted in Sea Surface Temperature and Sea Surface Salinity biases and hence an unbalanced ocean heat budget. This is why the 20CRv2 was adjusted according to satellite observations and CORE.v2. A detailed description of the correction, the different forcing components, and an evaluation of the data set is given in He et al. (2016). We acknowledge that the model has relatively coarse resolution, and it is difficult to say what impact this has on the transports through the FS and BSO. The simulation does not resolve mesoscale eddies and relies on eddy parameterizations such as Gent and Mcwilliams (1990) to represent cross shelf transport due to mesoscale eddies. In addition, parameterizations of surface processes in the mixed layer are also important to capture the right water mass transformation in the Nordic Seas where buoyancy fluxes are quite strong.

3.2. Observational Data

The observational data used in this study consist of several data sets. Time series of mean AW temperature is based on the NOAA Climatological Atlas of the Nordic Seas and Northern North Atlantic (hereafter referred to as NSA; Korablev et al., 2014). This data set is built on an enhanced collection of observations spanning over a period from the end of the 19th century to 2012. It is based on in situ data that have been considerably improved (data addition, editing, and quality control) within the framework of the Global Oceanographic Data Archeology and Rescue Project (Korablev et al., 2014). The uncertainty, instrumental error, signal-to-noise ratio, and method to calculate the annual means in this data set are being discussed in detail by Korablev et al. (2014). A major source for uncertainty is the number of stations. An error estimate is provided with the

data set, and we have used a threshold that excludes grid cells with a relative error higher than 0.25. In addition, we have performed a manual control of all annual profiles used in our analysis. To reduce the seasonal bias of the annual means, a threshold value was used with at least one winter and summer value before averaging. The standard error is larger in the beginning of our time series because of fewer observations. However, we argue that there is enough data to calculate an annual mean. In addition, temperature and salinity profiles from the N-ICE2015 drift expedition North of Svalbard (Meyer et al., 2017), the World Ocean Atlas (WOA13) global climatology (Boyer et al., 2013), the Polar Science Center Hydrographic Climatology (PHC3) (Steele et al., 2001), and a global monthly isopycnal upper-ocean climatology (MIMOC; Schmidtko et al., 2013) have been used to compare and quality control the model simulation. Profiles are shown in Supporting Information S1.

3.3. Approach

Direct comparisons of AW temperature anomalies in different regions, and between observations and model, are challenging. Several studies have used the maximum core temperature of the AW layer when discussing AW variability. In this study, we rather choose the mean AW temperature between 50 and 700 m. This choice is based on the fact that many of the historical observations are vertically interpolated or that they have coarse vertical resolution. Arctic wide heat transports are calculated across the whole strait (magenta lines in Figure 1), using a reference temperature of $T_{\mathrm{ref}} = 0\,^{\circ}\mathrm{C}$. Since the same reference temperature is used for all straits, we can compare them with each other. The heat transports that are computed in the model include both the advective and diffusive components at each of the grid cell boundaries. The same is true for simulated volume transports. Division into northward and southward AW flow through the FS and BSO is done off-line by summing up transports in all grid cells and at all depths with velocities in the meridional direction. The decomposition of heat transport into volume and temperature contributions ($v'\bar{T}c_p \varsigma\, \bar{v}T'c_p$) is also done off-line by using a mean temperature and mean volume transport averaged over the whole 120-year simulation period. Here the primes denote varying annual averages.

When low-passed filtered data are presented, a third-order Butterworth filter has been used with a cutoff period of 2 years to emphasize interannual and decadal variations. For the spatial correlation fields, detrended annual mean anomaly time series are correlated against detrended annual mean 2-D fields. All correlations in the text are significant with a significance level of 95%.

4. Results

4.1. Simulated Heat and Volume Transport Through Arctic Ocean Straits

Simulated volume transports from the NorESM20CR simulation for the period 1890–2009 are presented in Figure 2a, and the temporal evolution of the simulated heat transports through Arctic Ocean Straits is shown in Figure 2b. The northward-flowing AW in the FS and BSO combined stands for 80–90% of the total ocean heat transport toward the Arctic Ocean over the last century. Here the AW is defined as all water with positive northward velocities, with no temperature cutoff. We also find that nearly all ($r = 0.97$) of the year-to-year variability in total ocean heat transport can be explained by variations in AW heat. This is our motivation to assess the AW variability and the forcing mechanisms in closer detail. A major part of the AW already recirculates before it reaches the FS but also a portion recirculates back into the FS after it has reaches the Arctic. We note that eddies are not resolved in our model.

The simulated volume transport through the Bering Strait remains nearly constant at 0.8 Sv which is also consistent with observations and the CORE-II experiment (Ilıcak et al., 2016; Tsubouchi et al., 2018; Woodgate et al., 2005). The simulated outflow through Davis Strait is approximately 1–2 Sv, which Tsubouchi et al. (2018) estimated at 2.1 Sv based on observations from Curry et al. (2014). Cuny et al. (2005) estimated this to be approximately 2.6 Sv based on observations between 1987 and 1990. The multimodel mean from the CORE-II model comparison experiment (Ilıcak et al., 2016) is 1.75 Sv, a value consistent with our simulation.

Observation-based estimates of volume transport through Arctic Ocean straits by Tsubouchi et al. (2018) from 2005 to 2006 indicate a net southerly directed volume transport through the FS of about 1 Sv, consisting of a southerly directed transport in the East Greenland Current of about 8 Sv and a northward-directed transport in the West Spitsbergen Current of about 7 Sv. Earlier estimates from Schauer et al. (2008) and Beszczynska-Möller et al. (2011) for the period 1997 to 2006 indicate the same to a northward directed flow of 5–7 Sv and a southerly directed flow of 3–5 Sv. The simulated net volume transport through the FS varies between approximately 1 and 2 Sv southerly directed, which is in agreement with the observed 1 Sv (Tsubouchi et al., 2018). This is also in agreement with mean values from the CORE-II model comparison

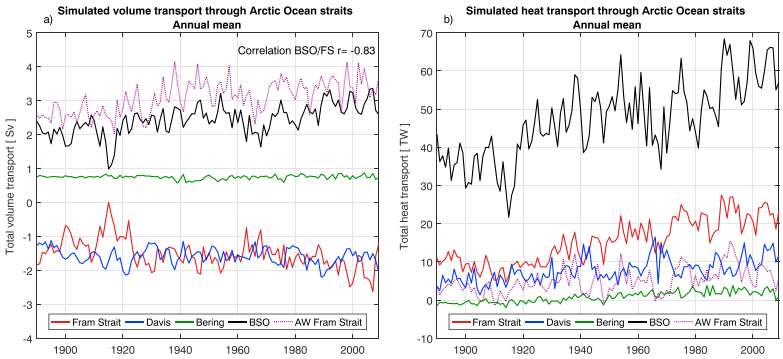

Figure 2. Time series of (a) simulated volume and (b) heat transports through the Arctic Ocean Straits from NorESM20CR. The violet-dotted line shows the heat and volume transport of only the northward-flowing part (AW) in the FS, while the red line shows the net transport of both the northward and the southward flow through FS. BSO = Barents Sea Opening; FS = Fram Strait; AW = Atlantic Water.

experiment (Ilıcak et al., 2016). In the CORE-II study it was noted, however, that the northward and southward transports were underestimated by a factor of two or more by all models. Most models in the CORE-II experiment were coarse like NorESM; most models had 1° horizontal resolution, three models had 0.5° resolution, and one model had 0.25° resolution. The same was found by Pietschnig et al. (2017), and this is also the case in our simulation, with a northward transport of about 3–4 Sv in the FS. In the BSO, Tsubouchi et al. (2018) estimated a volume transport just above 2 Sv, which is consistent with observations provided by Smedsrud et al. (2013) and the CORE-II experiment. From 1890 to 2009, NorESM20CR simulates a BSO volume transport ranging from 1 to 3 Sv with a mean of approximately 2.5 Sv and is thus also consistent with observations and CORE-II values. Note however that there is an increase in flow over the century of approximately 50% for AW in the FS and BSO. What causes this increase is still an open question. We have not investigated this in particular in this analysis but hope to include this in future work. Here we focus mainly on the interannual variations.

The BSO is the largest contributor of oceanic heat to the Arctic, followed by FS. In NorESM20CR, the BSO heat transport ranges from 30 to 60 TW and is a factor three larger than the FS heat transport which ranges from 10 to 30 TW. Because of its low temperature (less then 0 °C), the outflow through the Davis Strait also contributes to a positive northward heat transport of approximately 5–15 TW. The inflow of warm PW through the Bering Strait is the smallest provider of oceanic heat to the Arctic with approximately 0–5 TW in the simulation. The absolute values of the simulated oceanic heat transports are likely too small. As will be described in the following section, the simulated AW layer is colder than observed in the FS, and hence, the total heat transport will also be lower than observed. This was also noted by Ilıcak et al. (2016) who found the heat transport to vary significantly from model to model. We will therefore mostly focus on the variability when it comes to the simulated heat transports.

From Figures 2a and 2b, we see that, except for in the Bering Strait, all heat and volume transports experience relatively large year-to-year and multiannual to decadal variations. However, since the seasonal cycle is large in the Bering Strait, taking the annual mean damps the variations. If we investigate the summer variations only (not shown), we find that it varies as much as in the FS. The northward volume transport in the FS is correlated ($r = 0.65$) with the AW flow through the BSO and can vary up to 1 Sv from year to year. The AW volume transports are anticorrelated with the outflows through the East Greenland Current and Davis Strait ($r = -0.87$), because the volume in the Arctic Ocean is conserved. Both FS and the BSO volume and heat transports have prominent periods of 5–7 and 7–8 years. The volume transport through the BSO has shown an increasing trend since the 1960s, accompanied by a small decreasing trend in northward transport in the FS.

When we consider the long-term changes in simulated heat transport, all straits show a small increasing trend throughout the 120-year integration period. The trend is the largest in the FS and the BSO. However, the ETCW from the 1920s to 1930s followed by a colder period in the 1960s to 1970s can be seen in both BSO and FS heat transports. The BSO heat transport experiences the largest change as it almost doubles from 30 to

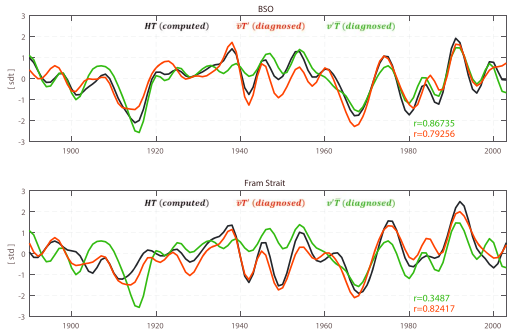

Figure 3. Inflow (northward) HT anomalies (low-pass filtered) across the BSO and the FS. HT is computed HT by the model. HT can be decomposed into a temperature component ($\bar{v}T'$) and a velocity component ($v'\bar{T}$). Red and green lines show the calculated components and numbers show the correlations with the computed HT. Because $\bar{T}$ is close to 0 in the FS, the magnitude of the green line in absolute values (TW) is smaller than the orange. This is why values are presented in standard deviations and not in TW. For both FS and BSO, 1 standard deviation in HT (black line) equals approximately 6 TW. BSO = Barents Sea Opening; HT = heat transport; FS = Fram Strait.

60 TW over a 100-year period. In the FS, it also doubles from approximately 10 to 20 TW. For both straits, there appears to be a regime shift around 1920, when we suddenly see a large increase in heat transport. Before the 1920s, there is no significant trend in neither of the straits, but after the sudden increase in 1920, the general trend remains positive. This might be due to the quality of the reanalysis forcing. We acknowledge the fact that in earlier years, the forcing data are more uncertain because of fewer observations, especially prior to the satellite era. Since we are interested in long-term variability, this is one of the few products available for 100 years and more simulations (He et al., 2016). The multimodel mean from the CORE-II model comparison by Ilıcak et al. (2016) also shows this positive trend in the BSO heat transport, while any FS trend is unclear. From visual inspection, we see that the variability in the BSO heat transport closely resembles the variability in the volume transport, indicating that the heat transport variations are dominated by velocity fluctuations rather than temperature fluctuations. However, the increasing temperatures also impact the heat transport. In the FS, the northward-flowing AW volume anomalies explains a small portion of the increase in heat transport. The increase in net heat transport through the FS is mainly due to increasing AW temperatures and increasing southward flow in the cold East Greenland Current. The increased outflow may partly be a response to the increasing BSO inflow.

Changes in heat transport may occur as a result of changes in temperature (T') or through changes in volume transport (v'). Figure 3 presents the detrended heat transport anomalies for the BSO and the northward-flowing AW in the FS decomposed into a temperature component ($\bar{v}T'$) and a velocity component ($v'\bar{T}$). The primes denote annual means (variations), while $\bar{v}$ is the mean volume transport over the whole period, and $\bar{T}$ is the mean temperature in the strait over the whole period. The components are presented as standard deviation, because we wish to illustrate how well v' and T' correlate with the total heat transport. The absolute magnitude of the two components is dependent on $\bar{v}$ and $\bar{T}$, and since the mean temperature in the FS is close to the reference temperature, $v'\bar{T}$ is smaller than $\bar{v}T'$. In BSO, the variability of heat transport is affected by both changes in volume and temperature, but volume transport dominates slightly ($r = 0.87$ for $v'\bar{T}$ and $r = 0.79$ for $\bar{v}T'$). This result is consistent with Smedsrud et al. (2013). In the FS, however, the result is opposite, and variability of heat transport appears to be dominated by temperature fluctuations ($\bar{v}T'$). The correlation of $\bar{v}T'$ with the computed heat transport is $r = 0.82$, while the correlation of $v'\bar{T}$ with the computed heat transport is only $r = 0.35$. This is likely because the volume transport is more steady here. Figure 3 also shows that the large heat transport anomaly during the 1930s to 1940s was dominated by temperature anomalies in both the BSO and the FS.

4.2. Observed AW Temperature Variability

Time series from 1920 to 2012 of observed AW temperature based on the NSA (Figure 4) show a gradual cooling along the northward-flowing Norwegian Atlantic Slope Current and into the Arctic Ocean (Figure 1). The AW mean temperature in the Svinøy section over this 90-year-long record is 5.2 °C. In the BSO, the water has cooled to approximately 4.5 °C, at Sørkapp (76° N) to 2.5 °C, and at the FS section to 2.1 °C. The time series of AW temperature shows prominent variations on both interannual and near-decadal time scales. In all sections, the year-to-year variations typically have a range of approximately 1 °C.

In the Svinøy section the AW temperature shows a range of 2.5 °C, whereas in the BSO and the FS the range is 2.9 and 2.2 °C, respectively. We note that before 1940, the data coverage is sparse, especially in the BSO and FS sections. From visual inspection, we see that prior to the 1960s, the variability was particularly high and fluctuations with short periods are dominant. After the 1920s, for example, in the FS and BSO, a quasi-regular fluctuation on near-decadal (7–9-year) time scales appears to be more pronounced, although this times cale is not statistically significant compared to a simulated red noise spectrum. Peaks can be produced even in a random process, and we therefore conclude that the peaks that do not stick out of the red noise spectrum are not necessarily real. In the Norwegian and Barents Seas, such near-decadal variability has previously been linked to the large-scale atmospheric pressure patterns, as reflected in the NAO (Ingvaldsen et al., 2003; Venegas & Mysak, 2000; Visbeck et al., 2001).

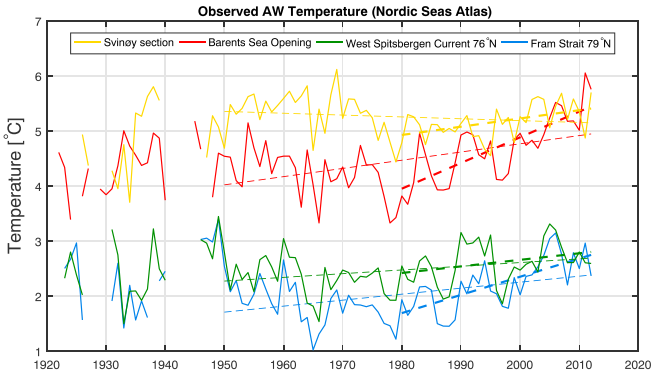

Figure 4. Time series of observed annual mean AW temperature (50–700 m) in four regions (Figure 1) along the pathway of the AW from 1920 to 2012. Thick-dashed lines show the linear trend from 1980 to 2012, and thin-dashed lines show the linear trend from 1950. AW = Atlantic Water.

A low-pass filter analysis (not shown) of the time series shows two distinct warm periods: (1) from the 1920s to the 1950s (ETCW; Bengtsson et al., 2004; Yamanouchi, 2011) and (2) from the 1980s to present with a relatively cold period in between. From the early 1980s, we observe a relatively strong warming trend in all regions. This trend is smallest in the Svinøy section and at Sørkapp (0.15 and 0.11 °C/decade, respectively). It is strongest in the BSO (0.47 °C/decade), but it is also relatively strong in the FS (0.33 °C/decade). This translates to approximately 1–1.5 °C warming from 1980 to 2012, comparable to the 1 °C warming between 1967 and 1999 documented by Dickson et al. (1988a). However, we observe that temperatures were as high also in the 1930s, possibly in the 1940s, and in the 1950s as well. Polyakov et al. (2004) suggested similar multidecadal variations in the central Arctic and so did Levitus et al. (2009) in the Barents Sea, who again linked it to the Atlantic Multidecadal Oscillation index of Sutton and Hodson (2005). From 1950, our time series show a positive trend in AW temperature in all sections apart from Svinøy.

4.3. Simulated AW Temperature Variability

The anomalous simulated annual AW temperature from NorESM20CR is presented and compared with the observed time series from the NSA in Figure 5. In general, the relative anomalies in the model agree fairly well with the observations. The model, however, has a climatological bias and looses AW heat too quickly northward from the Svinøy section toward FS. For example, at the Svinøy section, the model has a mean AW temperature of 6 °C, which is 1 °C higher than observed. Further north in the BSO, the simulated AW has cooled down to 3.5 °C which now is almost 1° below the observed. At Sørkapp, it has cooled down to approximately 2 °C which is close to the observed mean, but in the Northern FS, the AW layer is just above 1 °C, 1° below that indicated by the NSA. Thus, from the Svinøy section to 79° N, the simulated AW cools down with more than 5°, while the NSA only cools with 3°. From previous studies with NorESM and comparison with other similar Coupled Model Intercomparison Project Phase 5 models (CORE-II experiments), it is known that NorESM has a cold bias and loses oceanic heat to quickly in the Nordic Seas (Ilıcak et al., 2016). This is likely connected to the depth of the AW layer, cold water formation in the Barents Sea, and the vertical mixing parameterization (Ilıcak et al., 2016).

Despite the difference in the mean temperature, the simulated variations have high correlations with the observations. Highest correlation is found in the BSO ($r = 0.8$ for 1950–2009) and is also significant at Sørkapp ($r = 0.6$ for 1950–2009). At the Svinøy section and in the FS, correlation between the model and observations is lower ($r = 0.4$ and $r = 0.2$, respectively), but they still appear to agree on some prominent features in amplitude and timing (after 1980). The year-to-year variability typically has a range between 0.5 and 1.5 °C and is thus comparable to the observations, although somewhat smaller at the Svinøy section and in the FS than in the BSO and at Sørkapp. The variability is fairly constant throughout the whole 120-year period, with some more prominent fluctuations at the near-decadal (6–9-year) time scales in the latter part of the time series. Especially after the 1960s, the near-decadal variability is obvious in all regions.

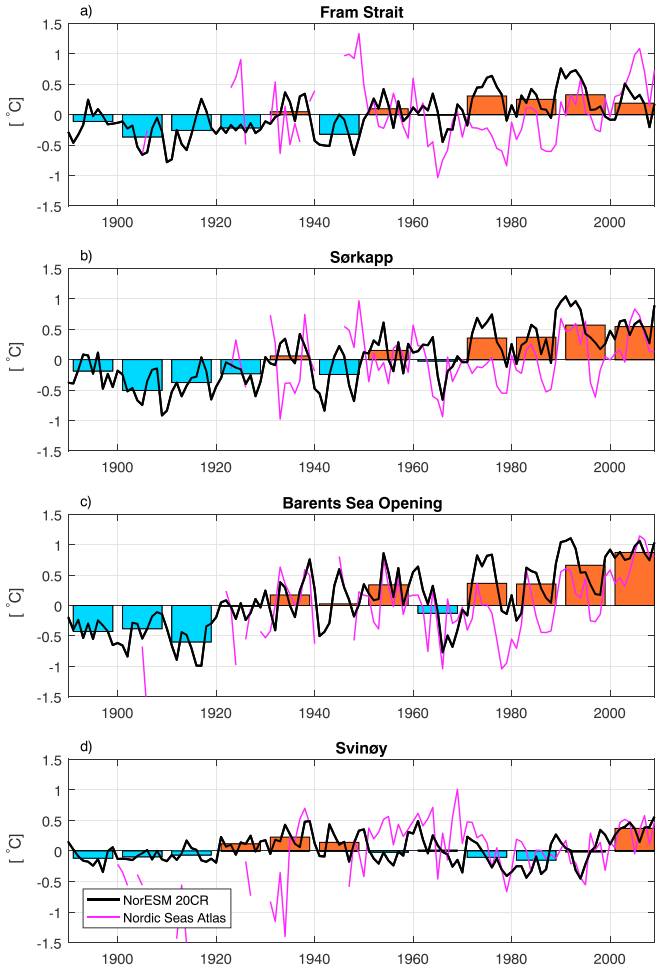

Figure 5. Anomaly time series of simulated (black lines) and observed (thin magenta lines) annual mean Atlantic Water temperature (50–700 m) in four regions (Figure 1) along the pathway of the Atlantic Water from 1890 to 2009, (a) Fram Strait, (b) Sørkapp, (c) the Barents Sea Opening, and (d) Svinøy. Red and blue bars denote the simulated decadal mean anomalies relative to the 120-year average. No detrending. NorESM = Norwegian Earth System Model.

The power spectrum of the AW temperature time series in Figure 6 reveals periods of 5–6 and 8–9 years for all sections. However, only the 5–6-year period peaks are significantly larger than expected from a red noise process in the BSO and at the Svinøy section. In the FS and at the Svinøy sections, only the 8–9-year periods stand out significantly. A 20-year peak (not shown in Figure 6), comparable to what is found by Årthun and Eldevik (2016), is visible in all sections, but it does not stand out compared to the red noise. We do not find any significant variations on longer time scales. One reason for this discrepancy could be model biases, but it may also be due to the shortness of our integration period. Since AW temperature anomalies are advective signals, all sections (Figure 5) have high-lagged (1–16 months) correlation (not shown), with values ranging between $r = 0.5$ and $r = 0.85$ from one region to another. This supports the findings that AW anomalies can be traced as a signal along the flow path (Årthun & Eldevik, 2016) over a longer time span (Figure S4). The Svinøy and BSO sections have maximum cross correlation with a lag of 11 months, indicating that a warm or

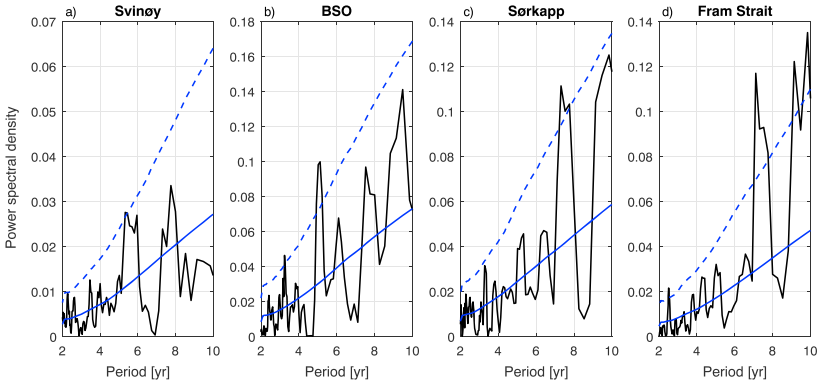

Figure 6. Power spectrum (black lines) of simulated Atlantic Water temperature based on unfiltered data for the 120-year-long series, (a) Fram Strait, (b) Sørkapp, (c) the Barents Sea Opening, and (d) Svinøy. The blue line represents the mean of 1,500 simulations of a fitted red noise spectrum, using a Monte-Carlo algorithm, and the dashed line is the 95% confidence limit about the red noise spectrum. BSO = Barents Sea Opening.

cold anomaly signal is advected in about 11 months time. The maximum cross correlation between Svinøy and Sørkapp sections has a lag of 15 months and between Sørkapp and the FS 4 months.

Simulated decadal anomalies shown in Figure 5 show small linear warming trends throughout the whole 120-year period for most sections (0.03–0.1 °C/decade or 0.4–1.4 °C of warming since 1890). The four last decades are the warmest for all sections except from Svinøy. No long-term trend can be observed at the Svinøy section, but since 1980, the AW has warmed with +0.28 °C/decade. In the BSO and at Sørkapp section, the simulated trends are 0.26 and 0.08 °C/decade, similar to observations (Figure 5). In the FS, however, the trend since 1980 is small, but negative, and not significant.

Removing the linear trend from Figure 5 uncovers multidecadal variations similar to Polyakov et al. (2004) and Polyakov, (2005; not shown). The ETCW (1930 to 1940) is very clear in the Svinøy section but also clearly visible in the BSO, the FS, and at Sørkapp. This warm period is followed by a relatively short cold period onward to the 1970s. The period prior to 1920 is relatively cold. During the ETCW, in the Svinøy section and the FS, the AW was as warm as during the early 2000s, while in the BSO and at Sorkapp, the 2000s are slightly warmer than during the ETCW.

5. Discussion

In our 20th century forcing simulation, we have established that the heat transport through the FS and BSO are dominating ocean heat transport anomalies toward the Arctic Ocean and that these depend on both fluctuations in volume and temperature. Furthermore, the relative importance of these vary in time. Next, forcing mechanisms of variations in heat and volume transport for both the BSO and the FS, and the relative roles of ocean advection and air-sea fluxes in driving these ocean heat anomalies, will be assessed.

5.1. Forcing Factors for Volume Transport Variability

In order to assess the overall Arctic volume transport variability, we examine the FS, the BSO, and the AW-dominated eastern part of the Nordic Seas (illustrated by the black box in Figure S3). These regions include most of the northward flow in the Nordic Seas. We now define the inflow of AW to the Arctic Ocean as the outflow from the Nordic Seas consisting of the FS and BSO combined. The anomalies (linear trend removed) of volume transport through the FS and BSO combined is shown in Figure 7b. Figure 7a shows the volume anomalies for the southern boundary of this region, at the Svinøy section, near the AW inflow across the Greenland Scotland ridge. The AW volume anomalies at the northern boundary (FS + BSO) and the volume anomalies at the Svinøy section appear to covary, but the correlation over the whole period is only $r = 0.47$ with a lag of 2 years. The relationship between the two varies over time, and a lagged gliding 30-year correlation (not shown) has values ranging from $r = 0.3$ to $r = 0.85$. This implies that the volume anomalies entering the Arctic Ocean are in some periods congruent with AW anomalies entering the Nordic Seas across

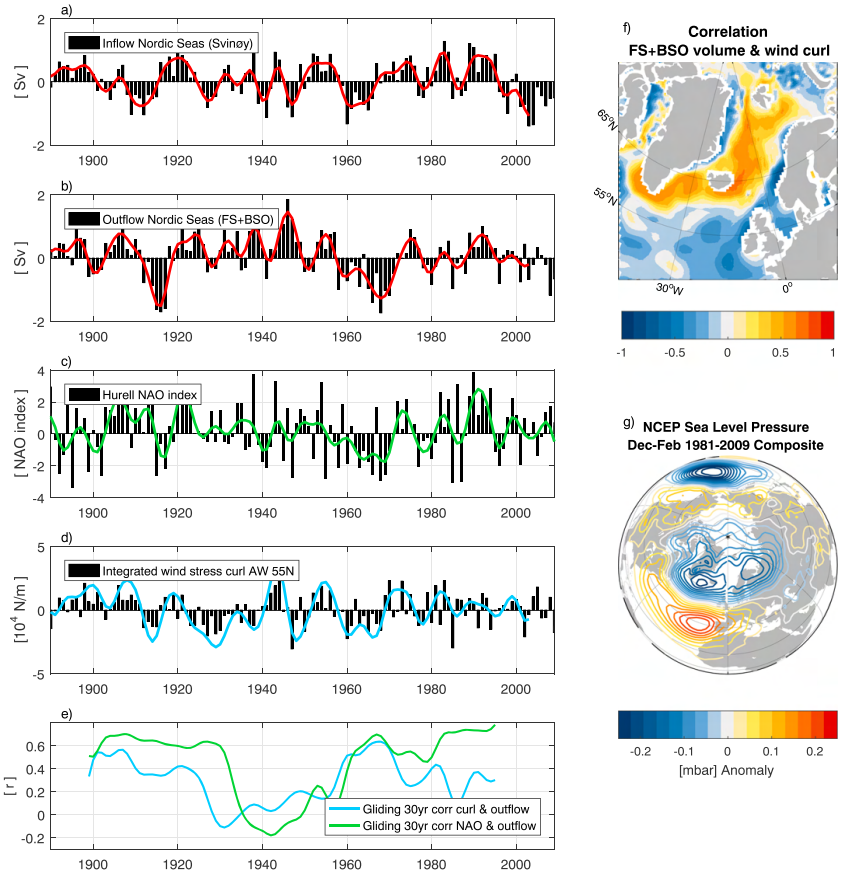

Figure 7. Nordic Seas AW volume transport (detrended anomalies) across (a) the inflow (Svinøy) and (b) outflow (BSO + FS). (c) shows the principal component time series of the leading Empirical Orthogonal Functions of seasonal (December through March) Sea Level Pressure anomalies over the Atlantic sector (20–80° N, 90° W–40° E), also known as the North Atlantic Oscillation (NAO) index (Hurrell, 1995). Anomalies of the integrated wind stress curl in a region across 55° N are shown in (d). (e) shows the gliding 30-year correlations of the NAO and curl with the outflow volume anomalies. Colored lines in (a)–(c) show a low-pass 3-year butterworth filtered, while in (d), it shows the low-pass filter of the 2-year accumulated wind stress curl. (f) shows the spatial correlation of annual mean outflow volume transport in the Nordic Seas (b) and annual mean wind stress curl. (g) shows the pattern of the mean winter sea level pressure anomaly from 1981 to 2009 explaining the NAO index. FS = Fram Strait; BSO = Barents Sea Opening; AW = Atlantic Water; NCEP = National Centers for Environmental Prediction.

the Greenland Scotland Ridge but not always. Also, the lag appears to change; for the time period before 1970, correlations are highest with a lag of 2 years, but after 1970, correlations are highest with zero lag. This indicates that there are different controlling mechanisms that contribute to generating these volume transport anomalies and these act over different time scales and in different regions.

We observe two periods with very low volume transport, one prior to the 1920s and one from the late 1950s and throughout the 1960s. These periods coincide with periods of low heat transport (Figure 8). The largest positive volume anomaly in the FS and BSO took place between 1940 and 1950; however, the Svinøy section anomaly was of the modest magnitude at this point, suggesting this was a period with a large inflow from the western AW branch or a spin-up of the internal Nordic Seas circulation. Note here that during the 1930s

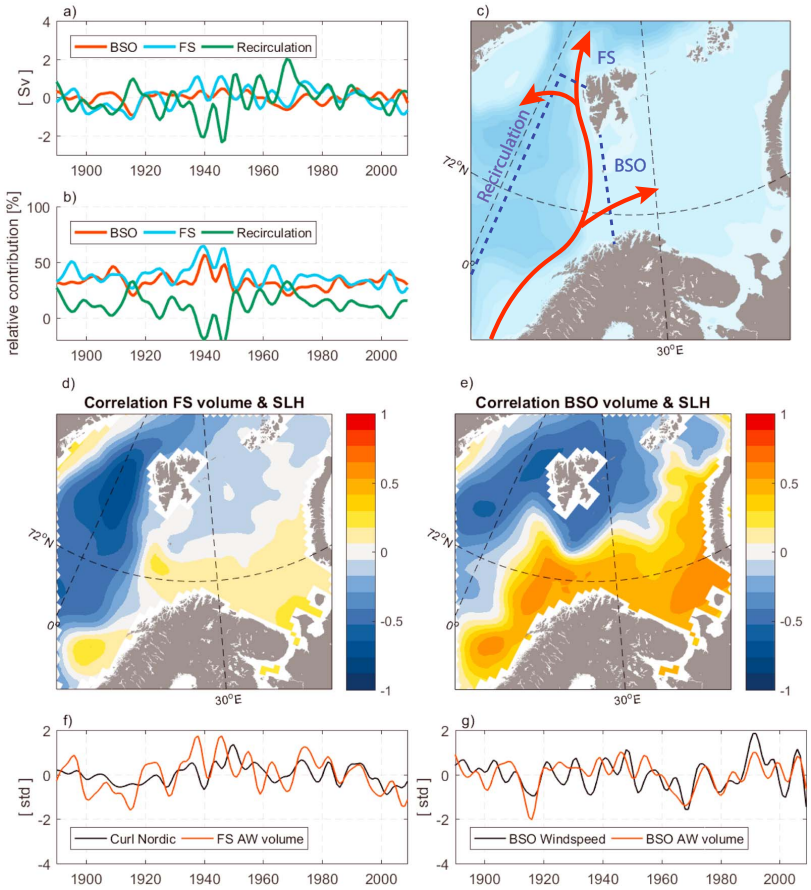

Figure 8. Volume transport anomalies (a) for the region indicated by blue lines in (c). Outflowing relative contribution for each of the three branches normalized to the inflowing volume is in (b). (d) and (e) show the spatial correlation with the SLH and outflowing volume anomalies for the FS and the BSO, respectively. (f) shows the volume anomaly through the FS section compared with the integrated wind stress curl in the whole Nordic Seas, while as (g) shows the volume anomaly through the BSO compared with the absolute wind speed here. BSO = Barents Sea Opening; AW = Atlantic Water; FS = Fram Strait; SLH = sea level height.

to 1940s, the volume anomaly is positive but relatively small both in south and in north, suggesting that the large heat anomaly during the ETCW is mainly a result of temperature, not volume, anomaly.

The North Atlantic westerlies and also the wind stress in the Nordic Seas are both central for the mechanical (wind) forcing. The leading mode of variability in this pattern is manifested in the NAO index, which is a measure of the difference in sea level pressure between the mean Azores High and Icelandic Low pressure as illustrated in Figure 7g. A positive NAO index leads to stronger westerlies and hence also a stronger cyclonic atmospheric circulation in the Nordic Seas and a stronger anticyclonic circulation further south in the North Atlantic. A time series of the NAO index by Hurrell and Deser (2009) is shown in Figure 7c. The negative NAO indices prior to the 1920s and between 1960 and 1970 coincide with low volume transports. The strong positive NAO in the 1920s, 1970s, and early 1990s also coincide with high AW volume transports. Correlation coefficients are given in Figure 7e and discussed further below. In Figure 7d, we present a time series of the 2-year accumulated zonally integrated wind stress curl at 55° N. Figure 7f confirms that the volume transport

through FS and BSO depends on this wind stress, with high spatial correlation between the volume transport and the wind stress curl. Strong positive curl (from cyclonic atmospheric circulation) leads to increased volume transport. This can be seen as a "pushing" mechanism that creates a divergence in the central Nordic Seas, by Ekman dynamics, piling up water toward the Norwegian and Greenland coasts. However, correlations are as high south of the zero curl, but with the opposite sign, meaning that strong negative curl (from anticyclonic atmospheric circulation) further south also leads to an increased AW inflow. The physical interpretation of this factor is to push the North Atlantic drift northeastward, toward the Greenland Scotland Ridge. Orvik and Skagseth (2003) found high correlations with the AW volume transport at the Svinøy section and the integrated wind stress curl over a band at 55° N, south of the zero curl.

In Figure 7e, we present a gliding 30-year correlation of the AW volume transport with the NAO index and the integrated wind stress curl at 55° N. Here we observe that we indeed have periods where the AW is highly correlated with both NAO and the wind stress curl but that this relationship is not stationary in time and that the relationship may break down completely. For example, during the 1930s and 1940s and during the ETCW, correlations are low. This points toward changes in the atmospheric circulation, where there are different regional variations in the wind forcing in the Nordic Seas and straits over time. In general, there is a good correlation between the large scale atmospheric circulation and the AW flow through the straits. However, when the relationship breaks down, we suggest that local atmospheric processes might be more important. Over certain periods, there appears to be a high correlation between the large scale wind patterns and the AW volume anomalies, but the relationship is not robust, and one can therefore not extrapolate based on this relationship. We also note that Figures 7e and 7f are essentially identical if we correlate with the Svinøy section volume instead of the BSO and FS volume. These findings support the theory that the long-term AW volume transport variability is partly dependent on the large scale atmospheric circulation as described in section 2.3. However, we acknowledge that the thermohaline forcing is also important but likely on longer time scales.

5.2. Covariability Between the Barent Sea Opening and the FS

AW heat that enters the Arctic Ocean through the FS is believed to directly impact the sea ice cover here (Ivanov et al., 2016; Onarheim et al., 2014; Polyakov et al., 2012). The AW that enters through the BSO prevents sea ice to form, and more of its heat is lost to the atmosphere (Smedsrud et al., 2013). Because the fate of AW heat is widely different if it enters through the FS or the BSO, the division between these two is examined. Although the volume transports of AW through the FS and the volume transport through the BSO are highly correlated ($r = 0.7$; Figure 2), we suggest that there are different processes at hand that govern how much of the northward-flowing AW that enters the Barents Sea and the FS.

In order to assess this division of the Norwegian Atlantic Slope Current, we have created a "box" with boundaries as shown in Figure 9c. Figure 9a shows the volume transport anomalies of the AW outflow anomalies through the FS, BSO, and the western boundary. Figure 9b shows the same but now normalized to the inflowing volume transport. Figure 9a reveals that the largest outflow variability is found at the western boundary, which can be interpreted as a recirculation branch. This tells us that most of the volume transport anomalies are actually being recirculated, and a smaller portion goes through the BSO and the FS. On average, both the FS and the BSO account for approximately 40% of inflow northward flow variability (Figure 9b). The remaining 20% is recirculated at the western boundary. During the 1930s and 1940s, a larger portion is carried through the FS and the BSO. The interpretation of the negative percentage through the western boundary is that there is a volume transport into the box here during these years.

We suggest that there is one forcing mechanism that controls how much of the northward-flowing AW that enters the BSO and that the remaining AW continues downstream toward the FS before a portion of the current recirculates and a portion continues northward toward the Arctic Ocean. On weekly and monthly time scales, Ingvaldsen et al. (2004b) and Lien et al. (2017) showed that the BSO volume transport depends on the local wind stress in the BSO and Barents Sea. These local winds would also depend on local sea level pressure in the Barents Sea that again results in a sea level height (SLH) gradient between Svalbard and the coast of Norway. Such a gradient would in turn set up a geostrophic current into the Barents Sea. This was also discussed by Lien et al. (2013), showing that on relatively short time scales, low SLH around Svalbard would lead to increased AW flow through the BSO. Here we test these existing relationships in a much longer time frame. Figure 9e supports that the BSO volume transport depends on the local winds. Here we see the spatial correlation between the BSO volume and the SLH spatial field is particularly high ($r = 0.6$) for the gradient in the BSO. Especially from the 1960s, there is a high correlation ($r = 0.8$) between the BSO volume and the

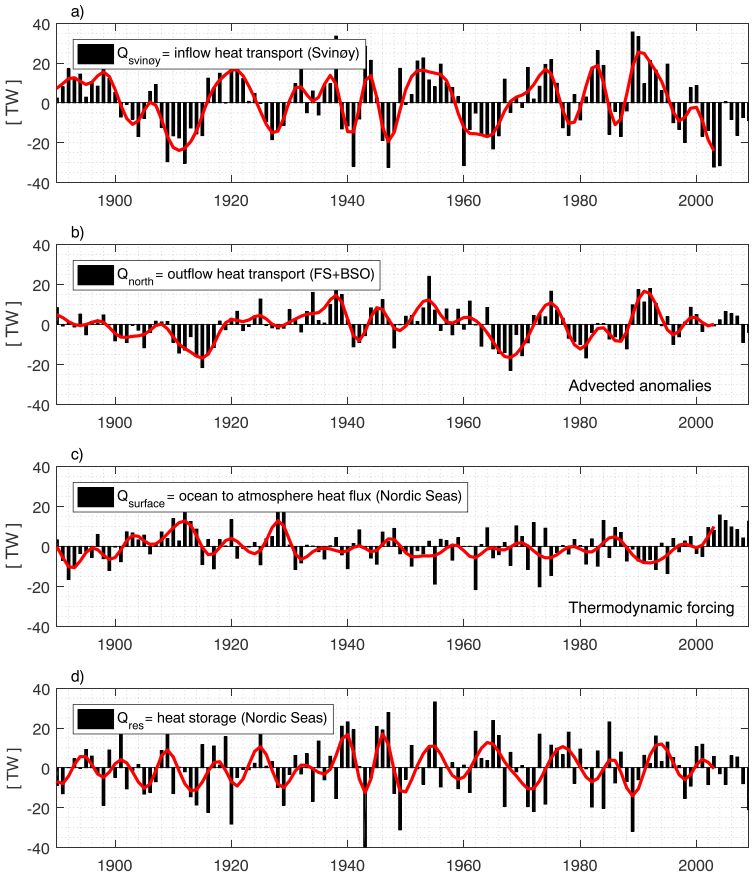

Figure 9. Nordic Seas AW heat transport (detrended anomalies) across (a) the inflow (Svinøy) and (b) outflow (BSO + FS). (c) shows the anomalies of ocean to atmosphere heat flux, and (d) shows the anomalies of the residual of the heat budget ($Q_{res} = Q_{north} - Q_{svinoy} - Q_{west} - Q_{surface}$) which can be interpreted as heat stored from one year to another. BSO = Barents Sea Opening; FS = Fram Strait.

mean absolute wind speed in the BSO (Figure 9g). We conclude that the low volume transports during the 1910s and the 1960s are caused by a drop in absolute wind speed locally in the BSO. Note that we here discuss the long-term annual averages. The local winds that promote enhanced volume transport through the BSO have, however, also been shown to be associated with the cyclonic pattern over the central Nordic Seas (Karcher, 2003).

While the BSO volume anomalies might be dominated by the local winds, the division further downstream is more complicated. By using a high-resolution ocean model, Hattermann et al. (2016) showed that eddy-driven recirculation is very important in the FS and that this explains a major part of the recirculation. Our model has too coarse horizontal resolution to resolve mesoscale eddies and only uses eddy parameterization and therefore likely simulate the FS processes with less realism. Also, Fieg et al. (2010) and Wekerle et al. (2017) showed the importance of high-resolution models when simulating volume transports in the FS and the Nordic Seas. Ilıcak et al. (2016) noted that the portion of recirculation in the FS differed a lot among the coarse CORE-II global climate models, adding to the uncertainty.

The spatial correlation between the FS AW volume anomalies and the SLH field is presented in Figure 9d. Strong negative correlations (up to $r = -0.7$) are seen throughout the central Nordic Seas, implying that low SLH in the central Nordic Seas results from a strong atmospheric cyclonic circulation and ocean divergence of the Ekman transport, leading to increased flow of AW through the FS. This is in accordance with Nøst and Isachsen (2003) who suggested that the large scale atmospheric circulation in the Nordic Seas drives the AW flow through the FS and circulation in the Arctic Ocean. The FS is different from the BSO in such that the local wind stress plays a less important role. In general, we have northerly winds in the FS and generally higher SLH in the Arctic Ocean than in the Nordic Seas, both acting against the AW flow. The AW current in the FS is also deeper, and more confined to the steep topography which likely makes it less influenced by the local winds. In Figure 9f, we present the AW inflow anomalies though the FS compared with the integrated wind stress curl within the Nordic Seas. Prior to 1930 and after 1970, there is relatively high correlation between these two quantities ($r = 0.5$ and $r = 0.6$). As previously stated, the FS volume anomalies and the recirculation volume anomalies are anticorrelated ($r = -0.5$; Figure 9a). As the FS volume is connected to the large-scale atmospheric circulation, we suggest that the recirculation increases when the the large scale circulation is weak and less AW is being pushed into the FS.

5.3. Drivers of Ocean Heat Anomalies

From the previous sections, it follows that the volume transport anomalies can partly explain the heat transport anomalies. However, advected temperature anomalies and local atmospheric thermodynamic forcing in the Nordic Seas are also of importance. Figure 8 shows the heat budget for the same region that was discussed in section 4.2 corresponding to the AW-dominated eastern Nordic Seas (black box in Figure S3). Figure 9a shows the heat transport anomalies at the Svinøy section and Figure 9b the heat transport anomalies at the FS and BSO combined. First, we note that there is a high correlation between the Svinøy section volume transport anomalies and the Svinøy section heat transport anomalies ($r = 0.96$). The correlation between the heat transport anomalies at the Svinøy section and those at the FS and BSO, however, is a lot lower ($r = 0.38$ with 1-year lag; Figures 8a and 8b), indicating that processes within the Nordic Seas influence the advected heat anomalies. If we split the FS and BSO heat transports, the correlations with the Svinøy heat transport anomalies are $r = 0.55$ and $r = 0.42$, respectively, both with 1-year lag.

Because the heat transport anomalies are largely dependent on temperature, we have investigated the propagation of temperature anomalies from the Svinøy section toward the north. In Figure S4a, we present a Hovmöller diagram of detrended standardized temperature anomalies from 60° N, along the AW pathway through the FS to 80° N. These anomalies have high-lagged correlations, and it takes approximately 20 months for the signals to propagate from 60° to 80° N. Periods with positive heat transport anomalies (Figure 8) generally coincide with positive temperature anomalies. Especially the 1930s, the 1960s, 1970s, 1990s, and after year 2000 stand out as warm periods. For comparison, Figure S4b shows salinity anomalies in the AW inflow. In most cases, both temperature and salinity anomalies fluctuate in phase at the different latitudes. The largest change in salinity was during the 1920s and the late 1930s, at the same time as the ETCW. Another large anomaly is during the cool 1970s, when the Great Salinity Anomaly propagated through the Nordic Seas (Dickson et al., 1988b), consistent with low AW inflow. The magnitude of the propagated anomalies can be both damped or amplified poleward, and in some cases, the anomalies are also generated within the Nordic Seas (Årthun & Eldevik, 2016; Furevik, 2001). While the warm anomaly in the first half of the 1920s weakened toward the north, the warm anomaly in the 1990s became stronger as it propagated northward. Furevik (2001) explained the latter with high air temperatures over the Nordic Seas, associated with an positive NAO index. We also see a transition at approximately 66° N which may be attributed to the long residence time of the AW in the Lofoten Basin (Poulain & Niiler, 1996).

A smoothened time series of ocean to atmosphere heat flux (Figure 8c) shows similar variability as the heat and volume transports, with near-decadal periods (not shown). Figure 8d displays the residual of the heat budget ($Q_{res} = Q_{north} - Q_{svinoy} - Q_{west} - Q_{surface}$) which can be interpreted as heat stored from one year to another. From Figure 8c, we also observe that the ocean to atmosphere heat flux is anticorrelated ($r = -0.68$) with the advected heat transport anomalies through the Svinøy section. This means that during years with strong heat advection, we have a large loss of heat to the atmosphere and vice versa. The atmosphere efficiently dampens the advected anomalies with approximately 50%. This is in accordance with Mork et al. (2014) who found that air-sea heat fluxes explained about half of the interannual variability in heat content in the Norwegian Sea. Carton et al. (2011), on the other hand, found that surface heat flux variations in some cases reinforce anomalies but that the contribution generally was small.

6. Conclusion

Northward ocean heat transport and its variability influence the Arctic sea ice cover, lead to surface warming or cooling, or simply warm or cool the Arctic Ocean interior. The variability thus likely plays an important role in Arctic Amplification, thermal expansion of the cold dense Arctic deep waters, or low-frequency variability of the Arctic sea ice cover (R. Zhang, 2015). Here we have investigated variability in heat transport, volume transport, and temperature using a forced global ocean model (NorESM20CR) aided by hydrographic observations since 1900. Generally, our simulations capture the mean hydrography and observed decadal heat variability well, despite a too strong poleward cooling.

The simulated net ocean heat transport toward the Arctic over the last century is about 68 TW, and 88% of this occurs in the Atlantic sector in the Barents Opening and the FS. Northward-flowing AW dominates this ocean heat transport and has typical variability of $\pm$40 TW over time scales between 5 and 10 years. Much of the variability is wind-driven and carried by associated changes in volume transport. The AW volume transport variability shows high correlations with the wind stress curl in the Nordic Seas and northern Atlantic and is clearly dependent on the large scale wind patterns also manifested in the NAO. However, gliding correlations show that the relationship between AW volume transport and wind stress curl or NAO are not stationary and may completely break down in certain periods, for example, during the 1930s and 1940s. The 1960s is a good example of low volume flow, that is, about 1 Sv less than 1900–2009 mean, occurring during a period with low NAO values.

Temperature variations of the AW also plays a vital role, with poleward flowing anomalies of $\pm$0.5 °C. The North Atlantic atmosphere generally dampens these heat anomalies in time, but they are also varying spatially. The atmospheric dampening of the advected heat anomalies in the Nordic Seas leads to about 45% of the total variability. The positive heat transport anomaly during the ETCW (1930s to 1940s) appears to be mainly a temperature anomaly and was also subject to weak atmospheric dampening. Temperature variability is thus a combination of advective processes and local thermodynamic forcing in the Nordic Seas. The trends appear to be stronger in the North and vary spatially. In future work, we plan to investigate the reason for this more in detail.

On a centennial time scale, the AW branch entering the Barents Sea is the largest advected heat source for the Arctic Ocean, contributing about 45 TW. Decomposition of the heat transport variability into mean volume and mean temperature contributions reveals that volume variability dominates slightly in the BSO. There are significant trends here, with values presently about 1 Sv higher in volume and +1.0 °C in temperature over the long-term mean. At the BSO, the AW volume transport depends largely on the local winds between Svalbard and the Northern Coast of Norway.

In the FS, the centennial mean heat advected northward is about 15 TW, with a large contribution from the colder than average southward-flowing water. The AW volume transport is comparable to that entering the Barents Sea, but it is more steady, so temperature variability dominates heat transport variability here. There is a complicated recirculation of AW in the FS, and the model bias is significant with a too strong cooling. The moderate volume transport variability here is more dependent on the large-scale atmospheric circulation in the Nordic Seas than local wind forcing. There are also variations in the other Arctic straits, but these are relatively small. The heat transport in the Davis strait is about 50% of the FS (10 TW), and less than 5 TW flow north in the Bering strait.

In both temperature and volume transport, we find prominent variability on 5–6- and on 8–9-year time scales. Both simulations and observations indicate the presence of multidecadal variability. Admittedly, AW observations do not stretch far enough back in time to resolve multidecadal variability properly; however, also our forced simulation has limitations due to the century-long integrations time, cyclic integration procedure, uncertainties in the reanalysis fields, and model deficiencies. Long simulations from fully coupled climate models may be useful to assess the variability on multidecadal time scales and beyond but with many of the above caveats in mind. To produce useful future predictions, a good understanding of the existing long-term variations is needed, and that is what we have have aimed at extracting here.

Acknowledgments
This work was partially supported by the Centre for Climate Dynamics (SKD) at the Bjerknes Centre for Climate Research. An extracted set of annual mean time series that have been used to make the figures is made available on the Bjerknes Climate Data Center (https://www.bcdc.no/). Analyzing scripts used in this study is available through the corresponding author by email at morven@uib.no. Dr Ilicak was partially supported by ITU Polar Research Center (PolRec; ITU-TGA-2017-40657). We would like to thank the reviewers for useful comments and feedback that helped improve this manuscript.

References

Aagaard, K. (1989). A synthesis of the Arctic Ocean circulation. *Rapports et proceès verbaux des réunions - Conseil international pour l'exploration de la mer*, *188*(1), 11–22.

Aagaard, K., & Carmack, E. C. (1989). The role of sea ice and other fresh water in the Arctic circulation. *Journal of Geophysical Research*, *94*(C10), 14,485–14,498. https://doi.org/10.1029/JC094iC10p14485

Alexeev, V. A., Ivanov, V. V., Kwok, R., & Smedsrud, L. H. (2013). North Atlantic warming and declining volume of Arctic sea ice. *The Cryosphere Discussions*, *7*(1), 245–265. https://doi.org/10.5194/tcd-7-245-2013

Årthun, M., & Eldevik, T. (2016). On anomalous ocean heat transport toward the Arctic and associated climate predictability. *Journal of Climate*, *29*(2), 689–704. https://doi.org/10.1175/JCLI-D-15-0448.1

Årthun, M., Eldevik, T., Smedsrud, L. H., Skagseth, O., & Ingvaldsen, R. B. (2012). Quantifying the influence of Atlantic heat on barents sea ice variability and retreat. *Journal of Climate*, *25*(13), 4736–4743. https://doi.org/10.1175/JCLI-D-11-00466.1

Banks, H. T., Wood, R. A., Gregory, J. M., Johns, T. C., & Jones, G. S. (2000). Are observed decadal changes in intermediate water masses a signature of anthropogenic climate change *Geophysical Research Letters*, *27*(18), 2961–2964. https://doi.org/10.1029/2000GL011601

Barnett, T. P., Pierce, D. W., AchutaRao, K. M., Gleckler, P. J., Santer, B. D., Gregory, J. M., & Washington, W. M. (2005). Penetration of human-induced warming into the world's oceans. *Science*, *309*(5732), 284–287. https://doi.org/10.1126/science.1112418

Barnett, T. P., Pierce, D. W., & Schnur, R. (2001). Detection of anthropogenic climate change in the world's oceans. *Science*, *292*(5515), 270–274. https://doi.org/10.1126/science.1058304

Bengtsson, L., Semenov, V. A., & Johannessen, O. M. (2004). The Early Twentieth-Century Warming in the Arctic—A possible mechanism. *Journal of Climate*, *17*(20), 4045–4057. https://doi.org/10.1175/1520-0442(2004)017<4045:TETWIT>2.0.CO;2

Bentsen, M., Bethke, I., Debernard, J. B., Iversen, T., Kirkevaag, A., Seland, O., et al. (2012). The Norwegian Earth System Model, NorESM1-M—Part 1: Description and basic evaluation. *Geoscientific Model Development Discussions*, *5*, 2843–2931. https://doi.org/10.5194/gmdd-5-2843-2012

Beszczynska-Möller, A., Fahrbach, E., Schauer, U., & Hansen, E. (2012). Variability in Atlantic water temperature and transport at the entrance to the Arctic Ocean, 1997–2010. *ICES Journal of Marine Science: Journal du Conseil*, *69*, fss056. https://doi.org/10.1093/icesjms/fss056

Beszczynska-Möller, A., Woodgate, R., Lee, C., Melling, H., & Karcher, M. (2011). A synthesis of exchanges through the main oceanic gateways to the Arctic Ocean. *Oceanography*, *24*(3), 82–99. https://doi.org/10.5670/oceanog.2011.59

Blindheim, J., Borovkov, V., Hansen, B., Malmberg, S.-A., Turrell, W. R., & Østerhus, S. (2000). Upper layer cooling and freshening in the Norwegian Sea in relation to atmospheric forcing. *Deep Sea Research Part I: Oceanographic Research Papers*, *47*(4), 655–680. https://doi.org/10.1016/S0967-0637(99)00070-9

Boyd, T., & Steele, M. (2002). Partial recovery of the Arctic Ocean halocline. *Geophysical Research Letters*, *29*(14), 1657. https://doi.org/10.1029/2001GL014047

Boyer, T. P., Antonov, J. I., Baranova, O. K., Coleman, C., Garcia, H. E., Grodsky, A., et al. (2013). World ocean database 2013, NOAA Atlas NESDIS 72, *NOAA Atlas* (pp. 209). Silver Spring, MD. https://doi.org/10.7289/V5NZ85MT

Burgard, C., & Notz, D. (2017). Drivers of arctic ocean warming in CMIP5 models. *Geophysical Research Letters*, *44*, 4263–4271. https://doi.org/10.1002/2016GL072342

Carmack, E. C., Macdonald, R. W., Perkin, R. G., McLaughlin, F. A., & Pearson, R. J. (1995). Evidence for warming of Atlantic water in the southern Canadian Basin of the Arctic Ocean, results from the Larsen 93 expedition. *Geophysical Research Letters*, *22*(9), 1061–1064. https://doi.org/10.1029/95GL00808

Carmack, E., Polyakov, I., Padman, L., Fer, I., Hunke, E., Hutchings, J., et al. (2015). Towards quantifying the increasing role of oceanic heat in sea ice loss in the new Arctic. *Bulletin of the American Meteorological Society*, *96*(12), 2079–2105. https://doi.org/10.1175/BAMS-D-13-00177.1

Carton, J. A., Chepurin, G. A., Reagan, J., & Hkkinen, S. (2011). Interannual to decadal variability of Atlantic Water in the Nordic and adjacent seas. *Journal of Geophysical Research*, *116*, C11035. https://doi.org/10.1029/2011JC007102

Chylek, P., Folland, C. K., Lesins, G., Dubey, M. K., & Wang, M. (2009). Arctic air temperature change amplification and the Atlantic Multidecadal Oscillation. *Geophysical Research Letters*, *36*, L14801. https://doi.org/10.1029/2009GL038777

Comiso, J. C. (2012). Large decadal decline of the arctic multiyear ice cover. *Journal of Climate*, *25*(4), 1176–1193. https://doi.org/10.1175/JCLI-D-11-00113.1

Compo, G. P., Whitaker, J. S., Sardeshmukh, P. D., Matsui, N., Allan, R. J., Yin, X., et al. (2011). The twentieth century reanalysis project. *Quarterly Journal of the Royal Meteorological Society*, *137*(654), 1–28. https://doi.org/10.1002/qj.776

Cuny, J., Rhines, P. B., & Kwok, R. (2005). Davis Strait volume, freshwater and heat fluxes. *Deep Sea Research Part I: Oceanographic Research Papers*, *52*(3), 519–542.

Curry, B., Lee, C. M., & Petrie, B. (2011). Volume, freshwater, and heat fluxes through Davis Strait, 2004-05*. *Journal of Physical Oceanography*, *41*(3), 429–436. https://doi.org/10.1175/2010JPO4536.1

Curry, B., Lee, C. M., Petrie, B., Moritz, R. E., & Kwok, R. (2014). Multiyear volume, liquid freshwater, and sea ice transports through Davis Strait, 2004-10. *Journal of Physical Oceanography*, *44*(4), 1244–1266.

Dickson, R. R., Meincke, J., Malmberg, S. A., & Lee, A. J. (1988a). The "great salinity anomaly" in the northern North Atlantic 1968–1982. *Progress in Oceanography*, *20*(2), 103–151. https://doi.org/10.1016/0079-6611(88)90049-3

Dickson, R. R., Meincke, J., Malmberg, S.-A., & Lee, A. J. (1988b). The "great salinity anomaly" in the northern North Atlantic 1968–1982. *Progress in Oceanography*, *20*(2), 103–151. https://doi.org/10.1016/0079-6611(88)90049-3

Dmitrenko, I. A., Polyakov, I. V., Kirillov, S. A., Timokhov, L. A., Frolov, I. E., Sokolov, V. T., et al. (2008). Toward a warmer Arctic Ocean: Spreading of the early 21st century Atlantic Water warm anomaly along the Eurasian Basin margins. *Journal of Geophysical Research*, *113*, C05023. https://doi.org/10.1029/2007JC004158

Dmitrenko, I. A., Polyakov, I. V., Kirillov, S. A., Timokhov, L. A., Simmons, H. L., Ivanov, V. V., & Walsh, D. (2006). Seasonal variability of Atlantic water on the continental slope of the Laptev Sea during 2002-2004. *Earth and Planetary Science Letters*, *244*(3-4), 735–743. https://doi.org/10.1016/j.epsl.2006.01.067

Fahrbach, E., Meincke, J., Østerhus, S., Rohardt, G., Schauer, U., Tverberg, V., & Verduin, J. (2001). Direct measurements of volume transports through Fram Strait. *Polar Research*, *20*(2), 217–224. https://doi.org/10.1111/j.1751-8369.2001.tb00059.x

Fieg, K., Gerdes, R., Fahrbach, E., Beszczynska-Möller, A., & Schauer, U. (2010). Simulation of oceanic volume transports through Fram Strait 1995-2005. *Ocean Dynamics*, *60*(3), 491–502. https://doi.org/10.1007/s10236-010-0263-9

Furevik, T. (1998). On the Atlantic Water flow in the Nordic Seas: Bifurcation and variability (PhD thesis), Geophysical Institute, University of Bergen, Allegt 70, 5011 Bergen, Norway.

Furevik, T. (2000). On anomalous sea surface temperatures in the Nordic Seas. *Journal of Climate*, *13*(5), 1044–1053. https://doi.org/10.1175/1520-0442(2000)013<1044:OASSTI>2.0.CO;2

Furevik, T. (2001). Annual and interannual variability of Atlantic Water temperatures in the Norwegian and Barents Seas: 1980-1996. *Deep-Sea Research Part I: Oceanographic Research Papers*, *48*(2), 383–404. https://doi.org/10.1016/S0967-0637(00)00050-9

Gent, P., & Mcwilliams, J. (1990). Isopycnal mixing in ocean circulation models. *Journal of Physical Oceanography*, *20*(1), 150–155. https://doi.org/10.1175/1520-0485(1990)020<0150:IMIOCM>2.0.CO;2
Glessmer, M. S., Eldevik, T., Vaage, K., Oie Nilsen, J. E., & Behrens, E. (2014). Atlantic origin of observed and modelled freshwater anomalies in the Nordic Seas. *Nature Geoscience*, *7*(11), 801–805. https://doi.org/10.1038/ngeo2259
Grotefendt, K., Logemann, K., Quadfasel, D., & Ronski, S. (1998). Is the Arctic Ocean warming? *Journal of Geophysical Research*, *103*(C12), 27,679–27,687. https://doi.org/10.1029/98JC02097
Hansen, B., Hátún, H., Kristiansen, R., Olsen, S. M., & Østerhus, S. (2010). Stability and forcing of the Iceland-Faroe inflow of water, heat, and salt to the Arctic. *Ocean Science*, *6*(4), 1013–1026. https://doi.org/10.5194/os-6-1013-2010
Hattermann, T., Isachsen, P. E., Von Appen, W. J., Albretsen, J., & Sundfjord, A. (2016). Eddy-driven recirculation of Atlantic Water in Fram Strait. *Geophysical Research Letters*, *43*, 3406–3414. https://doi.org/10.1002/2016GL068323
He, Y. C., Drange, H., Gao, Y., & Bentsen, M. (2016). Simulated Atlantic Meridional Overturning Circulation in the 20th century with an ocean model forced by reanalysis-based atmospheric data sets. *Ocean Modelling*, *100*, 31–48. https://doi.org/10.1016/j.ocemod.2015.12.011
Helland-Hansen, B., & Nansen, F. (1909). *The Norwegian Sea: Its physical oceanography based upon the Norwegian Researches 1900-1904*. Kristiania: Det Mallingske bogtrykkeri.
Herbaut, C., Houssais, M. N., Close, S., & Blaizot, A. C. (2017). On the spatial coherence of the Atlantic Water inflow across the Nordic Seas. *Journal of Geophysical Research: Oceans*, *122*, 4346–4363. https://doi.org/10.1002/2016JC012566
Holliday, N. P., Hughes, S. L., Bacon, S., Beszczynska-Möller, A., Hansen, B., Lavín, A., et al. (2008). Reversal of the 1960s to 1990s freshening trend in the northeast North Atlantic and Nordic Seas. *Geophysical Research Letters*, *35*, L03614. https://doi.org/10.1029/2007GL032675
Hunke, E. C., Lipscomb, W. H., Turner, A. K., Jeffery, N., & Elliott, S. (2008). CICE: The Los Alamos sea ice model, documentation and software, version 4.0. Los Alamos National Laboratory Tech. Rep. Los Alamos, NM.
Hurrell, J. W. (1995). Decadal trends in the North Atlantic Oscillation: Regional temperatures and precipitation. *Science*, *269*(5224), 676–679. https://doi.org/10.1126/science.269.5224.676
Hurrell, J. W., & Deser, C. (2009). North atlantic climate variability: The role of the North Atlantic Oscillation. *Journal of Marine Systems*, *78*(1), 28–41. https://doi.org/10.1016/j.jmarsys.2008.11.026
Hurrell, J. W., Holland, M. M., Gent, P. R., Ghan, S., Kay, J. E., Kushner, P. J., et al. (2013). The community earth system model: A framework for collaborative research. *Bulletin of the American Meteorological Society*, *94*(9), 1339–1360.
Ilıcak, M., Drange, H., Wang, Q., Gerdes, R., Aksenov, Y., Bailey, D., et al. (2016). An assessment of the Arctic Ocean in a suite of interannual CORE-II simulations. Part III: Hydrography and fluxes. *Ocean Modelling*, *100*, 141–161.
Ingvaldsen, R. B., Asplin, L., & Loeng, H. (2004a). The seasonal cycle in the Atlantic transport to the Barents Sea during the years 1997–2001. *Continental Shelf Research*, *24*(9), 1015–1032. https://doi.org/10.1016/j.csr.2004.02.011
Ingvaldsen, R. B., Asplin, L., & Loeng, H. (2004b). Velocity field of the western entrance to the Barents Sea. *Journal of Geophysical Research*, *109*, C03021. https://doi.org/10.1029/2003JC001811
Ingvaldsen, R. B., Loeng, H., Geir, O., & Bjorn, A. (2003). Climate variability in the Barents Sea during the 20th century with a focus on the 1990s. *ICES Journal of Marine Science*, *219*, 160–168.
Ivanov, V., Alexeev, V., Koldunov, N. V., Repina, I., Sando, A. B., Smedsrud, L. H., & Smirnov, A. (2016). Arctic Ocean heat impact on regional ice decay - a suggested positive feedback. *Journal of Physical Oceanography*, *46*(5), 1437–1456. https://doi.org/10.1175/JPO-D-15-0144.1
Karcher, M. J. (2003). Arctic warming: Evolution and spreading of the 1990s warm event in the Nordic Seas and the Arctic Ocean. *Journal of Geophysical Research*, *108*(C2), 3034. https://doi.org/10.1029/2001JC001265
Kay, J. E., Holland, M. M., & Jahn, A. (2011). Inter-annual to multi-decadal Arctic sea ice extent trends in a warming world. *Geophysical Research Letters*, *38*, L15708. https://doi.org/10.1029/2011GL048008
Koenigk, T., & Brodeau, L. (2017). Arctic climate and its interaction with lower latitudes under different levels of anthropogenic warming in a global coupled climate model. *Climate Dynamics*, *49*(1-2), 471–492. https://doi.org/10.1007/s00382-016-3354-6
Korablev, A., Smirnov, A., & Baranova, O. K. (2014). Climatological Atlas of the Nordic Seas and northern North Atlantic: NOAA Atlas NESDIS 77, 13(June), doihttps://doi.org/10.7289/V54B2Z78
Krahmann, G., Visbeck, M., & Reverdin, G. (2001). Formation and propagation of temperature anomalies along the North Atlantic Current. *Journal of Physical Oceanography*, *31*(5), 1287–1303.
Levitus, S., Antonov, J. I., Boyer, T. P., & Stephens, C. (2000). Warming of the world ocean. *Science*, *287*(5461), 2225–2229. https://doi.org/10.1126/science.287.5461.2225
Levitus, S., Matishov, G., Seidov, D., & Smolyar, I. (2009). Barents Sea multidecadal variability. *Geophysical Research Letters*, *36*, L19604. https://doi.org/10.1029/2009GL039847
Lien, V. S., Schlichtholz, P., Skagseth, Ø., & Vikebø, F. B. (2017). Wind-driven Atlantic Water flow as a direct mode for reduced Barents Sea ice cover. *Journal of Climate*, *30*(2), 803–812. https://doi.org/10.1175/JCLI-D-16-0025.1
Lien, V. S., Vikebø, F. B., & Skagseth, Ø. (2013). One mechanism contributing to co-variability of the Atlantic inflow branches to the Arctic. *Nature Communications*, *4*, 1–6. https://doi.org/10.1038/ncomms2505
Lind, S., & Ingvaldsen, R. B. (2012). Variability and impacts of Atlantic Water entering the Barents Sea from the north. *Deep-Sea Research Part I: Oceanographic Research Papers*, *62*, 70–88. https://doi.org/10.1016/j.dsr.2011.12.007
McLaughlin, F., Carmack, E., Macdonald, R., Melling, H., Swift, J., Wheeler, P., et al. (2004). The joint roles of Pacific and Atlantic-origin waters in the Canada Basin, 1997–1998. *Deep Sea Research Part I: Oceanographic Research Papers*, *51*(1), 107–128. https://doi.org/10.1016/j.dsr.2003.09.010
Meyer, A., Fer, I., Sundfjord, A., & Peterson, A. K. (2017). Mixing rates and vertical heat fluxes north of Svalbard from Arctic winter to spring. *Journal of Geophysical Research: Oceans*, *122*, 4569–4586. https://doi.org/10.1002/2016JC012441
Morison, J., Aagaard, K., & Steele, M. (2000). Recent environmental changes in the Arctic: A review. *Arctic*, *53*(4), 359–371. https://doi.org/10.14430/arctic867
Morison, J., Steele, M., & Andersen, R. (1998). Hydrography of the upper Arctic Ocean measured from the nuclear submarine U.S.S. Pargo. *Deep Sea Research Part I: Oceanographic Research Papers*, *45*(1), 15–38. https://doi.org/10.1016/S0967-0637(97)00025-3
Mork, K. A., Skagseth, O., Ivshin, V., Ozhigin, V., Hughes, S. L., & Valdimarsson, H. (2014). Advective and atmospheric forced changes in heat and fresh water content in the Norwegian Sea, 1951-2010. *Geophysical Research Letters*, *41*, 6221–6228. https://doi.org/10.1002/2014GL061038
Nansen, F. (1902). *The oceanography of the North Polar Basin* (Vol. 3). Longmans: Green, and Company.
Nøst, O. A., & Isachsen, P. E. (2003). The large-scale time-mean ocean circulation in the Nordic Seas and Arctic Ocean estimated from simplified dynamics. *Journal of Marine Research*, *61*(2), 175–210. https://doi.org/10.1357/002224003322005069
Onarheim, I. H., & Årthun, M. (2017). Toward an ice-free Barents Sea. *Geophysical Research Letters*, *44*, 8387–8395. https://doi.org/10.1002/2017GL074304

Onarheim, I. H., Eldevik, T., Årthun, M., Ingvaldsen, R. B., & Smedsrud, L. H. (2015). Skillful prediction of Barents Sea ice cover. *Geophysical Research Letters*, *42*, 5364–5371. https://doi.org/10.1002/2015GL064359

Onarheim, I. H., Eldevik, T., Smedsrud, L. H., & Stroeve, J. C. (2018). Seasonal and regional manifestation of Arctic sea ice loss. *Journal of Climate*, *31*(12), 4917–4932. https://doi.org/10.1175/JCLI-D-17-0427.1

Onarheim, I. H., Smedsrud, L. H., Ingvaldsen, R. B., & Nilsen, F. (2014). Loss of sea ice during winter north of Svalbard. *Tellus A*, *66*(1), 23933. https://doi.org/10.3402/tellusa.v66.23933

Orvik, K. A., & Niiler, P. (2002). Major pathways of Atlantic water in the northern North Atlantic and Nordic Seas toward Arctic. *Geophysical Research Letters*, *29*(19), 1896. https://doi.org/10.1029/2002GL015002

Orvik, K. A., & Skagseth, O. (2003). The impact of the wind stress curl in the North Atlantic on the Atlantic inflow to the Norwegian Sea toward the Arctic. *Geophysical Research Letters*, *30*(17), 1884. https://doi.org/10.1029/2003GL017932

Orvik, K. A., Skagseth, O., & Mork, M. (2001). Atlantic inflow to the Nordic Seas: Current structure and volume fluxes from moored current meters, VM-ADCP and SeaSoar-CTD observations, 1995-1999. *Deep-Sea Research Part I: Oceanographic Research Papers*, *48*(4), 937–957. https://doi.org/10.1016/S0967-0637(00)00038-8

Pietschnig, M., Mayer, M., Tsubouchi, T., Storto, A., & Haimberger, L. (2017). Volume and temperature transports through the main Arctic Gateways: A comparative study between an ocean reanalysis and mooring-derived data, (December).

Polyakov, I. V. (2005). One more step toward a warmer Arctic. *Geophysical Research Letters*, *32*, L17605. https://doi.org/10.1029/2005GL023740

Polyakov, I. V., Alekseev, G. V., Timokhov, L. a., Bhatt, U. S., Colony, R. L., Simmons, H. L., et al. (2004). Variability of the intermediate Atlantic Water of the Arctic Ocean over the last 100 years. *Journal of Climate*, *17*(23), 4485–4497. https://doi.org/10.1175/JCLI-3224.1

Polyakov, I. V., Alexeev, V. A., Bhatt, U. S., Polyakova, E. I., & Zhang, X. (2009). North Atlantic warming: Patterns of long-term trend and multidecadal variability. *Climate Dynamics*, *34*(2-3), 439–457. https://doi.org/10.1007/s00382-008-0522-3

Polyakov, I. V., Pnyushkov, A. V., Alkire, M. B., Ashik, I. M., Baumann, T. M., Carmack, E. C., et al. (2017). Greater role for Atlantic inflows on sea-ice loss in the Eurasian Basin of the Arctic Ocean. *Science*, *291*, 285–291. https://doi.org/10.1126/science.aai8204

Polyakov, I. V., Pnyushkov, A. V., & Timokhov, L. A. (2012). Warming of the intermediate Atlantic Water of the Arctic Ocean in the 2000s. *Journal of Climate*, *25*(23), 8362–8370. https://doi.org/10.1175/JCLI-D-12-00266.1

Polyakov, I. V., Timokhov, L. A., Alexeev, V. A., Bacon, S., Dmitrenko, I. A., Fortier, L., et al. (2010). Arctic Ocean warming contributes to reduced polar ice cap. *Journal of Physical Oceanography*, *40*(12), 2743–2756. https://doi.org/10.1175/2010JPO4339.1

Poulain, P., & Niiler, P. P. (1996). Near-surface circulation of the Nordic seas as measured by Lagrangian drifters. *Journal of Geophysical Research*, *101*, 18,237–18,258. https://doi.org/10.1029/96JC00506

Quadfasel, D., Sy, A., Wells, D., & Tunik, D. A. (1991). Warming in the Arctic. *Nature*, *350*, 385.

Richter, K., Furevik, T., & Orvik, K. A. (2009). Effect of wintertime low-pressure systems on the Atlantic inflow to the Nordic seas. *Journal of Geophysical Research*, *114*, C09006. https://doi.org/10.1029/2009JC005392

Richter, K., Segtnan, O. H., & Furevik, T. (2012). Variability of the Atlantic inflow to the Nordic Seas and its causes inferred from observations of sea surface height. *Journal of Geophysical Research*, *117*, C04004. https://doi.org/10.1029/2011JC007719

Rudels, B. (2015). Arctic Ocean circulation, processes and water masses: A description of observations and ideas with focus on the period prior to the International Polar Year 2007–2009. *Progress in Oceanography*, *132*, 22–67. https://doi.org/10.1016/j.pocean.2013.11.006

Rudels, B., Meyer, R., Fahrbach, E., Ivanov, V. V., Østerhus, S., Quadfasel, D., et al. (2000). Water mass distribution in Fram Strait and over the Yermak Plateau in summer 1997. *Annales Geophysicae*, *18*(6), 687–705. https://doi.org/10.1007/s00585-000-0687-5

Sandø, A. B., & Furevik, T. (2008). Relation between the wind stress curl in the North Atlantic and the Atlantic inflow to the Nordic Seas. *Journal of Geophysical Research*, *113*, C06028. https://doi.org/10.1029/2007JC004236

Sandø, A., Gao, Y., & Langehaug, H. R. (2014). Poleward ocean heat transport, sea ice processes, and Arctic sea ice variability in NorESM1-M simulations. *Journal of Geophysical Research: Oceans*, *119*, 2095–2108. https://doi.org/10.1002/2013JC009435

Sandø, A. B., Nilsen, J. E., Eldevik, T., & Bentsen, M. (2012). Mechanisms for variable North Atlantic-Nordic seas exchanges. *Journal of Geophysical Research*, *117*, C12006. https://doi.org/10.1029/2012JC008177

Schauer, U. (2004). Arctic warming through the Fram Strait: Oceanic heat transport from 3 years of measurements. *Journal of Geophysical Research*, *109*, C06026. https://doi.org/10.1029/2003JC001823

Schauer, U., & Beszczynska-Möller, A. (2009). Problems with estimation and interpretation of oceanic heat transport–conceptual remarks for the case of Fram Strait in the Arctic Ocean. *Ocean Science*, *5*(4), 487–494. https://doi.org/10.5194/os-5-487-2009

Schauer, U., Beszczynska-Möller, A., Walczowski, W., Fahrbach, E., Piechura, J., & Hansen, E. (2008). Variation of measured heat flow through the Fram Strait between 1997 and 2006 BT. In *Arctic subarctic ocean fluxes: Defining the role of the northern seas in climate* (pp. 65–85). Dordrecht, Netherlands: Springer.

Schauer, U., Loeng, H., Rudels, B., Ozhigin, V. K., & Dieck, W. (2002). Atlantic Water flow through the Barents and Kara Seas. *Deep Sea Research Part I: Oceanographic Research Papers*, *49*(12), 2281–2298. https://doi.org/10.1016/S0967-0637(02)00125-5

Schauer, U., Muench, R. D., Rudels, B., & Timokhov, L. (1997). Impact of eastern Arctic shelf waters on the Nansen Basin intermediate layers. *Journal of Geophysical Research*, *102*, 3371–3382.

Schmidtko, S., Johnson, G. C., & Lyman, J. M. (2013). MIMOC: A global monthly isopycnal upper-ocean climatology with mixed layers. *Journal of Geophysical Research: Oceans*, *118*, 1658–1672. https://doi.org/10.1002/jgrc.20122

Serreze, M. C., Barrett, A. P., Slater, A. G., Woodgate, R. a., Aagaard, K., Lammers, R. B., et al. (2006). The large-scale freshwater cycle of the Arctic. *Journal of Geophysical Research*, *111*, C11010. https://doi.org/10.1029/2005JC003424

Serreze, M. C., & Barry, R. G. (2011). Processes and impacts of Arctic amplification: A research synthesis. *Global and Planetary Change*, *77*(1–2), 85–96. https://doi.org/10.1016/j.gloplacha.2011.03.004

Shimada, K. (2004). Penetration of the 1990s warm temperature anomaly of Atlantic Water in the Canada Basin. *Geophysical Research Letters*, *31*, L20301. https://doi.org/10.1029/2004GL020860

Skagseth, Ø. (2004). Monthly to annual variability of the Norwegian Atlantic slope current: Connection between the northern North Atlantic and the Norwegian Sea. *Deep-Sea Research Part I: Oceanographic Research Papers*, *51*(3), 349–366. https://doi.org/10.1016/j.dsr.2003.10.014

Skagseth, Ø., Drinkwater, K. F., & Terrile, E. (2011). Wind-and buoyancy-induced transport of the Norwegian Coastal Current in the Barents Sea. *Journal of Geophysical Research*, *116*, C08007. https://doi.org/10.1029/2011JC006996

Skagseth, Ø., Furevik, T., Ingvaldsen, R. B., Loeng, H., Mork, K. A., Orvik, K. A., & Ozhigin, V. (2008). Volume and heat transports to the Arctic Ocean via the Norwegian and Barents Seas. In *Arctic-Subarctic Ocean Fluxes: Defining the role of the Northern Seas in Climate* (pp. 45–64). Dordrecht, Netherlands: Springer.

Skagseth, Ø., & Orvik, K. A. (2002). Identifying fluctuations in the Norwegian Atlantic Slope Current by means of empirical orthogonal functions. *Continental Shelf Research*, *22*(4), 547–563. https://doi.org/10.1016/S0278-4343(01)00086-3

Smedsrud, L. H., Esau, I., Ingvaldsen, R. B., Eldevik, T., Haugan, P. M., Li, C., et al. (2013). The role of the Barents Sea in the Arctic climate system. *Reviews of Geophysics*, *51*, 415–449. https://doi.org/10.1002/rog.20017

Steele, M., & Boyd, T. (1998). Retreat of the cold halocline layer in the Arctic Ocean. *Journal of Geophysical Research*, *103*, 10,419–10,435. https://doi.org/10.1029/98JC00580

Steele, M., Morley, R., & Ermold, W. (2001). PHC3 Updated from: A global ocean hydrography with a high quality Arctic Ocean. *Journal of Climate*, *14*(9), 2079–2087. https://doi.org/10.1175/1520-0442(2001)014<2079:PAGOHW>2.0.CO;2

Sutton, R. T., & Hodson, D. L. R. (2005). Atlantic Ocean forcing of North American and European summer climate. *Science*, *309*(5731), 115–118. https://doi.org/10.1126/science.1109496

Swift, J. H., Jones, E. P., Aagaard, K., Carmack, E. C., Hingston, M., Macdonald, R. W., et al. (1997). Waters of the Makarov and Canada basins. *Deep-Sea Research Part II: Topical Studies in Oceanography*, *44*(8), 1503–1529. https://doi.org/10.1016/S0967-0645(97)00055-6

Tereshchenko, V. V. (1996). Seasonal and year-to-year variations of temperature and salinity along the Kola meridian transect. *ICES CM*, *100*, 11.

Tsubouchi, T., Bacon, S., Aksenov, Y., Naveira Garabato, A. C., Beszczynska-Möller, A., Hansen, E., et al. (2018). The Arctic Ocean seasonal cycles of heat and freshwater fluxes: Observation-based inverse estimates. *Journal of Physical Oceanography*, *48*, 2029–2055. https://doi.org/10.1175/JPO-D-17-0239.1

Venegas, S. A., & Mysak, L. A. (2000). Is there a dominant timescale of natural climate variability in the Arctic? *Journal of Climate*, *13*(19), 3412–3434. https://doi.org/10.1175/1520-0442(2000)013<3412:ITADTO>2.0.CO;2

Visbeck, M. H., Hurrell, J. W., Polvani, L., & Cullen, H. M. (2001). The North Atlantic Oscillation: Past, present, and future. *Proceedings of the National Academy of Sciences of the United States of America*, *98*, 12,876–12,877. https://doi.org/10.1073/pnas.231391598

Wekerle, C., Wang, Q., von Appen, W., Danilov, S., Schourup-Kristensen, V., & Jung, T. (2017). Eddy-resolving simulation of the Atlantic Water circulation in the Fram Strait With focus on the seasonal cycle. *Journal of Geophysical Research: Oceans*, *122*, 8385–8405. https://doi.org/10.1002/2017JC012974

Woodgate, R. A (2005). Monthly temperature, salinity, and transport variability of the Bering Strait through flow. *Geophysical Research Letters*, *32*, L04601. https://doi.org/10.1029/2004GL021880

Woodgate, R. A., Aagaard, K., Swift, J. H., Falkner, K. K., & Smethie, W. M. (2005). Pacific ventilation of the Arctic Ocean's lower halocline by upwelling and diapycnal mixing over the continental margin. *Geophysical Research Letters*, *32*, L18609. https://doi.org/10.1029/2005GL023999

Woodgate, R. A., Aagaard, K., & Weingartner, T. J. (2006). Interannual changes in the Bering Strait fluxes of volume, heat and freshwater between 1991 and 2004. *Geophysical Research Letters*, *33*, L15609. https://doi.org/10.1029/2006GL026931

Woodgate, R. A., Weingartner, T., & Lindsay, R. (2010). The 2007 Bering Strait oceanic heat flux and anomalous Arctic sea-ice retreat. *Geophysical Research Letters*, *37*, L01602. https://doi.org/10.1029/2009GL041621

Yamanouchi, T. (2011). Early 20th century warming in the Arctic: A review. *Polar Science*, *5*(1), 53–71. https://doi.org/10.1016/j.polar.2010.10.002

Yashayaev, I., & Seidov, D. (2015). The role of the Atlantic Water in multidecadal ocean variability in the Nordic and Barents Seas. *Progress in Oceanography*, *132*, 68–127. https://doi.org/10.1016/j.pocean.2014.11.009

Zhang, R. (2015). Mechanisms for low-frequency variability of summer Arctic sea ice extent. *Proceedings of the National Academy of Sciences*, *112*(15), 4570–4575. https://doi.org/10.1073/pnas.1422296112

Zhang, J., Rothrock, D. A., & Steele, M. (1998). Warmin og the arctic ocea by a strengthened atlantic inflow: Model results. *Geophysical Research Letters*, *25*(10), 1745–1748. https://doi.org/10.1029/98GL01299

Supporting Information for "Atlantic Water heat transport variability in the 20th century Arctic Ocean from a global ocean model and observations"

Morven Muilwijk[1,2], Lars H. Smedsrud[1,2,3], Mehmet Ilicak[4], and Helge Drange[1,2]

[1]Geophysical Institute, University of Bergen, Norway.

[2]Bjerknes Centre for Climate Research, Bergen, Norway

[3]University Centre in Svalbard, Longyearbyen, Svalbard

[4]Eurasia Institute of Earth Sciences, Istanbul Technical University, Istanbul, Turkey

Contents

Corresponding author: Morven Muilwijk, morven@uib.no

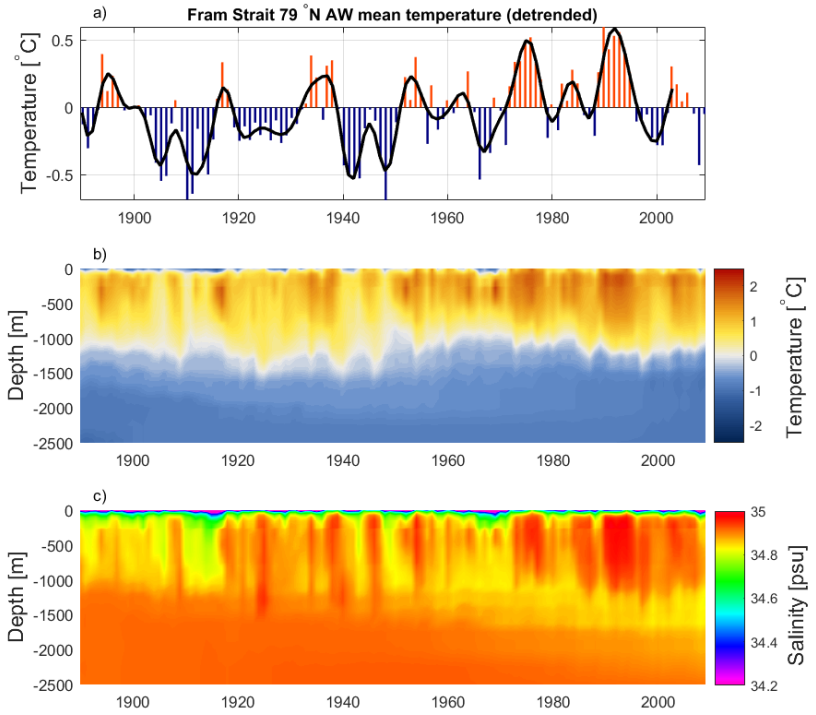

Figure 1. Simulated Atlantic Water mean temperature anomalies (a) and time-depth diagrams of temperature (b) and salinity (c) in the Fram Strait from NorESM20CR.

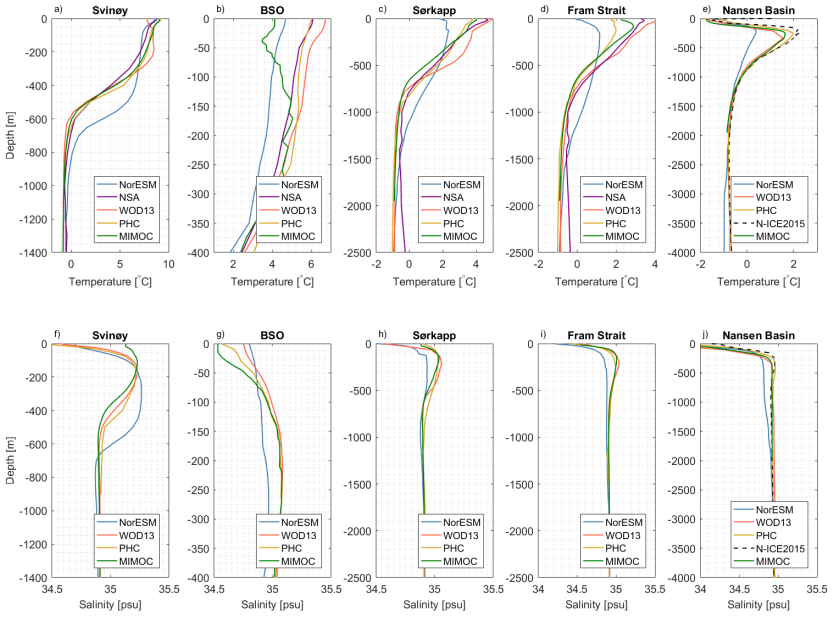

Figure 2. Horizontally averaged vertical temperature and salinity profiles in five regions along the Atlantic Water pathway (Fig. 1) from the Nordic Seas Atlas (NSA; Korablev et al., 2014), NorESM20CR (1890-2009) and three different climatologocial datasets: (i) the Polar Science Center Hydrographic Climatology (PHC3.0; Steele et al., 2001), (ii) World Ocean Database (WOD13; Boyer et al., 2013), and (iii) a monthly isopycnal/mixed-layer ocean climatology (MIMOC; Schmidtko et al., 2013). In the Nansen Basin the observed mean from the N-ICE2015 field campaign (Meyer et al., 2017) is also included.

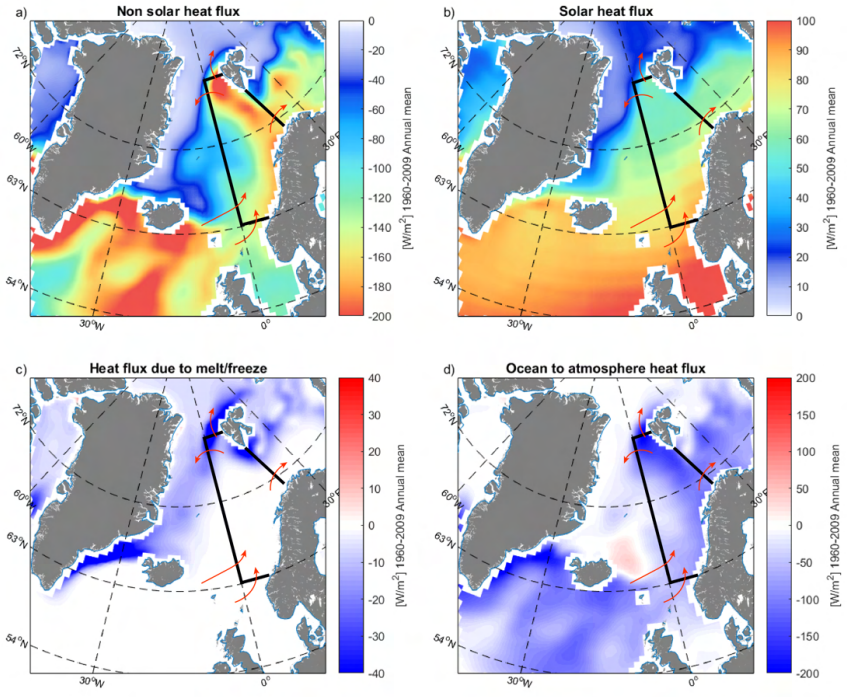

Figure 3. Annual mean spatial heat fluxes in the forced NorESM20CR simulation for the period of 1960-2009: non-solar heat flux (sensible + latent) (a), solar heat flux (short wave) (b), heat flux due to melting or freezing (c), and the net oceanic heat flux to the atmosphere (d). The box denotes the region for which we have calculated the heat budget and here the red arrows denote the direction of Atlantic Water heat transport into and out of the box.

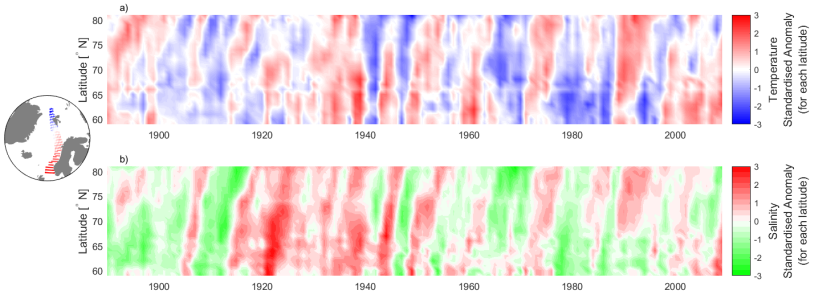

Figure 4. Standardized temperature (a) and salinity (b) anomalies for each latitude in sections along the Atlantic Water flow path (see map) from the southern Nordic Seas to north of the Fram Strait for the period 1890-2009.

Paper II

Arctic Ocean response to Greenland Sea wind anomalies in a suite of model simulations

Muilwijk, M., Ilicak, M., Cornish, S.B., Danilov, S., Gelderloos, R., Gerdes, R., Haid, V., Haine, T.W., Johnson, H.L., Kostov, Y., Kovács, T., Lique, C., Marson, J.M., Myers, P.G., Scott, J., Smedsrud, L.H., Talandier, C., Wang, Q.
Journal of Geophysical Research: Oceans, **124(8)** (2019)

JGR Oceans

RESEARCH ARTICLE
10.1029/2019JC015101

Special Section:
Forum for Arctic Modeling and Observational Synthesis (FAMOS) 2: Beaufort Gyre phenomenon

Arctic Ocean Response to Greenland Sea Wind Anomalies in a Suite of Model Simulations

Morven Muilwijk[1,2], Mehmet Ilicak[3], Sam B. Cornish[4], Sergey Danilov[5], Renske Gelderloos[6], Rüdiger Gerdes[5], Verena Haid[7], Thomas W. N. Haine[6], Helen L. Johnson[4], Yavor Kostov[8], Tamás Kovács[5], Camille Lique[7], Juliana M. Marson[9], Paul G. Myers[9], Jeffery Scott[1,10], Lars H. Smedsrud[1,2,11], Claude Talandier[7], and Qiang Wang[5]

[1]Geophysical Institute, University of Bergen, Bergen, Norway, [2]Bjerknes Centre for Climate Research, Bergen, Norway, [3]Eurasia Institute of Earth Sciences, Istanbul Technical University, Istanbul, Turkey, [4]Department of Earth Sciences, University of Oxford, Oxford, UK , [5]Alfred-Wegener-Institut Helmholtz-Zentrum für Polar- und Meeresforschung, Bremerhaven, Germany, [6]Department of Earth and Planetary Sciences, The Johns Hopkins University, Baltimore, USA, [7]Laboratoire d'Océanographie Physique et Spatiale, Univ. Brest, CNRS, IRD, Ifremer, IUEM, Brest, France, [8]Department of Physics, University of Oxford, Oxford, UK, [9]Department of Earth and Atmospheric Sciences, University of Alberta, Edmonton, Alberta, Canada, [10]Department of Earth, Atmospheric and Planetary Sciences, Massachusetts Institute of Technology, Cambridge, MA, USA, [11]University Centre in Svalbard, Longyearbyen, Svalbard, Norway

Abstract Multimodel Arctic Ocean "climate response function" experiments are analyzed in order to explore the effects of anomalous wind forcing over the Greenland Sea (GS) on poleward ocean heat transport, Atlantic Water (AW) pathways, and the extent of Arctic sea ice. Particular emphasis is placed on the sensitivity of the AW circulation to anomalously strong or weak GS winds in relation to natural variability, the latter manifested as part of the North Atlantic Oscillation. We find that anomalously strong (weak) GS wind forcing, comparable in strength to a strong positive (negative) North Atlantic Oscillation index, results in an intensification (weakening) of the poleward AW flow, extending from south of the North Atlantic Subpolar Gyre, through the Nordic Seas, and all the way into the Canadian Basin. Reconstructions made utilizing the calculated climate response functions explain ~50% of the simulated AW flow variance; this is the proportion of variability that can be explained by GS wind forcing. In the Barents and Kara Seas, there is a clear relationship between the wind-driven anomalous AW inflow and the sea ice extent. Most of the anomalous AW heat is lost to the atmosphere, and loss of sea ice in the Barents Sea results in even more heat loss to the atmosphere, and thus effective ocean cooling. Release of passive tracers in a subset of the suite of models reveals differences in circulation patterns and shows that the flow of AW in the Arctic Ocean is highly dependent on the wind stress in the Nordic Seas.

Plain Language Summary The North Atlantic Current is an extension of the Gulf Stream, which brings warm Atlantic Water northward as the current flows through the Nordic Seas. Eventually, it enters the cold deep Arctic Ocean basins through the Barents Sea and Fram Strait. Nine different numerical ocean ice models have been analyzed and compared in order to investigate (1) their ability to simulate this northward flow of Atlantic Water, (2) its dependence on wind forcing, and (3) its impact on Arctic sea ice. Consistently, in all models, stronger winds in the Greenland Sea result in a stronger northward flow of warm Atlantic Water. The response on ocean circulation occurs from the North Atlantic, through the Nordic Seas and the Barents Sea, to the deep Canadian Basin. The flow of warm Atlantic Water within the Arctic Ocean is thus highly dependent on the wind stress in the Nordic Seas. There is particularly clear response in the Barents and Kara Seas where a wind-driven anomalous warm inflow drives a smaller sea ice extent and thickness, and an increased heat transfer from the ocean to the atmosphere above. Weaker winds in the Greenland Sea produces weaker flow and hence a larger sea ice extent and thickness.

Key Points:
- Stronger/weaker winds over the Greenland Sea result in stronger/weaker flow of Atlantic Water in the Nordic Seas and into the Arctic Ocean
- In the Barents Sea there is a linear relationship between Atlantic Water volume and heat transport, surface heat loss, and sea ice extent
- There is potential for predictability of the Arctic-Atlantic circulation based on wind forcing anomalies and climate response functions

Supporting Information:
- Supporting Information S1
- Movie S1
- Movie S2
- Movie S3
- Movie S4
- Movie S5
- Movie S6

Correspondence to:
M. Muilwijk,
morven@uib.no

Citation:
Muilwijk, M., Ilicak, M., Cornish, S. B., Danilov, S., Gelderloos, R., Gerdes, R., et al. (2019). Arctic Ocean response to Greenland Sea wind anomalies in a suite of model simulations. *Journal of Geophysical Research: Oceans*, *124*. https://doi.org/10.1029/2019JC015101

Received 26 FEB 2019
Accepted 28 JUL 2019
Accepted article online 4 AUG 2019

1. Introduction

Changes in climate associated with global warming are particularly pronounced at high northern latitudes. Over the past decades the Arctic has warmed twice as fast as the global mean (IPCC, 2014), a characteristic

often termed "polar amplification" (Screen & Simmonds, 2010; Serreze & Barry, 2011). This Arctic warming manifests in many ways, for example, a dramatic and unprecedented decrease in sea ice extent (Carmack et al., 2015; Onarheim et al., 2018) and volume (Kwok, 2018). Since satellite observations began in the late 1970s, the Arctic summer sea ice extent has declined by approximately 50% (Vihma, 2014), and winter sea ice extent has steadily declined of 2.6% per decade (Cavalieri & Parkinson, 2012). Sea ice decline is projected to continue in the future, and these changes will alter Arctic ecosystems and fisheries (Dalpadado et al., 2014), influence transportation and exploitation of other natural resources (ACIA-Arctic Climate Impact Assessment, 2005), change the cycling of carbon (Hinzman et al., 2013), decrease the surface albedo Curry et al. (1995), and possibly affect climate and weather at lower latitudes (Liptak & Strong, 2014; Sorokina et al., 2016). For example, the decline of winter sea ice cover could increase the probability of cold winters in Europe (Cohen et al., 2014; Yang & Christensen, 2012).

Atmospheric forcing may be the biggest contributor to the sea ice loss (Serreze et al., 2007), but ocean heat storage and transport play an important role in certain regions (Carmack et al., 2015; Perovich & Richter-Menge, 2015; Polyakov et al., 2017). For example, the decline and variability in winter sea ice cover north of Svalbard and in the Barents and Kara Seas is linked to an increased and warmer inflow of Atlantic Water (AW; Årthun et al., 2012, 2017; Barton et al., 2018; Li et al., 2017; Onarheim et al., 2014, 2015, 2018). The Barents Sea experiences the fastest surface warming in the Arctic (Screen & Simmonds, 2010), and a recent study by Lind et al. (2018) found that the northern Barents Sea has transitioned from a cold Arctic to a warm Atlantic-dominated regime. It is expected that warming will continue, and projections from Onarheim and Arthun (2017) show that this region might become winter ice free in the time period 2061–2088 if the Representative Concentration Pathway scenario 8.5 (Moss et al., 2010) is followed. Although the recent Arctic surface changes have been well documented, the relative importance of the ocean remains uncertain and may increase in the future (Carmack et al., 2015). The observed trends in sea ice cover, atmospheric temperatures, and ocean heat transport due to increasing levels of greenhouse gases are superimposed on internal and natural variability. It is therefore of great interest to understand these current changes with respect to past change and to disentangle the different forcing factors in order to make skillful predictions for the future.

Variability in the Barents Sea sea ice extent has been attributed to a number of processes, and variations in the ocean heat transport is key (Årthun et al., 2012; Li et al., 2017; Smedsrud et al., 2013; Venegas & Mysak, 2000; Zhang, 2015). These heat anomalies result from either increased volume transport in the Norwegian Atlantic Current, a poleward extension of the North Atlantic Current (Muilwijk et al., 2018; Smedsrud et al., 2013), or temperature anomalies that are either generated locally (Schlichtholz & Houssais, 2011) or advected in from the south (Årthun & Eldevik, 2016; Furevik, 2001; Holliday et al., 2008; Skagseth et al., 2008). This has motivated several studies that have explored the effect of wind forcing on the AW volume and heat transport. Some studies focused on the impact of local wind forcing (Ingvaldsen et al., 2004; Lien et al., 2013, 2017; Skagseth et al., 2011), while others have described the influence of large-scale atmospheric forcing in terms of the North Atlantic Oscillation (NAO; Hurrell, 1995)—the dominant Northern Hemisphere (NH) mode of atmospheric variability (Dickson et al., 2000; Grotefendt et al., 1998; Orvik & Skagseth, 2003; Visbeck et al., 1998). As an example, Muilwijk et al. (2018) found a high correlation between the wind stress curl over the Nordic Seas and the ocean heat transport entering the Barents Sea.

Here, we further investigate the relationship between anomalous wind forcing, poleward ocean heat transport, and sea ice extent, with a particular focus on the Nordic, Barents, and Kara Seas using nine different climate and ocean sea ice-coupled general circulation models. Ocean sea ice-coupled general circulation models have been compared within the CORE2 project (Ilicak et al., 2016; Wang et al., 2016a, 2016b), and analyzed and improved during the last decades through the Arctic Ocean Model Intercomparison Project and its continuation, the Forum for Arctic Modeling and Observational Synthesis (https://famosarctic.com). Within this framework Marshall et al. (2017) proposed a coordinated modeling experiment with the goal to compute "climate response functions" (CRFs), the transient response of ocean and sea ice to abrupt "step" changes in external forcing fields. Here, we analyze how a suite of models respond to a step change in the Greenland Sea (GS) wind field (Figure 1), following the proposed protocol described in Marshall et al. (2017). We are motivated by three questions:

1. How does the general circulation of the Nordic Seas and poleward ocean heat transport into the Arctic Ocean respond to anomalous wind forcing over the GS?

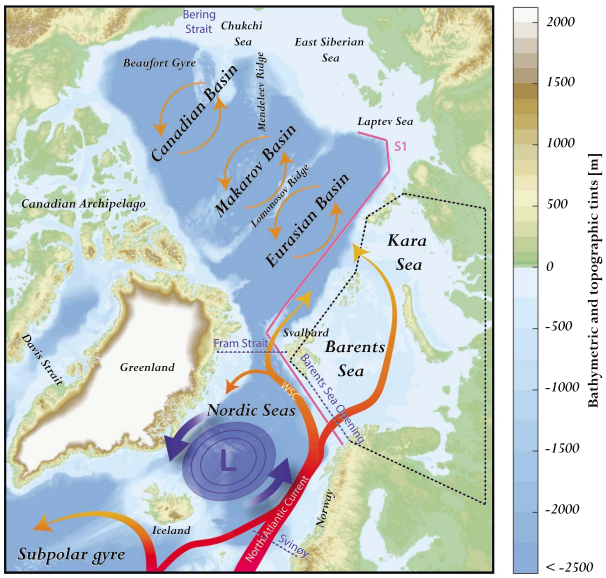

Figure 1. Overview map of the Arctic Ocean and its regional seas including the Atlantic Water inflow illustrated by the large red arrow. The blue arrows and low-pressure system illustrate the location of the Greenland Sea wind anomalies with stronger winds for the Greenland Sea Plus experiment and weaker winds for Greenland Sea Minus experiment. Orange arrows in the deep Arctic basins illustrate the circulation of intermediate Atlantic Water masses based on Carmack et al. (2015). Section S1 (presented in Figure S5) is shown in magenta, and the black dotted lines define the Barents and Kara Seas region.

2. What are the downstream effects of anomalous GS wind forcing on the deep Arctic Ocean basins and the Beaufort Gyre?
3. Does the system have any predictability?

Simulating the Arctic Ocean realistically is challenging due to the complexity of the dynamic and thermodynamic processes shaping its domain, in combination with the sparseness of long-term observations (Ilicak et al., 2016). Previous modeling studies document large differences in the mean state Arctic hydrography and AW inflow in different Arctic Ocean Model Intercomparison Project models (Holloway et al., 2007; Karcher et al., 2007) and Coupled Model Intercomparison Project models (Ilicak et al., 2016; Wang et al., 2016a, 2016b). The uniqueness and strength of the CRFs is that we study the model responses to external forcing rather than comparing their mean states. This allows us to focus on the forcing mechanism physics, similar to what is done in idealized studies such as Lique et al. (2015). A CRF approach also allows determination of time scales on which the system adjusts to changing forcing, which helps to understand the dynamical balance and predictability of the system. Here, step functions are useful because one can, if assuming linearity, reconstruct the response to any historical forcing based on the impulse response from the step function (Marshall et al., 2017). The ultimate goal is thus to learn how the Arctic Ocean responds to changes in external forcing. The differences and similarities across model responses give insights into the robustness of the results and the memory of the system.

The paper is organized as follows. A description of the region and a summary of previous studies investigating the relationship between wind forcing, ocean heat, and sea ice is given in section 2. The models and experimental setup are briefly described in section 3. In section 4 we explain the different responses to our perturbation experiment and investigate the potential for prediction based on a convolution of the CRFs with observed wind forcing. In section 5 we provide some further discussion on model differences and the redistribution of AW heat. We summarize our conclusions in section 6.

2. Background

Enclosed by the Eurasian and North American landmasses, the Arctic Ocean is the smallest of the world's five (major) oceans. The Arctic Basin has three subbasins deeper than 2,500 m: the Eurasian, Makarov, and Canadian Basins. These are separated by two ridges: the Lomonosov Ridge and the Mendeleev Ridge (Figure 1). Surrounding these deep basins are extensive continental shelf areas ($\lesssim$500 m) that cover a third of the total area: the Chukchi, the East Siberian, the Laptev, the Kara, and the Barents Seas. The Arctic Ocean is connected to the Pacific through the Bering Strait. We define the Nordic Seas—the Greenland, Iceland and Norwegian Seas—to be included in the Arctic Ocean, that is, in what Aagaard et al. (1985) termed the Arctic Mediterranean. This Arctic Ocean definition follows that of the International Hydrographic Office (Jakobsson & Macnab, 2006). The Fram Strait (FS) and the Barents Sea Opening (BSO) connect the deep Arctic basins with the Nordic Seas, while the Canadian Archipelago connects Arctic waters to the Labrador Sea through Baffin Bay. Most of the Arctic Ocean is characterized by a seasonally varying sea ice cover. With maximum extent in March and minimum extent in September, it influences ocean stratification, circulation, and freshwater and heat budgets (Haine et al., 2015).

2.1. AW Circulation and Atmospheric Forcing

AW that flows through the FS and the BSO is the dominant source of ocean heat and salt to the deep Arctic basins (Aagaard et al., 1987; Muilwijk et al., 2018). This AW current is an extension of the North Atlantic Current (Figure 1), which brings warm and saline water masses of subtropical origin into the Nordic Seas. In the Nordic Seas the AW flows in two main current branches, one that circulates and feeds the interior of the Nordic Seas, and one flowing northward as the Norwegian Atlantic Slope Current (Orvik et al., 2001; Wekerle et al., 2017). This current finally enters the BSO between Norway and Svalbard and enters the FS as the West Spitsbergen Current off the west coast of Svalbard (Beszczynska-Möller et al., 2012; Pérez-Hernández et al., 2019). A portion recirculates in FS (Hattermann et al., 2016; Wekerle et al., 2017), but the AW that does not circulates cyclonically in the Eurasian Basin, and a portion reaches the Makarov and Canadian basins, before it finally exits through the FS with the East Greenland Current or through the Canadian Archipelago (Carmack et al., 2015). The northward flow of AW in FS varies between 4 and 8 Sv (Beszczynska-Möller et al., 2012), while that in the BSO is close to 2 Sv (Smedsrud et al., 2010).

The NAO explains more than one third of the temporal variance in large-scale sea level pressure (SLP) in the North Atlantic. Its index is based on the difference between the subtropical (Azores) high and the subpolar low northeast of Iceland (Hurrell, 1995). Dickson et al. (2000) found that both the temperature and volume transport of AW to the Arctic Ocean increases during a strong positive NAO phase, which is characterized by an intense subpolar low and strong meridional pressure gradient. This strong pressure gradient results in stronger wind forcing in the North Atlantic, and thus an increased wind-driven northward AW current. The latter is supported by a comprehensive series of studies (Czaja & Marshall, 2001; Eden & Jung, 2001; Furevik, 2001; Langehaug et al., 2012; Lohmann et al., 2009; Medhaug et al., 2012; Muilwijk et al., 2018; Visbeck et al., 2013).

2.2. The Barents Sea and AW Impact on Sea Ice

The Barents Sea is a key region for determining the thermodynamic state of the Arctic Ocean. It dominates the region's heat storage, and more than 50% of the Arctic Ocean's surface heat loss occurs here (Serreze et al., 2007). In their pioneering work, Helland-Hansen and Nansen (1909) noted that varying inflow of AW influences the seasonal sea ice cover by determining the amount of winter freezing. This, and how the AW is modified before it exits the Barents Sea through the St. Anna Trough, has since been described by several other studies (Årthun & Schrum, 2010; Sandø et al., 2010; Smedsrud et al., 2010, 2013).

In the Arctic Basin, exchange from AW to the mixed layer and sea ice above is generally suppressed because of strong stratification (Carmack et al., 2015; Lind & Ingvaldsen, 2012; Lind et al., 2016). However, near the inflow regions such as the southern Barents Sea and north of Svalbard, where the AW layer is close to the surface or near steep topography, more of the heat reaches the surface and can contribute to direct bottom melting (Ivanov et al., 2016; Sandø et al., 2014). It has also been suggested that, with further warming of AW and increase of northward ocean heat transport, the warm AW might reach further into the Arctic Ocean. This so-called "Atlantification" represents an essential step toward a new Arctic climate state, with a substantially greater role for Atlantic inflow (Polyakov et al., 2017). As the sea ice becomes thinner, it is more mobile and less resistant to wind, surface, and tidal currents, facilitating the creation of more open-water areas. This may lead to a positive feedback. For example, increased input of momentum feeds turbulent

Table 1
Summary of the Models Participating in the Experiment in Alphabetical Order

Group	Ocean model	Ice model	Horiz. res.	Domain/grid	Forcing
Alberta	NEMO v3.4	LIM 2	Nominal 0.5°	Regional/ANHA2	2002–2016 CGRF (Smith et al., 2014)
AWI-MPI	MPIOM	MPIOM	Nominal 1.5°	Global/bipolar	Partially coupled, wind from NCEPcfsr (Saha et al., 2010)
FESOM	FESOM	FESIM	25km in Arctic	Global/bipolar	1948–2009 CORE-II (Griffies et al., 2012)
IFREMER	NEMO v3.6	LIM 3.5	Nominal 0.25°	Regional/CREG025	1979–2015 DFS 5.2 (Brodeau et al., 2010)
ITU-MOM	MOM5	SIS	Nominal 1°	Global/tripolar	1948–2009 CORE-II (Griffies et al., 2012)
JHU	MITgcm	MITgcm	Nominal 1/8°	Regional	ERA-Interim 1998 repeat year
MIT	MITgcm	MITgcm	36 km	Regional/cubedsphere	1979–2013 JRA-25 (Onogi et al., 2007)
NorESM	NorESM-O	CICE 4	Nominal 1°	Global/tripolar	1870–2009 20CR (He et al., 2016)
Ox-HiGEM	HiGEM	CICE 4	Nominal 1/3°	Global/bipolar	Fully coupled

mixing, which again could assist in bringing more AW heat to the surface (Peterson et al., 2017). Therefore, both the variation of the AW inflow and the local processes in the Barents Sea are important.

3. Experiment Setup for the Ocean-Only Models

In this coordinated study, the models considered have different resolutions, domains (both global and regional), and different atmospheric forcing (see Table 1). The common factor is that the models are perturbed by adding the exact same anomaly of wind/SLP to the original forcing. These wind anomalies affect all the forcing fields (and in particular the air-sea heat flux), which depend on the wind when estimated through a bulk formula. All other modeling choices are the preference of individual groups.

Prior to the sensitivity experiments, the models were run with an unperturbed atmospheric forcing covering a historical period. Several models use the CORE-II forcing (Griffies et al., 2012), but other reanalysis products are also used (Table 1). The perturbation experiment was then conducted by modifying the forcing field instantly after the models were "spun up" for a period of time (Marshall et al., 2017). Most perturbed runs were over the same time period (with the anomalous SLP field added in January 1980), and the difference between simulated fields in the perturbed and the control runs was used to evaluate the models responses. Exceptions are the Alberta model, which was run for the period 2002–2016 (and then repeated the 2002–2016 forcing to have a total of 30 model years like the other model runs), and the JHU setup, which uses repeat-year forcing.

The CRF of a certain diagnostic (e.g., the barotropic stream function, AW volume transport, or sea ice extent) was calculated as the difference between the perturbed and control simulation. The evaluation of step function anomalies and responses is used to distinguish between linear and nonlinear responses in the climate system (Gregory et al., 2015). From the CRFs, it is possible to construct the linear response to time history of the forcing (Marshall et al., 2014). One may calculate the evolution of the variable $R(t)$ by (see, e.g., Marshall et al., 2014)

$$R(t) = \int_0^t CRF(t - t')\frac{\partial F}{\partial t}(t')dt', \tag{1}$$

where F is the anomalous forcing (wind anomaly in the present study) and $CRF(t)$ is the time-dependent response to a unit step change in forcing.

3.1. Description of Models

We analyze monthly mean output from nine different models, five of which are global in extent. Key details of model configurations are given in Tables 1 and 2. The IFREMER and Alberta groups both use a regional model based on the Nucleus for European Modelling of the Ocean (Madec, 2014), but with different versions and resolution. The IFREMER version is a regional extraction (i.e., the "northfold" discontinuity of the global grid is removed) of the ORCA025 configuration, and the Alberta group uses a regional extraction of the ORCA05 configuration, both developed jointly by the Drakkar consortium and Mercator-Ocean (Barnier et al., 2009), encompassing the Arctic and parts of the North Atlantic down to 20° S. The Alberta

Table 2
Detailed Information About the Participating Models

Group	Vertical	Tracers	Background vertical diffusivity	Runoff
Alberta	z (50)	No	TKE model (Blanke & Delecluse, 1993)	Bamber et al. (2012), Dai and Trenberth (2002), (Dai et al., 2009)
AWI-MPI	z (40)	No	(Pacanowski & Philander, 1981) scheme	Coupled MPI-ESM
FESOM	z (47)	Yes	KPP scheme (Wang et al., 2014)	Dai and Trenberth (2002), Dai et al. (2009)
IFREMER	z (75)	no	TKE model (Blanke & Delecluse, 1993)	Bamber et al. (2012), Dai and Trenberth (2002), Dai et al. (2009)
ITU-MOM	z (50)	Yes	KPP scheme (Dunne et al., 2012)	Dai and Trenberth (2002), Dai et al. (2009)
JHU	z (50)	No	KPP scheme (Wang et al., 2014)	AOMIP
MIT	z (50)	Yes	KPP scheme (Wang et al., 2014)	Dai and Trenberth (2002), Dai et al. (2009)
NorESM	σ_2 (52)	Yes	TKE model (Fox-Kemper et al., 2008)	Dai and Trenberth (2002), Dai et al. (2009)
Ox-HiGEM	z (40)	No	Hybrid scheme (Shaffrey et al., 2009)	n/a

configuration has 50 geopotential levels in the vertical, and climatological conditions are provided by GLORYS2v3 (Masina et al., 2015). The IFREMER configuration has 75 geopotential levels and uses the initial conditions from World Ocean Atlas 2009 (Levitus et al., 2009).

The MITgcm is another regional Arctic Ocean simulation (Marshall et al., 1997) with a setup as described in Marshall et al. (2017). JHU (Stewart & Haine, 2013) is also a regional MITgcm configuration but uses 1998 repeat-year surface forcing and idealized open boundary conditions.

Of the five global models participating, the ocean component of the Norwegian Earth System Model (Bentsen et al., 2013) from the Bergen working group is the only model that has isopycnic layers (52 in number) in the vertical. For an in-depth analysis of physical mechanisms, a 120-year-long control simulation is used from NorESM, which is forced by a twentieth century reanalysis product. The setup of this model is similar to He et al. (2016), and an evaluation of the AW variability was performed by Muilwijk et al. (2018).

The only unstructured-mesh model in the analysis is FESOM Version 1.4 (Wang et al., 2014), a community ocean ice model developed and maintained by the Alfred Wegener Institute (AWI). FESOM is a global multiresolution ocean general circulation model using triangular meshes (Danilov et al., 2004; Wang et al., 2008). Its sea ice component is also formulated on the same surface triangular meshes (Danilov et al., 2015). In this study we employed a global setup at a nominal 1° horizontal resolution in most parts of the ocean and 24-km resolution north of 45° N. The resolution is refined along the coast and in the equatorial band. In the vertical, it has 47 z levels with 10-m resolution in the upper 100-m depth. This setup has been used in several previous studies with a focus on the Arctic Ocean (Wang et al., 2016a, 2016b, 2019).

The AWI-MPI group uses the fully coupled atmosphere-ocean-sea-ice-model MPI-ESM. A detailed description of the ocean component of the model can be found in Jungclaus et al. (2013). Wind anomalies are applied following the so-called Modini method, a partial coupling approach of Thoma et al. (2015). This method enables the ocean component of MPI-ESM to be driven by prescribed wind forcing, while maintaining consistency of heat and energy exchanges between the atmosphere and the ocean, and allowing feedbacks between climate system components.

The ocean component of the ITU-MOM uses the Modular Ocean Model (MOM5) code from Griffies (2012). MOM5 employs an Arakawa B-grid with nominal 1° horizontal grid resolution and bathymetry (refined meridionally to 1/3 degree at the equator) and a tripolar grid poleward of 65° N. The vertical grid has 50 levels, with 22 in the upper 220 m. This grid configuration was also used in the CORE-II intercomparison experiments (Danabasoglu et al., 2014; Farneti et al., 2015; Griffies et al., 2014). K-Profile (Large et al., 1994) and GM (Gent & Mcwilliams, 1990) parameterizations are used for vertical and isoneutral mixing, respectively. Further details of the numerical methods and physical parameterizations of the ocean are provided in Dunne et al. (2012).

Finally, we also analyze results from the Ox-HiGEM group with the fully coupled HiGEM climate model (Shaffrey et al., 2009). This model is not perturbed using the same approach as the forced simulations, but instead, multiple linear lagged regression is used to extract the responses to a hypothetical step increase in the principal components of Greenland Sea Plus (GSP) SLP pattern. This method is described by Kostov et al. (2017) and in section 3.3.

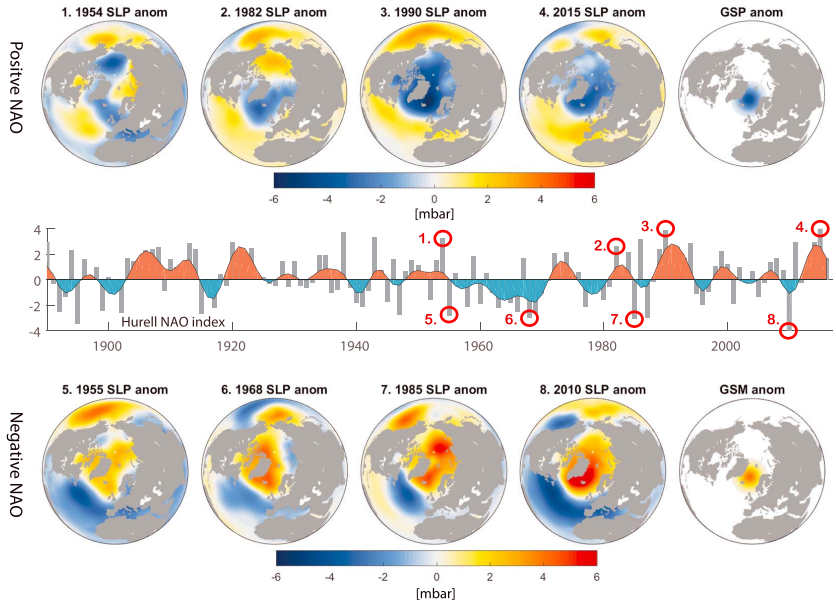

Figure 2. North Atlantic sea level pressure (SLP) anomalies over time. In the middle is the Hurell North Atlantic Oscillation (NAO) index with observed temporal variability. Maps of SLP anomalies for selected years with a strong positive NAO phase (1–4) are shown above, and selected years with a strong negative NAO phase (5–8) are plotted below. For comparison, the idealized SLP perturbation anomalies used for the Greenland Sea Plus (GSP) and Greenland Sea Minus (GSM) experiments are shown on the right. Note the GSP corresponds to anomalously low pressure over the Greenland Sea (stronger wind forcing) and GSM corresponds to anomalously high pressure (weaker wind forcing).

3.2. Wind Anomalies

The perturbation experiments consist of anomalous low/high SLP in the GS region, hereafter called the GSP/Greenland Sea Minus (GSM) experiments. GSP results in a stronger mean cyclonic atmospheric circulation, and GSM results in a weaker mean cyclonic atmospheric circulation. The anomalous pressure fields are shown in Figure 2. The center of the anomalies are located in the Greenland Sea at 70.55° N and 6.04° W (Figure 2) and have a magnitude of 4 mbar with a radius of influence of approximately 1,000 km. Compared to seasonal changes in SLP, reaching 20–30 mbar, the applied anomalies are relatively weak. The anomalous forcing is of the same order of magnitude as the long-term trends in the Arctic (Marshall et al., 2017), and comparable locally in the GS to the difference between a NAO neutral year and a strong positive/negative NAO year (Figure 2). The anomaly is located near the northern center of action of the NAO and is also termed the Icelandic Low. We use the term GS low from now on.

The center of this anomaly is similar to the first empirical orthogonal function of SLP in Thompson and Wallace (1998), who described the NAO as a regional manifestation of a hemispheric mode of variability that they named the Arctic Oscillation. The GS low is likely to be dominant during winter (Hurrell, 1995), and the anomaly center has shifted northeastward in recent decades (Moore et al., 2013; Zhang et al., 2008). Studies have shown that another center of SLP variability can be found in the Nordic Seas, named the Lofoten Low (Jahnke-Bornemann & Brümmer, 2009; Moore et al., 2012). Therefore, a perturbation experiment similar to our GS SLP perturbation was performed using the MIT model with the center of the anomaly shifted toward the Lofoten Low. Results from this experiment showed that the responses of the AW circulation were very similar to those in the GS perturbation experiment (not shown). Hence, we conclude that the GS anomaly is well located for our investigation of responses.

3.3. CRFs From the Fully Coupled HiGEM Simulation

The Ox-HiGEM CRFs are calculated from the coupled climate model HiGEM. The method, following Kostov et al. (2017), first identifies a target time series and a forcing time series, the latter of which is thought to exert some control on the former. The target time series is one of the metrics under investigation and is deseasonalized; the forcing time series is the regression of deseasonalized SLP variability onto the prescribed GSP anomaly pattern. The target time series is then considered as a convolution of the forcing time series with an unknown impulse response function. A solution for the impulse response function is found using multiple linear least squares regression of the target against the lagged forcing. Thousands of estimates are obtained for the impulse response function by varying (a) the cutoff lag, between 30 and 35 years; (b) the part; and (c) the length of the control run of the regression. The mean of these estimates for the impulses over the first 30 years is taken. Because this technique relies on a linear method, the symmetrical GSP and GSM forcing anomalies yield symmetrical responses. An estimate of uncertainty is derived from combining, in quadrature, the standard deviation of all estimates with a measure of the error associated with the fit between the original target and a convolution of each impulse estimate and the forcing, shown in Figure S8 in the supporting information. Finally, a step response is obtained by integrating the impulse response through time lags. The same technique was employed by Johnson et al. (2018) to probe the time-evolving relationship between Arctic freshwater and atmospheric circulation in HiGEM. This method is only used for the Ox-HiGEM CRFs.

3.4. Tracer Release

Passive tracers have been released "online" in four of the participating models (FESOM, ITU, MIT, and NorESM) in order to track the AW transport routes both in the climatology and perturbation experiments. The usage of "online" passive tracers in ocean circulation models is a useful method to investigate advection pathways and diffusion of water masses. One can view the tracers as a conservative dye that colors water particles with a certain concentration. At the release point the tracer concentration is set to 100% for every integration time step, starting in January 1980. It is then advected and diffused as the water masses circulate and mix. The passive tracers have been released in three locations along the AW flow (Figure 1): in the North Atlantic Current at the Svinøy section (63° N), in the BSO (70–74° N), and in the FS (79° N). Tracer diagnostics are computed as depth-integrated tracer volume for each grid cell.

4. Results

4.1. Circulation of AW in the Nordic Seas and Response to Wind Perturbations

In this section, the circulation of AW in the Nordic Seas and its relationship to the overlying atmospheric forcing is examined, followed by the responses of the AW flow to the two wind perturbation experiments, GSP and GSM.

In order to quantify the strength of the AW circulation in the Nordic Seas, an integrated quantity, like a "gyre index," is useful. To this end, the spatial pattern of the annual mean sea surface height (SSH) and the barotropic stream function have been examined using empirical orthogonal function analysis of the 120-year-long NorESM control simulation (Muilwijk et al., 2018). The barotropic stream function is here defined as

$$\psi = -\int_{\text{east}}^{\text{west}} v dx, \quad u = \frac{-\partial \psi}{\partial y} \quad \& \quad v = \frac{\partial \psi}{\partial x}, \tag{2}$$

where u and v are the depth-integrated currents in the x and y directions. As previously shown by Aagaard (1970), Nøst and Isachsen (2003), and Chatterjee et al. (2018), the leading mode features a barotropic cyclonic circulation in the Nordic Seas. Consequently, the area-average barotropic stream function over the central Nordic Seas (bounded by 66–76° N, 15° W to 10° E) can be used as an indicator of the strength of the Nordic Seas gyre circulation. A time series of the monthly mean NorESM barotropic stream function for the period 1880–2009 is shown in Figure S1. This time series shows that the NorESM barotropic circulation has a mean strength of approximately 6 Sv. Seasonally, it varies with a range of approximately 7 Sv, and interannual variations are approximately 1–3 Sv. Significant (with 95% confidence) positive correlations ($\bar{r} = 0.7$) are found between the area-averaged barotropic stream function and the wind stress curl in both the Nordic

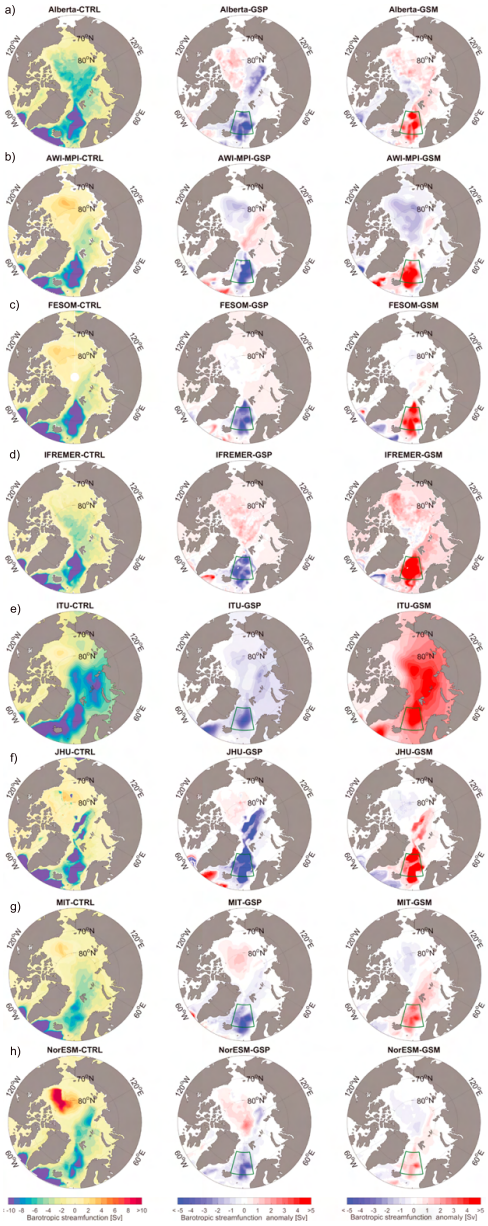

Figure 3. Annual mean barotropic stream function computed from each of the models. Negative values denote cyclonic circulation, and positive values denote anticyclonic circulation. Panels on the left show the control simulations. Middle panels show anomalies resulting from the Greenland Sea Plus (GSP) experiment (stronger wind forcing), and right panels show anomalies resulting from the Greenland Sea Minus (GSM) experiment (weaker wind forcing). All values are averaged over the last 10 years of integration (20–30 years after perturbation).

Seas and the Subpolar Gyre, and the NAO index (Figure S1c). Throughout the remainder of the text, all statistical significance has been determined using a Student's *t*-test.

4.1.1. Mean State

On average, all models have a similar spatial pattern in the Nordic Seas, a cyclonic ocean circulation that is strongest in the GS and Lofoten Basin (Figure 3). The cyclonic flow starts at the Greenland-Scotland Ridge and extends all the way north to FS in all models. This is due to a low in the SSH field in the central Nordic Seas caused by Ekman divergence as presented for NorESM in Figure 5a.

The absolute magnitude of the barotropic stream function generally varies between −8 and −10 Sv in the Nordic Seas (Figure S1c). An exception is the JHU model where the barotropic stream function is five times stronger than the other models. This has been investigated further and appears to be connected to strong deep circulation in the deep parts of the basins. Figure 3 clearly displays differences in the spatial pattern of the cyclonic flow between the models. Some models have a strong circulation throughout the entire Nordic Seas, while others are more confined to the smaller basins. Based on Nøst and Isachsen (2003), these differences are possibly linked to variations in Ekman pumping, the local bathymetry and its discrete representation, and the parameterization of the eddy field based on the actual hydrographic background states. The latter also results in different geostrophic currents. We will further explore these issues in section 5.1.

In the other Arctic basins the strength of the flow is less consistent between models (Figure 3), which could indicate different circulation patterns among the models. Further north, most models show a relatively strong cyclonic circulation in the Eurasian Basin, indicating that most of the AW recirculates here. A part of the AW continues to circumnavigate the Arctic Basin as a boundary current. As is shown by passive tracers in section 5.3, models differ by how the AW crosses the Lomonosov Ridge and extends into the Canadian Basin. The Alberta and ITU-MOM models have relatively strong cyclonic circulation throughout most of the Arctic Basin. An anticyclonic barotropic stream function is observed in the Beaufort Gyre for the AWI-MPI, FESOM, ITU-MOM, JHU, MIT, and NorESM models, but its magnitude and spatial pattern vary considerably. In the Beaufort Gyre the cyclonic circulation in the AW layer sits beneath the anticyclonic surface layer, so differences in the barotropic stream function, which integrates the two, may be a product of different halocline depths between models (Steiner et al., 2004). In the Beaufort Gyre, differences in the circulation may also be due to differences in vertical mixing (Zhang & Steele, 2007) or the simulated sea ice cover (not shown), as explained by the "ice-ocean governor" theory of Meneghello et al. (2018) and Wang et al. (2019). They argue that when wind blows over the ice, the ice drags the ocean, but when the gyre spins up, the geostrophic current catches up with the ice, and the surface stress is reduced. To first order, if simulated sea ice states are different among the models, the momentum transfer from the air to the ocean will also be different. Due to the lack of ocean current observations in the Arctic Ocean, the real barotropic stream function is not well known. We can therefore only compare the models with each other.

4.1.2. Response to Perturbations

Stronger cyclonic atmospheric wind forcing in the GSP enhances the Ekman divergence, leading to a deepening of the SSH trough in the Nordic Seas, as is seen for NorESM in the middle panel of Figure 4a. The perturbation also causes a stronger SSH gradient between the Arctic Basin and the Nordic Seas, which results in an increased barotropic flow as is seen in the center panels of Figure 3. All models behave consistently in this respect, and the average response is a 50% increase of the average barotropic stream function in the Nordic Seas. The JHU barotropic response is approximately five times stronger than that for the other models. All models show a slightly weaker, and in some cases opposite, response in the Eurasian Basin. We note that a local wind anomaly in the GS sets up a barotropic response extending over the entire Arctic Ocean, consistent with Peralta-Ferriz et al. (2014), and also upstream into the Subpolar Gyre (Figure S4) for most models. The weakened cyclonic atmospheric wind forcing in the GSM experiments results in a nearly identical, but opposite, response. This is consistent with previous analyses based on observations (Curry & McCartney, 2001) and model simulations (Brauch & Gerdes, 2005).

The spatially averaged barotropic stream function anomalies in the Nordic Seas governed by the GSP and GSM experiments are shown in Figure 5a. The amplitude of the response varies between 2–4 Sv in the GSP case and 1–5 Sv in the GSM case. Some asymmetry is seen among the responses, with the strongest response and largest spread for GSM. It also appears that the variability in the GSM case is larger than in the GSP case and that the ITU-MOM and IFREMER models do not reach equilibrium after 30 years. Ox-HiGEM has the weakest response for both cases, but this response increases over time. NorESM has

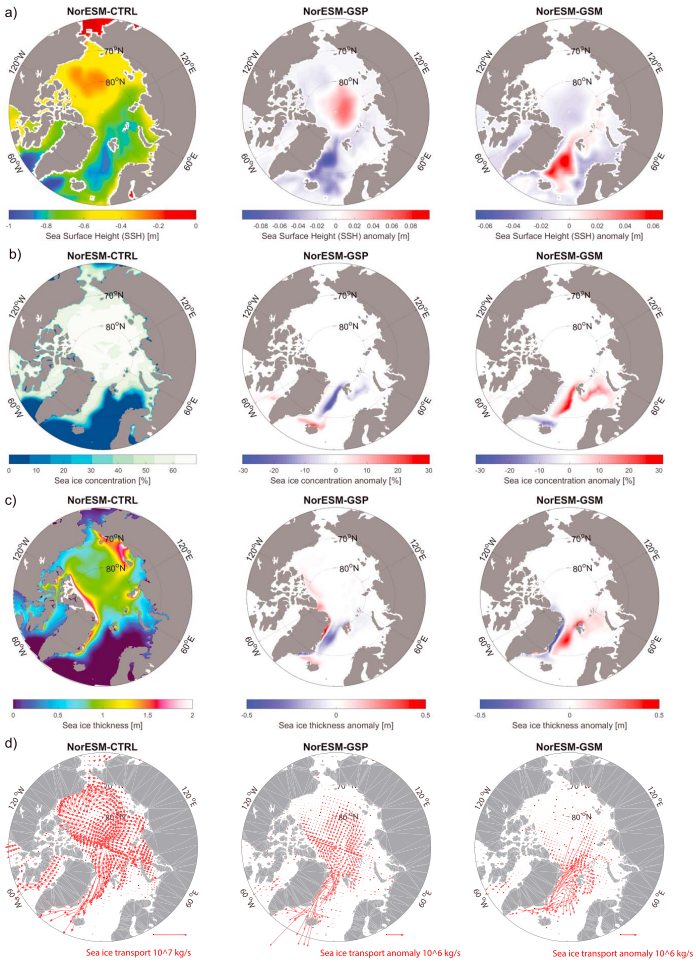

Figure 4. Annual mean and mean response for sea ice and SSH) in the NorESM model due to wind forcing. Panels on the left show the control simulation, middle panels show anomalies resulting from the stronger GSP forcing, and right panels show anomalies from the weaker Greenland Sea Minus (GSM) forcing. All values are averaged over the last 10 years of integration (20–30 years after perturbation). (a) SSH, (b) sea ice concentration, (c) sea ice thickness, and (d) sea ice transport. GSP = Greenland Sea Plus.

the lowest response of the models without an atmosphere, but otherwise, these are relatively similar. The response began in 1980 for most models, with a typical 2- to 5-year dynamic adjustment time before a new quasi-equilibrium state was obtained, in qualitative agreement with the findings in He et al. (2016). We find that the barotropic response to the wind anomalies is immediate and happens in the first month. This is also why the largest response is seen in the first year. The adjustment time scale is mainly set by dynamical adjustment of temperature and salinity. For NorESM this is investigated by looking at the depth-evolution of isopycnal layers (Figure S10). The perturbation results in a slow uplifting of the isopycnals, and the response in the intermediate and deep layers is therefore delayed by some years. A part of this delayed response might be advective, but it might also be related to convective mixing. This is discussed further in the upcoming sections.

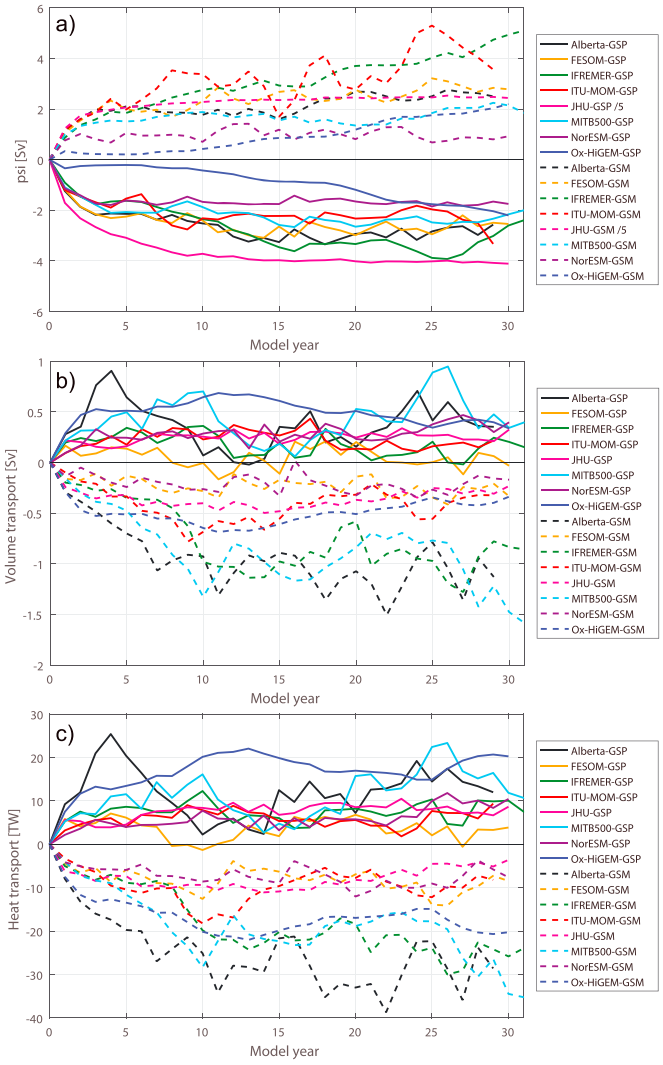

Figure 5. Annual mean Nordic Seas and Barents Sea climate response functions for the Greenland Sea Plus (GSP) and Greenland Sea Minus (GSM) wind anomalies. (a) Nordic Seas barotropic stream function strength (negative GSP values indicate stronger cyclonic circulation), (b) Barents Sea Opening inflow volume, and (c) Barents Sea Opening heat transport. The 4-mbar GSP and GSM forcing is shown in Figure 2, and the Nordic Seas area in Figure 3. The JHU response in (a) has been divided by 5 to scale with the other models.

4.2. Volume and Heat Transport Through the BSO

Ocean heat transport varies due to changes in both temperature and volume, and its absolute value depends on the chosen reference temperature (Schauer, 2004). We have chosen 0 ° C as a reference temperature for the inflow. Årthun et al. (2012) and Schauer et al. (2002) showed that 0 ° C is a representative value for the cold waters exiting the Barents Sea to the deep Arctic Basin, and we therefore simplify and refer to this transport as a heat transport and not a temperature transport. We acknowledge, however, that a physically consistent

Table 3
Climatological Values Obtained From the Control Simulations of the Different Models

Group	Barotropic stream function Nordic Seas (Sv)	Inflow volume transport BSO (Sv)	Inflow heat transport BSO (TW)	Sea ice extent Barent and Kara Seas (10^{11} m^2)	Sea ice extent NH (10^{12} m^2)	Net surface heat flux Barents and Kara Seas [TW]
Alberta	−8.0 (0.7)	+4.3 (0.5)	+100.2 (15.8)	+10.0 (1.7)	+10.4 (0.3)	-82.1 (21.7)
AWI-MPI	−8.8 (0.7)	+3.5 (0.3)	+99.2 (8.3)	+11.1 (0.9)	+11.1 (0.2)	-109.0 (13.3)
FESOM	−7.7 (0.8)	+3.4 (0.3)	+68.4 (8.8)	+11.7 (1.1)	+12.9 (0.3)	-82.3 (10.0)
IFREMER	−4.8 (1.1)	+2.8 (0.3)	+53.4 (7.6)	+13.6 (1.1)	+11.5 (0.2)	-71.9 (10.1)
ITU-MOM	−7.9 (1.1)	+2.2 (0.4)	+38.9 (8.6)	+13.8 (1.5)	+12.0 (0.4)	-55.0 (10.1)
JHU	−32.0 (0.0)	+3.6 (0.0)	+67.6 (0.0)	+16.9 (0.0)	+12.3 (0.0)	-32.6 (0.0)
MIT	−5.9 (0.7)	+3.3 (0.4)	+58.8 (11.7)	+13.5 (1.2)	+12.1 (0.3)	-42.0 (13.9)
NorESM	−6.5 (1.0)	+2.9 (0.3)	+51.7 (7.8)	+13.6 (1.0)	+12.0 (0.3)	-73.1 (10.1)
Ox-HiGEM	−7.9 (1.8)	3.4 (0.8)	+93.6 (18.7)	+9.1 (1.3)	+8.7 (0.3)	-254.7 (40.3)

Note. Values represent annual means averaged over the time period 1980–2005, with the exception of the Alberta model, which covers the period 2002–2016, and the JHU model, which utilizes a 1998 repeat year. We note that observational values also do not cover the exact same time period as the model averages. The observed value of the net surface heat flux only covers the Barents Sea and not the combined Barents and Kara Seas. Values in parenthesis are the standard deviations (annual cycle not included).

ocean heat budget independent of reference temperature results only from the heat convergence of a closed mass budget (Montgomery, 1974; Schauer & Beszczynska-Möller, 2009). To calculate such a closed heat budget for the Barents and Kara Sea region would require calculating the $V'T'$ terms on very short time scales at all grid points. This diagnostic was regrettably not available for all the models.

Temperature fluctuations are important for the BSO heat transport, but it is dominated by volume fluctuations (Muilwijk et al., 2018; Smedsrud et al., 2013). The CRFs of the associated heat transports are calculated relative to 0 ° C, and overall, there is consistent CRF response among the models for the eastward volume and heat transport (Figure 5). There is some interannual variability in the CRFs, and it is still an ongoing research project to fully understand this, but we believe that this variability is a nonlinear response to the daily forcing of the models. Volume and heat transport through the BSO in the AWI-MPI model show interannual variability that is much larger than the response to the forcing anomalies. Therefore, the response cannot be clearly identified. As a consequence, responses further downstream in the Arctic are also obscured by large variability. The AWI-MPI model results concerning the BSO fluxes and Arctic metrics are therefore excluded from the following analysis and are shown instead in Figure S9.

In the case of GSP, models show an increased flow of AW into the Barents Sea (Figure 5b). On average, the GSP response is +0.3 Sv, resulting in an advected heat anomaly of approximately 7 TW. For comparison, the multimodel mean volume and heat transports are 3.3 Sv and 62 TW, respectively. Thus, GSP results in roughly 10% increase in the transports. The multimodel mean is slightly elevated compared to observations indicating 2.3 Sv of total inflow in the BSO (Smedsrud et al., 2013). However, because observations are only available for AW inflow since 1998, there are substantial uncertainties in variations in the strength and extent of the Norwegian Coastal Current, and there are no observations available between Bear Island and Svalbard where models indicate a small net inflow. The simulated multimodel mean heat transport is smaller than the observation-based estimate of 70 TW (Smedsrud et al., 2013), with only one model exceeding the observation-based value (Alberta; 100 TW; Table 3). This implies that in most models water flowing east in the BSO is too cold.

There is a connection between the barotropic circulation anomalies in the Nordic Seas (Figure 5a) and the BSO volume transport anomalies (Figure 5b). A strong Nordic Seas cyclonic circulation due to GSP, resulting in negative stream function anomalies, occurs simultaneously to a stronger BSO inflow. However, the BSO transport anomalies are more variable and have a wider spread. Also, one model (FESOM) crosses the zero line several years after the initial response. There may be several reasons for these large differences among the models. First, the branching of the North Atlantic Current (between the BSO, FS, and recirculation near the FS) and the connection between the AW flow in the Nordic Seas and the BSO transport appear

Figure 6. Correlations between key diagnostics from each model. Top, summer (July), and bottom, winter (February). All time series are detrended, and their means are removed. Boxes containing "n.s." mean no significant correlation with a 95% confidence level. Correlations: (1) mean barotropic stream function (Psi) in the Nordic Seas and Barents Sea Opening (BSO) zonal volume transport, (2) mean barotropic stream function (Psi) in the Nordic Seas and Fram Strait (FS) northward volume transport (not net), (3) BSO zonal volume transport and BSO zonal heat transport, (4) BSO zonal heat transport and sea extent in the Barents and Kara Seas, (5) BSO zonal heat transport and sea volume in the Barents and Kara Seas, and (6) BSO zonal volume transport and FS northward volume transport. The JHU model is not included because it uses a repeat-year forcing and does not have realistic interannual variability.

to differ greatly between the models. Second, this connection is not steady in time and appears to vary seasonally. Figure 6 shows correlation values for summer (Figure 6a) and winter (Figure 6b) between different time series for all the model control simulations. Most models have a high correlation between the strength of the barotropic circulation in the Nordic Seas and the volume transport through the BSO (Figure 6). The Alberta model is an exception with no correlation during summer. During winter, however, the correlation is high also for the Alberta model, and higher for all models than during summer, meaning that the relationship between the barotropic circulation in the Nordic Seas and the BSO volume transport is generally stronger during winter. The correlation values between the barotropic circulation in the Nordic Seas and the FS volume transport are generally low, and much lower than for the BSO (Figure 6). During winter, these values are also slightly higher, and the Nordic Seas circulation in NorESM has a relatively high correlation with the FS volume transport ($r = 0.60$). Overall, the relationship between the barotropic stream function and the BSO volume transport is stronger than the relationship between the barotropic stream function and the FS volume transport. Most models show no significant correlation between the northeastward BSO volume transport and the northward FS volume transport. Exceptions are FESOM, which has a correlation of $r = 0.45$ during summer, and ITU, which has a correlation of $r = 0.41$ during winter.

The BSO transport responses to GSM are larger than to GSP (Figures 5 b and 5c), with even greater differences than the Nordic Seas barotropic stream function (Figure 5a). One possible explanation is that in GSM, the Nordic Sea gyre weakens but also contracts, while for GSP it only strengthens but cannot expand. The volume and heat transport anomalies resulting from GSM vary between 0.3 and 1.2 Sv and between 4 and 30 TW, respectively, a reduction of 7–50%. The adjustment time scale of the CRFs in the BSO is also approximately 2 to 3 years, but with substantial response the first year. We believe that the adjustment time scale in the BSO follows directly from the adjustment of the Nordic Seas barotropic circulation. The barotropic response time is days to weeks, but the baroclinic response also has to be taken into account. The baroclinic response time is likely slower due to advection of temperature and salinity anomalies that result from circulation changes.

The wind forcing in the GS is not the only forcing mechanism driving variations in the inflow at the BSO. The inflow is primarily driven by the strength of the local westerly winds following the coastline of northern Norway, which in turn sets up an Ekman transport toward the coast (Furevik, 2001; Ingvaldsen, 2004; Lien et al., 2017; Muilwijk et al., 2018; Sandø et al., 2010). These local wind patterns may or may not correlate with the NAO pattern, and thus the GS wind stress and barotropic stream function in the Nordic Seas. For example, Zhang et al. (1998) and Lien et al. (2017) showed that in recent decades with strong positive NAO index, the BSO AW inflow was strong and had an anomalous eastward extent, but Muilwijk et al. (2018) showed that this relationship is not stationary over long time scales. For the long NorESM control simulation, there is on average a relatively high correlation ($r = 0.5 - 0.8$) between the strength of the barotropic circulation in the Nordic Seas and BSO inflow volume transport, but there are also periods when this relationship completely breaks down, for instance between 1930 and 1950 (Figure S1).

We note that AW exits the Nordic Seas through both the BSO and FS; however, we focus on the BSO and the northeastward flow through the Barents Sea. The dynamics in FS are more complex, with both a northward AW flow in the West Spitsbergen Current, and a southward flow in the East Greenland Current on the western side. Although there is a clear connection between the flow through FS and the circulation in the Nordic Seas (Nøst & Isachsen, 2003), the responses in both inflow and outflow due to the GSP and GSM experiments are less consistent across the models. We believe this is in part because the balance between the BSO AW-branch, the FS AW-branch, and the FS outflow is different across the suite of models we investigated. The FS is also a region with recirculation (Hattermann et al., 2016; Wekerle et al., 2017), and the volume transport varies a lot depending on where the sections are defined (Marnela et al., 2013). Here the models are likely to be different, and the response in recirculation due to GSP and GSM can also differ. Additional complications in the FS are the strong northerly winds, especially during winter, and the steep topography, possibly resulting in large differences in eddy activity depending on model resolution. The complexities of FS demand further investigation using higher-resolution models. However, we discuss the role of the FS branch briefly in section 5.

Although there are some differences among the models, there is a clear relationship between the GS wind stress, the circulation of AW in the Nordic Seas, and the volume transport through the BSO. We find that there is a linear relationship between volume transport anomalies and heat transport anomalies for all models which will be discussed in more detail in the following section.

4.3. Sea Ice Response

The sea ice responses in the NH, and in the combined Barents and Kara Seas, are consistent across the models for the GSP and GSM experiments (Figures 7a and 7b). With an increased GSP wind stress and increased BSO heat transport, all models show a significant reduction of sea ice extent in the Barents and Kara Seas. On average, the annual mean reduction is 50,000 km^2, approximately 5% of the simulated annual mean in the Barents and Kara Sea region. The spatial pattern of sea ice anomalies (Figures 4b and 4c) shows that the response of sea ice area and thickness is confined to the Barents and Kara Seas, North of Svalbard, and the ice edge in the GS, all regions near the AW inflow. Figure 4 shows the NorESM model, but other models behave similarly. As is discussed in the upcoming sections, the response of sea ice in the Barents and Kara Seas occurs mainly during winter. As for the other CRFs, the response of the sea ice cover is also asymmetric between the GSP and GSM cases (Figures 7a and 7b). Due to the reduced GSM wind stress and ocean heat transport through the BSO, all models experience an increase of sea ice extent in the Barents and Kara seas, which is more than double the GSP reduction. The increase in sea ice extent varies from 30,000 to 150,000 km^2, an increase of 3–13%. In general, the sea ice response from the fully coupled Ox-HiGEM model

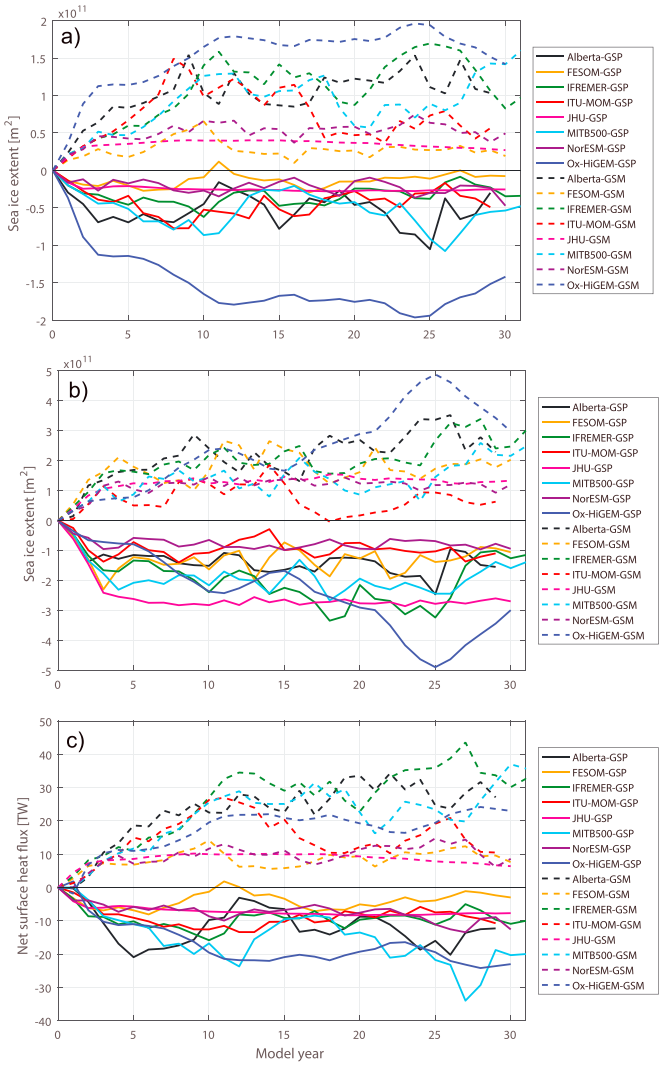

Figure 7. Annual mean climate response functions for sea ice and heat loss. (a) Sea ice extent in the Barents and Kara Seas region, (b) Northern Hemisphere sea ice extent, and (c) spatially integrated net surface heat flux in the Barents and Kara Seas region. The 4-mbar Greenland Sea Plus (GSP) and Greenland Sea Minus (GSM) forcing is shown in Figure 2, and the Barents and Kara Seas area in Figure 1.

is larger than for other models. We believe this is due to the ocean-atmosphere feedback mechanisms related to the surface heat fluxes, which are not captured in the forced simulations. These feedback mechanisms are discussed at the end of the section 4.4. Here it is also important to remember that the Ox-HiGEM responses are symmetric by construction, because we assume linearity. The sea ice extent response in the whole NH is significantly larger than in the Barents and Kara Seas region, mainly due to the large response in the GS (Figure 4). The NH multimodel mean sea ice extent response is approximately 13% for both the GSP and GSM.

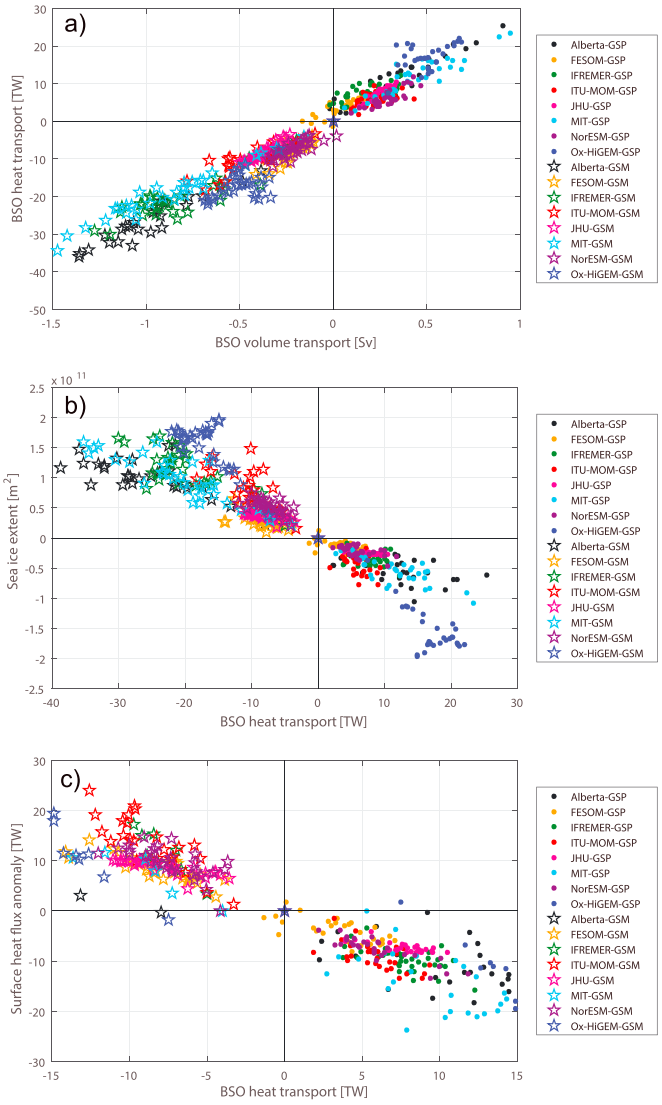

Figure 8. Annual mean values from the climate response functions of Barents and Kara Sea transport, sea ice and heat flux anomalies plotted against each other: (a) heat transport through the Barents Sea Opening (BSO) as a function of volume transport; (b) sea ice extent as a function of BSO heat transport; and (c) integrated net surface heat flux over the Barents and Kara Seas as a function of BSO heat transport. GSP = Greenland Sea Plus; GSM = Greenland Sea Minus.

We find a linear relationship between volume transport anomalies and heat transport anomalies for all models (Figure 8a). There is also a near linear relationship between the advected BSO heat transport anomalies and Barents and Kara sea ice extent anomalies (Figure 8b). Because a larger heat transport leads to less ice, the correlation is negative. On average, a 10-TW heat transport anomaly will result in a change of 50.000 km^2 sea ice area. The direct influence of AW heat anomalies on Barents sea ice has previously been suggested and was estimated by Årthun et al. (2012) to be 70.000 km^2 per 10 TW. An effect of AW heat anomalies has

also been suggested for the area north of Svalbard by Onarheim et al. (2014), and here the sea ice is observed to melt effectively if advected over warm AW in the surface layer (Peterson et al., 2017). The AW heat can thus reduce the sea ice cover through direct bottom melt (Sandø et al., 2014) and the reduction of sea ice growth during winter. The latter has been suggested to be the most important in the Barents Sea, and this is why the influence of AW is mainly a winter signal (Onarheim et al., 2018). Another recent study by Barton et al. (2018) showed that since 2005, the winter sea ice edge in the Barents Sea has been restrained by an increase in temperature gradient across the Polar Front, which is a potential vorticity constrained shelf slope current in the eastern Barents Sea. This change may be driven by an increase in AW temperature (Barton et al., 2018). During summer, the Barents Sea is mainly ice free, and therefore, the influence of AW is much smaller.

Changes in sea ice cover involve a complex interplay between atmospheric and ocean forcing. During winter, the ocean often plays a more important role because of the cold air temperatures and lack of solar radiation, but untangling these two driving forces is complicated. In our study, the atmospheric variability in the Barents Sea region is not altered, and only the remote winds are perturbed, which results in an increased ocean heat transport here. We therefore know that the changes in sea ice must largely be related to changes in ocean heat transport. Another possible explanation for altered sea ice cover is changes in sea ice advection. Change in sea ice transport due to GSP and GSM wind anomalies is shown for NorESM in Figure 4d. Response is small in the Barents Sea, but the climatic mean FS sea ice southward export is increased by ~10% due to GSP and decreases similarly for GSM. The downstream GS ice cover increases with GSM for both sea ice thickness (Figure 4c) and extent (Figure 4b) and decreases for GSP, suggesting that the strong GSP winds also bring more AW to the northern GS and melt ice there. It is possible that ice transport anomalies in the Northern Barents Sea explain a part of the sea ice extent anomalies in the Barents and Kara Seas.

Although the response of the sea ice cover is generally consistent across the suite of models, there is some spread in the CRFs, and we believe that this is partly linked to spread in the heat transport CRFs and partly due to differences in the mean sea ice state of the models. For example, models that already have a large sea ice cover experience a small GSM response, and models with a small sea ice cover experience a large increase during GSM. The mean sea ice extent for each of the models is given in the supporting information. NorESM, FESOM, and JHU are the models with smallest GSM response (Figure 7a) and have the largest ice cover in the control simulations. We anticipate a southern maximum limit set by radiative fluxes for the sea ice edge in the Barents and Kara Seas, even with a strongly reduced ocean heat transport. Other models have less ice in their control simulation and therefore grow more ice before they reach the same limit. The forcing of the Alberta model covers a later time period than all other models and therefore has a warmer climatic mean state, and a reduced sea ice cover in comparison to the other models. This might explain why it also has the strongest response during the GSM experiments.

Because the AW influence on sea ice cover in the Barents Sea is mainly a winter signal, we need to ensure that the models have a realistic seasonal cycle. We have therefore compared the variability in the different control simulations to satellite observations. Figure S3 presents a Taylor diagram of the model's seasonal cycle (a) and interannual variability (b), for the time period 1980–2010 in comparison to satellite observations from the National Snow and Ice Data Center (NSIDC; Cavalieri et al., 1996). All models simulate the seasonal cycle well, with correlations higher than $r = 0.97$, but with relatively large differences in standard deviation. There is a relatively large difference between the observed and simulated interannual variability. The ITU-MOM, IFREMER, and FESOM models are closest to the NSIDC variability with correlation coefficients higher than 0.8. The ITU-MOM and FESOM models share the same forcing data set and are therefore expected to have similar variability.

The third from bottom and second from bottom rows of Figure 6 represent the correlation values over the control simulation between the heat transport through the BSO and the sea ice extent and volume in the Barents and Kara Seas. As expected, in summer the correlation values are low. During summer, most of the area is ice free, and the relatively warm atmosphere and incoming solar radiation appear to control the remaining interannual variability. During winter, however, the atmosphere is generally cold; there is no melting due to solar radiation, and hence, we expect the ocean to play a more important role. Indeed, winter correlation values are generally high for all models. There is, for example, a significant correlation (with a significance level of 95%) between BSO heat transport and sea ice extent, with values ranging between $r = 0.37$ and $r = 0.61$. NorESM has the highest correlation ($r = 0.61$), followed by MIT ($r = 0.57$). The

IFREMER model has the lowest correlation ($r = 0.37$) between BSO heat transport and sea ice extent. For most models, with an exception of ITU-MOM, the correlation is higher with sea ice extent than with sea ice volume.

4.4. Air-Ocean Heat Exchange in the Barents Sea

The Barents Sea occupies only 10% of the Arctic Ocean, and the mean depth is 230 m, creating favorable conditions for cooling of the inflowing AW. In wintertime, when the incoming solar radiation is negligible, this heat loss from the ocean increases, but sea ice also limits this ocean heat loss. Figure 9 displays the annual mean net ocean-atmosphere surface heat flux (averaged over the last 10 years of simulation for all models) and the response due to GSP and GSM. Negative values represent a cooling of the ocean. In general, the mean values are negative in the Nordic Seas and the Barents Sea, with the largest fluxes found along the pathway of the North Atlantic Current. As expected, the surface heat fluxes in the Barents and Kara Seas are highly dependent on the sea ice cover. The average values for the integrated surface heat fluxes and sea ice area in the Barents and Kara seas for the control simulations of the different models are given in Table 3. While the JHU and MIT models have relatively low surface heat flux in the Barents Sea, most models are close to the estimated 76 TW for this region (Table 3; Smedsrud et al., 2013). The fully coupled Ox-HiGEM model has three times the net surface heat flux. Models with a small ice cover, such as Alberta and FESOM, generally lose more heat than models with a larger ice cover. For the majority of models the heat loss is largest toward the north, where the atmosphere is colder and cold-air outbreaks occur. A prominent feature in most models is also large heat loss in the West Spitsbergen Current and near the sea ice edge in the GS. In the FESOM, IFREMER, JHU, and NorESM models there is an annual mean surface heating in the Norwegian and Iceland Seas, a feature that is not prominent in the Alberta, ITU-MOM, and MIT models.

Center and right panels in Figure 9 show a consistent response in surface heat fluxes due to GSP and GSM across the suite of models. The stronger atmospheric GSP forcing causes increased northward ocean heat transport, increased heat loss from the Barents Sea, west of Svalbard, and near the sea ice edge in the GS. Due to the faster GSP circulation, less heat is lost in the Norwegian and Iceland Seas, and warmer anomalies reach further north and increase heat loss there. The opposite is true for decreased GSM atmospheric forcing. The response in the Barents Sea is mainly confined to the northern Barents Sea and linked to the retreat of the winter sea ice edge. On an annual basis this region has more open water and therefore loses more heat. The CRFs of the integrated surface heat fluxes over the Barents and Kara Sea are presented in Figure 7c. The multimodel mean response is approximately 10 W/m^2 for GSP and 20 W/m^2 for GSM, approximately 15–30% relative to the control annual mean. The time scale of this response is slightly longer than for the BSO fluxes and sea ice, approximately 10 years. Again, we believe the spread for GSM is mainly connected to the differences in sea ice state. Models with a large mean sea ice cover tend to have a larger response in sea ice during GSP and open up a large area of open water resulting in a large response in surface heat fluxes. The opposite is true for the GSM case. Heat transport anomalies through the BSO may warm the Barents and Kara Seas, enter the deep Arctic basins, or be lost to the atmosphere. A scatter plot of the surface heat flux anomalies versus the ocean heat transport anomalies is shown in Figure 8c. Although the spread between models is slightly bigger than for Figures 7a and 7b, the scatter plot indicates a near linear relationship between the ocean heat transport anomalies and the surface heat flux anomalies. Direct comparison of the surface heat flux anomaly with the ocean heat transport anomaly is difficult since we do not have a closed heat budget. Figure 8c suggests that a large portion of the advected heat anomalies are lost to the atmosphere in the Barents and Kara Sea region. This is mainly because the positive AW heat anomalies prevent formation of sea ice increasing the open-water area, cooling the AW more efficiently. Årthun et al. (2012) showed that the BSO inflow heat transport carries 79% of the annual variance in the net advective heat convergence in the Barents Sea, and 94% if monthly values are considered. The variabilities of the heat convergence and the inflow are thus closely related, and the temperature variability in the water exiting the Barents Sea is small. This supports the theory that most heat anomalies are not advected into the deep Arctic basins but are either completely lost to the atmosphere or change the heat content locally. This is discussed further in section 5.2.

Several positive feedback loops in the coupled Barents Sea ocean-ice-atmosphere system are possible (Smedsrud et al., 2013). For example, increased surface heat loss from the ocean to the atmosphere, resulting from anomalous ocean heat transport, has been proposed to reinforce the ocean heat transport (Ikeda, 1990; Ikeda et al., 2001; Smedsrud et al., 2013). The increased surface heat loss would lead to a reduction in SLP, and hence, the resulting cyclonic atmospheric circulation anomaly would produce stronger westerly winds over the BSO. Smedsrud et al. (2013) also hypothesized another positive "ocean-feedback" mechanism, where the

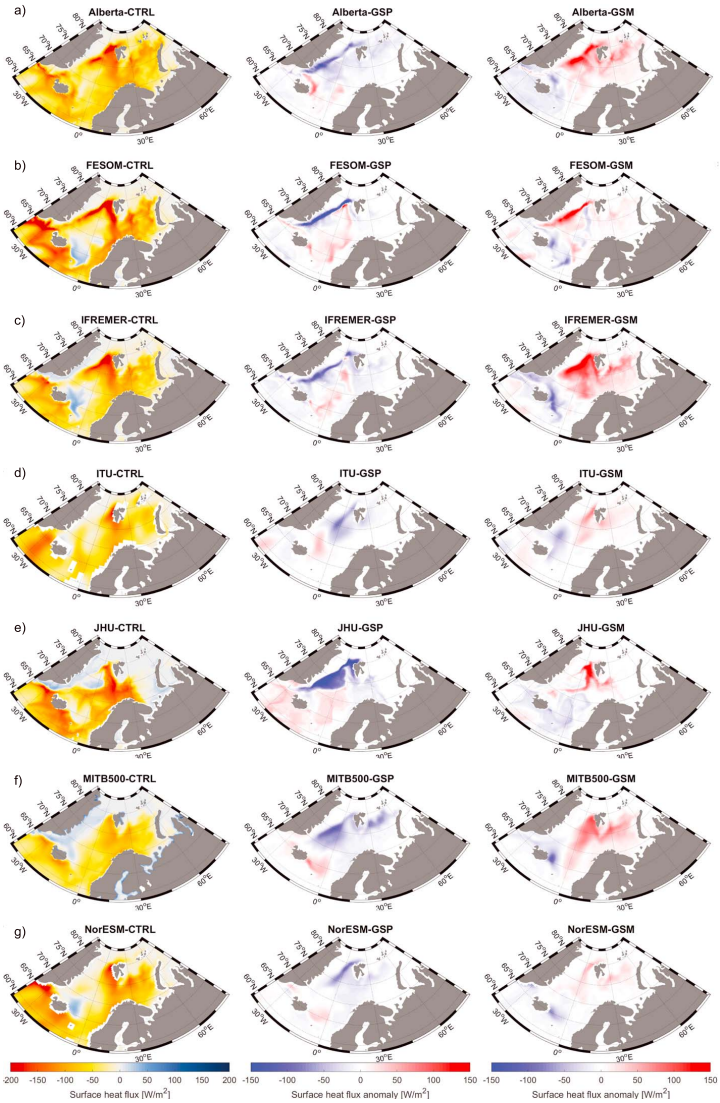

Figure 9. Surface heat flux from the different models. Negative values denote heat loss from the ocean to the atmosphere. Panels on the left show the control simulations, middle panels show Greenland Sea Plus (GSP) anomalies (stronger wind forcing), and right panels show Greenland Sea Minus (GSM) anomalies (weaker wind forcing). All values are averaged over the last 10 years of integration (20–30 years after perturbation).

increased ocean heat loss results in more dense water formation in the Barents Sea and a stronger outflow in the northern Barents Sea, which has to be compensated by a stronger inflow of AW through the BSO.

The models included in Figures 8c and 7c do not include the possibility for any ocean-atmosphere feedback mechanisms, so we believe that the relationship and the response shown there might be different in a fully

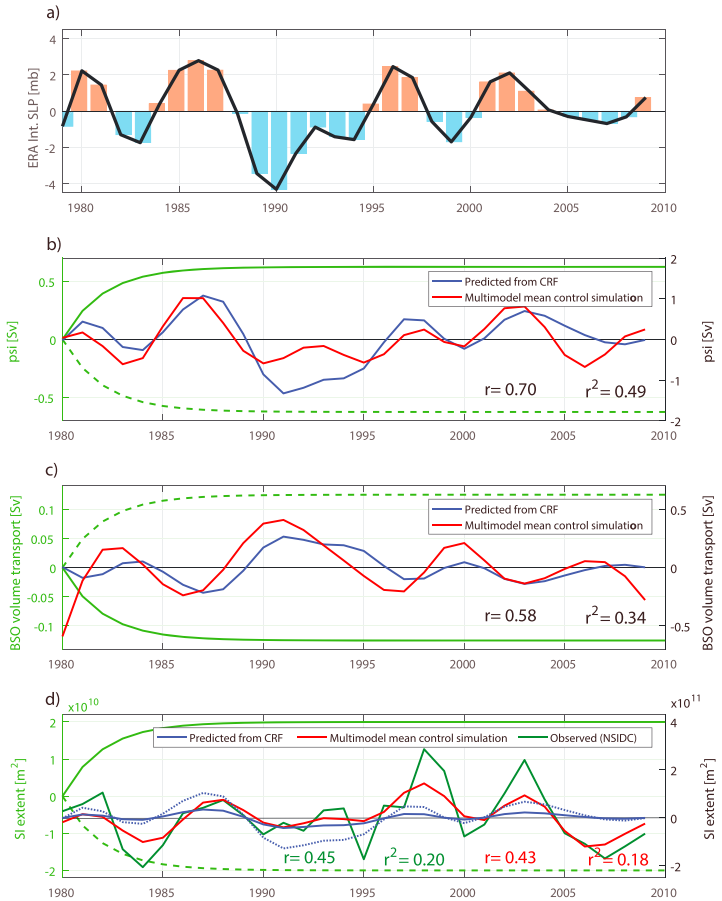

Figure 10. Historical low-pass filtered sea level pressure (SLP) anomalies in the central Greenland Sea from ERA-Interim reanalysis (W_{GS} in equation (4)). (b) Analytical fit (green curves) of the multimodel barotropic stream function climate response function (CRF; C, equation (3)), and anomalous strength of the barotropic stream function, BTS_{NS}, predicted by the CRFs (equation (4); blue curve) and directly simulated by the models (red curve). Note that the green curve has a different scale compared to the red and blue curves and that this is per mb. (c) Analytical fit (green curves) of the multimodel Barents Sea Opening (BSO) volume transport CRF, and anomalous BSO volume transport, VT_{BSO}, predicted by the CRFs (blue curve) and directly simulated by the models (red curve). (d) Analytical fit (green curves) of the multimodel Barents and Kara Seas sea ice extent CRF, and anomalous Barents and Kara Seas sea ice extent, SI_{BK}: observed from National Snow and Ice Data Center (NSIDC; dark green curve), predicted by the CRFs (blue curve) and directly simulated by the models (red curve). Green values denote the correlation between the predicted and the observed time series, and red values denote the correlation values between the predicted and simulated sea ice extent. All time series are detrended. The blue dotted line represents a hypothetical prediction if we assume the CRF has an amplitude three times larger than the multimodel mean.

coupled system. In our simulations, while sea ice cover responds to the changing ocean conditions, the reanalyzed atmospheric forcing remains unaltered and is based on the prescribed sea ice cover of the reanalysis product. Air temperatures over ice covered regions are indeed lower than over open ocean. For new open water regions, these cold temperatures over regions that used to be ice covered will probably be too cold. This is an uncertainty because we only simulate a part of the naturally occurring coupling. For example, the sea ice response to increased AW heat input could be a low-end estimate because of strong heat loss where

the atmosphere is too cold. The Ox-HiGEM CRFs are calculated from multiple linear lagged regression in a coupled model control run and, as such, partly incorporate atmospheric feedbacks related to surface heat fluxes. This may explain the stronger Ox-HiGEM sea-ice response.

The negative correlation between BSO ocean heat transport and sea ice extent suggests that ocean variability is an important driver of sea ice variability. The increased ocean heat transport from the GSP anomalies results in a smaller sea ice cover in the Barents and Kara Seas. The larger open water area hence results in increased ocean-to-atmosphere heat fluxes in all models. Similar dependence was found from direct observations by Ivanov et al. (2003) and Smedsrud et al. (2013).

4.5. Convolution of the CRFs and Potential for Prediction

Having described the response resulting from anomalous SLP in the GS and the form of some key CRFs, we now use this to compute the response to a historical time series of SLP anomalies in the GS (Figure 10a). These "hindcasts" are then compared to calculations from the different models and observations. This comparison gives a sanity check on the utility of the CRFs and can provide us with information on how much of the simulated (or observed) variability can be explained by the GS SLP anomalies. The methodology follows the same procedure as described in Marshall et al. (2017). Here, the focus will be on the relationship between the GS SLP anomalies and the CRFs of the barotropic stream function in the Nordic Seas (Figure 5a), BSO volume transport (Figure 5b), and sea ice extent in the Barents and Kara Seas (Figure 7a).

We define C (units Sv/mbar) as the response function per unit forcing of the mean barotropic stream function strength in the Nordic Seas. $\widehat{BTS}_{NS}$ (units Sv) is the amplitude of the resulting change in the barotropic stream function induced by pressure anomalies over the GS. We fit an analytical expression to the multimodel mean CRFs shown in Figure 5a and assume that the responses to GSP and GSM are roughly equal of magnitude but of opposite sign. All calculations have also been performed with the CRFs of the individual models (not shown), but since we did not find notably different results, we have chosen to only present the fit based on the multimodel mean. The following analytical expression broadly captures the form of C:

$$C \times W_{\text{step}} = \widehat{BTS}_{NS}(1 - \exp(-\gamma t)), \tag{3}$$

where the scaling factor W_{step} is the magnitude of the step function in forcing (4 mbar in our case). The time scale of response is very short, as described earlier. An analytical fit based on Figure 5a suggests that $\gamma = \frac{1}{2}\ \text{y}^{-1}$ (i.e., an e-folding response time of 2 years) with $\widehat{BTS}_{NS} = 2.5$ Sv (green lines in Figure 10b). Following equation (1), we may now write

$$BTS_{NS}(t) = \int_0^t C(t - t')\frac{\partial W_{GS}}{\partial t}(t')dt', \tag{4}$$

where W_{GS} (units mbar) is a time series of historical pressure anomalies over the GS, as shown in Figure 10a from the ERA-Interim reanalysis (Dee et al., 2011). We have also tested other reanalysis products, but the results are not sensitive to the product being used. The solution of equation (4) gives us an estimate of the barotropic stream function solely based on GS SLP anomalies and our analytical CRF and is presented in Figure 10b. Unfortunately, there are no observations of the Nordic Seas barotropic circulation strength with which to compare, but comparison with the multimodel mean from the control simulations gives high correlations ($r = 0.7$). These results lend strong support to a close relationship between anomalous SLP in the GS and the barotropic circulation in the Nordic Seas. The success of the convolution in reconstructing the variability in the strength of the Nordic Seas barotropic circulation suggests that almost all of the variability in this circulation is driven by the imposed wind pattern, we have imposed, and that the relationship is relatively linear.

A similar exercise can be repeated for the BSO volume transport, which we will define as VT_{BSO}. As explained above, we can fit an analytical expression similar to equation (3) to the multimodel CRFs shown in Figure 5b. The green curves in Figure 10c represent the fitted analytical response function C (units Sv/mbar) for the BSO volume transport with $\gamma = \frac{1}{2}\ \text{y}^{-1}$ and $\widehat{VT}_{BSO} = 0.5$ Sv. The blue curve in Figure 10c shows the solution of the convolution (as equation (4)) for the BSO volume transport CRF. The estimated volume transport compares well with the simulated multimodel mean, and their correlations are relatively high ($r = 0.58$). The skill on this estimate is somewhat lower than for the barotropic stream function in the Nordic Seas, but this is expected because we are further away from the perturbation location and also expect other mechanisms to influence the variations in the BSO volume transport. For example, the local wind direction in the BSO is

likely to be important (Muilwijk et al., 2018). Also, the models we use differ in how well correlated the BSO volume transport is with the Nordic Seas barotropic circulation, and hence with the winds in this region. This will be further discussed in section 5.2. In general, we conclude that there is also a relatively close relationship between anomalous SLP in the GS and the volume transport through the BSO.

Finally, we investigate the convolutions of CRFs from sea ice extent in the Barents and Kara Seas, which we define as SI_{BK}. A multimodel analytical fit of the CRFs presented in Figure 7a is shown in green in Figure 10d. Again, the analytical fit, C (units m^2/mbar), may be expressed like equation (3), now with the coefficients $\gamma = \frac{1}{2}$ y^{-1} and $\widehat{SI}_{BK} = 0.8 \cdot 10^{11}$ m^2. For sea ice extent in the Barents and Kara Seas a good observational record can be obtained from NSIDC passive microwave satellite data (Cavalieri et al., 1996). In Figure 10d, the observed sea ice extent anomalies in the Barents and Kara Seas region are compared with the simulated multimodel mean sea ice extent anomalies, and with the prediction based on the convolution of the analytical CRF and the GS SLP time series (similar to equation (4)). First we would like to point out that although the multimodel mean anomalies are somewhat smaller than the observed anomalies, the correlation between these two time series is high ($r = 0.84$, not shown). The correlation of the time series from individual models with the observed sea ice data was discussed in section 4.3 and can also be seen in the Taylor diagram in Figure S3. Because these are simulations with a forced "realistic" atmosphere, it is expected that they simulate the sea ice variability quite well (Ilicak et al., 2016). The estimated sea ice variability based on the analytical CRF and the GS SLP anomalies is shown in blue in Figure 10d. Its correlation with the observed sea ice anomalies is $r = 0.45$, and the correlation with the simulated multimodel mean anomalies is $r = 0.43$, thus much smaller than for the barotropic flow or the BSO volume transport. Also, the amplitude of the anomalies from the convolution time series is smaller than what is observed and simulated.

The limited success of the reconstructed sea ice variability based on GS SLP anomalies is not unexpected. First, as discussed in section 4.3, there may be several nonlinear responses and feedback mechanisms that are not captured in our CRFs due to the nature of our forced simulations. Hence, we hypothesize that our sea ice response is underestimated (an argument supported by the CRF results from the fully coupled Ox-HiGEM simulation). If our CRFs were to reach an equilibrium that is larger than $\widehat{SI}_{BK} = 0.8 \cdot 10^{11}$ m^2, the estimate would slightly improve. This is illustrated by the dotted blue line in Figure 10d, which shows the convolution based on a hypothetical CRF with an amplitude three times larger than the multimodel mean CRF, and slightly larger than the Ox-HiGEM CRF in Figure 7a. Second, and most importantly, although we do observe a clear linear response in the Barents and Kara Seas sea ice cover following the GS SLP anomalies (Figure 8), there may be other atmospheric and oceanic remote effects that have a potential impact but are not captured in our CRF convolution (Nakanowatari et al., 2014). For example, Onarheim et al. (2015) presented a framework for skillful prediction of sea ice in the Barents Sea based on ocean heat transport, but ocean heat transport is affected by both temperature and volume transport anomalies. Advected temperature anomalies from the south also influence the ocean heat transport into the Barents and Kara Seas (Årthun et al., 2017; Muilwijk et al., 2018). In our CRF experiment we mainly perturb the volume transport.

Hence, we conclude that our CRFs provide a good potential for prediction on relatively short time scales (2 years) of the Nordic Seas barotropic circulation and the BSO volume transport, but not for sea ice extent. The convolutions allow us to produce an estimate of the variability in Nordic Seas circulation directly from knowledge of the winds, without running a model. They also underpin the utility of our perturbation experiments and the value of computing CRFs. Further investigation of the convolution procedure is a current research focus, and this method will likely be refined in future work.

5. Discussion

5.1. Ekman Pumping and the Resulting Circulation

The barotropic circulation results presented in Figure 3 are in accordance with Isachsen et al. (2003), who presented a lowest order theory of the temporal variability for circulation in the Nordic Seas, and related it to Ekman-dynamics. Isachsen et al. (2003) found that anomalous Ekman convergence contributes to a spin-up (or spin-down) of the gyres within regions enclosed by contours of constant f/H, where f is the Coriolis parameter and H is the water depth. In this barotropic model, gyres will spin up cyclonically for cyclonic wind stress anomalies and vice versa. The barotropic response we see from our GSP and GSM experiments is also bounded by f/H contours (not shown) and thus consistent with the simple model of Nøst and Isachsen (2003). However, cyclonic wind stress is likely not the only explanation for the mean cyclonic gyre circulation

in the Nordic Seas because baroclinic pressure terms will eventually balance the surface Ekman pumping (Nøst & Isachsen, 2003). The cyclonic circulation in the Nordic Seas and the narrow cyclonic AW boundary current in the Arctic Basin is likely also partially explained by eddy-topography interaction, or the so-called "Neptune effect" (Holloway, 1987).

From Figure 3 we see that there are relatively large differences across the suite of models in regard to the strength and spatial patterns of barotropic circulation. The barotropic circulation is mainly wind driven, and hence dependent on surface stress and Ekman pumping. Nøst and Isachsen (2003) simulated the barotropic circulation in the Arctic Ocean by using the Ekman Pumping and the hydrographic forcing resulting from the geostrophic shear as "forcing terms." The Ekman Pumping velocity (W_{ek}) can be calculated from the surface stress (τ_s) and is given as

$$W_{ek} = \nabla \times \frac{\tau_s}{\rho_0 f}. \tag{5}$$

The hydrographic forcing resulting from geostrophic shear (W_g) can be calculated from the density field and is given as

$$W_g = -V_s \cdot \nabla f / f, \tag{6}$$

where

$$V_s = \frac{1}{\rho_0 f}\mathbf{k} \times \int_{-H}^{0} (\nabla p - \nabla p|_{z=-H}) dz. \tag{7}$$

Here V_s is the geostrophic shear, p the hydrostatic pressure, f the Coriolis parameter, H the water depth, and ρ_0 a reference density of 1,027.8 kg/m^3. Based on their results we explore whether major model differences in the barotropic circulation in the Nordic Seas are a result of either differences in W_{ek} or differences in W_g, the latter being mainly dependent on the mean hydrography. Differences in the resolution dependent representation of bottom topography in the models may also influence the barotropic circulation. The topography might be especially important for the division of the North Atlantic Current into the BSO or FS branches.

Figure 11 shows maps of the annual mean strength of W_{ek} in the control simulations. In general, most models share similar Ekman pumping behavior, but regional differences are visible, particularly in the Barents Sea region. The strongest upwelling is found in the Irminger Basin, Iceland Sea, and southern part of the GS. The strong Ekman pumping in the Irminger Basin is related to the Greenland tip-jet. Nearly all models experience a modest upwelling in the Norwegian Sea and GS, with a minimum in the center of the Basin. NorESM shows relatively large upward Ekman velocities in the GS and Lofoten Basin but also downward Ekman velocities in the central Norwegian Sea. This downwelling is related to the position of the climatological atmospheric low-pressure center in NorESM. While most models experience one large low-pressure system over the Nordic Seas in their long-term mean, NorESM experiences a SLP structure (not shown) with a second low-pressure center centralized over the Lofoten Basin and one low-pressure center over Iceland. Both these centers create Ekman divergences and upwelling, but where they meet in the central Norwegian Sea, they create a convergence zone and downwelling. The wave-like structure in Ekman pumping in NorESM is a result of the topography of Greenland and Iceland. ITU-MOM has the largest regions with strong upwelling in the GS and Irminger Basin.

Relatively strong coastal downwelling is found east of Greenland and Svalbard and is strongest for the FESOM model. All models also experience general downwelling in the Canadian Basin, this is strongest in the JHU model. The values noted in Figure 11 represent long-term average values of the mean Ekman pumping strength for the central Nordic Seas region, and also the mean strength of the Ekman pumping anomalies due to GSP and GSM. From these values we observe that there are relatively large variations in the mean Ekman pumping strength in this region. Spatial maps of W_{ek} anomalies due to the GS experiments are shown in Figure S11.

There is no clear link between the average strength of Ekman Pumping (values noted on Figure 11) and average strength of the barotropic stream function in the same region (Table 3). From the models with relatively low Ekman pumping strength (Alberta, IFREMER, and MIT), only IFREMER and MIT have a relatively weak barotropic circulation. NorESM is another model with relatively weak barotropic circulation, but NorESM has relatively strong Ekman pumping. All models have relatively similar Ekman pumping

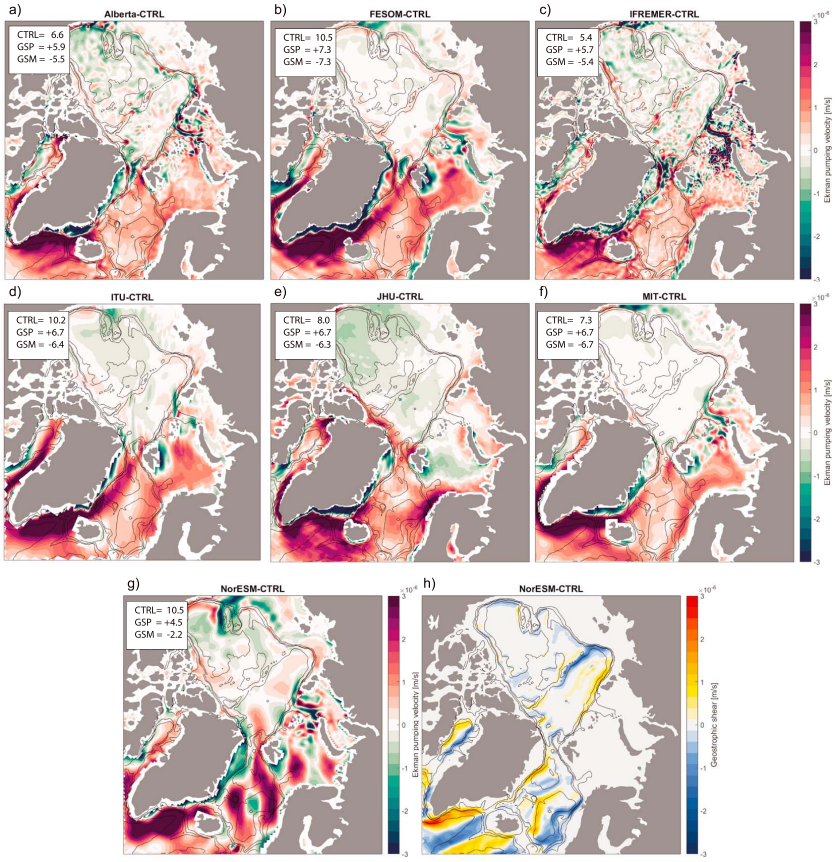

Figure 11. (a–g) Map of the annual mean Ekman pumping ($\nabla \times \tau_s/\rho_0 f$) field computed from the model control simulations. Positive values denote upward velocities. Values in the upper left represent the long-term mean (and anomalies due to Greenland Sea Plus [GSP] and Greenland Sea Minus [GSM]) Ekman pumping averaged over the Nordic Seas region (green box Figure 3). Values are given in 10^{-7} m/s. (h) Map of the annual mean "hydrographic forcing" (given by the geostrophic shear, $-V_s \cdot \nabla f/f$) computed from the NorESM control simulation. All values are averaged over model years 20–25. Black lines show f/H contours. Maps of the spatial anomalies due to GSP and GSM are given in the Supporting Information (Figure S11).

anomalies in response to the GSP and GSM forcings (Figures 11 and S11). NorESM, however, has relatively weak anomalies, and this might explain the relatively weak response for the barotropic stream function (Figure 5a). Based on these results, we hypothesize that differences in the mean (and anomalous) barotropic circulation may partially be explained by spatial differences in the Ekman pumping, possibly related to differences in sea ice cover. Differences in Ekman pumping (Figure 10) may also result from differences in model resolution or differences in the bulk formula, which may impact the barotropic circulation.

Another possible explanation for differences in the barotropic circulation may be differences in mean state hydrography (Nøst & Isachsen, 2003). Differences in hydrography will be manifested in differences in geostrophic currents as a result of equation (7)). The spatial hydrographic forcing from the geostrophic shear (equation (7)) has only been calculated for the NorESM model and is presented in Figure 11h. On average, this forcing results in a much smaller contribution compared to the Ekman pumping contribution. However,

where f/H contours are close to each other, the geostrophic shear is relatively large. The GS is such a region with relatively large topographic changes. Differences in mean state hydrography here will likely result in different geostrophic shear in this region, which will in turn affect the barotropic circulation. As is shown in section 5.2, the models have substantial differences in hydrography in this region, making this a plausible partial explanation for the differences in barotropic circulation. The GS is also a region with convective mixing resulting in colder and fresher waters at intermediate depth. Differences in convective mixing in the models may thus also affect the mean state hydrography here, and hence the circulation.

5.2. Fate of the AW Heat Distribution and Its Dependence on the Wind

Local increase and decrease in wind stress affects the barotropic circulation strength in the Nordic Seas and the northward heat transport through the Barents Sea (Figure 5). But how far into the Arctic Ocean basins does this anomaly propagate? The GS wind likely also affects the division of the North Atlantic Current between the BSO and FS and, as is described in further detail in section 5.3, it also affects the AW pathways inside the Arctic Basin. The fate of the ocean heat carried by the FS and BSO branches is substantially different. The BSO branch releases a vast amount of heat to the atmosphere in the Barents Sea (Figure 7c), resulting in a strong local cooling of the AW and relatively cold outflow through the St. Anna Trough into the Arctic Basin. Where the FS branch meets the sea ice edge north of Svalbard, the upper layer melts ice, but at intermediate depth the AW continues into the Arctic Basin releasing heat more gradually over a much larger area (Rudels et al., 1996). Changes in the division of the North Atlantic Current between the FS and BSO will likely affect the fate of the AW heat.

Total vertically and horizontally integrated heat content relative to a reference temperature of 0 ° C shows a clear evolution over time for the different regions (Figure 12, left panels). For the Nordic Seas (Figure 12a), there is an overall cooling for stronger GSP wind stress and warming due to weaker GSM wind stress across the suite of models. This is mainly the result of a temperature change of the upper 1,000 m, which can be observed from the long-term mean profiles (Figure 12b). On average, the models experience a warming or cooling of 0.1–0.5 ° C in the Nordic Seas AW layer as a result of the wind perturbations. Generally, cooling is associated with a slight freshening of the AW layer and warming is associated with a slightly saltier AW layer. Change in the vertically integrated heat content comes from changes in the surface heat fluxes (increased or decreased heat loss) and heat flux divergence due to lateral fluxes. The anomalies in heat content are, consistently in all our models, largely explained by changes in lateral fluxes, but local processes in the Nordic Seas are also important, and these result might be slightly different in a system with a coupled atmosphere. We note that there are also substantial differences in the mean Nordic Seas hydrography for the different models. NorESM and IFREMER generally have a cold and shallow intermediate layer, while the ITU-MOM model, for example, has a very deep and warm intermediate layer. These differences translate into large differences in total heat content for the control simulations.

Concerning changes in lateral fluxes, we hypothesize that the reduction in heat content in the Nordic Seas in the GSP case is mainly a result of enhanced AW export in the north and enhanced import of cold Polar Water in the EGC. Another process causing decreased heat content under the GSP forcing is increased Ekman pumping leading to a lifting of the colder water (around 0° C) from below 1000 m. The gyre spin up is associated with a doming of deep isopycnals, and import of more cold deep water from outside the domain, which then contributes to a general decrease of heat content. Tesdal et al. (2018) showed that this also happens in the Subpolar Gyre. Concerning local forcing, the stronger winds lead to stronger heat loss by increasing the turbulent fluxes of sensible and latent heat. Asbjørnsen et al. (2019) have recently shown that 50% of the variability in the Nordic Seas ocean heat content can be attributed to local surface forcing, and although we have not investigated this in depth, we speculate that the changes in heat content arise due to a combination of advection and local forcing. Note that the accelerated Norwegian Current (and resulting greater heat transport from the south) is mainly excluded from the Nordic Seas box shown in Figure 3.

The CRFs of heat content in the Barents and Kara Seas region are shown in Figure 12c. Although the responses are less consistent between models than in the Nordic Seas, most models, with the exception of MIT and JHU, experience an increase in total heat content due to GSP and decrease due to GSM. An increase in heat content is consistent with the increase in heat transport through the BSO (Figure 5) and associated with a slight warming of the whole water column (Figure 12d). The opposite is true for the decrease. This is consistent with Årthun et al. (2012) and strengthens the theory that heat anomalies advected through the BSO mainly affect the surface heat fluxes (Figure 8c) and the heat content locally. A closed heat budget anal-

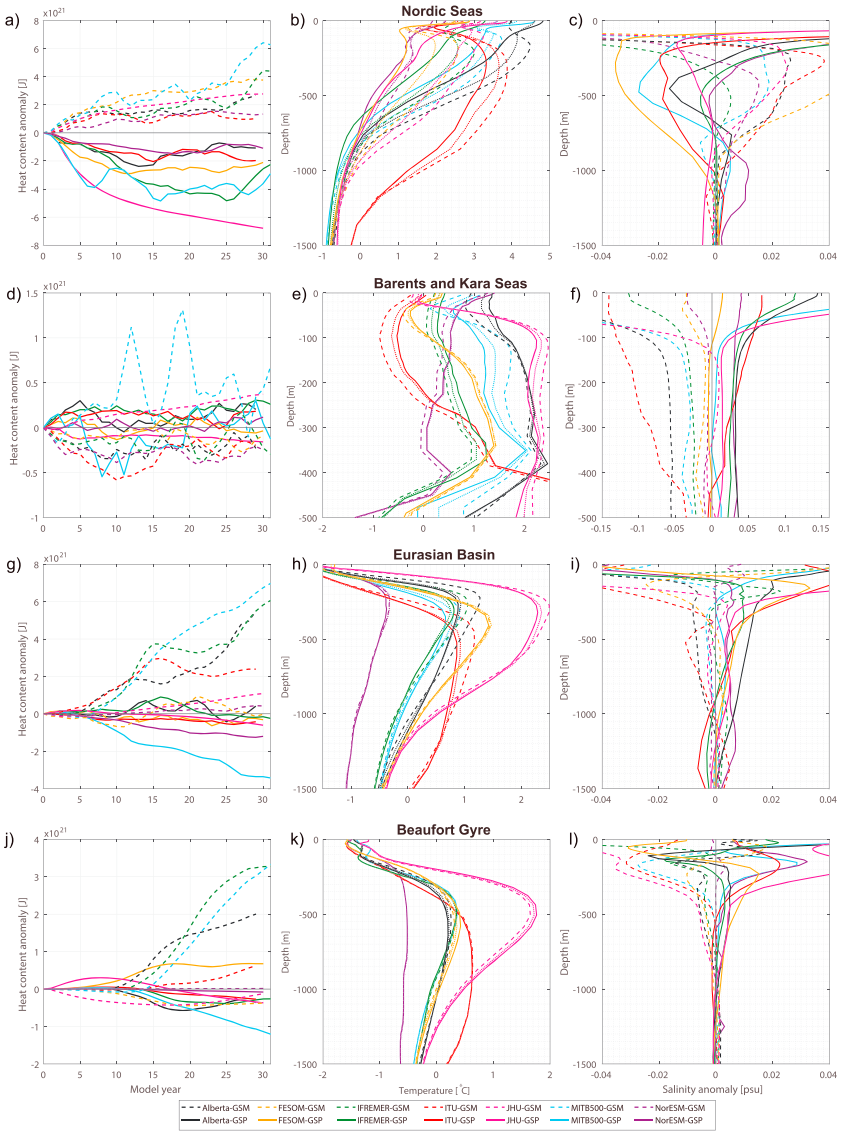

Figure 12. Arctic Ocean heat anomalies, mean temperature profiles, and salt anomalies. Left: climate response functions of vertically and horizontally integrated heat content relative to 0 ° C for the Greenland Sea Plus (GSP) and Greenland Sea Minus (GSM) wind anomalies. Solid lines represent the GSP simulations, and dashed lines represent the GSM simulations. Note that GSP implies a stronger cyclonic forcing over the Nordic Seas and increased barotropic circulation strength in the Nordic Seas. Heat content is calculated over the full depth. Middle and right: annual mean temperature profiles and salinity anomalies for the different basins and models averaged over the last 10 years of integration (20–30 years after perturbation). Solid lines represent the control simulations, dotted lines represent the GSP simulations, and dashed lines represent the GSM simulations. Note that for temperature the actual profiles are shown, but for salinity, only the anomalies are shown.

ysis is needed to confirm this. The only models that do not experience a warming in the Barents and Kara Seas region are MIT and JHU. This might be due to changes in sea ice cover, such that heat loss outweighs the increased heat input. The temperature distribution in the Barents and Kara Sea is relatively uniform throughout the water column, but there are large contrasts between the models, with a difference of more than 2 ° C. We believe this is mainly due to advection.

The GSP and GSM perturbations have a consistent impact on the heat content in the deep Arctic Basins (Figure 12). The response here is delayed, but after approximately 5 years all models experience an increase in heat content in the Eurasian Basin as a result of the GSM perturbation. The MIT, JHU, NorESM, and ITU-MOM models also experience a decrease in heat content in the Eurasian Basin resulting from GSP, but Alberta, IFREMER, and FESOM show no clear response.

There is also a response downstream in the Beaufort Gyre. As in the Eurasian Basin, most models experience a small decrease in heat content from GSP and a slightly larger increase in heat content due to GSM. During GSP the AW layer in the Beaufort Gyre becomes slightly colder and saltier, and during GSM, the AW layer becomes warmer and fresher. It seems likely that less ice and larger surface heat loss in the Barents Sea during GSP result in colder water ultimately entering the Eurasian Basin. After approximately 10 years this anomaly is subsequently advected into the Beaufort Gyre. The opposite is true for GSM, with the AW entering the Arctic through the St. Anna Trough retaining more of its heat due to a more extensive ice cover and less heat loss in the Barents Sea. As is shown from passive tracer results (section 5.3), during GSP, more AW enters the deep Arctic Basins. Because more AW volume is inconsistent with a decrease in heat content, the temperature of the AW must be lower. It is to be noted that the GSP and GSM anomalies are relatively small, and smaller than both the anomalies from the individual models and the differences between the different models. Overall, the effect of the GSP and GSM experiments on the Beaufort Gyre region is not very strong. The FESOM and JHU models show the opposite responses to the other models in the Beaufort Gyre. In section 5.3 we show that the FESOM model is the model with least response in total AW volume in the deep Arctic Basins, which might explain the lack of response in heat content. The JHU model may behave similarly, but unfortunately, this model did not have passive tracers implemented.

Generally, the models have a more similar hydrography in the Eurasian Basin and Beaufort Gyre, but NorESM stands out with a cold bias, and ITU-MOM with a slight warm bias. This is well known and discussed in detail in Ilicak et al. (2016). JHU has a warm bias only in the AW layer. We hypothesize that the change in heat content in the deep Arctic basins is mainly connected to the increased or decreased cooling of AW in the Barents and Kara Seas, and the changing circulation pathways. The lack of response in the Eurasian Basin in the Alberta and IFREMER models might result from redistribution between the different basins. Possibly, the AW is colder, but at the same time more AW stays in the Eurasian Basin. These two processes might outweigh each other. Unfortunately, the IFREMER and Alberta models did not have passive tracers implemented to allow us to check this.

5.3. AW Flow From Passive Tracer Release

To further investigate the circulation of AW, we consider the advection and diffusion of passive tracers that were released in four of the models. These tracers were released continuously at three locations along the AW flow path for approximately 30 years, starting in 1980 (Svinøy, BSO, and FS). Figure 13 shows the mean concentration of a passive tracer 20–25 years after release in the BSO. The tracer concentrations are standardized by depth in order to visualize the differences between the shallow Barents Sea and deep Eurasian Basin. By this we mean that all tracer volumes have been divided by water depth, and it can be interpreted as a fraction of the water column that is filled with tracer. Figures S6 and S7 show the same for the Svinøy and FS tracers. For the BSO tracer we also show the surface concentration and the concentration at the depth of the AW layer (400 m) in Figures S12 and S13, respectively. Most of the Barents Sea is quickly filled up with AW from the BSO, and this eventually enters the Eurasian Basin through the St. Anna Trough. In all models the AW continues to circulate cyclonically in the deep Arctic basins, but the bulk does not cross the Lomonosov Ridge and remains in the Eurasian Basin. After some modification, here the AW circulates back to the Nordic Seas through FS. Animations of these passive tracer concentrations are available in the supporting information.

The tracer release experiments reveal substantial differences in advection between these four different control simulations (Figure 13). The ITU-MOM and FESOM models have the strongest circulation inside the Arctic Basin, where a substantial portion of the BSO tracer ends up in the Canadian and Makarov basins. In

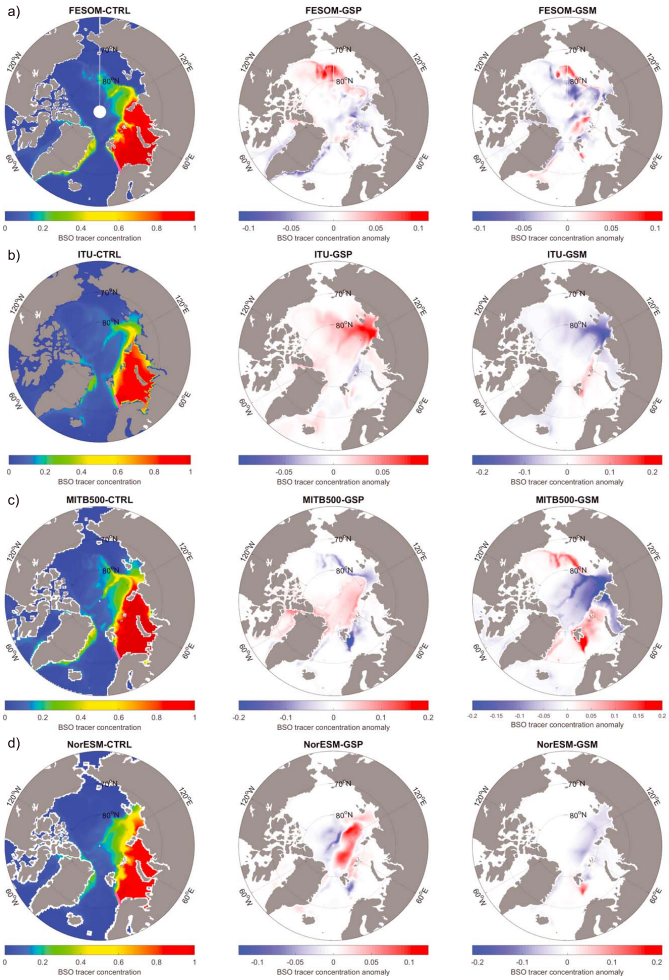

Figure 13. Vertically integrated concentration of passive tracer released continuously at all depths in the Barents Sea Opening (BSO) in four models. Panels on the left show the control simulations, middle panels show anomalies resulting from the GSP experiment (stronger wind forcing), and right panels show anomalies resulting from the GSM experiment (weaker wind forcing). All values are averaged over model years 20–25. Tracer release started simultaneously with the beginning of the perturbation. All values are standardized by depth. The pink line marks the tracer release location.

the MIT simulation less of the BSO tracer crosses the Lomonosov Ridge, and most of the BSO tracer remains in the Eurasian Basin, whereas in NorESM nearly none of the BSO tracer crosses the Lomonosov Ridge. Observations of the circulation in this area are scarce, but Karcher et al. (2012) make the point that the ability of the AW to cross the Lomonosov Ridge might vary over time. One possible explanation is that the MIT and the NorESM models create more dense water in the Barents Sea, and this subsequently has trouble crossing over the Lomonosov Ridge. This is likely related to numerics in the model. The Lomonosov Ridge creates a potential vorticity barrier, so differences between the momentum advection schemes and momentum closure schemes (i.e., viscosity operator) might lead to differences among the models. The tracers released in the FS and at Svinøy also show that there are large differences in how much of the AW recirculates in the

FS. Both MIT and NorESM have relatively high recirculation in the FS whereas ITU-MOM and FESOM generally transport AW further into the Arctic Ocean (Figures S6 and S7).

In general, GSP results in an increased volume of BSO tracer in the deep Arctic Basins for all models and vice versa for GSM after 20–25 years (Figure 13). Because the heat content of these basins goes down (Figure 12), this AW must be colder than before. There is a very limited response in the Barents and Kara seas, because these regions were already filled with AW from the BSO. However, the spatial distribution is also very different from the control simulations. For NorESM and MIT, the AW originating from the BSO and the FS (Figures S6 and S7) is more confined to the southern part of the Eurasian Basin in the GSP case. Here, the Nansen Basin experiences an increased volume of AW, while the Amundsen Basin experiences a decreased volume of AW after 25 years. More AW enters the Arctic Basin in the GSP case, but it does not reach as far north and west into the deep basins. For these two models the increased circulation results also in a quicker recirculation and shorter residence time; as more AW enters, the "throughflow" in the Arctic Basin increases, and more AW exits through FS. This could also contribute to a lower heat content. The opposite is true for the GSM case, where a lower wind stress in the Nordic Seas results in less AW in the deep Arctic Basins. For MIT there is a positive AW volume anomaly in the Makarov and Canadian basins for the GSM case, meaning the AW reaches further to the north and west when the circulation is weak. This contributes to the positive anomaly in heat content of the Beafort Gyre in the GSM case (Figure 12).

The ITU-MOM and FESOM models behave slightly differently than MIT and NorESM. The ITU-MOM model also experiences an increased AW volume in the deep Arctic basins in the GSP case, but here the increase mainly results in more tracer volume further away from the inflow region, toward the Laptev Sea, Makarov Basin, and Canadian Basin (Figure 13). This increase is Arctic-wide for ITU-MOM, but with the strongest response in the Laptev Sea. Because this increase of AW volume is related to a decrease in heat content (Figure 12), the AW must be colder than before. FESOM actually experiences a decrease of AW volume in the Nansen Basin and an increase in the Makarov and Canadian Basins. For FESOM, the GSP case does result in a longer AW residence time in the Arctic Basin, and hence less AW volume in the outflowing East Greenland Current. In the GSM case, the ITU-MOM model also experiences an overall decrease of AW volume in all the deep Arctic basins. Again, the response is strongest in the Laptev Sea. For FESOM there is also a general decrease in AW for GSM, but also a small increase in the Nansen Basin and the southern parts of the Canadian Basin. In the Barents and Kara Seas we see an initial response due to the stronger circulation, which tells us that the Barents and Kara Seas fill up with AW faster due to the GSP perturbations and slower due to the GSM perturbations. In 20 years an equilibrium is reached because the seas are completely filled with AW originating in the BSO. The BSO tracer increases steadily in the Eurasian Basin during the GSP case for the ITU-MOM, MIT, and NorESM models and vice versa for GSM. The FESOM model has an initial response, which is similar to the other models, but in the long term there is no change in absolute tracer volume in the Eurasian Basin. Overall, in the Eurasian and Canadian Basins, an increase of total AW volume is related to a decrease in total heat content, thus the AW temperature is lower than before. The model with least clear response in AW volume in these deep basins (FESOM) is also the model with the smallest response in heat content change.

The change in temperature in the Eurasian Basin has been investigated thoroughly for the NorESM (Figure S5). The average annual mean temperature shows a thick near-surface layer of relatively warm AW entering through FS. This layer cools but continues at depth toward the Laptev Sea. We note that NorESM has a cold bias (Ilicak et al., 2016) and that the absolute temperatures are therefore too low. The GSP perturbation results in a stronger AW circulation and a warmer intermediate and surface layer, but colder temperatures at depth and near the inflow region (Figure S5b). This is consistent with a stronger throughflow in the Nordic Seas combined with a more effective lifting of the colder deep water due to the stronger GSP wind forcing. In the Eurasian Basin the temperatures are colder from the surface to the bottom, apart from just downstream of the FS at intermediate depth. As discussed in section 5.2 this is likely due to the stronger "throughflow" and cooling in the Barents Sea, increasing the proportion of AW that has been effectively cooled and densified, and which ends up at depth in the Eurasian Basin. The cooling could also result from increased transport of colder waters from the Western Arctic.

We conclude that the changing GS wind forcing clearly affects the AW pathways and its residence time in the different seas and basins of the Arctic Ocean. Likely, the strength of the barotropic circulation also affects the vertical distribution, temperature, and possibly also salinity of the AW in the Arctic Ocean. When it comes

to the AW pathways, there are, however, larger differences across the suite of models, both in the mean state and in the responses.

6. Summary and Conclusions

We have here analyzed a suite of different Arctic Ocean model simulations to understand the effect of anomalous wind forcing over the GS. We examined similarities and differences in Nordic Seas circulation, poleward ocean heat transport, AW pathways, and Arctic sea ice. This coordinated model comparison grew out of the Forum for Arctic Modeling and Observational Synthesis community, and one main goal here is to compute CRFs for the Atlantic sector of the Arctic Ocean to understand climate and model sensitivity to changes in wind forcing. We have successfully shown that CRFs based on SLP anomalies have a potential for prediction purposes and that there is a clear link between the GS winds, northward ocean heat transport, and sea ice. Overall, there is a strong general agreement between the different models, but for some aspects the models behave differently and had different biases, which underlines the value of doing cross-model comparisons.

We focus on the sensitivity of AW circulation to stronger and weaker GS winds. The stronger wind forcing, termed GSP, is the geostrophic wind increase related to a 4-mbar drop in surface pressure in the central GS. The weaker forcing is opposite in strength and termed GSM, and they are both comparable to observed Nordic Seas annual mean SLP anomalies that resemble the NAO variability.

A stronger GS wind stress results in stronger cyclonic barotropic circulation in the Nordic Seas and increased northward transport of AW volume and heat through the BSO. A weaker GS wind stress results in the opposite. The responses in the BSO have a response time of 1–5 years where most of the response happens during the first year after the perturbation begins. The change in AW flow extends from south of the Subpolar Gyre, through the Nordic Seas, and all the way north into the Canadian Basin. There is a corresponding net decrease in the depth-integrated heat content in the Nordic Seas, Eurasian Basin, and eventually in the Canadian Basin due to GSP. This net decrease in Nordic Seas heat content is likely connected to increased input of cold water from the north, uplifting of cold waters from the deep ocean, and increased heat loss within the Barents and Kara Seas. In a similar way, the weaker GSM forcing leads to an increased depth-integrated heat content along the AW inflow pathway.

The GS experiments impact the AW flow all the way downstream into the Canadian Basin, but overall, the effect of the GSP and GSM experiments on the Beaufort Gyre region is not very strong. During GSP, the AW layer in the Beaufort Gyre becomes slightly colder and saltier, and during GSM, the AW layer becomes warmer and fresher. The response in this region is relatively small, and the GSP/GSM anomalies are not larger than the temporal anomalies in the control simulations from the individual models or the differences between the different models.

The higher GS wind stress of the GSP experiment results in an increased transport of warmer AW into the Barents and Kara Seas. Likewise, the weaker GSM wind stress leads to a smaller AW inflow volume transport. This response is clear in all models, but the strength of the response varies. The most remarkable result is the very close-to-linear response in the heat transport into the Barents Sea, the heat content in the Barents/Kara Seas, the heat loss to the atmosphere, and the change in sea ice extent. The response integrated over the whole Arctic amounts to a loss of about 10% of the annual mean sea ice area for a 4-mbar SLP anomaly over the GS. The positive AW inflow volume anomaly due to GSP leads to a higher ocean heat transport into the Barents Sea, a local warming, less sea ice, and a stronger heat loss to the atmosphere. The opposite is true for the weaker GSM forcing. This response is similar to the main cause of Barents Sea variability examined over the last 2,500 years by Smedsrud et al. (2013), but our results increase the confidence in this response by demonstrating that it appears across a suite of models.

The CRFs have a 2- to 5-year dynamic adjustment time, suggesting that there is potential for predictability on these time scales. A reconstruction of the strength of the barotropic circulation in the Nordic Seas based solely on a linear convolution of SLP anomalies in the GS with the CRFs explains 49% of the variance simulated by the models. Also, for the AW volume transport into the Barents Sea there is high correlation ($r = 0.58$) between the CRF hindcast and the direct calculations from the models, explaining approximately 34% of the variance. For sea ice extent, the reconstructions based on GS SLP anomalies are not well correlated with observed or simulated variability. This is likely due to a combination of missing ocean-atmosphere

Acknowledgments
The first author is particularly grateful to Prof. John Marshall and Prof. Helge Drange for constructive discussions and comments that helped to improve the manuscript, Evangelia Efstathiou for good suggestions, and the consortium supporting the development of the NorESM model. M. M. and L. H. S. were supported by the Centre for Climate Dynamics at the Bjerknes Centre for Climate Research, funded by the Norwegian Research Council. M. I. was partially supported by the ITU (ITU-TGA-2017-40657). Computing resources used in this work for ITU was provided by the National Center for High Performance Computing of Turkey (UHeM) under Grant 5004782017. R. Gelderloos and TWNH were financially supported by NOAA Grant NA15OAR4310172. C. L., C. T., and V. H. were supported through the projects ArcticMix, supported by the Copernicus Marine Environment Monitoring Service (CMEMS), and FREDY, supported by the French LEFE/INSU program. Q. W. was supported by the Helmholtz Climate Initiative REKLIM. T. K. and R. Gerdes are supported by the cooperative project 03F0729E (RACE II, Regional Atlantic Circulation and Global Climate), funded by the German Federal Ministry for Education and Research (BMBF). R. G. gratefully acknowledges funding by the Deutsche Forschungsgemeinschaft (DFG, German Research Foundation), Projektnummer 268020496, TRR 172, within the Transregional Collaborative Research Center "ArctiC Amplification: Climate Relevant Atmospheric and SurfaCe Processes, and Feedback Mechanisms" (AC). S. C., H. J., and Y. K. are grateful for funding from the U.K. Natural Environment Research Council, via the UK-OSNAP project (NE/K010948/1) and a DTP studentship. The HiGEM coupled climate model data are available from NERC's Centre for Environmental Data Analysis (CEDA; http://badc.nerc.ac.uk). This model was developed from the Met Office Hadley Centre Model by the U.K. High-Resolution Modelling (HiGEM) Project and the U.K. Japan Climate Collaboration (UJCC). HiGEM was supported by a NERC High Resolution Climate Modelling Grant (R8/H12/123). UJCC was supported by the Foreign and Commonwealth Office Global Opportunities Fund, and jointly funded by NERC and the DECC/Defra Met Office Hadley Centre Climate Programme (GA01101). The HiGEM model integrations were performed using the Japanese Earth Simulator supercomputer, supported by JAMSTEC. The work of Pier Luigi Vidale and Malcolm Roberts in leading the effort in Japan is particularly

feedback mechanisms and the fact that there are other major forcing mechanisms influencing ocean heat transport and sea ice extent. One of these important mechanisms, which are captured to limited extend in our CRF prediction, is the propagation of temperature anomalies from the south, which Årthun et al. (2017) has shown also strongly affect the ocean heat transport and, hence, the sea ice extent in the Barents Sea.

Increased ocean heat transport into the Barents Sea results in an increased net surface heat loss, and a net cooling effect on the AW that exits the Barents Sea. As most of our models are forced with atmospheric reanalysis, this strong cooling might be overestimated because the atmosphere is not able to respond to such increased heat fluxes. This is not the case for the CRFs from the Ox-HiGEM group, which are calculated by multiple linear lagged regression in a fully coupled ocean-ice-atmosphere simulation. Consequently, the response in sea ice is stronger in this coupled system, because there is less heat loss to the atmosphere to dampen the initial sea ice loss, and more AW heat available to prevent sea ice growth. The Ox-HiGEM results show that ocean-atmosphere feedback mechanisms in the Barents Sea are important and that the sea ice response might be underestimated in the forced simulations we focus on here.

Passive tracers show that anomalous wind stress in the Nordic Seas results in different AW pathways in the Arctic Ocean. This is consistent with Ilicak et al. (2016), who found substantial differences between Arctic Ocean simulations. Differences in barotropic circulation between models can be attributed to different climatological states, differences in AW pathways, and differences in Ekman pumping. The details of the circulation pathways, including the relative intensity of AW recirculation, FS, and Barents Sea inflows, will likely depend on the exact position of the wind anomaly, but we nevertheless expect the conclusions drawn here to be robust. In general, the CRF approach appears valuable for comparing climate models and their response to key drivers of climate variability, and for extracting the governing processes within the large and dynamic present-day changes occurring in the Arctic Ocean.

Author Contributions

John Marshall had the initial idea to compare Arctic Models using Climate Response Functions, and the different model simulations were run by the different groups. Data analysis was done by Morven Muilwijk in collaboration with Mehmet Illicak. Morven Muilwijk wrote the text with input from Lars H. Smedsrud, and all authors contributed to describing their own model and suggested improvements.

References

ACIA-Arctic Climate Impact Assessment (2005). *Arctic climate impact assessment*. Cambridge: Cambridge University Press.

Aagaard, K. (1970). Wind-driven transports in the Greenland and Norwegian seas. *Deep Sea Research and Oceanographic Abstracts*, *17*, 281–291. https://doi.org/10.1016/0011-7471(70)90021-5

Aagaard, K., Foldvik, A., & Hillman, R. S. (1987). The West Spitsbergen Current: Disposition and water mass transformation. *Journal of Geophysical Research*, *92*(C4), 3778–3784. https://doi.org/10.1029/JC092iC04p03778

Aagaard, K., Swift, J. H., Jolla, L., Carmack, E. C., Vancouver, W., & Columbia, B. (1985). Thermohaline circulation in the Arctic. *Deep Sea Research Part I: Oceanographic Research Papers*, *90*, 4833–4846. https://doi.org/10.1029/JC090iC03p04833

Årthun, M., & Eldevik, T. (2016). On anomalous ocean heat transport toward the Arctic and associated climate predictability. *Journal of Climate*, *29*(2), 689–704. https://doi.org/10.1175/1301JCLI-D-15-0448.1

Årthun, M., Eldevik, T., Smedsrud, L. H., Skagseth, O., & Ingvaldsen, R. B. (2012). Quantifying the influence of Atlantic heat on Barents sea ice variability and retreat. *Journal of Climate*, *25*(13), 4736–4743. https://doi.org/10.1175/JCLI-D-11-00466.1

Årthun, M., Eldevik, T., Viste, E., Drange, H., Furevik, T., Johnson, H. L., & Keenlyside, N. S. (2017). Skillful prediction of northern climate provided by the ocean. *Nature Communications*, *8*(May), 15875. https://doi.org/10.1038/ncomms15875

Årthun, M., & Schrum, C. (2010). Ocean surface heat flux variability in the Barents Sea. *Journal of Marine Systems*, *83*(1-2), 88–98. https://doi.org/10.1016/j.jmarsys.2010.07.003

Asbjørnsen, H., Arthun, M., Skagseth, Ø., & Eldevik, T. (2019). Mechanisms of ocean heat anomalies in the Norwegian Sea. *Journal of Geophysical Research: Oceans*, *124*, 2908–2923. https://doi.org/10.1029/2018JC014649

Bamber, J., van den Broeke, M., Ettema, J., Lenaerts, J., & Rignot, E. (2012). Recent large increases in freshwater fluxes from Greenland into the North Atlantic. *Geophysical Research Letters*, *39*, L19501. https://doi.org/10.1029/2012GL052552

Barnier, B., Madec, G., Penduff, T., Molines, J.-M., Treguier, A.-M., Le Sommer, J., et al. (2009). Impact of partial steps and momentum advection schemes in a global ocean circulation model at eddy-permitting resolution. *Ocean Dynamics*, *59*(3), 537. https://doi.org/10.1007/s10236-009-0180-y

Barton, B. I., Lenn, Y.-D., & Lique, C. (2018). Observed Atlantification of the Barents Sea causes the polar front to limit the expansion of winter sea ice. *Journal of Physical Oceanography*, *48*(8), 1849–1866. https://doi.org/10.1175/JPO-D-18-0003.1

Bentsen, M., Bethke, I., Debernard, J. B., Iversen, T., Kirkevaag, A., Seland, O., et al. (2013). The Norwegian Earth System Model, NorESM1-M - Part 1: Description and basic evaluation. *Geoscientific Model Development Discussions*, *5*, 2843–2931. https://doi.org/10.5194/gmdd-5-2843-2012

Beszczynska-Möller, A., Fahrbach, E., Schauer, U., & Hansen, E. (2012). Variability in Atlantic water temperature and transport at the entrance to the Arctic Ocean, 1997-2010. *ICES Journal of Marine Science*, *69*, 852–863. https://doi.org/10.1093/icesjms/fss056

valued. The Alberta team gratefully acknowledge the financial and logistic support of grants from the Natural Sciences and Engineering Research Council (NSERC) of Canada (RGPIN 04357 and RGPCC 433898), as well as Polar Knowledge Canada (PKC-NST-1617-0003). We are grateful to the NEMO development team and the Drakkar project for providing the model and continuous guidance and to Westgrid and Compute Canada for computational resources. For more details on the Alberta configuration, visit http://knossos.eas.ualberta.ca/anha/anhatable.php. An extracted set of time series from the various model simulations that have been used to make the figures are made available on the Bjerknes Climate Data Center (https://www.bcdc.no/).

Blanke, B., & Delecluse, P. (1993). Variability of the tropical Atlantic Ocean simulated by a general circulation model with two different mixed-layer physics. *Journal of Physical Oceanography*, *23*(7), 1363–1388. https://doi.org/10.1175/1520-0485(1993)023h1363:VOTTAOi2.0.CO;2

Brauch, J. P., & Gerdes, R. (2005). Response of the northern North Atlantic and Arctic oceans to a sudden change of the North Atlantic Oscillation. *Journal of Geophysical Research*, *110*, C11018. https://doi.org/10.1029/2004JC002436

Brodeau, L., Barnier, B., Treguier, A.-M., Penduff, T., & Gulev, S. (2010). An ERA40-based atmospheric forcing for global ocean circulation models. *Ocean Modelling*, *31*(3-4), 88–104. https://doi.org/10.1016/j.ocemod.2009.10.005

Carmack, E., Polyakov, I., Padman, L., Fer, I., Hunke, E., Hutchings, J., et al. (2015). Towards quantifying the increasing role of oceanic heat in sea ice loss in the New Arctic. *Bulletin of the American Meteorological Society*, *96*(12), 2079–2105. https://doi.org/10.1175/BAMS-D-13-00177.1

Cavalieri, D. J., & Parkinson, C. L. (2012). Arctic sea ice variability and trends, 1979–2010. *Cryosphere*, *6*(4), 881–889. https://doi.org/10.5194/tc-6-881-2012

Cavalieri, D., Parkinson, C., Gloersen, P., & Zwally, H. J. (1996). *Sea ice concentrations from Nimbus-7 SMMR and DMSP SSM/I-SSMIS passive microwave data, Version 1*. Boulder, CO: NASA National Snow and Ice Data Center Distributed Active Archive Center. https://doi.org/10.5067/8GQ8LZQVL0VL

Chatterjee, S., Raj, R. P., Bertino, L., Skagseth, R. M., & Johannessen, O. M. (2018). Role of Greenland Sea gyre circulation on Atlantic water temperature variability in the Fram Strait. *Geophysical Research Letters*, *45*, 8399–8406. https://doi.org/10.1029/2018GL079174

Cohen, J., Screen, J. A., Furtado, J. C., Barlow, M., Whittleston, D., Coumou, D., et al. (2014). Recent Arctic amplification and extreme mid-latitude weather. *Nature Geoscience*, *7*(9), 627. https://doi.org/10.1038/NGEO2234

Curry, R. G., & McCartney, M. S. (2001). Ocean gyre circulation changes associated with the North Atlantic Oscillation. *Journal of Physical Oceanography*, *31*(12), 3374–3400. https://doi.org/10.1175/1520-0485(2001)031h3374:OGCCAWi2.0.CO;2

Curry, J. A., Schramm, J. L., & Ebert, E. E. (1995). Sea ice-albedo climate feedback mechanism. *Journal of Climate*, *8*(2), 240–247. https://doi.org/10.1175/1520-0442(1995)008h0240:SIACFMi2.0.CO;2

Czaja, A., & Marshall, J. (2001). Observation of atmosphere ocean coupling in the North Atlantic. *Quarterly Journal of Royal Meteorological Soceity*, *127*(December 2000), 1893–1916. https://doi.org/10.1002/qj.49712757603

Dai, A., Qian, T., Trenberth, K. E., & Milliman, J. D. (2009). Changes in continental freshwater discharge from 1948 to 2004. *Journal of Climate*, *22*(10), 2773–2792. https://doi.org/10.1175/2008JCLI2592.1

Dai, A., & Trenberth, K. E. (2002). Estimates of freshwater discharge from continents: Latitudinal and seasonal variations. *Journal of Hydrometeorology*, *3*(6), 660–687. https://doi.org/10.1175/1525-7541(2002)003h0660:EOFDFCi2.0.CO;2

Dalpadado, P., Arrigo, K. R., Hjøllo, S. S., Rey, F., Ingvaldsen, R. B., Sperfeld, E., et al. (2014). Productivity in the Barents Sea—Response to recent climate variability. *PLoS ONE*, *9*(5), e95273. https://doi.org/10.1371/journal.pone.0095273

Danabasoglu, G., Yeager, S. G., Bailey, D., Behrens, E., Bentsen, M., Bi, D., et al. (2014). North Atlantic simulations in coordinated ocean-ice reference experiments phase II (CORE-II). Part I: Mean states. *Ocean Modelling*, *73*, 76–107. https://doi.org/10.1016/j.ocemod.2013.10.005

Danilov, S., Kivman, G., & Schröter, J. (2004). A finite-element ocean model: Principles and evaluation. *Ocean Modelling*, *6*(2), 125–150. https://doi.org/10.1016/S1463-5003(02)00063-X

Danilov, S., Wang, Q., Timmermann, R., Iakovlev, N., Sidorenko, D., Kimmritz, M., et al. (2015). Finite-element sea ice model (FESIM), version 2. *Geoscientific Model Development*, *8*(6), 1747–1761. https://doi.org/10.5194/gmd-8-1747-2015

Dee, D. P., Uppala, S. M., Simmons, A. J., Berrisford, P., Poli, P., Kobayashi, S., et al. (2011). The ERA-Interim reanalysis: Configuration and performance of the data assimilation system. *Quarterly Journal of the Royal Meteorological Society*, *137*(656), 553–597. https://doi.org/10.1002/qj.828

Dickson, R. R., Osborn, T. J., Hurrell, J. W., Meincke, J., Blindheim, J., Adlandsvik, B., et al. (2000). The Arctic Ocean response to the North Atlantic oscillation. *Journal of Climate*, *13*(15), 2671–2696. https://doi.org/10.1175/1520-0442(2000)013h2671:TAORTTi2.0.CO;2

Dunne, J. P., John, J. G., Adcroft, A. J., Griffies, S. M., Hallberg, R. W., Shevliakova, E., et al. (2012). GFDL's ESM2 global coupled climate-carbon earth system models. Part I: Physical formulation and baseline simulation characteristics. *Journal of Climate*, *25*(19), 6646–6665. https://doi.org/10.1175/JCLI-D-11-00560.1

Eden, C., & Jung, T. (2001). North Atlantic interdecadal variability: Oceanic response to the North Atlantic oscillation (1865-1997). *Journal of Climate*, *14*(5), 676–691. https://doi.org/10.1175/1520-0442(2001)014h0676:NAIVORi2.0.CO;2

Farneti, R., Downes, S. M., Griffies, S. M., Marsland, S. J., Behrens, E., Bentsen, M., et al. (2015). An assessment of Antarctic Circumpolar Current and Southern Ocean meridional overturning circulation during 1958-2007 in a suite of interannual CORE-II simulations. *Ocean Modelling*, *93*, 84–120. https://doi.org/10.1016/j.ocemod.2015.07.009

Fox-Kemper, B., Ferrari, R., & Hallberg, R. (2008). Parameterization of mixed layer eddies. Part I: Theory and diagnosis. *Journal of Physical Oceanography*, *38*(6), 1145–1165. https://doi.org/10.1175/2007JPO3792.1

Furevik, T. (2001). Annual and interannual variability of Atlantic Water temperatures in the Norwegian and Barents Seas: 1980-1996. *Deep-Sea Research Part I: Oceanographic Research Papers*, *48*(2), 383–404. https://doi.org/10.1016/S0967-0637(00)00050-9

Gent, P. R., & Mcwilliams, J. C. (1990). Isopycnal mixing in ocean circulation models. *Journal of Physical Oceanography*, *20*(1), 150–155. https://doi.org/10.1175/1520-0485(1990)020h0150:IMIOCMi2.0.CO;2

Gregory, J. M., Andrews, T., & Good, P. (2015). The inconstancy of the transient climate response parameter under increasing CO2. *Philosophical Transactions of the Royal Society A: Mathematical, Physical and Engineering Sciences*, *373*(2054), 20140417. https://doi.org/10.1098/rsta.2014.0417

Griffies, S. M. (2012). Elements of the modular ocean model (MOM). GFDL Ocean Group Tech. Rep, 7, 620.

Griffies, S. M., Winton, M., Samuels, B., Danabasoglu, G., Yeager, S., Marsland, S., et al. (2012). Datasets and protocol for the CLIVAR WGOMD Coordinated Ocean-sea ice Reference Experiments (COREs). WCRP Report, 21, 1–21.

Griffies, S. M., Yin, J., Durack, P. J., Goddard, P., Bates, S. C., Behrens, E., et al. (2014). An assessment of global and regional sea level for years 1993–2007 in a suite of interannual CORE-II simulations. *Ocean Modelling*, *78*, 35–89.

Grotefendt, K., Logemann, K., Quadfasel, D., & Ronski, S. (1998). Is the Arctic Ocean warming? *Journal of Geophysical Research*, *103*(C12), 27679. https://doi.org/10.1029/98JC02097

Haine, ThomasW. N., Curry, B., Gerdes, R., Hansen, E., Karcher, M., Lee, C., et al. (2015). Arctic freshwater export: Status, mechanisms, and prospects. *Global and Planetary Change*, *125*, 13–35. https://doi.org/10.1016/j.gloplacha.2014.11.013

Hattermann, T., Isachsen, P. E., Von Appen, W. J., Albretsen, J., & Sundfjord, A. (2016). Eddy-driven recirculation of Atlantic Water in Fram Strait. *Geophysical Research Letters*, *43*, 3406–3414. https://doi.org/10.1002/2016GL068323

He, Y. C., Drange, H., Gao, Y., & Bentsen, M. (2016). Simulated Atlantic Meridional Overturning Circulation in the 20th century with an ocean model forced by reanalysis-based atmospheric data sets. *Ocean Modelling*, *100*, 31–48. https://doi.org/10.1016/j.ocemod.2015.12.011

Helland-Hansen, B., & Nansen, F. (1909). *The Norwegian Sea: Its physical oceanography based upon the Norwegian researches 1900-1904*. Kristiania: Det Mallingske bogtrykkeri.

Hinzman, L. D., Deal, C. J., Mcguire, A. D., Mernild, S. H., Polyakov, I. V., & Walsh, J. E. (2013). Trajectory of the Arctic as an integrated system. *Ecological Applications*, *23*(8), 1837–1868. https://doi.org/10.1890/11-1498.1

Holliday, N. P., Hughes, S. L., Bacon, S., Beszczynska-Möller, A., Hansen, B., Lavín, A., et al. (2008). Reversal of the 1960s to 1990s freshening trend in the northeast North Atlantic and Nordic Seas. *Geophysical Research Letters*, *35*, L03614. https://doi.org/10.1029/2007GL032675

Holloway, G. (1987). Systematic forcing of large-scale geophysical flows by eddy-topography interaction. *Journal of Fluid Mechanics*, *184*, 463–476. https://doi.org/10.1017/S0022112087002970

Holloway, G., Dupont, F., Golubeva, E., Häkkinen, S., Hunke, E., Jin, M., et al. (2007). Water properties and circulation in Arctic Ocean models. *Journal of Geophysical Research*, *112*, 1–18. https://doi.org/10.1029/2006JC003642

Hurrell, J. W. (1995). Decadal trends in the North Atlantic Oscillation: Regional temperatures and precipitation. *Science*, *269*(5224), 676–679. https://doi.org/10.1126/science.269.5224.676

IPCC (2014). *Climate Change 2013—The Physical Science Basis: Working Group I Contribution to the Fifth Assessment Report of the Intergovernmental Panel on Climate Change*. Cambridge: Cambridge University Press. https://doi.org/10.1017/CBO9781107415324

Ikeda, M. (1990). Decadal oscillations of the air-ice-ocean system in the Northern Hemisphere. *Atmosphere-Ocean*, *28*(1), 106–139. https://doi.org/10.1080/07055900.1990.9649369

Ikeda, M., Wang, J., & Zhao, J. (2001). Hypersensitive decadal oscillations in the Arctic/subarctic climate. *Geophysical research letters*, *28*(7), 1275–1278. https://doi.org/10.1029/2000GL011773

Ilicak, M., Drange, H., Wang, Q., Gerdes, R., Aksenov, Y., Bailey, D., et al. (2016). An assessment of the Arctic Ocean in a suite of interannual CORE-II simulations. Part III: Hydrography and fluxes. *Ocean Modelling*, *100*, 141–161. https://doi.org/10.1016/j.ocemod.2016.02.004

Ingvaldsen, R. (2004). The Atlantic inflow to the Barents Sea. *Continental Shelf Research*, *10*(1), 5817. https://doi.org/10.1029/2001JC001039.Ottersen

Ingvaldsen, R. B., Asplin, L., & Loeng, H. (2004). Velocity field of the western entrance to the Barents Sea. *Journal of Geophysical Research*, *109*, 1–12. https://doi.org/10.1029/2003JC001811

Isachsen, P. E., LaCasce, J. H., Mauritzen, C., & Hakkinen, S. (2003). Wind-driven variability of the large-scale recirculating flow in the Nordic Seas and Arctic Ocean. *Journal of Physical Oceanography*, *33*(12), 2534–2550. https://doi.org/10.1175/1520-0485(2003)033h2534:WVOTLRi2.0.CO;2

Ivanov, V., Alexeev, V., Koldunov, N. V., Repina, I., Sando, A. B., Smedsrud, L. H., & Smirnov, A. (2016). Arctic Ocean heat impact on regional ice decay - a suggested positive feedback. *Journal of Physical Oceanography*, *46*(5), 1437–1456. https://doi.org/10.1175/JPO-D-15-0144.1

Ivanov, B. V., Gerland, S., Winther, J.-G., & Goodwin, H. (2003). Energy exchange processes in the marginal ice zone of the Barents Sea, Arctic Ocean, during spring 1999. *Journal of Glaciology*, *49*(166), 415–419. https://doi.org/10.3189/172756503781830557

Jahnke-Bornemann, A., & Brümmer, B. (2009). The Iceland-Lofotes pressure difference: Different states of the North Atlantic low-pressure zone. *Tellus, Series A: Dynamic meteorology and oceanography*, *61*(4), 466–475. https://doi.org/10.1111/j.1600-0870.2009.00401.x

Jakobsson, M., & Macnab, R. (2006). A comparison between GEBCO Sheet 5.17 and the International Bathymetric Chart of the Arctic Ocean (IBCAO) version 1.0. *Marine Geophysical Researches*, *27*(1), 35–48. https://doi.org/10.1007/s11001-005-7760-0

Johnson, H. L., Cornish, S. B., Kostov, Y., Beer, E., & Lique, C. (2018). Arctic Ocean freshwater content and its decadal memory of sea-level pressure. *Geophysical Research Letters*, *45*, 4991–5001. https://doi.org/10.1029/2017GL076870

Jungclaus, J. H., Fischer, N., Haak, H., Lohmann, K., Marotzke, J., Matei, D., et al. (2013). Characteristics of the ocean simulations in the Max Planck Institute Ocean Model (MPIOM) the ocean component of the MPI Earth system model. *Journal of Advances in Modeling Earth Systems*, *5*, 422–446. https://doi.org/10.1002/jame.20023

Karcher, M., Kauker, F., Gerdes, R., Hunke, E., & Zhang, J. (2007). On the dynamics of Atlantic Water circulation in the Arctic Ocean. *Journal of Geophysical Research*, *112*, C04S02. https://doi.org/10.1029/2006JC003630

Karcher, M., Smith, J. N., Kauker, F., Gerdes, R., & Smethie, W. M. (2012). Recent changes in Arctic Ocean circulation revealed by iodine-129 observations and modeling. *Journal of Geophysical Research*, *117*, C08007. https://doi.org/10.1029/2011JC007513

Kostov, Y., Marshall, J., Hausmann, U., Armour, K. C., Ferreira, D., & Holland, M. M. (2017). Fast and slow responses of Southern Ocean sea surface temperature to SAM in coupled climate models. *Climate Dynamics*, *48*(5-6), 1595–1609. https://doi.org/10.1007/s00382-016-3162-z

Kwok, R. (2018). Arctic sea ice thickness, volume, and multiyear ice coverage: Losses and coupled variability (1958-2018). *Environmental Research Letters*, *13*(10), 105005. https://doi.org/10.1088/1748-9326/aae3ec

Langehaug, H. R., Medhaug, I., Eldevik, T., & Otterå, O. H. (2012). Arctic/Atlantic exchanges via the subpolar gyre. *Journal of Climate*, *25*(7), 2421–2439. https://doi.org/10.1175/JCLI-D-11-00085.1

Large, W. G., McWilliams, J. C., & Doney, S. C. (1994). Oceanic vertical mixing: A review and a model with a nonlocal boundary layer parameterization. *Reviews of Geophysics*, *32*(4), 363–403. https://doi.org/10.1029/94RG01872

Levitus, S., Matishov, G., Seidov, D., & Smolyar, I. (2009). Barents Sea multidecadal variability. *Geophysical Research Letters*, *36*, L19604. https://doi.org/10.1029/2009GL039847

Li, D., Zhang, R., & Knutson, T. R. (2017). On the discrepancy between observed and CMIP5 multi-model simulated Barents Sea winter sea ice decline. *Nature Communications*, *8*, 1–7. https://doi.org/10.1038/ncomms14991

Lien, V. S., Schlichtholz, P., Skagseth, Ø., & Vikebø, F. B. (2017). Wind-Driven Atlantic Water Flow as a Direct Mode for Reduced Barents Sea Ice Cover. *Journal of Climate*, *30*(2), 803–812. https://doi.org/10.1175/JCLI-D-16-0025.1

Lien, V. S., Vikebø, F. B., & Skagseth, Ø. (2013). One mechanism contributing to co-variability of the Atlantic inflow branches to the Arctic. *Nature Communications*, *4*, 1–6. https://doi.org/10.1038/ncomms2505

Lind, S., & Ingvaldsen, R. B. (2012). Variability and impacts of Atlantic Water entering the Barents Sea from the north. *Deep-Sea Research Part I: Oceanographic Research Papers*, *62*, 70–88. https://doi.org/10.1016/j.dsr.2011.12.007

Lind, S., Ingvaldsen, R. B., & Furevik, T. (2016). Arctic layer salinity controls heat loss from deep Atlantic layer in seasonally ice-covered areas of the Barents Sea. *Geophysical Research Letters*, *43*, 5233–5242. https://doi.org/10.1002/2016GL068421

Lind, S., Ingvaldsen, R. B., & Furevik, T. (2018). Sea linked to declining sea-ice import. *Nature Climate Change*, *8*(634), 634–639. https://doi.org/10.1038/s41558-018-0205-y

Liptak, J., & Strong, C. (2014). The winter atmospheric response to sea ice anomalies in the Barents Sea. *Journal of Climate*, *27*(2), 914–924. https://doi.org/10.1175/JCLI-D-13-00186.1

Lique, C., Johnson, H. L., & Davis, P. E. D. (2015). On the interplay between the circulation in the surface and the intermediate layers of the Arctic Ocean. *Journal of Physical Oceanography*, *45*(5), 1393–1409. https://doi.org/10.1175/JPO-D-14-0183.1

Lohmann, K., Drange, H., & Bentsen, M. (2009). Response of the North Atlantic subpolar gyre to persistent North Atlantic oscillation like forcing. *Climate Dynamics*, *32*(2-3), 273–285. https://doi.org/10.1007/s00382-008-0467-6

Madec, G. (2014). NEMO ocean engine (*27*). Institut Pierre-Simon Laplace.

Marnela, M., Rudels, B., Houssais, M. N., Beszczynska-Möller, A., & Eriksson, P. B. (2013). Recirculation in the Fram Strait and transports of water in and north of the Fram Strait derived from CTD data. *Ocean Science*, *9*(3), 499–519. https://doi.org/10.5194/os-9-499-2013

Marshall, J., Adcroft, A., Hill, C., Perelman, L., & Heisey, C. (1997). A finite-volume, incompressible Navier Stokes model for studies of the ocean on parallel computers. *Journal of Geophysical Research*, *102*(C3), 5753–5766. https://doi.org/10.1029/96JC02775

Marshall, J., Armour, K. C., Scott, J. R., Kostov, Y., Hausmann, U., Ferreira, D., et al. (2014). The ocean's role in polar climate change: asymmetric Arctic and Antarctic responses to greenhouse gas and ozone forcing. *Philosophical Transactions of the Royal Society A*, *372*, 20130040. https://doi.org/10.1098/rsta.2013.0040

Marshall, J., Scott, J., & Proshutinsky, A. (2017). Climate Response Functions for the Arctic Ocean: a proposed coordinated modeling experiment. *Geoscientific Model Development Discussions*, *10*(January), 1–25. https://doi.org/10.5194/gmd-2016-316

Masina, S., Storto, A., Ferry, N., Valdivieso, M., Haines, K., Balmaseda, M., et al. (2015). An ensemble of eddy-permitting global ocean reanalyses from the MyOcean project. *Climate Dynamics*, *49*(3), 813–841. https://doi.org/10.1007/s00382-015-2728-5

Medhaug, I., Langehaug, H. R., Eldevik, T., Furevik, T., & Bentsen, M. (2012). Mechanisms for decadal scale variability in a simulated Atlantic meridional overturning circulation. *Climate Dynamics*, *39*(1-2), 77–93. https://doi.org/10.1007/s00382-011-1124-z

Meneghello, G., Marshall, J., Campin, J.-M., Doddridge, E., & Timmermans, M.-L. (2018). The Ice-Ocean governor: ice-ocean stress feedback limits Beaufort Gyre spin up. *Geophysical Research Letters*, *45*, 293–299. https://doi.org/10.1029/2018GL080171

Montgomery, R. B. (1974). Comments on seasonal variability of Florida Current-Niiler and Richardson. *Journal of Marine Research*, *32*(3), 533–534.

Moore, G. W. K., Renfrew, I. A., & Pickart, R. S. (2012). Spatial distribution of air-sea heat fluxes over the sub-polar North Atlantic Ocean. *Geophysical Research Letters*, *39*, L18806. https://doi.org/10.1029/2012GL053097

Moore, G. W. K., Renfrew, I. A., & Pickart, R. S. (2013). Multidecadal mobility of the north atlantic oscillation. *Journal of Climate*, *26*(8), 2453–2466. https://doi.org/10.1175/JCLI-D-12-00023.1

Moss, R. H., Edmonds, J. A., Hibbard, K. A., Manning, M. R., Rose, S. K., Van Vuuren, D. P., et al. (2010). The next generation of scenarios for climate change research and assessment. *Nature*, *463*(7282), 747. https://doi.org/10.1038/nature08823

Muilwijk, M., Smedsrud, L. H., Ilicak, M., & Drange, H. (2018). Atlantic Water heat transport variability in the 20th century Arctic Ocean from a global ocean model and observations. *Journal of Geophysical Research: Oceans*, *123*, 8159–8179. https://doi.org/10.1029/2018JC014327

Nakanowatari, T., Sato, K., & Inoue, J. (2014). Predictability of the Barents Sea ice in early winter: Remote effects of oceanic and atmospheric thermal conditions from the North Atlantic. *Journal of Climate*, *27*(23), 8884–8901. https://doi.org/10.1175/JCLI-D-14-00125.1

Nøst, O. A., & Isachsen, P. E. (2003). The large-scale time-mean ocean circulation in the Nordic Seas and Arctic Ocean estimated from simplified dynamics. *Journal of Marine Research*, *61*(2), 175–210. https://doi.org/10.1357/002224003322005069

Onarheim, I. H., & Arthun, M. (2017). Toward an ice-free Barents Sea. *Geophysical Research Letters*, *44*, 8387–8395. https://doi.org/10.1002/2017GL074304

Onarheim, I. H., Eldevik, T., Årthun, M., Ingvaldsen, R. B., & Smedsrud, L. H. (2015). Skillful prediction of Barents Sea ice cover. *Geophysical Research Letters*, *42*, 5364–5371. https://doi.org/10.1002/2015GL064359

Onarheim, I. H., Eldevik, T., Smedsrud, L. H., & Stroeve, J. C. (2018). Seasonal and regional manifestation of Arctic sea ice loss. *Journal of Climate*, *31*(12), 4917–4932. https://doi.org/10.1175/JCLI-D-17-0427.1

Onarheim, I. H., Smedsrud, L. H., Ingvaldsen, R. B., & Nilsen, F. (2014). Loss of sea ice during winter north of Svalbard. *Tellus A*, *66*(1), 23933. https://doi.org/10.3402/tellusa.v66.23933

Onogi, K., Tsutsui, J., Koide, H., Sakamoto, M., Kobayashi, S., Hatsushika, H., et al. (2007). The JRA-25 reanalysis. *Journal of the Meteorological Society of Japan. Ser. II*, *85*(3), 369–432. https://doi.org/10.2151/jmsj.85.369

Orvik, K. A., & Skagseth, O. (2003). The impact of the wind stress curl in the North Atlantic on the Atlantic inflow to the Norwegian Sea toward the Arctic. *Geophysical Research Letters*, *30*(17), 1884. https://doi.org/10.1029/2003GL017932

Orvik, K. A., Skagseth, O., & Mork, M. (2001). Atlantic inflow to the Nordic Seas: Current structure and volume fluxes from moored current meters, VM-ADCP and SeaSoar-CTD observations, 1995-1999. *Deep-Sea Research Part I: Oceanographic Research Papers*, *48*(4), 937–957. https://doi.org/10.1016/S0967-0637(00)00038-8

Pérez-Hernández, M., S. Pickart, R., Torres, D., Bahr, F., Sundfjord, A., Ingvaldsen, R., et al. (2019). Structure, Transport, and Seasonality of the Atlantic Water Boundary Current North of Svalbard: Results From a Yearlong Mooring Array. *Journal of Geophysical Research: Oceans*, *124*, 1679–1698. https://doi.org/10.1029/2018JC014759

Pacanowski, R. C., & Philander, S. G. H. (1981). Parameterization of vertical mixing in numerical models of tropical oceans. *Journal of Physical Oceanography*, *11*(11), 1443–1451. https://doi.org/10.1175/1520-0485(1981)011h1443:POVMINi2.0.CO;2

Peralta-Ferriz, C., Morison, J. H., Wallace, J. M., Bonin, J. A., & Zhang, J. (2014). Arctic ocean circulation patterns revealed by GRACE. *Journal of Climate*, *27*(4), 1445–1468. https://doi.org/10.1175/JCLI-D-13-00013.1

Perovich, D. K., & Richter-Menge, J. A. (2015). Regional variability in sea ice melt in a changing Arctic. *Philosophical Transactions of the Royal Society A: Mathematical, Physical and Engineering Sciences*, *373*(2045), 20140165. https://doi.org/10.1098/rsta.2014.0165

Peterson, A. K., Fer, I., McPhee, M. G., & Randelhoff, A. (2017). Turbulent heat and momentum fluxes in the upper ocean under Arctic sea ice. *Journal of Geophysical Research: Oceans*, *122*, 1439–1456. https://doi.org/10.1002/2016JC012283

Polyakov, I. V., Pnyushkov, A. V., Alkire, M. B., Ashik, I. M., Baumann, T. M., Carmack, E. C., et al. (2017). Greater role for Atlantic inflows on sea-ice loss in the Eurasian Basin of the Arctic Ocean. *Science*, *291*(April), 285–291. https://doi.org/10.1126/science.aai8204

Rudels, B., Anderson, L. G., & Jones, E. P. (1996). Formation and evolution of the surface mixed layer and halocline of the Arctic Ocean. *Journal of Geophysical Research*, *101*, 8807–8821. https://doi.org/10.1029/96JC00143

Saha, S., Moorthi, S., Pan, H.-L., Wu, X., Wang, J., Nadiga, S., et al. (2010). The NCEP climate forecast system reanalysis. *Bulletin of the American Meteorological Society*, *91*(8), 1015–1058. https://doi.org/10.1175/2010BAMS3001.1

Sandø, A, Gao, Y., & Langehaug, H. R. (2014). Poleward ocean heat transport, sea ice processes, and Arctic sea ice variability in NorESM1-M simulations. *Journal of Geophysical Research: Oceans*, *119*, 2095–2108. https://doi.org/10.1002/2013JC009435

Sandø, A. B., Nilsen, J. E., Gao, Y., & Lohmann, K. (2010). Importance of heat transport and local air-sea heat fluxes for Barents Sea climate variability. *Journal of Geophysical Research*, *115*, C07013. https://doi.org/10.1029/2009JC005884

Schauer, U. (2004). Arctic warming through the Fram Strait: Oceanic heat transport from 3 years of measurements. *Journal of Geophysical Research*, *109*, C06026. https://doi.org/10.1029/2003JC001823

Schauer, U., & Beszczynska-Möller, A. (2009). Problems with estimation and interpretation of oceanic heat transport-conceptual remarks for the case of Fram Strait in the Arctic Ocean. *Ocean Science*, *5*(4), 487–494. https://doi.org/10.5194/os-5-487-2009

Schauer, U., Loeng, H., Rudels, B., Ozhigin, V. K., & Dieck, W. (2002). Atlantic Water flow through the Barents and Kara Seas. *Deep Sea Research Part I: Oceanographic Research Papers*, *49*(12), 2281–2298. https://doi.org/10.1016/S0967-0637(02)00125-5

Schlichtholz, P., & Houssais, M. N. (2011). Forcing of oceanic heat anomalies by air-sea interactions in the Nordic Seas area. *Journal of Geophysical Research*, *116*, 1–21. https://doi.org/10.1029/2009JC005944

Screen, J. A., & Simmonds, I. (2010). The central role of diminishing sea ice in recent Arctic temperature amplification. *Nature*, *464*(7293), 1334–1337. https://doi.org/10.1038/nature09051

Serreze, M. C., & Barry, R. G. (2011). Processes and impacts of Arctic amplification: A research synthesis. *Global and Planetary Change*, *77*(1-2), 85–96. https://doi.org/10.1016/j.gloplacha.2011.03.004

Serreze, M. C., Holland, M. M., & Stroeve, J. (2007). Perspectives on the Arctic's shrinking sea-ice cover. *Science*, *315*(5818), 1533–1536. https://doi.org/10.1126/science.1139426

Shaffrey, LCoauthors, Stevens, I., Norton, WA, Roberts, MJ, Vidale, P. L., Harle, JD, et al. (2009). UK HiGEM: The new UK high-resolution global environment model—Model description and basic evaluation. *Journal of Climate*, *22*(8), 1861–1896. https://doi.org/10.1175/2008JCLI2508.1

Skagseth, Ø., Drinkwater, K. F., & Terrile, E. (2011). Wind-and buoyancy-induced transport of the Norwegian Coastal Current in the Barents Sea. *Journal of Geophysical Research*, *116*, C08007. https://doi.org/10.1029/2011JC006996

Skagseth, Ø., Furevik, T., Ingvaldsen, R. B., Loeng, H., Mork, K. A., Orvik, K. A., & Ozhigin, V. (2008). Volume and heat transports to the Arctic Ocean via the Norwegian and Barents Seas. In *Arctic-Subarctic Ocean Fluxes: Defining the role of the Northern Seas in Climate* (pp. 45–64). Dordrecht: Springer.

Smedsrud, L. H., Esau, I., Ingvaldsen, R. B., Eldevik, T., Haugan, P. M., Li, C., et al. (2013). The role of the Barents Sea in the Arctic climate system. *Reviews of Geophysics*, *51*, 415–449. https://doi.org/10.1002/rog.20017

Smedsrud, L. H., Ingvaldsen, R., Nilsen, J. E. Ø., & Skagseth, Ø (2010). Heat in the Barents Sea: Transport, storage, and surface fluxes. *Ocean Science*, *6*(1), 219–234. https://doi.org/10.5194/os-6-219-2010

Smith, G. C., Roy, F., Mann, P., Dupont, F., Brasnett, B., Lemieux, J., et al. (2014). A new atmospheric dataset for forcing ice-ocean models: Evaluation of reforecasts using the Canadian global deterministic prediction system. *Quarterly Journal of the Royal Meteorological Society*, *140*(680), 881–894. https://doi.org/10.1002/qj.2194

Sorokina, S. A., Li, C., Wettstein, J. J., & Kvamstø, N. G. (2016). Observed atmospheric coupling between Barents Sea ice and the warm-Arctic cold-Siberian anomaly pattern. *Journal of Climate*, *29*(2), 495–511. https://doi.org/10.1175/JCLI-D-15-0046.1

Steiner, N., Holloway, G., Gerdes, R., Häkkinen, S., Holland, D., Karcher, M., et al. (2004). Comparing modeled streamfunction, heat and freshwater content in the Arctic Ocean. *Ocean Modelling*, *6*(3-4), 265–284. https://doi.org/10.1016/S1463-5003(03)00013-1

Stewart, K. D., & Haine, T. W. N. (2013). Wind-driven Arctic freshwater anomalies. *Geophysical Research Letters*, *40*, 6196–6201. https://doi.org/10.1002/2013GL058247

Tesdal, J.-E., Abernathey, R. P., Goes, J. I., Gordon, A. L., & Haine, T. W. N. (2018). Salinity trends within the upper layers of the subpolar North Atlantic. *Journal of Climate*, *31*(7), 2675–2698. https://doi.org/10.1175/JCLI-D-17-0532.1

Thoma, M., Gerdes, R., Greatbatch, R. J., & Ding, H. (2015). Partially coupled spin-up of the MPI-ESM: Implementation and first results. *Geoscientific Model Development*, *8*(1), 51–68. https://doi.org/10.5194/gmd-8-51-2015

Thompson, D. W., & Wallace, J. M. (1998). The Arctic oscillation signature in the wintertime geopotential height and temperature fields. *Geophysical Research Letters*, *25*(9), 1297–1300. https://doi.org/10.1029/98GL00950

Venegas, S. A., & Mysak, L. A. (2000). Is there a dominant timescale of natural climate variability in the Arctic? *Journal of Climate*, *13*(19), 3412–3434. https://doi.org/10.1175/1520-0442(2000)013h3412:ITADTOi2.0.CO;2

Vihma, T. (2014). Effects of Arctic Sea ice decline on weather and climate: A review. *Surveys in Geophysics*, *35*(5), 1175–1214. https://doi.org/10.1007/s10712-014-9284

Visbeck, M., Chassignet, E., Curry, R. G., Delworth Thomas, D. R. R., & Krahmann, G. (2013). The ocean's response to North Atlantic Oscillation variability. In *The North Atlantic Oscillation: Climatic Significance and Environmental Impact* (pp. 113–145). Washington, DC: American Geophysical Union. https://doi.org/10.1029/134GM06

Visbeck, M., Cullen, H., Krahmann, G., & Naik, N. (1998). Ocean model's response to North Atlantic Oscillation-like wind forcing. *Geophysical Research Letters*, *25*(24), 4521–4524. https://doi.org/Doi10.1029/1998gl900162

Wang, Q., Danilov, S., & Schröter, J. (2008). Finite element ocean circulation model based on triangular prismatic elements, with application in studying the effect of topography representation. *Journal of Geophysical Research*, *113*, C05015. https://doi.org/10.1029/2007JC004482

Wang, Q., Danilov, S., Sidorenko, D., Timmermann, R., Wekerle, C., Wang, X., et al. (2014). The Finite Element Sea Ice-Ocean Model (FESOM) v. 1.4: Formulation of an ocean general circulation model. *Geoscientific Model Development*, *7*(2), 663–693. https://doi.org/10.5194/gmd-7-663-2014

Wang, Q., Ilicak, M., Gerdes, R., Drange, H., Aksenov, Y., Bailey, D. A., et al. (2016a). An assessment of the Arctic Ocean in a suite of interannual CORE-II simulations. Part II: Liquid freshwater. *Ocean Modelling*, *99*, 86–109. https://doi.org/10.1016/j.ocemod.2015.12.009

Wang, Q., Ilicak, M., Gerdes, R., Drange, H., Aksenov, Y., Bailey, D. A., et al. (2016b). An assessment of the Arctic Ocean in a suite of interannual CORE-II simulations. Part II: Liquid freshwater. *Ocean Modelling*, *99*, 86–109. https://doi.org/10.1016/j.ocemod.2015.12.009

Wang, Q., Marshall, J., Scott, J., Meneghello, G., Danilov, S., & Jung, T. (2019). On the feedback of ice-ocean stress coupling from geostrophic currents in an anticyclonic wind regime over the Beaufort Gyre. *Journal of Physical Oceanography*, *49*(2019), 369–383. https://doi.org/10.1175/JPO-D-18-0185.1

Wekerle, C., Wang, Q., Danilov, S., Schourup-Kristensen, V., von Appen, W.-J., & Jung, T. (2017). Atlantic Water in the Nordic Seas: Locally eddy-permitting ocean simulation in a global setup. *Journal of Geophysical Research: Oceans*, *122*, 914–940. https://doi.org/10.1002/2016JC012121

Wekerle, C., Wang, Q., von Appen, W., Danilov, S., Schourup-Kristensen, V., & Jung, T. (2017). Eddy-resolving simulation of the Atlantic Water circulation in the Fram Strait with focus on the seasonal cycle. *Journal of Geophysical Research: Oceans*, *122*, 8385–8405. https://doi.org/10.1002/2017JC012974

Yang, S., & Christensen, J. H. (2012). Arctic sea ice reduction and European cold winters in CMIP5 climate change experiments. *Geophysical Research Letters*, *39*, L20707. https://doi.org/10.1029/2012GL053338

Zhang, R. (2015). Mechanisms for low-frequency variability of summer Arctic sea ice extent. *Proceedings of the National Academy of Sciences*, *112*(15), 4570–4575. https://doi.org/10.1073/pnas.1422296112

Zhang, J., Lindsay, R., Steele, M., & Schweiger, A. (2008). What drove the dramatic retreat of arctic sea ice during summer 2007? *Geophysical Research Letters*, *35*, L11505. https://doi.org/10.1029/2008GL034005

Zhang, J., Rothrock, D. A., & Steele, M. (1998). Warming of the Arctic Ocean by a strengthened Atlantic inflow: Model results. *Geophysical Research Letters*, *25*(10), 1745–1748. https://doi.org/10.1029/98GL01299

Zhang, J., & Steele, M. (2007). Effect of vertical mixing on the Atlantic Water layer circulation in the Arctic Ocean. *Journal of Geophysical Research*, *112*, C04S04. https://doi.org/10.1029/2006JC003732

Supporting Information for

"Arctic response to Greenland Sea wind anomalies in a suite of model simulations"

Morven Muilwijk[1,2], Mehmet Ilicak[3], Sam B. Cornish[4], Sergey Danilov[5], Renske Gelderloos[6], Rüdiger Gerdes[5], Verena Haid[7], Thomas W. N. Haine[6], Helen L. Johnson[4], Yavor Kostov[8], Tamás Kovács[5], Camille Lique[7], John Marshall[9], Juliana M. Marson[10], Paul G. Myers[10], Jeffery Scott[9], Lars H. Smedsrud[1,2,11], Claude Talandier[7], Qiang Wang[5]

[1]Geophysical Institute, University of Bergen, Norway.

[2]Bjerknes Centre for Climate Research, Bergen, Norway

[3]Eurasia Institute of Earth Sciences, Istanbul Technical University, Istanbul, Turkey

[4]Department of Earth Sciences, University of Oxford, Oxford, UK

[5]Alfred-Wegener-Institut Helmholtz-Zentrum für Polar- und Meeresforschung, Bremerhaven, Germany

[6]Department of Earth and Planetary Sciences, The Johns Hopkins University, Baltimore, USA

[7]Laboratoire d'Océanographie Physique et Spatiale, Univ. Brest, CNRS, IRD, Ifremer, IUEM, Brest, France

[8]Department of Physics, University of Oxford, Oxford, UK

[9]Department of Earth, Atmospheric and Planetary Sciences, Massachusetts Institute of Technology, Cambridge, USA

[10]University of Alberta, Edmonton, Canada

[11]University Centre in Svalbard, Longyearbyen, Svalbard

Contents

Corresponding author: Morven Muilwijk, Morven@uib.no

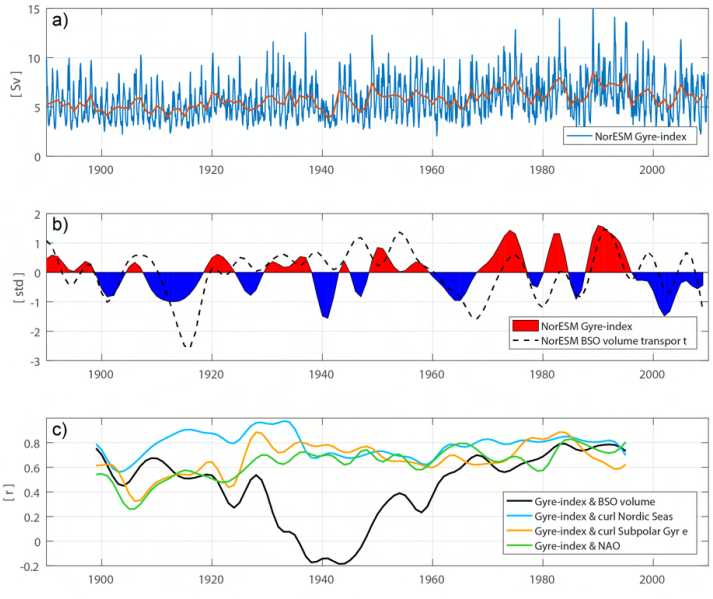

Figure 1. Circulation in the Nordic Seas and related forcing over the last century. a) The mean barotropic streamfunction strength ("Gyre-index") from the forced NorESM 130 year control simulation. Blue line shows monthly values and the red line shows the annual mean. b) Low-pass filtered anomalies of the annual mean barotropic streamfunction (as above) expressed in standard deviations (red and blue) compared with anomalies of annual mean Atlantic Water inflow volume transport through the Barents Sea Opening (BSO, positive north-eastward). Positive values show years with a strong cyclonic barotropic circulation regime and negative values show weak cyclonic circulation . c) Gliding 30-year correlations of the "Gyre-index" anomalies and NAO-index, BSO inflow volume transport, mean wind stress curl strength in the Nordic Seas, and mean wind stress curl strength in the Subpolar Gyre. NAO=North Atlantic Oscillation.

Figure 2. Model mean states from the start of simulation. Note that the Alberta model is simulated over a different period as the others. The JHU model has no variability since it is forced with repeated 1998 forcing.

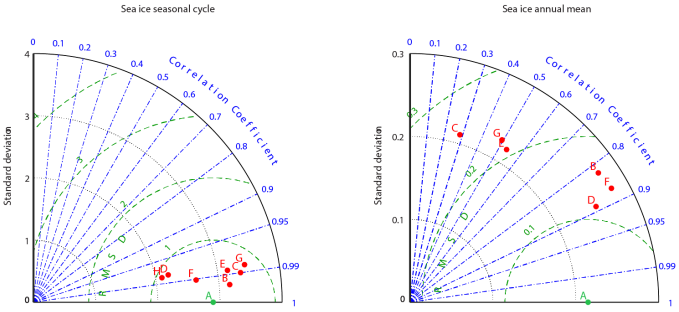

Figure 3. Taylor diagram of the Northern Hemisphere sea ice cover variability from different model control simulations (B=ITU, C=MITB500, D=IFREMER, E=NorESM, F=FESOM, G=JHU and H=Alberta) compared to NSIDC satellite observations (A). Values that appear closest to the (A) in the Taylor diagram are closest to the observations. JHU is not included in the right panel because it utilizes a repeat year forcing and hence has no realistic interannual variability.

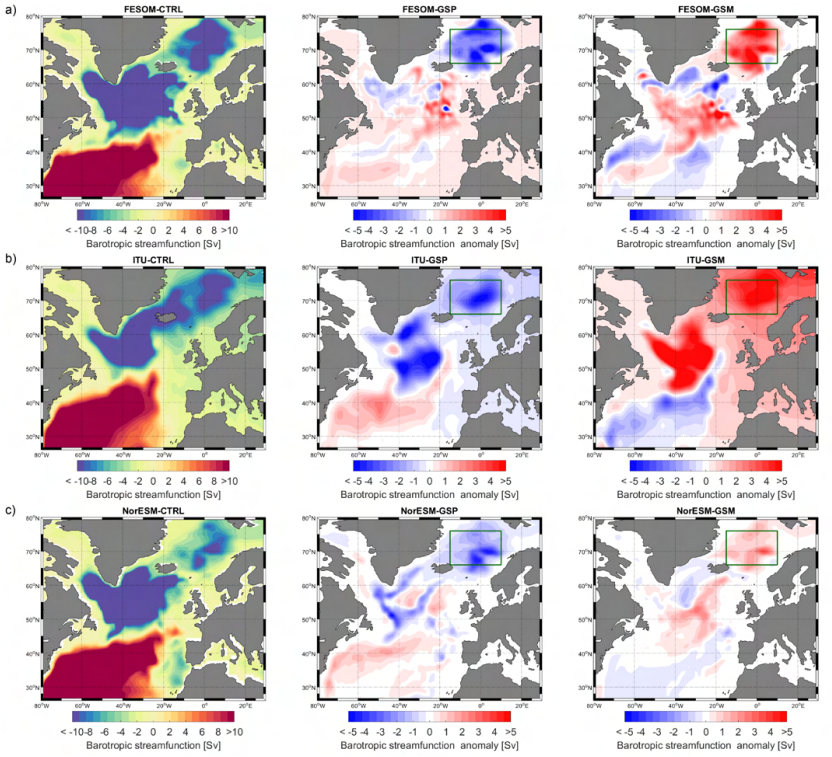

Figure 4. The annual mean response to a 4mb surface pressure anomaly on the barotropic streamfunction in the subpolar gyre region computed from three of the global CRF-models. Negative values denote cyclonic circulation and positive values denote anticyclonic circulation. Panels on the left show the control simulations, middle panels show anomalies resulting from the GSP experiment (stronger wind forcing), and right panels show anomalies resulting from the GSM experiment (weaker wind forcing). All values are averaged over the last 10 years of integration (20-30 years after perturbation).

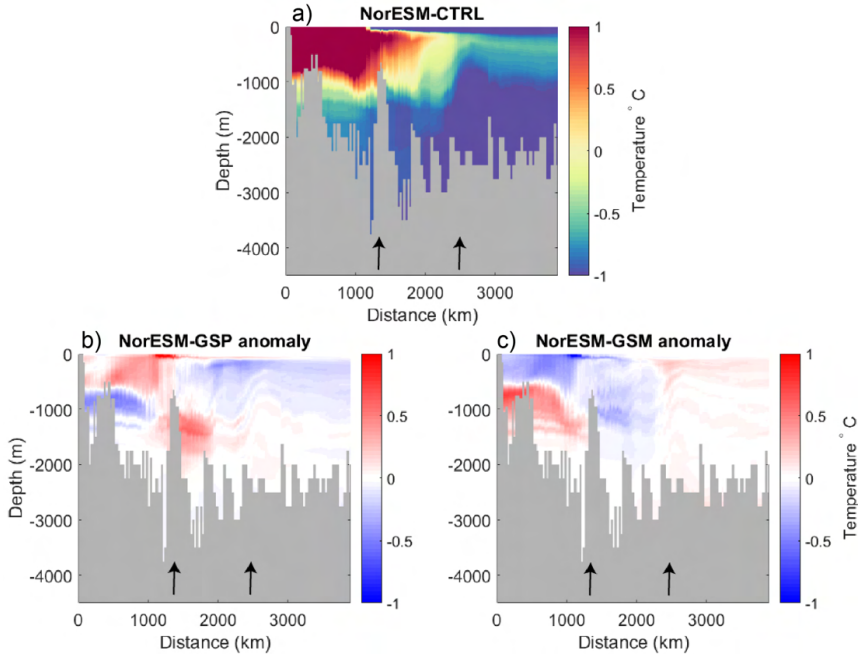

Figure 5. Vertical section of the mean temperature field along the Atlantic Water inflow path for NorESM (section S1 shown in Figure 1). Upper figure shows the mean values, lower figures anomalies resulting from the GSP and GSM experiments. The left arrow in all panels shows Fram Strait while the right arrow shows the St. Anna Trough where water from the Barents Sea exits into the Arctic Basin.

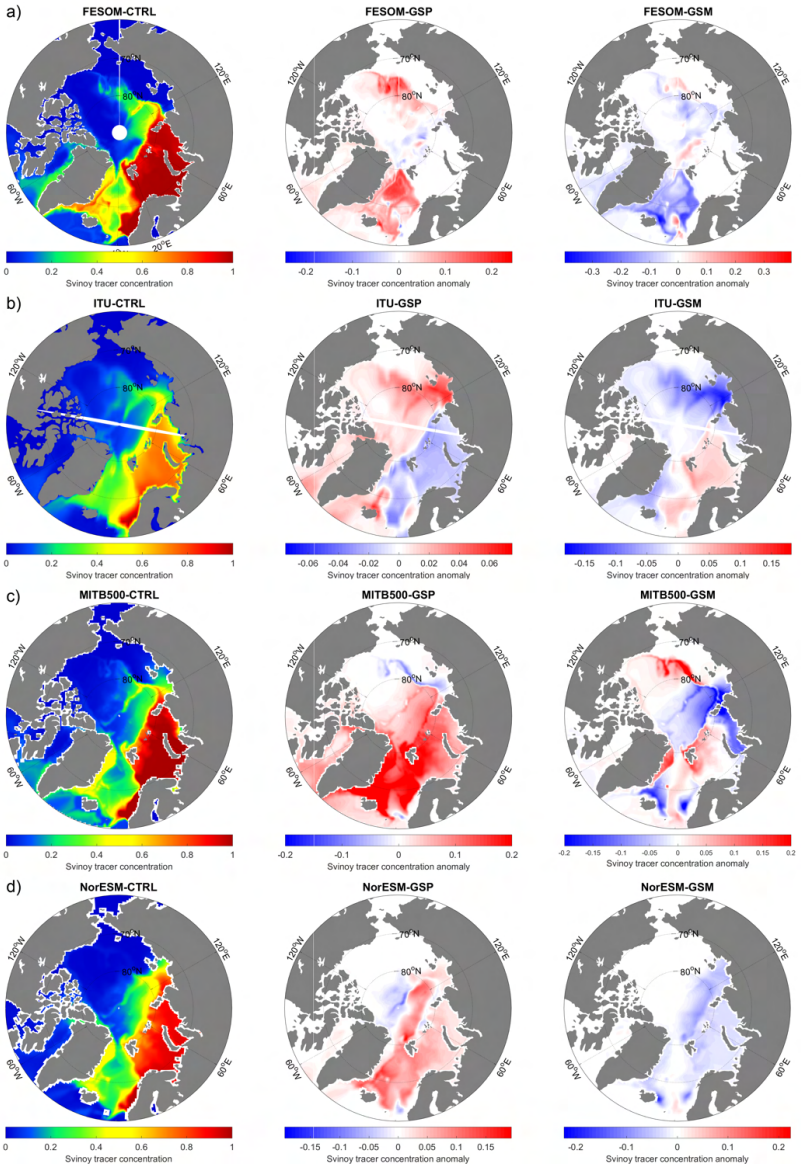

Figure 6. Vertically integrated volume of passive tracer released continuously at all depths at SvinÃÿy in four models. Panels on the left show the control simulations, middle panels show anomalies resulting from the GSP experiment (stronger wind forcing), and right panels show anomalies resulting from the GSM experiment (weaker wind forcing). All values are averaged over the last 10 years of integration (20-30 years after perturbation). Tracer release started simultaneously with the perturbation start. All values are standardized by depth.

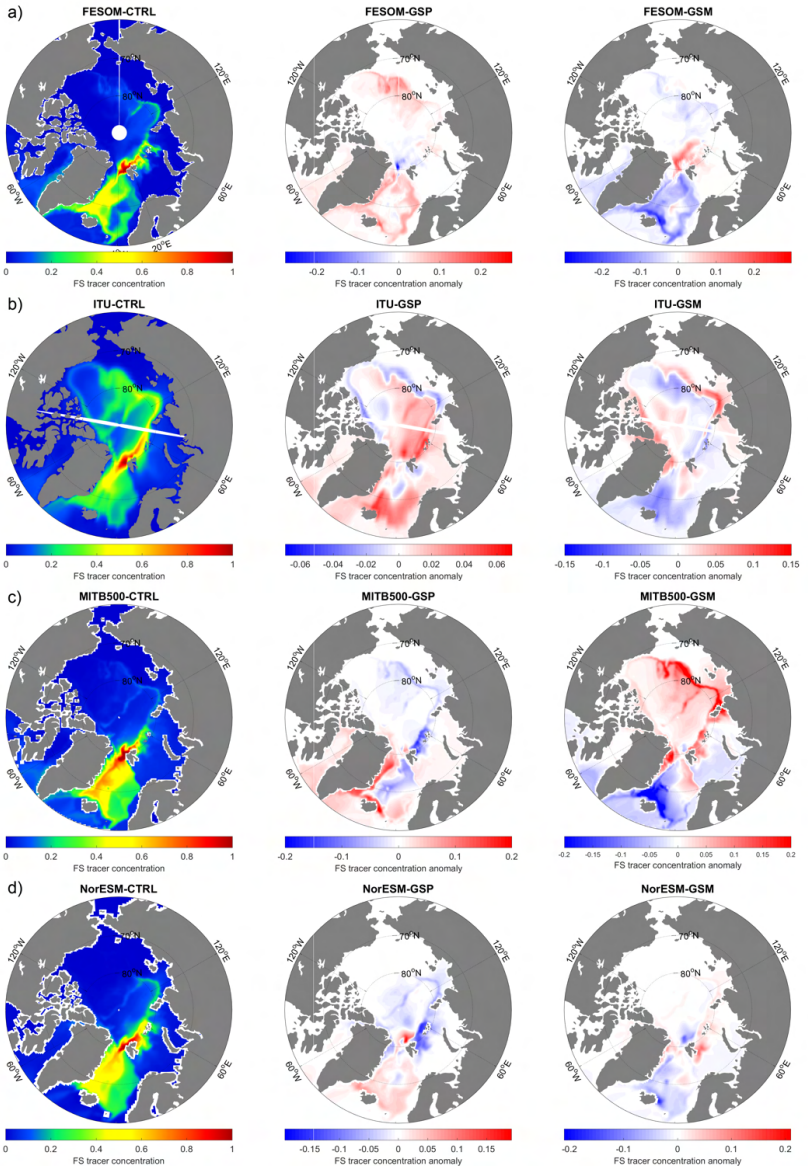

Figure 7. Vertically integrated volume of passive tracer released continuously at all depths in the Fam Strait in four models. Panels on the left show the control simulations, middle panels show anomalies resulting from the GSP experiment (stronger wind forcing), and right panels show anomalies resulting from the GSM experiment (weaker wind forcing). All values are averaged over the last 10 years of integration (20-30 years after perturbation). Tracer release started simultaneously with the perturbation start. All values are standardized by depth.

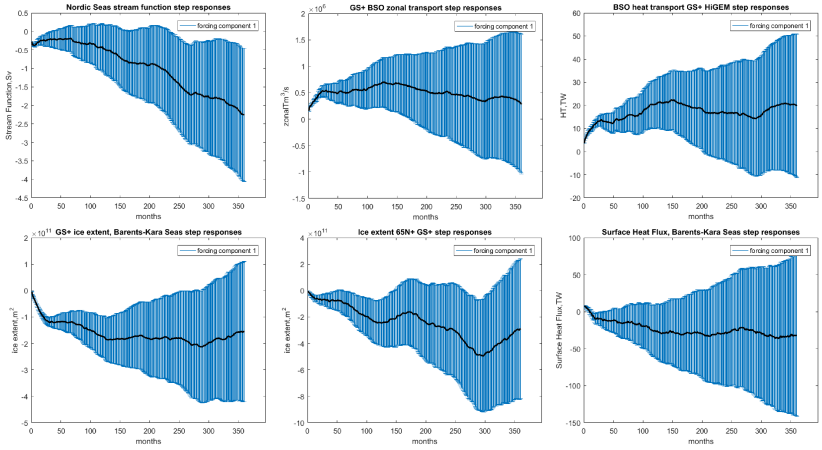

Figure 8. Errors that arise from the multiple linear regression method used to calculate CRFs from the fully coupled Ox-HiGEM simulation.

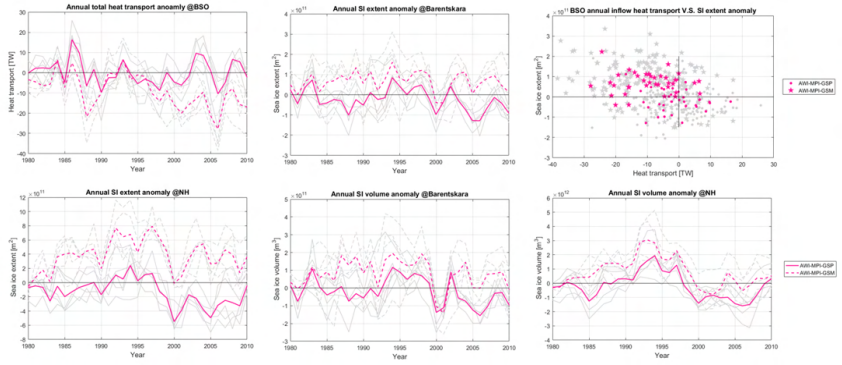

Figure 9. CRF responses from the partial coupled AWI-MPI simulation. Grey lines represent six different ensembles, and the pink lines show the ensemble mean CRF response.

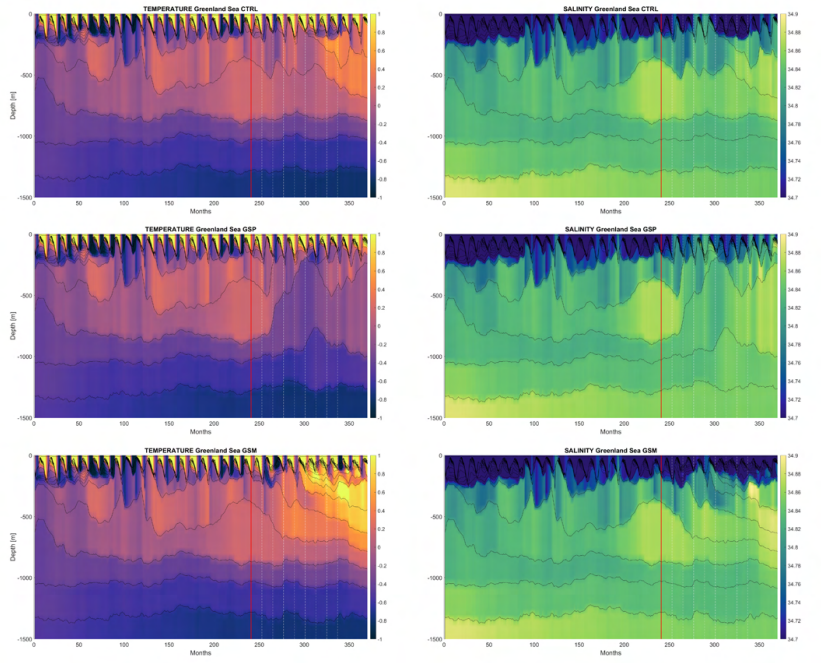

Figure 10. Time evolution of the density field in the central GS before and after the GSP and GSM experiments from the NorESM simulations. Color shading in the left panels shows the temperature by depth for each month, and on the right panels it shows the salinity by depth. Black contours mark different isopycnal layers. Top panels represent the control simulation, middle panels represent the GSP experiment, and lower panels represent the GSM experiment. The red line marks the start of wind perturbation (1980), and dashed white lines each mark one year after the perturbation is applied.

Bibliography

Aagaard, K., and E. C. Carmack (1989), The role of sea ice and other fresh water in the Arctic circulation, *Journal of Geophysical Research*, *94*(C10), 14,485, doi: 10.1029/JC094iC10p14485. 2.1.2, 2.4, 2.1.3

Aagaard, K., and L. K. Coachman (1968), The East Greenland current north of Denmark Strait: part I, *Arctic*, pp. 181–200. 2.1.2

Aagaard, K., L. K. Coachman, and E. Carmack (1981), On the halocline of the Arctic Ocean, *Deep Sea Research Part A, Oceanographic Research Papers*, *28*(6), 529–545, doi:10.1016/0198-0149(81)90115-1. 2.1.3

Aagaard, K., J. H. Swift, L. Jolla, E. C. Carmack, W. Vancouver, and B. Columbia (1985), Thermohaline Circulation in the Arctic, *Deep Sea Research Part I: Oceanographic Research Papers*, *90*, 4833–4846, doi:10.1029/JC090iC03p04833. 2.1.1, 2.1.3, 2.2.2

Anderson, L. G., G. Björk, O. Holby, E. P. Jones, G. Kattner, K. P. Koltermann, B. Liljeblad, R. Lindegren, B. Rudels, and J. Swift (1994), Water masses and circulation in the Eurasian Basin: results from the Oden 91 expedition, *Journal of Geophysical Research*, *99*(C2), 3273–3283, doi:10.1029/93JC02977. 2.1.3

Andresen, C. S., K. K. Kjeldsen, B. Harden, N. Nørgaard-Pedersen, and K. H. Kjær (2014), Outlet glacier dynamics and bathymetry at Upernavik Isstrøm and Upernavik Isfjord, North-West Greenland, doi:10.34194/geusb.v31.4668. 3.2.4

Årthun, M., and T. Eldevik (2016), On anomalous ocean heat transport toward the Arctic and associated climate predictability, *Journal of Climate*, *29*(2), 689–704, doi: 10.1175/JCLI-D-15-0448.1. 2.2.1

Arthun, M., R. Ingvaldsen, L. Smedsrud, and C. Schrum (2011), Dense water formation and circulation in the Barents Sea, *Deep Sea Research Part I: Oceanographic Research Papers*, *58*(8), 801–817, doi:10.1016/j.dsr.2011.06.001. 2.1.3, 2.3.3

Årthun, M., T. Eldevik, L. H. Smedsrud, O. Skagseth, and R. B. Ingvaldsen (2012), Quantifying the Influence of Atlantic Heat on Barents Sea Ice Variability and Retreat, *Journal of Climate*, *25*(13), 4736–4743, doi:10.1175/JCLI-D-11-00466.1. 2.2.1, 2.3.1, 5.1

Årthun, M., T. Eldevik, E. Viste, H. Drange, T. Furevik, H. L. Johnson, and N. S. Keenlyside (2017), Skillful prediction of northern climate provided by the ocean, *Nature Communications*, *8*(May), doi:10.1038/ncomms15875. 2.3.1, 5.2

Årthun, M., T. Eldevik, and L. H. Smedsrud (2019), The role of Atlantic heat transport in future Arctic winter sea ice loss, *Journal of Climate*, *32*(11), 3327–3341, doi: 10.1175/JCLI-D-18-0750.1. 2.2.1, 2.2.2, 2.3.1, 5.2

Årthun, M., I. H. Onarheim, J. Dörr, and T. Eldevik (2021), The seasonal and regional transition to an icefree Arctic, *Geophysical Research Letters*, *48*(1), e2020GL090,825. 2.1.1, 2.3.3

Asbjørnsen, H., M. Årthun, Skagseth, and T. Eldevik (2019), Mechanisms of ocean heat anomalies in the Norwegian Sea, *Journal of Geophysical Research: Oceans*, *124*(4), 2908–2923, doi:10.1029/2018JC014649. 2.2.1, 2.3.3, 4, 5.1

Asbjørnsen, H., M. Årthun, Skagseth, and T. Eldevik (2020), Mechanisms Underlying Recent Arctic Atlantification, *Geophysical Research Letters*, *47*(15), e2020GL088,036, doi:10.1029/2020GL088036. 2.2.1

Athanase, M., C. Provost, M. D. PérezHernández, N. Sennéchael, C. Bertosio, C. Artana, G. Garric, and J. Lellouche (2020), Atlantic Water Modification North of Svalbard in the Mercator Physical System From 2007 to 2020, *Journal of Geophysical Research: Oceans*, *125*(10), e2020JC016,463, doi:10.1029/2020JC016463. 5.3

Auclair, G., and B. Tremblay (2018), The role of ocean heat transport in rapid sea ice declines in the Community Earth System Model Large Ensemble, *Journal of Geophysical Research: Oceans*, doi:10.1029/2018JC014525. 2.2.1

Bamber, J., M. van den Broeke, J. Ettema, J. Lenaerts, and E. Rignot (2012), Recent large increases in freshwater fluxes from Greenland into the North Atlantic, *Geophysical Research Letters*, *39*(19), doi:10.1029/2012GL052552. 2.3.2

Bamber, J. L., A. J. Tedstone, M. D. King, I. M. Howat, E. M. Enderlin, M. R. van den Broeke, and B. Noel (2018), Land ice freshwater budget of the Arctic and North Atlantic Oceans: 1. Data, methods, and results, *Journal of Geophysical Research: Oceans*, *123*(3), 1827–1837, doi:10.1002/2017JC013605. 2.3.2, 5.4

Behrendt, A., H. Sumata, B. Rabe, and U. Schauer (2018), UDASH - Unified Database for Arctic and Subarctic Hydrography, *Earth System Science Data*, *10*(2), 1119–1138, doi:10.5194/essd-10-1119-2018. 3.2.3

Bentsen, M., I. Bethke, J. B. Debernard, T. Iversen, A. Kirkevaag, O. Seland, H. Drange, C. Roelandt, I. a. Seierstad, C. Hoose, and J. E. Kristjánsson (2013), The Norwegian Earth System Model, NorESM1-M - Part 1: Description and basic evaluation, *Geoscientific Model Development Discussions*, *5*, 2843–2931, doi: 10.5194/gmdd-5-2843-2012. 3.2.1

Beszczynska-Möller, A., E. Fahrbach, U. Schauer, and E. Hansen (2012), Variability in Atlantic water temperature and transport at the entrance to the Arctic Ocean, 1997-2010, *ICES Journal of Marine Science: Journal du Conseil*, p. fss056, doi: 10.1093/icesjms/fss056. 2.1.2, 2.2.1

Böning, C. W., E. Behrens, A. Biastoch, K. Getzlaff, and J. L. Bamber (2016), Emerging impact of Greenland meltwater on deepwater formation in the North Atlantic Ocean, *Nature Geoscience*, *9*(7), 523–527, doi:10.1038/ngeo2740. 2.3.2

Boyer, T. P., J. I. Antonov, O. K. Baranova, C. Coleman, H. E. Garcia, A. Grodsky, D. R. Johnson, R. a. Locarnini, A. V. Mishonov, T. D. O'Brien, C. R. Paver, J. R. Reagan, D. Seidov, I. V. Smolyar, M. M. Zweng, T. D. O. Brien, C. R. Paver, J. R. Reagan, D. Seidov, I. V. Smolyar, M. M. Zweng, and K. D. Sullivan (2013), WORLD OCEAN DATABASE 2013, NOAA Atlas NESDIS 72, *Sydney Levitus, Ed.; Alexey Mishonoc, Technical Ed.*, *NOAA Atlas*, 209 pp, doi:10.7289/V5NZ85MT. 3.2.3

Brakstad, A., K. Våge, L. Håvik, and G. W. K. Moore (2019), Water mass transformation in the Greenland Sea during the period 19862016, *Journal of Physical Oceanography*, *49*(1), 121–140, doi:10.1175/JPO-D-17-0273.1. 2.1.3, 2.3.3

Bringedal, C., T. Eldevik, Skagseth, M. A. Spall, and S. Østerhus (2018), Structure and forcing of observed exchanges across the GreenlandScotland Ridge, *Journal of Climate*, *31*(24), 9881–9901, doi:10.1175/JCLI-D-17-0889.1. 2.2.2, 5.2

Caesar, L., G. D. McCarthy, D. J. R. Thornalley, N. Cahill, and S. Rahmstorf (2021), Current Atlantic Meridional Overturning Circulation weakest in last millennium, *Nature Geoscience*, pp. 1–3, doi:https://doi.org/10.1038/s41561-021-00699-z. 2.3.2

Carmack, E., I. Polyakov, L. Padman, I. Fer, E. Hunke, J. Hutchings, J. Jackson, D. Kelley, R. Kwok, C. Layton, H. Melling, D. Perovich, O. Persson, B. Ruddick, M.-L. Timmermans, J. Toole, T. Ross, S. Vavrus, and P. Winsor (2015), Towards Quantifying the Increasing Role of Oceanic Heat in Sea Ice Loss in the New Arctic, *Bulletin of the American Meteorological Society*, *96*(12), 2079–2105, doi:10.1175/BAMS-D-13-00177.1. 2.3.1, 2.3.1

Carmack, E. C. (2007), The alpha/beta ocean distinction: A perspective on freshwater fluxes, convection, nutrients and productivity in high-latitude seas, *Deep Sea Research Part II: Topical Studies in Oceanography*, *54*(23-26), 2578–2598, doi:10.1016/j.dsr2.2007.08.018. 2.1.3

Carmack, E. C., M. Yamamoto-Kawai, T. W. N. Haine, S. Bacon, B. A. Bluhm, C. Lique, H. Melling, I. V. Polyakov, F. Straneo, M. L. Timmermans, and W. J. Williams (2016), Freshwater and its role in the Arctic Marine System: Sources, disposition, storage, export, and physical and biogeochemical consequences in the Arctic and global oceans, *Journal of Geophysical Research G: Biogeosciences*, *121*(3), 675–717, doi:10.1002/2015JG003140. 2.1.2

Carton, J. A., G. A. Chepurin, J. Reagan, and S. Hkkinen (2011), Interannual to decadal variability of Atlantic Water in the Nordic and adjacent seas, *Journal of Geophysical Research: Oceans*, *116*(11), 1–13, doi:10.1029/2011JC007102. 2.2.1

Chafik, L., and T. Rossby (2019), Volume, heat, and freshwater divergences in the subpolar North Atlantic suggest the Nordic Seas as key to the state of the meridional overturning circulation, *Geophysical Research Letters*, *46*(9), 4799–4808, doi:10.1029/2019GL082110. 2.3.3

Chatterjee, S., R. P. Raj, L. Bertino, S. H. Mernild, M. P. Subeesh, N. Murukesh, and M. Ravichandran (2021), Combined influence of oceanic and atmospheric circulations on Greenland sea ice concentration, *The Cryosphere*, *15*(3), 1307–1319, doi: 10.5194/tc-15-1307-2021. 2.3.3

Chepurin, G. A., and J. A. Carton (2012), Subarctic and Arctic sea surface temperature and its relation to ocean heat content 19822010, *Journal of Geophysical Research: Oceans*, *117*(C6), doi:10.1029/2011JC007770. 2.2.1

Chevallier, M., G. C. Smith, F. Dupont, J.-F. Lemieux, G. Forget, Y. Fujii, F. Hernandez, R. Msadek, K. A. Peterson, and A. Storto (2017), Intercomparison of the Arctic sea ice cover in global oceansea ice reanalyses from the ORA-IP project, *Climate Dynamics*, *49*(3), 1107–1136, doi:10.1007/s00382-016-2985-y. 2.3.1

Childers, V. A., and J. M. Brozena (2005), Long-range aircraft as an Arctic Oceanographic platform, *Deep Sea Research Part I: Oceanographic Research Papers*, *52*(12), 2366–2375, doi:10.1016/j.dsr.2005.07.004. 3.2.4

Chylek, P., C. K. Folland, G. Lesins, M. K. Dubey, and M. Wang (2009), Arctic air temperature change amplification and the Atlantic Multidecadal Oscillation, *Geophysical Research Letters*, *36*(14), 2–6, doi:10.1029/2009GL038777. 2.2.1

Chylek, P., C. K. Folland, G. Lesins, and M. K. Dubey (2010), Twentieth century bipolar seesaw of the Arctic and Antarctic surface air temperatures, *Geophysical Research Letters*, *37*(8), doi:10.1029/2010GL042793. 2.2.1

Cohen, J., J. A. Screen, J. C. Furtado, M. Barlow, D. Whittleston, D. Coumou, J. Francis, K. Dethloff, D. Entekhabi, and J. Overland (2014), Recent Arctic amplification and extreme mid-latitude weather, *Nature geoscience*, *7*(9), 627, doi: 10.1038/NGEO2234. 2.1.1

Cohen, J., X. Zhang, J. Francis, T. Jung, R. Kwok, J. Overland, T. J. Ballinger, U. S. Bhatt, H. W. Chen, and D. Coumou (2020), Divergent consensuses on Arctic amplification influence on midlatitude severe winter weather, *Nature Climate Change*, *10*(1), 20–29, doi:10.1038/s41558-019-0662-y. 2.1.1

Comiso, J. C., W. N. Meier, and R. Gersten (2017), Variability and trends in the A rctic S ea ice cover: Results from different techniques, *Journal of Geophysical Research: Oceans*, *122*(8), 6883–6900, doi:10.1002/2017JC012768. 2.3.1

Compo, G. P., J. S. Whitaker, P. D. Sardeshmukh, N. Matsui, R. J. Allan, X. Yin, B. E. Gleason, R. S. Vose, G. Rutledge, and P. Bessemoulin (2011), The twentieth century reanalysis project, *Quarterly Journal of the Royal Meteorological Society*, *137*(654), 1–28, doi:10.1002/qj.776. 3.2.1

Cornish, S. B., Y. Kostov, H. L. Johnson, and C. Lique (2020), Response of Arctic freshwater to the Arctic Oscillation in coupled climate models, *Journal of Climate*, *33*(7), 2533–2555, doi:10.1175/JCLI-D-19-0685.1. 3.2.2

Danabasoglu, G., S. G. Yeager, W. M. Kim, E. Behrens, M. Bentsen, D. Bi, A. Biastoch, R. Bleck, C. Böning, and A. Bozec (2016), North Atlantic simulations in Coordinated Ocean-ice Reference Experiments phase II (CORE-II). Part II: Inter-annual to decadal variability, *Ocean Modelling*, *97*, 65–90, doi:10.1016/j.ocemod.2015.11.007. 2.1.1, 3.2

Davy, R., and S. Outten (2020), The Arctic surface climate in CMIP6: status and developments since CMIP5, *Journal of Climate*, *33*(18), 8047–8068. 2.1.1

Day, J. J., J. C. Hargreaves, J. D. Annan, and A. Abe-Ouchi (2012), Sources of multi-decadal variability in Arctic sea ice extent, *Environmental Research Letters*, *7*(3), 34,011, doi:10.1088/1748-9326/7/3/034011. 2.2.1

de Steur, L., E. Hansen, R. Gerdes, M. Karcher, E. Fahrbach, and J. Holfort (2009), Freshwater fluxes in the East Greenland Current: A decade of observations, *Geophysical Research Letters*, *36*(23), doi:10.1029/2009GL041278. 2.1.2

Delworth, T. L., and K. W. Dixon (2000), Implications of the recent trend in the Arctic/North Atlantic Oscillation for the North Atlantic thermohaline circulation, *Journal of Climate*, *13*(21), 3721–3727, doi:10.1175/1520-0442(2000)013<3721:IOTRTI>2.0.CO;2. 2.2.1

Delworth, T. L., and F. Zeng (2016), The impact of the North Atlantic Oscillation on climate through its influence on the Atlantic meridional overturning circulation, *Journal of Climate*, *29*(3), 941–962. 2.2.2

Deser, C., R. A. Tomas, and L. Sun (2015), The role of oceanatmosphere coupling in the zonal-mean atmospheric response to Arctic sea ice loss, *Journal of Climate*, *28*(6), 2168–2186, doi:10.1175/JCLI-D-14-00325.1. 2.1.1

Desmarais, A., and B. Tremblay (2021), Assessment of decadal variability in sea ice in the Community Earth System Model against a long-term regional observational record: implications for the predictability of an ice-free Arctic, *Journal of Climate*, doi:10.1175/jcli-d-20-0561.1. 2.1.1

Dickson, R. R., J. Meincke, S. A. Malmberg, and A. J. Lee (1988), The "great salinity anomaly" in the Northern North Atlantic 1968-1982, *Progress in Oceanography*, *20*(2), 103–151, doi:10.1016/0079-6611(88)90049-3. 2.2.1

Dickson, R. R., T. J. Osborn, J. W. Hurrell, J. Meincke, J. Blindheim, B. Adlandsvik, T. Vinje, G. Alekseev, and W. Maslowski (2000), The Arctic Ocean response to the North Atlantic oscillation, *Journal of Climate*, *13*(15), 2671–2696, doi:10.1175/1520-0442(2000)013<2671:TAORTT>2.0.CO;2. 2.2.2

Dmitrenko, I. a., I. V. Polyakov, S. a. Kirillov, L. a. Timokhov, I. E. Frolov, V. T. Sokolov, H. L. Simmons, V. V. Ivanov, and D. Walsh (2008), Toward a warmer Arctic Ocean: Spreading of the early 21st century Atlantic Water warm anomaly along the Eurasian Basin margins, *Journal of Geophysical Research*, *113*(C5), doi:10.1029/2007JC004158. 2.2.1

Docquier, D., R. Fuentes-Franco, T. Koenigk, and T. Fichefet (2020), Sea IceOcean Interactions in the Barents Sea Modeled at Different Resolutions, *Frontiers in Earth Science*, *8*, doi:10.3389/feart.2020.00172. 5.1

Drinkwater, K. F., M. Miles, I. Medhaug, O. H. Otterå, T. Kristiansen, S. Sundby, and Y. Gao (2014), The Atlantic Multidecadal Oscillation: Its manifestations and impacts with special emphasis on the Atlantic region north of 60 N, *Journal of Marine Systems*, *133*, 117–130, doi:10.1016/j.jmarsys.2013.11.001. 2.2.1

Duarte, P., A. Sundfjord, A. Meyer, S. R. Hudson, G. Spreen, and L. H. Smedsrud (2020), Warm Atlantic water explains observed sea ice melt rates north of Svalbard, *Journal of Geophysical Research: Oceans*, *125*(8), e2019JC015,662, doi:10.1029/2019JC015662. 2.3.1

Eldevik, T., and J. E. Nilsen (2013), The ArcticAtlantic thermohaline circulation, *Journal of climate*, *26*(21), 8698–8705, doi:0.1175/JCLI-D-13-00305.1. 2.1.2, 2.2.2, 5.2

Eldevik, T., J. E. Nilsen, D. Iovino, K. A. Olsson, A. B. Sandø, and H. Drange (2009), Observed sources and variability of Nordic seas overflow, *Nature Geoscience*, *2*(6), 406–410, doi:10.1038/ngeo518. 2.2.2, 2.3.3

Eldevik, T., I. H. Onarheim, L. H. Smedsrud, M. Steele, P. Dodd, M. Muilwijk, and M. Årthun (2021), How Atlantic heat makes Arctic sea ice retreat, *In preperation*. 2.2.1, 2.3.1

Environmental Working Group, V. (1997), Joint US-Russian atlas of the Arctic Ocean for the winter period, *Natl Snow and Ice Data Cent*. 3.2.3

Eyring, V., S. Bony, G. A. Meehl, C. A. Senior, B. Stevens, R. J. Stouffer, and K. E. Taylor (2016), Overview of the Coupled Model Intercomparison Project Phase 6 (CMIP6) experimental design and organization, *Geoscientific Model Development*, *9*(5), 1937–1958, doi:10.5194/gmd-9-1937-2016. 3.2.1

Fahrbach, E., J. Meincke, S. Østerhus, G. Rohardt, U. Schauer, V. Tverberg, and J. Verduin (2001), Direct measurements of volume transports through Fram Strait, *Polar Research*, *20*(2), 217–224, doi:10.1111/j.1751-8369.2001.tb00059.x. 2.1.2, 2.2.1

Fenty, I., J. K. Willis, A. Khazendar, S. Dinardo, R. Forsberg, I. Fukumori, D. Holland, M. Jakobsson, D. Moller, and J. Morison (2016), Oceans melting Greenland: early results from NASA's ocean-ice mission in Greenland, *Oceanography*, *29*(4), 72–83, doi:10.5670/oceanog.2018.211. 3.2.4

Fer, I., M. Müller, and A. Peterson (2015), Tidal forcing, energetics, and mixing near the Yermak Plateau, *Ocean Science*, *11*(2), 287–304, doi:10.5194/os-11-287-2015. 2.1.3

Fer, I., Z. Koenig, I. E. Kozlov, M. Ostrowski, T. P. Rippeth, L. Padman, A. Bosse, and E. Kolås (2020), Tidally forced lee waves drive turbulent mixing along the Arctic Ocean margins, *Geophysical Research Letters*, *47*(16), e2020GL088,083, doi:10.1029/2020GL088083. 2.1.3

Fichefet, T., C. Poncin, H. Goosse, P. Huybrechts, I. Janssens, and H. Le Treut (2003), Implications of changes in freshwater flux from the Greenland ice sheet for the climate of the 21st century, *Geophysical Research Letters*, *30*(17), doi: 10.1029/2003GL017826. 5.2

Forget, G., J.-M. Campin, P. Heimbach, C. N. Hill, R. M. Ponte, and C. Wunsch (2015), ECCO version 4: An integrated framework for non-linear inverse modeling and global ocean state estimation, *Geoscientific Model Development*, *8*(10), 3071–3104, doi:https://doi.org/10.5194/gmd-8-3071-2015. 3.2.3

Fox-Kemper, B., A. Adcroft, C. W. Böning, E. P. Chassignet, E. Curchitser, G. Danabasoglu, C. Eden, M. H. England, R. Gerdes, and R. J. Greatbatch (2019), Challenges and prospects in ocean circulation models, *Frontiers in Marine Science*, *6*, 65. 3.2

Frajka-Williams, E., J. L. Bamber, and K. Våge (2016), Greenland melt and the Atlantic meridional overturning circulation, *Oceanography*, *29*(4), 22–33, doi:10.5670/oceanog.2016.96. 2.3.2

Francis, J. A., and S. J. Vavrus (2012), Evidence linking Arctic amplification to extreme weather in mid latitudes, *Geophysical Research Letters*, *39*(6), doi:10.1029/2012GL051000. 2.1.1, 3.1

Furevik, T. (2000), On anomalous sea surface temperatures in the nordic seas, *Journal of Climate*, *13*(5), 1044–1053, doi:10.1175/1520-0442(2000)013<1044:OASSTI>2.0.CO;2. 2.2.1

Fyfe, J. C., K. Von Salzen, N. P. Gillett, V. K. Arora, G. M. Flato, and J. R. McConnell (2013), One hundred years of Arctic surface temperature variation due to anthropogenic influence, *Scientific Reports*, *3*(1), 1–7. 2.1.1

Gebbie, G., and P. Huybers (2011), How is the ocean filled?, *Geophysical Research Letters*, *38*(6), doi:10.1029/2011GL046769. 2.3.3

Gent, P. R., and J. C. Mcwilliams (1990), Isopycnal mixing in ocean circulation models, *Journal of Physical Oceanography*, *20*(1), 150–155, doi:10.1175/1520-0485(1990)020<0150:IMIOCM>2.0.CO;2. 3.2.1

Gidden, M. J., K. Riahi, S. J. Smith, S. Fujimori, G. Luderer, E. Kriegler, D. P. v. Vuuren, M. v. d. Berg, L. Feng, and D. Klein (2019), Global emissions pathways under different socioeconomic scenarios for use in CMIP6: a dataset of harmonized emissions trajectories through the end of the century, *Geoscientific model development*, *12*(4), 1443–1475, doi:10.5194/gmd-12-1443-2019. 3.2.1

Gillard, L. C., X. Hu, P. G. Myers, and J. L. Bamber (2016), Meltwater pathways from marine terminating glaciers of the Greenland ice sheet, *Geophysical Research Letters*, *43*(20), doi:10.1002/2016GL070969. 2.3.2

Glessmer, M. S., T. Eldevik, K. Vaage, J. E. Oie Nilsen, and E. Behrens (2014), Atlantic origin of observed and modelled freshwater anomalies in the Nordic Seas, *Nature Geoscience*, *7*(11), 801–805, doi:10.1038/ngeo2259. 2.2.1, 2.3.3

Goncalves-Araujo, R. (2016), Tracing environmental variability in the changing Arctic Ocean with optical measurements of dissolved organic matter., Ph.D. thesis. 2.4

González-Pola, C., K. M. H. Larsen, P. Fratantoni, and A. Beszczynska-Moller (2018), ICES Report on Ocean Climate 2018, *ICES Cooperative Research Report*, (349). 2.2.1

Good, P., J. M. Gregory, and J. A. Lowe (2011), A stepresponse simple climate model to reconstruct and interpret AOGCM projections, *Geophysical Research Letters*, *38*(1), doi:10.1029/2010GL045208. 3.2.2

Good, S. A., M. J. Martin, and N. A. Rayner (2013), EN4: Quality controlled ocean temperature and salinity profiles and monthly objective analyses with uncertainty estimates, *Journal of Geophysical Research: Oceans*, *118*(12), 6704–6716, doi:10.1002/2013JC009067. 3.2.2, 3.2.3

Gorshkov, S. G. (1980), Atlas of Oceans. Arctic Ocean, *Minist. of Def. of the USSR, Moscow*. 3.2.3

Griffies, S. M., M. Winton, B. Samuels, G. Danabasoglu, S. Yeager, S. Marsland, H. Drange, and M. Bentsen (2012), Datasets and protocol for the CLIVAR WGOMD Coordinated Ocean-sea ice Reference Experiments (COREs), *WCRP Report*, (21), 1–21. 3.2.1

Griffies, S. M., G. Danabasoglu, P. J. Durack, A. J. Adcroft, V. Balaji, C. W. Böning, E. P. Chassignet, E. Curchitser, J. Deshayes, H. Drange, B. Fox-Kemper, P. J. Gleckler, J. M. Gregory, H. Haak, R. W. Hallberg, P. Heimbach, H. T. Hewitt, D. M. Holland, T. Ilyina, J. H. Jungclaus, Y. Komuro, J. P. Krasting, W. G. Large, S. J. Marsland, S. Masina, T. J. McDougall, A. J. George Nurser, J. C. Orr, A. Pirani, F. Qiao, R. J. Stouffer, K. E. Taylor, A. M. Treguier, H. Tsujino, P. Uotila, M. Valdivieso, Q. Wang, M. Winton, and S. G. Yeager (2016), OMIP contribution to CMIP6: Experimental and diagnostic protocol for the physical component of the Ocean Model Intercomparison Project, *Geoscientific Model Development*, *9*(9), 3231–3296, doi:10.5194/gmd-9-3231-2016. 3.2.1

Haine, T. W., B. Curry, R. Gerdes, E. Hansen, M. Karcher, C. Lee, B. Rudels, G. Spreen, L. de Steur, K. D. Stewart, and R. Woodgate (2015), Arctic freshwater export: Status, mechanisms, and prospects, *Global and Planetary Change*, *125*, 13–35, doi:10.1016/j.gloplacha.2014.11.013. 2.1.2, 2.1.3

Haine, T. W. N. (2020), Arctic Ocean Freshening Linked to Anthropogenic Climate Change: All Hands on Deck, *Geophysical Research Letters*, *47*(22), e2020GL090,678, doi:10.1029/2020GL090678. 2.1.1, 2.1.3

Hansen, B., and S. Østerhus (2007), Faroe bank channel overflow 19952005, *Progress in Oceanography*, *75*(4), 817–856, doi:10.1016/j.pocean.2007.09.004. 2.1.1

Hansen, B., S. Østerhus, W. R. Turrell, S. Jónsson, H. Valdimarsson, H. Hátún, and S. M. Olsen (2008), The inflow of Atlantic water, heat, and salt to the nordic seas across the GreenlandScotland ridge, in *ArcticSubarctic Ocean Fluxes*, pp. 15–43, Springer. 2.1.2, 2.7

Hasselmann, K. (1993), Optimal fingerprints for the detection of time-dependent climate change, *Journal of Climate*, *6*(10), 1957–1971, doi:10.1175/1520-0442(1993)006<1957:OFFTDO>2.0.CO;2. 3.2.2

Hattermann, T., P. E. Isachsen, W. J. Von Appen, J. Albretsen, and A. Sundfjord (2016), Eddy-driven recirculation of Atlantic Water in Fram Strait, *Geophysical Research Letters*, *43*(7), 3406–3414, doi:10.1002/2016GL068323. 2.1.2

Håvik, L., M. Almansi, K. Våge, and T. W. N. Haine (2019), Atlantic-origin overflow water in the east Greenland current, *Journal of Physical Oceanography*, *49*(9), 2255–2269, doi:10.1175/JPO-D-18-0216.1. 2.1.3

He, Y. C., H. Drange, Y. Gao, and M. Bentsen (2016), Simulated Atlantic Meridional Overturning Circulation in the 20th century with an ocean model forced by reanalysis-based atmospheric data sets, *Ocean Modelling*, *100*, 31–48, doi:10.1016/j.ocemod.2015.12.011. 3.2.1

Held, I. M., and B. J. Soden (2006), Robust responses of the hydrological cycle to global warming, *Journal of climate*, *19*(21), 5686–5699, doi:10.1175/JCLI3990.1. 2.1.3

Helland-Hansen, B., and F. Nansen (1909), *The Norwegian Sea: its physical oceanography based upon the Norwegian researches 1900-1904*, Det Mallingske bogtrykkeri. 2.1.3, 2.1.3, 2.2.1, 2.3.1, 2.3.3

Heuzé, C. (2017), North Atlantic deep water formation and AMOC in CMIP5 models, *Ocean Science*, *13*(4), 609–622, doi:10.5194/os-13-609-2017. 2.3.3

Heuzé, C., and M. Årthun (2019), The Atlantic inflow across the Greenland-Scotland ridge in global climate models (CMIP5), *Elementa: Science of the Anthropocene*, *7*, doi:10.1525/elementa.354. 2.1.1

Hinzman, L. D., C. J. Deal, A. D. Mcguire, S. H. Mernild, I. V. Polyakov, and J. E. Walsh (2013), Trajectory of the Arctic as an integrated system, *Ecological Applications*, *23*(8), 1837–1868, doi:10.1890/11-1498.1. 3.1

Holland, D. M., R. H. Thomas, B. De Young, M. H. Ribergaard, and B. Lyberth (2008), Acceleration of Jakobshavn Isbræ triggered by warm subsurface ocean waters, *Nature geoscience*, *1*(10), 659–664, doi:10.1038/ngeo316. 2.3.2

Holliday, N. P., S. L. Hughes, S. Bacon, A. Beszczynska-Möller, B. Hansen, A. Lavín, H. Loeng, K. a. Mork, S. Østerhus, T. Sherwin, and W. Walczowski (2008), Reversal of the 1960s to 1990s freshening trend in the northeast North Atlantic and Nordic Seas, *Geophysical Research Letters*, *35*(3), doi:10.1029/2007GL032675. 2.2.1

Holmes, R. M., J. W. McClelland, B. J. Peterson, S. E. Tank, E. Bulygina, T. I. Eglinton, V. V. Gordeev, T. Y. Gurtovaya, P. A. Raymond, D. J. Repeta, R. Staples, R. G. Striegl, A. V. Zhulidov, and S. A. Zimov (2012), Seasonal and Annual Fluxes of Nutrients and Organic Matter from Large Rivers to the Arctic Ocean and Surrounding Seas, *Estuaries and Coasts*, *35*(2), 369–382, doi:10.1007/s12237-011-9386-6. 2.1.3

Hopkins, T. S. (1991), The GIN SeaA synthesis of its physical oceanography and literature review 19721985, *Earth-Science Reviews*, *30*(3-4), 175–318, doi:10.1016/0012-8252(91)90001-V. 2.1.1

Huang, J., R. S. Pickart, R. X. Huang, P. Lin, A. Brakstad, and F. Xu (2020), Sources and upstream pathways of the densest overflow water in the Nordic Seas, *Nature communications*, *11*(1), 1–9, doi:10.1038/s41467-020-19050-y. 2.3.3, 3.2.3

Hunke, E. C., W. H. Lipscomb, A. K. Turner, N. Jeffery, and S. Elliot (2015), CICE : the Los Alamos Sea Ice Model Documentation and Software Users Manual Version 5.1 LA-CC-06-012, *Los Alamos National Laboratory Tech. Rep. LA-CC-06-012*, (March 17), 76. 3.2.1

Hunkins, K. L. (1974), Subsurface eddies in the Arctic ocean, *Deep-Sea Research and Oceanographic Abstracts*, *21*(12), 1017–1033, doi:10.1016/0011-7471(74)90064-3. 2.1.2

IHO (1953), *Limits of oceans and seas*, 23, International Hydrographic Organization. 2.1.1

Ilicak, M., H. Drange, Q. Wang, R. Gerdes, Y. Aksenov, D. Bailey, M. Bentsen, A. Biastoch, A. Bozec, and C. Böning (2016), An assessment of the Arctic Ocean in a suite of interannual CORE-II simulations. Part III: Hydrography and fluxes, *Ocean Modelling*, *100*, 141–161, doi:10.1016/j.ocemod.2016.02.004. 2.1.1, 3.2, 3.3, 5.1

Ilcak, M., T. M. Özgökmen, H. Peters, H. Z. Baumert, and M. Iskandarani (2008), Performance of two-equation turbulence closures in three-dimensional simulations of the Red Sea overflow, *Ocean Modelling*, *24*(3-4), 122–139, doi:10.1016/j.ocemod.2008.06.001. 3.2.1

Ingvaldsen, R. (2004), The Atlantic inflow to the Barents Sea, *10*(1), 5817, doi:10.1029/2001JC001039.Ottersen. 2.2.1

Ingvaldsen, R., H. Loeng, and L. Asplin (2002), Variability in the Atlantic inflow to the Barents Sea based on a one-year time series from moored current meters, *Continental Shelf Research*, *22*(3), 505–519, doi:10.1016/S0278-4343(01)00070-X. 2.1.2, 2.2.1

IPCC, H. Portner, D. Roberts, V. Masson-Delmotte, P. Zhai, M. Tignor, E. Poloczanska, K. Mintebeck, M. Nicolai, A. Okem, J. Petzold, B. Rama, and N. Weyer (2019), IPCC The Ocean and Cryosphere in a Changing Climate Summary for Policmakers, *IPCC Special Report on the Ocean and Cryosphere in a Changing Climate*, (September), SPM–1–SPM–42. 2.1.1, 2.1.1, 2.3.1, 2.3.2, 3.1

Ivanov, V., V. Alexeev, N. V. Koldunov, I. Repina, A. B. Sando, L. H. Smedsrud, and A. Smirnov (2016), Arctic Ocean heat impact on regional ice decay - a suggested positive feedback, *Journal of Physical Oceanography*, *46*(5), 1437–1456, doi:10.1175/JPO-D-15-0144.1. 2.3.1, 2.3.1

Ivanov, V. V., V. A. Alexeev, I. Repina, N. V. Koldunov, and A. Smirnov (2012), Tracing Atlantic Water signature in the Arctic sea ice cover east of Svalbard, *Advances in Meteorology*, *2012*, doi:10.1155/2012/201818. 2.3.1

Jakobsson, M., and R. Macnab (2006), A comparison between GEBCO Sheet 5.17 and the International Bathymetric Chart of the Arctic Ocean (IBCAO) version 1.0, *Marine Geophysical Researches*, *27*(1), 35–48, doi:10.1007/s11001-005-7760-0. 2.1.1

Jakobsson, M., L. A. Mayer, J. Nilsson, C. Stranne, B. Calder, M. ORegan, J. W. Farrell, T. M. Cronin, V. Brüchert, and J. Chawarski (2020), Ryder Glacier in northwest Greenland is shielded from warm Atlantic water by a bathymetric sill, *Communications Earth & Environment*, *1*(1), 1–10, doi:10.1038/s43247-020-00043-0. 5.4

Johnson, H. L., S. B. Cornish, Y. Kostov, E. Beer, and C. Lique (2018), Arctic Ocean freshwater content and its decadal memory of sea-level pressure, *Geophysical Research Letters*, *45*(10), 4991–5001, doi:10.1029/2017GL076870. 3.2.2

Jones, E. P. (2001), Circulation in the Arctic Ocean, *Polar Research*, *20*(2), 139–146, doi:10.1111/j.1751-8369.2001.tb00049.x. 2.1.2

Karcher, M. J. (2003), Arctic warming: Evolution and spreading of the 1990s warm event in the Nordic seas and the Arctic Ocean, *Journal of Geophysical Research*, *108*(C2), 3034, doi:10.1029/2001JC001265. 2.1.2

Karstensen, J., P. Schlosser, D. W. R. Wallace, J. L. Bullister, and J. Blindheim (2005), Water mass transformation in the Greenland Sea during the 1990s, *Journal of Geophysical Research: Oceans*, *110*(C7), doi:10.1175/JPO-D-17-0273.1. 2.3.3

Kay, J. E., M. M. Holland, and A. Jahn (2011), Inter-annual to multi-decadal Arctic sea ice extent trends in a warming world, *Geophysical Research Letters*, *38*(15), doi:10.1029/2011GL048008. 2.2.1

Keen, A., E. Blockley, D. A. Bailey, J. Boldingh Debernard, M. Bushuk, S. Delhaye, D. Docquier, D. Feltham, F. Massonnet, and S. O'Farrell (2021), An intercomparison of the mass budget of the Arctic sea ice in CMIP6 models, *The Cryosphere*, *15*(2), 951–982, doi:10.5194/tc-15-951-2021. 2.1.1

Kinnard, C., C. M. Zdanowicz, D. A. Fisher, E. Isaksson, A. de Vernal, and L. G. Thompson (2011), Reconstructed changes in Arctic sea ice over the past 1,450 years, *Nature*, *479*(7374), 509–512, doi:10.1038/nature10581. 2.1.1

Klenke, M., and H. W. Schenke (2002), A new bathymetric model for the central Fram Strait, *Marine Geophysical Researches*, *23*(4), 367–378. 2.1.1

Koenig, Z., C. Provost, N. VillacierosRobineau, N. Sennéchael, and A. Meyer (2016), Winter oceanice interactions under thin sea ice observed by I AOOS platforms during NI CE2015: Salty surface mixed layer and active basal melt, *Journal of Geophysical Research: Oceans*, *121*(10), 7898–7916, doi:10.1002/2016JC012195. 2.3.1

Koenigk, T., and L. Brodeau (2017), Arctic climate and its interaction with lower latitudes under different levels of anthropogenic warming in a global coupled climate model, *Climate Dynamics*, *49*(1-2), 471–492, doi:10.1007/s00382-016-3354-6. 2.3.1

Korablev, A., A. Smirnov, and O. K. Baranova (2014), Climatological Atlas of the Nordic Seas and Northern North Atlantic: NOAA Atlas NESDIS 77, *13*(June), doi: 10.7289/V54B2Z78. 3.2.3, 3.4

Kostov, Y., J. Marshall, U. Hausmann, K. C. Armour, D. Ferreira, and M. M. Holland (2017), Fast and slow responses of Southern Ocean sea surface temperature to SAM in coupled climate models, *Climate dynamics*, *48*(5-6), 1595–1609, doi: 10.1007/s00382-016-3162-z. 3.2.2

Krahmann, G., M. Visbeck, and G. Reverdin (2001), Formation and propagation of temperature anomalies along the North Atlantic Current, *Journal of Physical Oceanography*, *31*(5), 1287–1303, doi:10.1175/1520-0485(2001)031<1287: FAPOTA>2.0.CO;2. 2.2.1

Kwok, R. (2018), Arctic sea ice thickness, volume, and multiyear ice coverage: Losses and coupled variability (1958-2018), *Environmental Research Letters*, *13*(10), doi: 10.1088/1748-9326/aae3ec. 2.3.1

Lambert, E., T. Eldevik, and P. M. Haugan (2016), How northern freshwater input can stabilise thermohaline circulation, *Tellus A: Dynamic Meteorology and Oceanography*, *68*(1), 31,051, doi:10.3402/tellusa.v68.31051. 2.1.2, 2.2.2

Lambert, E., A. Nummelin, P. Pemberton, and M. Ilcak (2019), Tracing the imprint of river runoff variability on Arctic water mass transformation, *Journal of Geophysical Research: Oceans*, *124*(1), 302–319, doi:10.1029/2017JC013704. 3.2.2, 5.2

Landrum, L., and M. M. Holland (2020), Extremes become routine in an emerging new Arctic, *Nature Climate Change*, *10*(12), 1108–1115, doi:10.1038/ s41558-020-0892-z. 2.1.1, 3.1

Langehaug, H. R., A. B. Sandø, M. Årthun, and M. Ilcak (2019), Variability along the Atlantic water pathway in the forced Norwegian Earth System Model, *Climate dynamics*, *52*(1), 1211–1230, doi:10.1007/s00382-018-4184-5. 2.2.1

Lannuzel, D., L. Tedesco, M. Van Leeuwe, K. Campbell, H. Flores, B. Delille, L. Miller, J. Stefels, P. Assmy, and J. Bowman (2020), The future of Arctic sea-ice biogeochemistry and ice-associated ecosystems, *Nature Climate Change*, *10*(11), 983–992, doi:10.1038/s41558-020-00940-4. 2.1.1

Large, W. G., J. C. McWilliams, and S. C. Doney (1994), Oceanic vertical mixing: A review and a model with a nonlocal boundary layer parameterization, *Reviews of Geophysics*, *32*(4), 363–403, doi:10.1029/94RG01872. 3.2.1

Latarius, K., and D. Quadfasel (2016), Water mass transformation in the deep basins of the Nordic Seas: Analyses of heat and freshwater budgets, *Deep Sea Research Part I: Oceanographic Research Papers*, *114*, 23–42, doi:10.1016/j.dsr.2016.04.012. 2.3.3

Lauvset, S. K., A. Brakstad, K. Våge, A. Olsen, E. Jeansson, and K. A. Mork (2018), Continued warming, salinification and oxygenation of the Greenland Sea gyre, *Tellus A: Dynamic Meteorology and Oceanography*, *70*(1), 1–9, doi:10.1080/16000870. 2018.1476434. 2.3.3

Laxon, S. W., K. a. Giles, A. L. Ridout, D. J. Wingham, R. Willatt, R. Cullen, R. Kwok, A. Schweiger, J. Zhang, C. Haas, S. Hendricks, R. Krishfield, N. Kurtz, S. Farrell, and M. Davidson (2013), CryoSat-2 estimates of Arctic sea ice thickness and volume, *Geophysical Research Letters*, *40*(4), 732–737, doi:10.1002/grl.50193. 2.3.1

Le Bras, I., F. Straneo, M. Muilwijk, L. H. Smedsrud, F. Li, M. S. Lozier, and N. P. Holliday (2021), How much Arctic fresh water participates in the subpolar overturning circulation?, *Journal of Physical Oceanography*, doi:10.1175/jpo-d-20-0240.1. 2.1.2, 2.1.3, 2.3.2, 2.12, 2.13, 3.2.1, 5.1

LeBlond, P. H. (1980), On the surface circulation in some channels of the Canadian Arctic Archipelago, *Arctic*, pp. 189–197, doi:10.14430/arctic2554. 2.1.2

Lecomte, O., T. Fichefet, M. Vancoppenolle, F. Domine, F. Massonnet, P. Mathiot, S. Morin, and P.-Y. Barriat (2013), On the formulation of snow thermal conductivity in largescale sea ice models, *Journal of Advances in Modeling Earth Systems*, *5*(3), 542–557, doi:10.1002/jame.20039. 3.2.1

Lehner, F., C. C. Raible, D. Hofer, and T. F. Stocker (2012), The freshwater balance of polar regions in transient simulations from 1500 to 2100 AD using a comprehensive coupled climate model, *Climate dynamics*, *39*(1-2), 347–363, doi:10.1007/s00382-011-1199-6. 2.1.3

Lemke, P., and T. O. Manley (1984), The seasonal variation of the mixed layer and the pycnocline under polar sea ice, *Journal of Geophysical Research*, *89*(C4), 6494, doi:10.1029/JC089iC04p06494. 2.1.3

Li, G., L. Cheng, J. Zhu, K. E. Trenberth, M. E. Mann, and J. P. Abraham (2020), Increasing ocean stratification over the past half-century, *Nature Climate Change*, *10*(12), 1116–1123, doi:10.1038/s41558-020-00918-2. 4

Lien, V. S., P. Schlichtholz, Ø. Skagseth, and F. B. Vikebø (2017), Wind-Driven Atlantic Water Flow as a Direct Mode for Reduced Barents Sea Ice Cover, *Journal of Climate*, *30*(2), 803–812, doi:10.1175/JCLI-D-16-0025.1. 2.3.1

Lind, S., R. B. Ingvaldsen, and T. Furevik (2016), Arctic layer salinity controls heat loss from deep Atlantic layer in seasonally ice-covered areas of the Barents Sea, *Geophysical Research Letters*, *43*(10), 5233–5242, doi:10.1002/2016GL068421. 2.3.1

Lind, S., R. B. Ingvaldsen, and T. Furevik (2018), Sea linked to declining sea-ice import, *Nature Climate Change*, *8*(634), doi:10.1038/s41558-018-0205-y. 2.2.1

Lindeman, M. R., F. Straneo, N. J. Wilson, J. M. Toole, R. A. Krishfield, N. L. Beaird, T. Kanzow, and J. Schaffer (2020), Ocean circulation and variability beneath Nioghalvfjerdsbræ (79 North Glacier) ice tongue, *Journal of Geophysical Research: Oceans*, *125*(8), e2020JC016,091, doi:10.1029/2020JC016091. 2.3.2

Liptak, J., and C. Strong (2014), The winter atmospheric response to sea ice anomalies in the barents sea, *Journal of Climate*, *27*(2), 914–924, doi:10.1175/JCLI-D-13-00186.1. 2.1.1, 3.1

Lique, C., and M. D. Thomas (2018), Latitudinal shift of the Atlantic Meridional Overturning Circulation source regions under a warming climate, *Nature Climate Change*, *8*(11), 1013–1020, doi:10.1038/s41558-018-0316-5. 2.3.3, 5.3

Locarnini, M., A. V. Mishonov, O. K. Baranova, T. P. Boyer, M. M. Zweng, H. E. Garcia, D. Seidov, K. Weathers, C. Paver, and I. Smolyar (2018), World ocean atlas 2018, volume 1: Temperature, *Mishonov Technical Ed.; NOAA Atlas NESDIS 81, 52 pp.* 3.2.3

Lozier, M. S. (2012), Overturning in the north atlantic, *Annual review of marine science*, *4*, 291–315, doi:10.1146/annurev-marine-120710-100740. 5.2

Lozier, M. S., F. Li, S. Bacon, F. Bahr, A. S. Bower, S. A. Cunningham, M. F. De Jong, L. De Steur, B. DeYoung, and J. Fischer (2019), A sea change in our view of overturning in the subpolar North Atlantic, *Science*, *363*(6426), 516–521. 2.3.3, 2.3.3, 5.2

Lubchenco, J. (1998), Entering the century of the environment: a new social contract for science, *Science*, *279*(5350), 491–497, doi:10.1126/science.279.5350.491. 1

Lundesgaard, A. Sundfjord, and A. H. H. Renner (2021), Drivers of Interannual Sea Ice Concentration Variability in the Atlantic Water Inflow Region North of Svalbard, *Journal of Geophysical Research: Oceans*, *126*(4), e2020JC016,522, doi:10.1029/2020JC016522. 2.3.1

MacKinnon, J. A., H. L. Simmons, J. Hargrove, J. Thomson, T. Peacock, M. H. Alford, B. I. Barton, S. Boury, S. D. Brenner, N. Couto, S. L. Danielson, E. C. Fine, H. C. Graber, J. Guthrie, J. E. Hopkins, S. R. Jayne, C. Jeon, T. Klenz, C. M. Lee, Y.-D. Lenn, A. J. Lucas, B. Lund, C. Mahaffey, L. Norman, L. Rainville, M. M. Smith, L. N. Thomas, S. Torres-Valdés, and K. R. Wood (2021), A warm jet in a cold ocean, *Nature Communications*, *12*(1), 2418, doi:10.1038/s41467-021-22505-5. 2.1.2, 2.1.3

Mann, M. E., B. A. Steinman, D. J. Brouillette, and S. K. Miller (2021), Multidecadal climate oscillations during the past millennium driven by volcanic forcing, *Science*, *371*(6533), 1014–1019, doi:10.1126/science.abc5810. 2.2.1, 2.2.1, 5.1

Marshall, J., and A. R. Plumb (2008), *Atmosphere, Ocean, and Climate Dynamics: An Introductory Text*, 117–120 pp., Elsevier Academic Press. 2.1.1

Marshall, J., K. C. Armour, J. R. Scott, Y. Kostov, U. Hausmann, D. Ferreira, T. G. Shepherd, and C. M. Bitz (2014), The ocean's role in polar climate change: asymmetric Arctic and Antarctic responses to greenhouse gas and ozone forcing, *Phil. Trans. R. Soc. A*, *372*, 20130,040, doi:10.1098/rsta.2013.0040. 3.2.2

Marshall, J., J. Scott, and A. Proshutinsky (2017), Climate Response Functions for the Arctic Ocean: a proposed coordinated modeling experiment, *Geoscientific Model Development Discussions*, (January), 1–25, doi:10.5194/gmd-2016-316. 3.2.2, 3.2.2, 5.2

Massonnet, F., T. Fichefet, H. Goosse, C. M. Bitz, G. Philippon-Berthier, M. M. Holland, and P.-Y. Barriat (2012), Constraining projections of summer Arctic sea ice, *The Cryosphere*, *6*(6), 1383–1394, doi:10.5194/tc-6-1383-2012. 2.1.1

Mauritzen, C. (1996), Production of dense overflow waters feeding the North Atlantic across the Greenland-Scotland Ridge. Part 1: Evidence for a revised circulation scheme, *Deep Sea Research Part I: Oceanographic Research Papers*, *43*(6), 769–806, doi:10.1016/0967-0637(96)00038-6. 2.2.2

McLaughlin, F., E. Carmack, R. Macdonald, H. Melling, J. Swift, P. Wheeler, B. Sherr, and E. Sherr (2004), The joint roles of Pacific and Atlantic-origin waters in the Canada Basin, 19971998, *Deep Sea Research Part I: Oceanographic Research Papers*, *51*(1), 107–128, doi:10.1016/j.dsr.2003.09.010. 2.1.3

Mclaughlin, F. A., E. C. Carmack, R. W. Macdonald, J. K. B. Bishop, and B. Samples (1996), Physical and geochemical properties across the Atlantic / Pacific the Canadian Ridge into the station between the Atlantic and is freshet in the Makarov Basin lies above Ridge and is marked, *Journal of Geophysical Research*, *101*, 1183–1197. 2.1.2

McWilliams, J. C. (1996), Modeling the oceanic general circulation, *Annual Review of Fluid Mechanics*, *28*(1), 215–248. 3.2

Meier, W. N., G. K. Hovelsrud, B. E. H. Van Oort, J. R. Key, K. M. Kovacs, C. Michel, C. Haas, M. A. Granskog, S. Gerland, and D. K. Perovich (2014), Arctic sea ice in transformation: A review of recent observed changes and impacts on biology and human activity, *Reviews of Geophysics*, *52*(3), 185–217, doi:10.1002/2013RG000431. 2.1.1

Meincke, J., S. Jónsson, and J. H. Swift (1992), Variability of convective conditions in the Greenland Sea, in *ICES Mar. Sci. Symp*, vol. 195, pp. 32–39. 2.3.3

Meincke, J., B. Rudels, and H. J. Friedrich (1997), The Arctic OceanNordic Seas thermohaline system, *ICES Journal of Marine Science*, *54*(3), 283–299. 2.1.3

Meneghello, G., J. Marshall, J.-M. Campin, E. Doddridge, and M.-L. Timmermans (2018), The Ice-Ocean governor: ice-ocean stress feedback limits Beaufort Gyre spin up, *Geophysical Research Letters*, pp. 293–299, doi:10.1029/2018GL080171. 3.2.2

Meneghello, G., J. Marshall, C. Lique, P. E. Isachsen, E. Doddridge, J.-M. Campin, H. Regan, and C. Talandier (2021), Genesis and decay of mesoscale baroclinic eddies in the seasonally ice-covered interior Arctic Ocean, *Journal of Physical Oceanography*, *51*(1), 115–129, doi:10.1175/JPO-D-20-0054.1. 2.1.2

Morison, J., R. Kwok, S. Dickinson, R. Andersen, C. Peralta-Ferriz, D. Morison, I. Rigor, S. Dewey, and J. Guthrie (2021), The Cyclonic Mode of Arctic Ocean Circulation, *Journal of Physical Oceanography*, *51*(4), 1053–1075, doi:10.1175/JPO-D-20-0190.1. 2.1.2, 2.1.2, 2.2.2

Mork, K. A., O. Skagseth, V. Ivshin, V. Ozhigin, S. L. Hughes, and H. Valdimarsson (2014), Advective and atmospheric forced changes in heat and fresh water content in the Norwegian Sea, 1951-2010, *Geophysical Research Letters*, *41*(17), 6221–6228, doi:10.1002/2014GL061038. 2.2.1, 2.3.3, 4, 5.1

Mork, K. A., Skagseth, and H. Søiland (2019), Recent warming and freshening of the Norwegian Sea observed by Argo data, *Journal of Climate*, *32*(12), 3695–3705, doi: 10.1175/JCLI-D-18-0591.1. 2.3.3

Morrison, A. L., J. E. Kay, H. Chepfer, R. Guzman, and V. Yettella (2018), Isolating the liquid cloud response to recent Arctic sea ice variability using spaceborne lidar observations, *Journal of Geophysical Research: Atmospheres*, *123*(1), 473–490, doi: 10.1002/2017JD027248. 2.3.1

MOSJ (2021), MOSJ Environmental monitoring of Svalbard and Jan Mayen: Temperature and Salinity in the Fram Strait, doi:https://www.mosj.no/en/climate/ocean/temperature-salinity-fram-strait.html. 2.2.1

Mouginot, J., E. Rignot, A. A. Bjørk, M. Van Den Broeke, R. Millan, M. Morlighem, B. Noël, B. Scheuchl, and M. Wood (2019), Forty-six years of Greenland Ice Sheet mass balance from 1972 to 2018, *Proceedings of the National Academy of Sciences*, *116*(19), 9239–9244, doi:https://doi.org/10.1073/pnas.1904242116. 2.3.2

Muilwijk, M. (2016), Bottom melting of Arctic Sea Ice in the Nansen Basin due to Atlantic Water influence [Master's Thesis]. 2.2.1, 2.3.1

Münchow, A., H. Melling, and K. K. Falkner (2006), An observational estimate of volume and freshwater flux leaving the Arctic Ocean through Nares Strait, *Journal of Physical Oceanography*, *36*(11), 2025–2041, doi:10.1175/JPO2962.1. 2.1.2

Najafi, M. R., F. W. Zwiers, and N. P. Gillett (2015), Attribution of Arctic temperature change to greenhouse-gas and aerosol influences, *Nature Climate Change*, *5*(3), 246–249, doi:10.1038/nclimate2524. 2.1.1

Nansen, F. (1902), *The oceanography of the north polar basin*, vol. 3, Longmans, Green, and Company. 2.1.3, 2.1.3, 3.1, 3.2.3

Nilsen, J. E. Y. Gao, H. Drange, T. Furevik, and M. Bentsen (2003), Simulated North AtlanticNordic Seas water mass exchanges in an isopycnic coordinate OGCM, *Geophysical Research Letters*, *30*(10), doi:10.1029/2002gl016597. 2.2.2

Nilsen, J. E. H. Hátún, K. A. Mork, and H. Valdimarsson (2008), The NISE dataset, *Technical Report. Torshavn, Faroe Islands.*, *117*. 3.2.3

Nøst, O. A., and P. E. Isachsen (2003), The large-scale time-mean ocean circulation in the Nordic Seas and Arctic Ocean estimated from simplified dynamics, *Journal of Marine Research*, *61*(2), 175–210, doi:10.1357/002224003322005069. 2.1.2, 2.8, 2.2.2

Notz, D. (2017), Arctic sea ice seasonal-to-decadal variability and long-term change, *Past Global Changes Magazine*, *25*(1), 14–19, doi:10.22498/pages.25.1.14. 2.3.1

Notz, D., and S. Community (2020), Arctic Sea Ice in CMIP6, *Geophysical Research Letters*, *47*(10), e2019GL086,749, doi:10.1029/2019GL086749. 2.1.1, 2.3.3, 3.1

Notz, D., and J. Marotzke (2012), Observations reveal external driver for Arctic sea-ice retreat, *Geophysical Research Letters*, *39*(8), doi:10.1029/2012GL051094. 2.3.1

Notz, D., and J. Stroeve (2016), Observed Arctic sea-ice loss directly follows anthropogenic CO 2 emission, *Science*, *354*(6313), 747–750, doi:10.1126/science.aag2345. 2.3.1

Nummelin, A., C. Li, and L. H. Smedsrud (2015), Response of Arctic Ocean stratification to changing river runoff in a column model, *Journal of Geophysical Research: Oceans*, *120*(4), 2655–2675, doi:10.1002/2014JC010571. 2.1.3

Nummelin, A., C. Li, and P. J. Hezel (2017), Connecting ocean heat transport changes from the midlatitudes to the Arctic Ocean, *Geophysical Research Letters*, *44*(4), 1899–1908, doi:10.1002/2016GL071333. 2.2.2, 5.2

Oldenburg, D., K. C. Armour, L. Thompson, and C. M. Bitz (2018), Distinct mechanisms of ocean heat transport into the Arctic under internal variability and climate change, *Geophysical Research Letters*, *45*(15), 7692–7700, doi:10.1029/2018GL078719. 2.2.2

Olonscheck, D., T. Mauritsen, and D. Notz (2019), Arctic sea-ice variability is primarily driven by atmospheric temperature fluctuations, *Nature Geoscience*, doi:10.1038/s41561-019-0363-1. 2.3.1

OMG Mission (2020), Conductivity, Temperature and Depth (CTD) data from the ocean survey. Ver. 0.1., *OMG SDS, CA, USA. Dataset accessed [2020-01-02]*, doi:https://dx.doi.org/10.5067/OMGEV-AXCTD. 3.2.4

Onarheim, I. H., and M. Årthun (2017), Toward an ice-free Barents Sea, *Geophysical Research Letters*, *44*(16), doi:10.1002/2017GL074304. 2.3.1

Onarheim, I. H., L. H. Smedsrud, R. B. Ingvaldsen, and F. Nilsen (2014), Loss of sea ice during winter north of Svalbard, *Tellus A*, *66*(1), 23,933, doi:10.3402/tellusa.v66.23933. 2.3.1

Onarheim, I. H., T. Eldevik, M. Årthun, R. B. Ingvaldsen, and L. H. Smedsrud (2015), Skillful prediction of Barents Sea ice cover, *Geophysical Research Letters*, *42*(13), 5364–5371, doi:10.1002/2015GL064359. 2.3.1, 5.2

Onarheim, I. H., T. Eldevik, L. H. Smedsrud, and J. C. Stroeve (2018), Seasonal and regional manifestation of Arctic sea ice loss, *Journal of Climate*, *31*(12), 4917–4932, doi:10.1175/JCLI-D-17-0427.1. 2.3.1, 2.3.1

Orvik, K. A., and P. Niiler (2002), Major pathways of Atlantic water in the northern North Atlantic and Nordic Seas toward Arctic, *Geophysical Research Letters*, *29*(19), 2–1, doi:10.1029/2002GL015002. 2.1.2

Orvik, K. A., O. Skagseth, and M. Mork (2001), Atlantic inflow to the Nordic Seas: Current structure and volume fluxes from moored current meters, VM-ADCP and SeaSoar-CTD observations, 1995-1999, *Deep-Sea Research Part I: Oceanographic Research Papers*, *48*(4), 937–957, doi:10.1016/S0967-0637(00)00038-8. 2.2.1

Østerhus, S., R. Woodgate, H. Valdimarsson, B. Turrell, L. d. Steur, D. Quadfasel, S. M. Olsen, M. Moritz, C. M. Lee, and K. M. H. Larsen (2019), Arctic Mediterranean exchanges: a consistent volume budget and trends in transports from two decades of observations, *Ocean Science*, *15*(2), 379–399, doi:10.5194/os-15-379-2019. 2.1.2

Otterå, O. H., M. Bentsen, H. Drange, and L. Suo (2010), External forcing as a metronome for Atlantic multidecadal variability, *Nature Geoscience*, *3*(10), 688–694, doi:10.1038/ngeo955. 2.2.1, 2.2.1, 5.1

Overland, J. E., and M. Wang (2010), Large-scale atmospheric circulation changes are associated with the recent loss of Arctic sea ice, *Tellus A: Dynamic Meteorology and Oceanography*, *62*(1), 1–9, doi:10.1111/j.1600-0870.2009.00421.x. 2.1.1, 3.1

Padman, L., and T. M. Dillon (1987), Vertical heat fluxes through the Beaufort Sea thermohaline staircase, *Journal of Geophysical Research*, *92*(C10), 10,799, doi:10.1029/JC092iC10p10799. 2.3.1

PérezHernández, M. D., R. S. Pickart, D. J. Torres, F. Bahr, A. Sundfjord, R. Ingvaldsen, A. H. H. Renner, A. BeszczynskaMöller, W. Appen, and V. Pavlov (2019), Structure, Transport, and Seasonality of the Atlantic Water Boundary Current North of Svalbard: Results From a Yearlong Mooring Array, *Journal of Geophysical Research: Oceans*, *124*(3), 1679–1698, doi:10.1029/2018JC014759. 2.3.3, 5.3

Peterson, A. K., I. Fer, M. G. McPhee, and A. Randelhoff (2017), Turbulent heat and momentum fluxes in the upper ocean under Arctic sea ice, *Journal of Geophysical Research: Oceans*, *122*(2), 1439–1456, doi:10.1002/2016JC012283. 2.3.1

Pistone, K., I. Eisenman, and V. Ramanathan (2019), Radiative Heating of an IceFree Arctic Ocean, *Geophysical Research Letters*, *46*(13), 7474–7480, doi:10.1029/2019GL082914. 2.1.1, 2.1.1, 2.3.1

Polyak, L., R. B. Alley, J. T. Andrews, J. Brigham-Grette, T. M. Cronin, D. A. Darby, A. S. Dyke, J. J. Fitzpatrick, S. Funder, and M. Holland (2010), History of sea ice in the Arctic, *Quaternary Science Reviews*, *29*(15-16), 1757–1778, doi:10.1016/j.quascirev.2010.02.010. 2.1.1

Polyakov, I. V. (2005), One more step toward a warmer Arctic, *Geophysical Research Letters*, *32*(17), L17,605, doi:10.1029/2005GL023740. 2.1.2, 2.2.1

Polyakov, I. V., G. V. Alekseev, R. V. Bekryaev, U. S. Bhatt, R. Colony, M. A. Johnson, V. P. Karklin, D. Walsh, and A. V. Yulin (2003), Long-term ice variability in Arctic marginal seas, *Journal of Climate*, *16*(12), 2078–2085, doi:10.1175/1520-0442(2003)016<2078:LIVIAM>2.0.CO;2. 3.2.3

Polyakov, I. V., G. V. Alekseev, L. a. Timokhov, U. S. Bhatt, R. L. Colony, H. L. Simmons, D. Walsh, J. E. Walsh, and V. F. Zakharov (2004), Variability of the Intermediate Atlantic Water of the Arctic Ocean over the Last 100 Years, *Journal of Climate*, *17*(23), 4485–4497, doi:10.1175/JCLI-3224.1. 2.2.1, 3.2.3, 3.2.3

Polyakov, I. V., V. A. Alexeev, G. I. Belchansky, I. A. Dmitrenko, V. V. Ivanov, S. A. Kirillov, A. A. Korablev, M. Steele, L. A. Timokhov, and I. Yashayaev (2008), Arctic Ocean freshwater changes over the past 100 years and their causes, *Journal of Climate*, *21*(2), 364–384, doi:10.1175/2007JCLI1748.1. 3.2.3

Polyakov, I. V., V. a. Alexeev, U. S. Bhatt, E. I. Polyakova, and X. Zhang (2009), North Atlantic warming: patterns of long-term trend and multidecadal variability, *Climate Dynamics*, *34*(2-3), 439–457, doi:10.1007/s00382-008-0522-3. 2.2.1

Polyakov, I. V., L. a. Timokhov, V. a. Alexeev, S. Bacon, I. a. Dmitrenko, L. Fortier, I. E. Frolov, J.-C. Gascard, E. Hansen, V. V. Ivanov, S. Laxon, C. Mauritzen, D. Perovich, K. Shimada, H. L. Simmons, V. T. Sokolov, M. Steele, and J. Toole (2010), Arctic Ocean Warming Contributes to Reduced Polar Ice Cap, *Journal of Physical Oceanography*, *40*(12), 2743–2756, doi:10.1175/2010JPO4339.1. 2.1.1, 2.2.1

Polyakov, I. V., A. V. Pnyushkov, and L. a. Timokhov (2012), Warming of the Intermediate Atlantic Water of the Arctic Ocean in the 2000s, *Journal of Climate*, *25*(23), 8362–8370, doi:10.1175/JCLI-D-12-00266.1. 2.2.1

Polyakov, I. V., A. V. Pnyushkov, R. Rember, L. Padman, E. C. Carmack, and J. M. Jackson (2013), Winter Convection Transports Atlantic Water Heat to the Surface Layer in the Eastern Arctic Ocean, *Journal of Physical Oceanography*, *43*(10), 2142–2155, doi:10.1175/JPO-D-12-0169.1. 3.2.3

Polyakov, I. V., A. V. Pnyushkov, M. B. Alkire, I. M. Ashik, T. M. Baumann, E. C. Carmack, I. Goszczko, J. Guthrie, V. V. Ivanov, T. Kanzow, R. Krishfield, R. Kwok, A. Sundfjord, J. Morison, R. Rember, and A. Yulin (2017), Greater role for Atlantic inflows on sea-ice loss in the Eurasian Basin of the Arctic Ocean, *Science*, *291*(April), 285–291, doi:10.1126/science.aai8204. 2.2.1, 2.6, 2.3.1

Polyakov, I. V., A. V. Pnyushkov, and E. C. Carmack (2018), Stability of the arctic halocline: A new indicator of arctic climate change, *Environmental Research Letters*, *13*(12), doi:10.1088/1748-9326/aaec1e. 3.2.3

Polyakov, I. V., M. B. Alkire, B. A. Bluhm, K. A. Brown, E. C. Carmack, M. Chierici, S. L. Danielson, I. Ellingsen, E. A. Ershova, K. Gårdfeldt, R. B. Ingvaldsen, A. V. Pnyushkov, D. Slagstad, and P. Wassmann (2020), Borealization of the Arctic Ocean in Response to Anomalous Advection From Sub-Arctic Seas, *Frontiers in Marine Science*, *7*, doi:10.3389/fmars.2020.00491. 2.1.1, 2.1.3, 2.2.1, 2.2.1, 3.2.3

Proshutinsky, A., Y. Aksenov, J. C. Kinney, R. Gerdes, E. Golubeva, D. Holland, G. Holloway, A. Jahn, M. Johnson, and E. Popova (2011), Recent advances in Arctic ocean studies employing models from the Arctic Ocean Model Intercomparison Project, *Oceanography*, *24*(3), 102–113, doi:10.5670/oceanog.2011.61. 3.2.1

Proshutinsky, A., M. Steele, and M. Timmermans (2016), Forum for Arctic Modeling and Observational Synthesis (FAMOS): Past, current, and future activities, *Journal of Geophysical Research: Oceans*, *121*(6), 3803–3819, doi:10.1002/2016JC011898. 3.2.1

Proshutinsky, A., R. Krishfield, J. M. Toole, M. Timmermans, W. Williams, S. Zimmermann, M. YamamotoKawai, T. W. K. Armitage, D. Dukhovskoy, and E. Golubeva (2019), Analysis of the Beaufort Gyre freshwater content in 20032018, *Journal of Geophysical Research: Oceans*, *124*(12), 9658–9689, doi:10.1029/2019JC015281. 2.1.3

Proshutinsky, A. Y., and M. A. Johnson (1997), Two circulation regimes of the wind-driven Arctic Ocean, *Journal of Geophysical Research: Oceans*, *102*(C6), 12,493–12,514, doi:10.1029/97JC00738. 3.2.2

Provost, C., N. Sennéchael, J. Miguet, P. Itkin, A. Rösel, Z. Koenig, N. VillacierosRobineau, and M. A. Granskog (2017), Observations of flooding and snowice formation in a thinner Arctic seaice regime during the NICE2015 campaign: Influence of basal ice melt and storms, *Journal of Geophysical Research: Oceans*, *122*(9), 7115–7134, doi:10.1002/2016JC012011. 2.3.1

Rabe, B., M. Karcher, F. Kauker, U. Schauer, J. M. Toole, R. A. Krishfield, S. Pisarev, T. Kikuchi, and J. Su (2014), Arctic Ocean basin liquid freshwater storage trend 19922012, *Geophysical Research Letters*, *41*(3), 961–968, doi:10.1002/2013GL058121. 2.1.3

Reigstad, M., P. Wassmann, C. W. Riser, S. Øygarden, and F. Rey (2002), Variations in hydrography, nutrients and chlorophyll a in the marginal ice-zone and the central Barents Sea, *Journal of Marine Systems*, *38*(1-2), 9–29, doi:10.1016/S0924-7963(02)00167-7. 2.2.1

Renner, A. H. H., S. Gerland, C. Haas, G. Spreen, J. F. Beckers, E. Hansen, M. Nicolaus, and H. Goodwin (2014), Evidence of Arctic sea ice thinning from direct observations, *Geophysical Research Letters*, *41*(14), doi:10.1002/2014GL060369. 2.3.1

Rignot, E., I. Fenty, D. Menemenlis, and Y. Xu (2012), Spreading of warm ocean waters around Greenland as a possible cause for glacier acceleration, *Annals of Glaciology*, *53*(60), 257–266, doi:doi:10.3189/2012AoG60A136. 2.3.2

Rudels, B. (1987), *On the mass balance of the Polar Ocean, with special emphasis on the Fram Strait*, 188, 53 pp. 2.1.2

Rudels, B. (2015), Arctic Ocean circulation, processes and water masses: A description of observations and ideas with focus on the period prior to the International Polar Year 20072009, *Progress in Oceanography*, *132*, 22–67, doi:10.1016/j.pocean.2013.11.006. 2.1.1, 2.1.2, 2.1.2, 2.1.3, 2.4, 2.1.3, 2.3.3

Rudels, B. (2016), Arctic Ocean stability: The effects of local cooling, oceanic heat transport, freshwater input, and sea ice melt with special emphasis on the Nansen Basin, *Journal of Geophysical Research: Oceans*, *121*(7), 4450–4473, doi:10.1002/2015JC011045. 2.3.1

Rudels, B., E. P. Jones, L. G. Anderson, and G. Kattner (1994), On the intermediate depth waters of the Arctic Ocean, *The polar oceans and their role in shaping the global environment*, *85*, 33–46, doi:10.1029/gm085p0033. 2.1.2

Rudels, B., R. Meyer, E. Fahrbach, V. V. Ivanov, S. Østerhus, D. Quadfasel, U. Schauer, V. Tverberg, and R. A. Woodgate (2000), Water mass distribution in Fram Strait and over the Yermak Plateau in summer 1997, *Annales Geophysicae*, *18*(6), 687–705, doi:10.1007/s00585-000-0687-5. 2.2.1

Sandø, A., Y. Gao, and H. R. Langehaug (2014), Poleward ocean heat transport, sea ice processes, and Arctic sea ice variability in NorESM1-M simulations, *Journal of Geophysical Research: Oceans*, *119*(3), 2095–2108, doi:10.1002/2013JC009435. 2.3.1, 2.3.1

Sayedi, S. S., B. W. Abbott, B. F. Thornton, J. M. Frederick, J. E. Vonk, P. Overduin, C. Schädel, E. A. G. Schuur, A. Bourbonnais, and N. Demidov (2020), Subsea permafrost carbon stocks and climate change sensitivity estimated by expert assessment, *Environmental Research Letters*, *15*(12), 124,075. 2.1.1

Schaffer, J., T. Kanzow, W.-J. von Appen, L. von Albedyll, J. E. Arndt, and D. H. Roberts (2020), Bathymetry constrains ocean heat supply to Greenlands largest glacier tongue, *Nature Geoscience*, *13*(3), 227–231, doi:10.1038/s41561-019-0529-x. 2.3.2

Schauer, U. (1997), Impact of eastern Arctic shelf waters on the Nansen Basin intermediate layers, *Journal of Geophysical Research C: Oceans*, *102*(C2), 3371–3382, doi:10.1029/96JC03366. 2.2.1, 2.3.3

Schauer, U. (2004), Arctic warming through the Fram Strait: Oceanic heat transport from 3 years of measurements, *Journal of Geophysical Research*, *109*, doi:10.1029/2003JC001823. 2.1.2

Schauer, U., and A. Beszczynska-Möller (2009), Problems with estimation and interpretation of oceanic heat transport-conceptual remarks for the case of Fram Strait in the Arctic Ocean, *Ocean Science*, *5*(4), 487–494, doi:10.5194/os-5-487-2009. 2.1.2, 5.1

Schauer, U., H. Loeng, B. Rudels, V. K. Ozhigin, and W. Dieck (2002), Atlantic Water flow through the Barents and Kara Seas, *Deep Sea Research Part I: Oceanographic Research Papers*, *49*(12), 2281–2298, doi:10.1016/S0967-0637(02)00125-5. 2.1.2, 2.1.3, 2.2.1

Schmidtko, S., G. C. Johnson, and J. M. Lyman (2013), MIMOC: A global monthly isopycnal upper-ocean climatology with mixed layers, *Journal of Geophysical Research: Oceans*, *118*(4), doi:10.1002/jgrc.20122. 2.4, 3.2.3

Schuur, E. A. G., A. D. McGuire, C. Schädel, G. Grosse, J. W. Harden, D. J. Hayes, G. Hugelius, C. D. Koven, P. Kuhry, and D. M. Lawrence (2015), Climate change and the permafrost carbon feedback, *Nature*, *520*(7546), 171–179. 2.1.1

Screen, J. A. (2017), Simulated atmospheric response to regional and pan-Arctic sea ice loss, *Journal of Climate*, *30*(11), 3945–3962, doi:10.1175/JCLI-D-16-0197.1. 2.1.1, 3.1

Seale, A., P. Christoffersen, R. I. Mugford, and M. O'Leary (2011), Ocean forcing of the Greenland Ice Sheet: Calving fronts and patterns of retreat identified by automatic satellite monitoring of eastern outlet glaciers, *Journal of Geophysical Research: Earth Surface*, *116*(F3), doi:10.1029/2010JF001847. 2.3.2

Seland, M. Bentsen, L. Seland Graff, D. Olivié, T. Toniazzo, A. Gjermundsen, J. B. Debernard, A. K. Gupta, Y. He, A. Kirkevåg, J. Schwinger, J. Tjiputra, K. Schancke Aas, I. Bethke, Y. Fan, J. Griesfeller, A. Grini, C. Guo, M. Ilicak, I. H. Hafsahl Karset, O. Landgren, J. Liakka, K. Onsum Moseid, A. Nummelin, C. Spensberger, H. Tang, Z. Zhang, C. Heinze, T. Iverson, and M. Schulz (2020), The Norwegian Earth System Model, NorESM2 Evaluation of theCMIP6 DECK and historical simulations, *Geoscientific Model Development Discussions*, (February), 1–68, doi:10.5194/gmd-2019-378. 3.2.1

Semper, S., R. S. Pickart, K. Våge, K. M. H. Larsen, H. Hátún, and B. Hansen (2020), The Iceland-Faroe Slope Jet: a conduit for dense water toward the Faroe Bank Channel overflow, *Nature communications*, *11*(1), 1–10, doi:10.1038/s41467-020-19049-5. 2.1.3

Serreze, M. C., M. M. Holland, and J. Stroeve (2007), Perspectives on the Arctic's shrinking sea-ice cover., *Science*, *315*(5818), 1533–1536, doi:10.1126/science.1139426. 2.1.1, 3.1

Sévellec, F., A. V. Fedorov, and W. Liu (2017), Arctic sea-ice decline weakens the Atlantic meridional overturning circulation, *Nature Climate Change*, *7*(8), 604–610, doi:10.1038/NCLIMATE3353. 2.1.1, 3.1

Shepherd, A., E. Ivins, E. Rignot, B. Smith, M. van den Broeke, I. Velicogna, P. Whitehouse, K. Briggs, I. Joughin, and G. Krinner (2020), Mass balance of the Greenland Ice Sheet from 1992 to 2018, *Nature*, *579*(7798), 233–239, doi:https://doi.org/10.1038/s41586-019-1855-2. 2.3.2, 2.3.2

Shu, Q., Q. Wang, J. Su, X. Li, and F. Qiao (2019), Assessment of the Atlantic water layer in the Arctic Ocean in CMIP5 climate models, *Climate Dynamics*, *53*(9), 5279–5291, doi:10.1007/s00382-019-04870-6. 2.1.1

Shu, Q., Q. Wang, Z. Song, F. Qiao, J. Zhao, M. Chu, and X. Li (2020), Assessment of sea ice extent in CMIP6 with comparison to observations and CMIP5, *Geophysical Research Letters*, *47*(9), e2020GL087,965, doi:10.1029/2020GL087965. 2.1.1

Skagseth, T. Eldevik, M. Årthun, H. Asbjørnsen, V. S. Lien, and L. H. Smedsrud (2020), Reduced efficiency of the Barents Sea cooling machine, *Nature Climate Change*, *10*(7), 661–666, doi:10.1038/s41558-020-0772-6. 2.2.1, 5.1, 5.3

Slater, D. A., F. Straneo, D. Felikson, C. M. Little, H. Goelzer, X. Fettweis, and J. Holte (2019), Estimating Greenland tidewater glacier retreat driven by submarine melting, *Cryosphere*, *13*(9), 2489–2509, doi:10.5194/tc-13-2489-2019. 2.3.2, 2.11

Smedsrud, L. H., I. Esau, R. B. Ingvaldsen, T. Eldevik, P. M. Haugan, C. Li, V. S. Lien, A. Olsen, A. M. Omar, B. Risebrobakken, A. B. Sandø, V. A. Semenov, and S. A. Sorokina (2013), The role of the Barents Sea in the Arctic climate system, *Reviews of Geophysics*, *51*(3), 415–449, doi:10.1002/rog.20017. 2.1.2

Smedsrud, L. H., M. H. Halvorsen, J. C. Stroeve, R. Zhang, and K. Kloster (2017), Fram Strait sea ice export variability and September Arctic sea ice extent over the last 80 years, *Cryosphere*, *11*(1), 65–79, doi:10.5194/tc-11-65-2017. 2.1.2, 5.2

Smedsrud, L. H., A. Brakstad, E. Madonna, M. Muilwijk, S. K. Lauvset, C. Spensberger, A. Born, T. Eldevik, H. Drange, and E. Jeansson (2021), Nordic Seas Heat Loss, Atlantic Inflow, and Arctic Sea Ice cover over the last century, *Earth and Space Science Open Archive ESSOAr*, doi:10.1002/essoar.10506171.1. 2.1.2, 2.1.3, 2.2.1, 2.2.1, 2.2.2, 2.2.2, 2.2.2, 2.3.2, 2.11, 2.3.3, 2.12, 2.3.3, 3.2.3, 5.1, 5.2

Solomon, A., C. Heuzé, B. Rabe, S. Bacon, L. Bertino, P. Heimbach, J. Inoue, D. Iovino, R. Mottram, and X. Zhang (2020), Freshwater in the Arctic Ocean 20102019, *Ocean Science Discussions*, pp. 1–28, doi:10.5194/os-2020-113. 2.1.1, 2.1.3

Sorokina, S. A., C. Li, J. J. Wettstein, and N. G. Kvamstø (2016), Observed atmospheric coupling between Barents Sea ice and the warm-Arctic cold-Siberian anomaly pattern, *Journal of Climate*, *29*(2), 495–511, doi:10.1175/JCLI-D-15-0046.1. 2.1.1, 3.1

Spall, M. a. (2013), On the Circulation of Atlantic Water in the Arctic Ocean, *Journal of Physical Oceanography*, *43*(11), 2352–2371, doi:10.1175/JPO-D-13-079.1. 2.2.2

Steele, M. (2004), Circulation of summer Pacific halocline water in the Arctic Ocean, *Journal of Geophysical Research*, *109*(C2), doi:10.1029/2003JC002009. 2.1.3

Steele, M., and T. Boyd (1998), Retreat of the cold halocline layer in the Arctic Ocean, *Journal of Geophysical Research: Oceans*, *103*, 10,419–10,435, doi:10.1029/98JC00580. 2.1.3

Steele, M., G. L. Mellor, and M. G. Mcphee (1989), Role of the Molecular Sublayer in the Melting or Freezing of Sea Ice, *Journal of Physical Oceanography*, *19*(1), 139–147, doi:10.1175/1520-0485(1989)019<0139:rotmsi>2.0.co;2. 2.1.3

Steele, M., R. Morley, and W. Ermold (2001), PHC3 Updated from: A global ocean hydrography with a high quality Arctic Ocean, *Journal of Climate*, *14*(9), 2079–2087, doi:10.1175/1520-0442(2001)014<2079:PAGOHW>2.0.CO;2. 3.2.3

Stocker, A. N., A. H. H. Renner, and M. Knol-Kauffman (2020), Sea ice variability and maritime activity around Svalbard in the period 20122019, *Scientific reports*, *10*(1), 1–12, doi:10.1038/s41598-020-74064-2. 2.1.1

Straneo, F., and C. Cenedese (2015), The Dynamics of Greenland s Glacial Fjords and Their Role in Climate, doi:10.1146/annurev-marine-010213-135133. 2.3.2

Straneo, F., R. G. Curry, D. a. Sutherland, G. S. Hamilton, C. Cenedese, K. Våge, and L. a. Stearns (2011), Impact of fjord dynamics and glacial runoff on the circulation near Helheim Glacier, *Nature Geoscience*, *4*(5), 322–327, doi:10.1038/ngeo1109. 5.4

Straneo, F., D. A. Sutherland, D. Holland, C. Gladish, G. S. Hamilton, H. L. Johnson, E. Rignot, Y. Xu, and M. Koppes (2012), Characteristics of ocean waters reaching greenland's glaciers, *Annals of Glaciology*, *53*(60), 202–210, doi:10.3189/2012AoG60A059. 2.3.2, 5.4

Straneo, F., P. Heimbach, O. Sergienko, G. Hamilton, G. Catania, S. Griffies, R. Hallberg, A. Jenkins, I. Joughin, R. Motyka, W. T. Pfeffer, S. F. Price, E. Rignot, T. Scambos, M. Truffer, and A. Vieli (2013), Challenges to understanding the dynamic response of Greenland's marine terminating glaciers to oc eanic and atmospheric forcing, *Bulletin of the American Meteorological Society*, *94*(8), 1131–1144, doi:10.1175/BAMS-D-12-00100.1. 2.3.2, 2.11

Stroeve, J., and D. Notz (2018), Changing state of Arctic sea ice across all seasons, *Environmental Research Letters*, *13*(10), 103,001, doi:10.1088/1748-9326/aade56. 2.3.1

Sutherland, D. A., F. Straneo, and R. S. Pickart (2014), Characteristics and dynamics of two major Greenland glacial fjords, *Journal of Geophysical Research: Oceans*, *119*(6), 3767–3791, doi:https://doi.org/10.1002/2013JC009786. 5.4

Sutton, R. T., and M. R. Allen (1997), Decadal predictability of North Atlantic sea surface temperature and climate, *Nature*, *388*(6642), 563–567, doi:10.1038/41523. 2.2.1

Sutton, R. T., and D. L. R. Hodson (2005), Atlantic Ocean Forcing of North American and European Summer Climate, *Science*, *309*(5731), 115–118, doi:10.1126/science.1109496. 2.2.1

Svendsen, L., N. Keenlyside, I. Bethke, Y. Gao, and N.-E. Omrani (2018), Pacific contribution to the early twentieth-century warming in the Arctic, *Nature Climate Change*, *8*(9), 793–797, doi:10.1038/s41558-018-0247-1. 2.2.1, 2.2.1

Svendsen, L., N. Keenlyside, M. Muilwijk, I. Bethke, N. Omrani, and Y. Gao (2021), Pacific contribution to decadal surface temperaturetrends in the Arctic during the twentieth century, *In review at Climate Dynamics*. 2.2.1

Sverdrup, H. U., M. W. Johnson, and R. H. Fleming (1942), *The Oceans: Their physics, chemistry, and general biology*, vol. 1087, Prentice-Hall New York. 2.1.1

Swart, N. C., J. C. Fyfe, E. Hawkins, J. E. Kay, and A. Jahn (2015), Influence of internal variability on Arctic sea-ice trends, *Nature Climate Change*, *5*(2), 86–89, doi:10.1038/nclimate2483. 2.1.1

Swift, J. H., and K. Aagaard (1981), Seasonal transitions and water mass formation in the Iceland and Greenland seas, *Deep Sea Research Part A. Oceanographic Research Papers*, *28*(10), 1107–1129, doi:10.1016/0198-0149(81)90050-9. 2.1.3

Swingedouw, D., C. B. Rodehacke, E. Behrens, M. Menary, S. M. Olsen, Y. Gao, U. Mikolajewicz, J. Mignot, and A. Biastoch (2013), Decadal fingerprints of freshwater discharge around Greenland in a multi-model ensemble, *Climate Dynamics*, *41*(3-4), 695–720, doi:10.1007/s00382-012-1479-9. 5.2

Terhaar, J., L. Kwiatkowski, and L. Bopp (2020), Emergent constraint on Arctic Ocean acidification in the twenty-first century, *Nature*, *582*(7812), 379–383, doi:10.1038/s41586-020-2360-3. 2.1.1

Thomas, D. N., and G. S. Diekmann (2003), *Sea Ice, An introduction to its Physics, Chemestry, biology and Geology*, Blackwell. 2.1.1

Timmermans, M. L., and J. Marshall (2020), Understanding Arctic Ocean Circulation: A Review of Ocean Dynamics in a Changing Climate, *Journal of Geophysical Research: Oceans*, *125*(4), 1–70, doi:10.1029/2018JC014378. 2.1.2, 2.3, 2.1.3, 2.1.3, 2.2.2, 2.2.2, 2.8, 2.2.2, 5.2

Timmermans, M.-L., J. Toole, and R. Krishfield (2018), Warming of the interior Arctic Ocean linked to sea ice losses at the basin margins, *Science advances*, *4*(8), eaat6773, doi:10.1126/sciadv.aat6773. 2.1.1

Treshnikov, A. F. (1985), Arctic atlas, *Head Administration of Geodesy and Cartography of the Soviet Ministry, Moscow*, p. 204. 3.2.3

Tsubouchi, T., K. Våge, B. Hansen, K. M. H. Larsen, S. Østerhus, C. Johnson, S. Jónsson, and H. Valdimarsson (2021), Increased ocean heat transport into the Nordic Seas and Arctic Ocean over the period 19932016, *Nature Climate Change*, *11*(1), 21–26, doi:10.1038/s41558-020-00941-3. 2.1.2, 2.2.1

Tsujino, H., S. Urakawa, H. Nakano, R. J. Small, W. M. Kim, S. G. Yeager, G. Danabasoglu, T. Suzuki, J. L. Bamber, and M. Bentsen (2018), JRA-55 based surface dataset for driving oceansea-ice models (JRA55-do), *Ocean Modelling*, *130*, 79–139, doi:10.1016/j.ocemod.2018.07.002. 3.2.1

Tsujino, H., L. S. Urakawa, S. M. Griffies, G. Danabasoglu, A. J. Adcroft, A. E. Amaral, T. Arsouze, M. Bentsen, R. Bernardello, and C. W. Böning (2020), Evaluation of global oceansea-ice model simulations based on the experimental protocols of the Ocean Model Intercomparison Project phase 2 (OMIP-2), *Geoscientific Model Development*, *13*(8), 3643–3708, doi:10.5194/gmd-13-4595-2020. 3.2

Umlauf, L., and H. Burchard (2005), Second-order turbulence closure models for geophysical boundary layers. A review of recent work, *Continental Shelf Research*, *25*(7-8), 795–827, doi:10.1016/j.csr.2006.02.008. 3.2.1

Våge, K., G. W. K. Moore, S. Jónsson, and H. Valdimarsson (2015), Water mass transformation in the Iceland Sea, *Deep Sea Research Part I: Oceanographic Research Papers*, *101*, 98–109, doi:10.1016/j.dsr.2015.04.001. 2.3.3

Våge, K., L. Papritz, L. Håvik, M. A. Spall, and G. W. K. Moore (2018), Ocean convection linked to the recent ice edge retreat along east Greenland, *Nature communications*, *9*(1), 1–8. 2.3.3

van der Linden, E. C., D. Le Bars, R. Bintanja, and W. Hazeleger (2019), Oceanic heat transport into the Arctic under high and low CO2 forcing, *Climate Dynamics*, *53*(7), 4763–4780, doi:10.1007/s00382-019-04824-y. 2.2.1

Visbeck, M., J. Fischer, and F. Schott (1995), Preconditioning the Greenland Sea for deep convection: Ice formation and ice drift, *Journal of Geophysical Research: Oceans*, *100*(C9), 18,489–18,502, doi:10.1029/95jc01611. 2.3.3

Walsh, J. E., F. Fetterer, J. Scott Stewart, and W. L. Chapman (2017), A database for depicting Arctic sea ice variations back to 1850, *Geographical Review*, *107*(1), 89–107, doi:10.1111/j.1931-0846.2016.12195.x. 2.2

Wang, Q., M. Ilicak, R. Gerdes, H. Drange, Y. Aksenov, D. A. Bailey, M. Bentsen, A. Biastoch, A. Bozec, C. Böning, C. Cassou, E. Chassignet, A. C. Coward, B. Curry, G. Danabasoglu, S. Danilov, E. Fernandez, P. G. Fogli, Y. Fujii, S. M. Griffies, D. Iovino, A. Jahn, T. Jung, W. G. Large, C. Lee, C. Lique, J. Lu, S. Masina, A. J. G. Nurser, B. Rabe, C. Roth, D. Salas y Mélia, B. L. Samuels, P. Spence, H. Tsujino, S. Valcke, A. Voldoire, X. Wang, and S. G. Yeager (2016a), An assessment of the Arctic Ocean in a suite of interannual CORE-II simulations. Part II: Liquid freshwater, *Ocean Modelling*, *99*, 86–109, doi:10.1016/j.ocemod.2015.12.009. 2.1.1

Wang, Q., M. Ilicak, R. Gerdes, H. Drange, Y. Aksenov, D. A. Bailey, M. Bentsen, A. Biastoch, A. Bozec, C. Böning, C. Cassou, E. Chassignet, A. C. Coward, B. Curry, G. Danabasoglu, S. Danilov, E. Fernandez, P. G. Fogli, Y. Fujii, S. M. Griffies, D. Iovino, A. Jahn, T. Jung, W. G. Large, C. Lee, C. Lique, J. Lu, S. Masina, A. J. G. Nurser, B. Rabe, C. Roth, D. Salas y Mélia, B. L. Samuels, P. Spence, H. Tsujino, S. Valcke, A. Voldoire, X. Wang, and S. G. Yeager (2016b), An assessment of the Arctic Ocean in a suite of interannual CORE-II simulations. Part II: Liquid freshwater, *Ocean Modelling*, *99*, 86–109, doi:10.1016/j.ocemod.2015.12.009. 3.2

Wang, S., Q. Wang, M. Wang, G. Lohmann, and F. Qiao (2021), Arctic Ocean liquid freshwater in CMIP6 coupled models, *Earth and Space Science Open Archive ESSOAr*, doi:10.1002/essoar.10505861.1. 2.1.3

Wassmann, P., E. Bauerfeind, M. Fortier, M. Fukuchi, B. Hargrave, B. Moran, T. Noji, E.-M. Nöthig, K. Olli, and R. Peinert (2004), Particulate organic carbon flux to the Arctic Ocean sea floor, in *The organic carbon cycle in the Arctic Ocean*, pp. 101–138, Springer, doi:10.1007/978-3-642-18912-8{_}5. 2.2.1

Wassmann, P., C. M. Duarte, S. Agusti, and M. K. Sejr (2011), Footprints of climate change in the Arctic marine ecosystem, *Global change biology*, *17*(2), 1235–1249, doi:10.1111/j.1365-2486.2010.02311.x. 2.1.1, 3.1

Wei, T., Q. Yan, W. Qi, M. Ding, and C. Wang (2020), Projections of Arctic sea ice conditions and shipping routes in the twenty-first century using CMIP6 forcing scenarios, *Environmental Research Letters*, *15*(10), 104,079, doi:10.1088/1748-9326/abb2c8. 2.1.1

Weller, R. A., D. J. Baker, M. M. Glackin, S. J. Roberts, R. W. Schmitt, E. S. Twigg, and D. J. Vimont (2019), The challenge of sustaining ocean observations, *Frontiers in Marine Science*, *6*, 105, doi:10.3389/fmars.2019.00105. 3.2

Wilson, N. J., and F. Straneo (2015), Water exchange between the continental shelf and the cavity beneath Nioghalvfjerdsbræ (79 North Glacier), *Geophysical Research Letters*, *42*(18), 7648–7654, doi:10.1002/2015GL064944. 2.3.2

Winton, M. (2008), Sea ice-albedo feedback and nonlinear Arctic climate change, *Arctic sea ice decline: Observations, projections, mechanisms, and implications, Geophys. Monogr*, *180*, 111–131. 5

Wood, M., E. Rignot, I. Fenty, D. Menemenlis, R. Millan, M. Morlighem, J. Mouginot, and H. Seroussi (2018), Oceaninduced melt triggers glacier retreat in Northwest Greenland, *Geophysical Research Letters*, *45*(16), 8334–8342, doi:10.1029/2018GL078024. 2.3.2

Wood, M., E. Rignot, I. Fenty, L. An, A. Bjørk, M. van den Broeke, C. Cai, E. Kane, D. Menemenlis, and R. Millan (2021), Ocean forcing drives glacier retreat in Greenland, *Science Advances*, *7*(1), eaba7282, doi:doi:10.1126/sciadv.aba7282. 2.3.2

Woodgate, R. (2013), Arctic Ocean circulation: Going around at the top of the world, *Nature Education Knowledge*, *4*(8), 8. 2.1.2

Woodgate, R. A. (2018), Increases in the Pacific inflow to the Arctic from 1990 to 2015, and insights into seasonal trends and driving mechanisms from year-round Bering Strait mooring data, *Progress in Oceanography*, *160*, 124–154, doi:10.1016/j.pocean.2017.12.007. 2.1.1

Woodgate, R. a., K. Aagaard, R. D. Muench, J. Gunn, G. Björk, B. Rudels, a. Roach, and U. Schauer (2001), The Arctic Ocean Boundary Current along the Eurasian slope and the adjacent Lomonosov Ridge: Water mass properties, transports and transformations from moored instruments, *Deep Sea Research Part I: Oceanographic Research Papers*, *48*(8), 1757–1792, doi:10.1016/S0967-0637(00)00091-1. 2.1.2

Woodgate, R. a., K. Aagaard, J. H. Swift, K. K. Falkner, and W. M. Smethie (2005), Pacific ventilation of the Arctic Ocean's lower halocline by upwelling and diapycnal mixing over the continental margin, *Geophysical Research Letters*, *32*(18), doi:10.1029/2005GL023999. 2.1.3

Woodgate, R. a., K. Aagaard, and T. J. Weingartner (2006), Interannual changes in the Bering Strait fluxes of volume, heat and freshwater between 1991 and 2004, *Geophysical Research Letters*, *33*(15), L15,609, doi:10.1029/2006GL026931. 2.1.2

Woodgate, R. a., T. Weingartner, and R. Lindsay (2010), The 2007 Bering Strait oceanic heat flux and anomalous Arctic sea-ice retreat, *Geophysical Research Letters*, *37*(1), doi:10.1029/2009GL041621. 2.1.2, 2.1.3

Woodgate, R. a., T. J. Weingartner, and R. Lindsay (2012), Observed increases in Bering Strait oceanic fluxes from the Pacific to the Arctic from 2001 to 2011 and their impacts on the Arctic Ocean water column, *Geophysical Research Letters*, *39*(24), doi:10.1029/2012GL054092. 2.1.3

Woods, C., and R. Caballero (2016), The role of moist intrusions in winter Arctic warming and sea ice decline, *Journal of Climate*, *29*(12), 4473–4485, doi:10.1175/JCLI-D-15-0773.1. 2.3.1

Wunsch, C., and R. Ferrari (2018), 100 years of the ocean general circulation, *Meteorological Monographs*, *59*, 1–7, doi:10.1175/amsmonographs-d-18-0002.1. 3.2

Yamanouchi, T. (2011), Early 20th century warming in the Arctic: A review, *Polar Science*, *5*(1), 53–71, doi:10.1016/j.polar.2010.10.002. 2.2.1

Yang, S., and J. H. Christensen (2012), Arctic sea ice reduction and European cold winters in CMIP5 climate change experiments, *Geophysical Research Letters*, *39*(20), 1–7, doi:10.1029/2012GL053338. 2.1.1, 3.1

Yashayaev, I., and D. Seidov (2015), The role of the Atlantic Water in multidecadal ocean variability in the Nordic and Barents Seas, *Progress in Oceanography*, *132*(December 2014), 68–127, doi:10.1016/j.pocean.2014.11.009. 2.2.1, 2.2.1

Yeager, S. G., A. R. Karspeck, and G. Danabasoglu (2015), Predicted slowdown in the rate of Atlantic sea ice loss, *Geophysical Research Letters*, *42*(24), 10–704, doi:10.1002/2015GL065364. 2.2.2, 5.2

Yu, L., Y. Gao, and O. H. Otterå (2016), The sensitivity of the Atlantic meridional overturning circulation to enhanced freshwater discharge along the entire, eastern and western coast of Greenland, *Climate Dynamics*, *46*(5-6), 1351–1369, doi:10.1007/s00382-015-2651-9. 5.2

Zanowski, H., A. Jahn, and M. M. Holland (2021), Arctic Ocean freshwater in CMIP6 Ensembles: Declining Sea Ice, Increasing Ocean Storage and Export, *Journal of Geophysical Research: Oceans*, p. e2020JC016930. 5.3

Zhang, R. (2015), Mechanisms for low-frequency variability of summer Arctic sea ice extent, *Proceedings of the National Academy of Sciences*, *112*(15), 4570–4575, doi:10.1073/pnas.1422296112. 2.2.1, 2.2.2, 5.2

Zhao, M., and M. Timmermans (2015), Vertical scales and dynamics of eddies in the Arctic Ocean's Canada Basin, *Journal of Geophysical Research: Oceans*, *120*(12), 8195–8209, doi:10.1002/2015JC011251. 2.1.2

Graphic design: Communication Division, UiB / Print: Skipnes Kommunikasjon AS

uib.no

ISBN: 9788230841709 (print)
9788230866306 (PDF)